Applications of planar oxygen optodes in biological aquatic systems

**Dissertation zur Erlangung des Doktorgrades
der Naturwissenschaften**

**Dem Fachbereich Biologie/Chemie
der Universität Bremen vorgelegt von**

Ulrich Franke

Bremen im Januar 2005

Die vorliegende Arbeit wurde in der Zeit von Oktober 2000 bis Januar 2005 am Max-Planck-Institut für marine Mikrobiologie in Bremen angefertigt.

Gutachter

Prof. Dr. Gunter Otto Kirst
Prof. Dr. Bo Barker Jørgensen

Prüfer

Prof. Dr. Friedrich Widdel
Dr. Dirk de Beer

Weitere Mitglieder des Prüfungsausschusses

Dipl. Biologin Susanne Hinck
Stud. rer. nat. Nina Linde

Datum des Promotionskolloquiums: 18. April 2005

Acknowledgements

I would like to thank Prof. Bo Barker Jørgensen for accepting me as a PhD student and for supporting this work.

I am grateful to my mentor Dr. Gerhard Holst, who greatly supported me in numerous ways during the first 1.5 years of my PhD and introduced me into the "secrets" of the planar optode technique.

Dr. Markus Hüttel is thanked very much for a lot of help and for sharing his great experience in the field of sandy sediments from the planning of wave tank experiments, fruitful discussions all the way to critical manuscript reading.

Dr. Dirk de Beer is thanked for valuable discussions as well as numerous ideas concerning planing and enforcement of several studies.

I am very grateful to Lubos Polerecky, who supported me like a mentor and often it was his ability to separate important from irrelevant things that helped a lot, especially when the writing process started.

I'd further like to thank Prof. B. B. Jørgensen and Prof. G. O. Kirst for examination of this PhD thesis. Together with Prof. F. Widdel, Dr. D. de Beer, S. Hinck, and N. Linde they are also acknowledged for participating as committee members in the thesis defense.

Special thanks go to all the technicians that contributed to the construction of diverse experimental setups and electronic parts: Volker Meyer, Paul Färber, Harald Osmers, Georg Herz, Alfred Kutsche.

Claudia Schröder, Ingo Klimant and Gregor Liebsch are thanked very much for their supply with planar optodes, very pleasant times in Regensburg and helping me to start producing them here.

My long time office members, Björn Grunwald and Lubos Polerecky are thanked very much for a lot of help with trigger-boxes, cameras, nasty camera cards and computers, for discussion, and for keeping me in a good mood. Without their programming skills this work would not have been possible.

I am indebted to the following people for their help and technical assistance in the laboratory: Gabi Eickert, Ines Schröder, Anja Eggers and Cäcilia Wigand.

My colleagues in the Microsensor and Flux Group in the Biogeochemistry Department and across the house are thanked for their warmth which made the period of my PhD a very pleasant time. Unfortunately too many people to mention here.

Special thanks go to Lubos Polerecky, Elimar Precht, Peter Stief, Rebecca Ludwig, Uschi Werner, Markus Billerbeck, Henk Jonkers, Felix Janssen and Fanni Aspetsberger for their friendship, for fruitful discussions that largely improved this thesis, and for their help in the finalizing stage.

The "Mensa-team" Uschi, Rebecca, Markus, Eva, Henk, Björn, Lubos and Anja is thanked for disport, relaxing times which made the lunch and coffee breaks very pleasant times.

The credit for every sentence in this thesis without grammatical or spelling errors as well as constructive comments go to Lubos, Peter, Rebecca, Uschi, Eli and Henk.

My parents are thanked very much for supporting me both financially and with their strong belief that I would finish the thesis some day and my grandmother for showing that high spirits make live much easier. My uncle Walter is thanked for the help of the development of the prototype of the squared sediment corer which is nicely working and extremely handy.

Most of all, I am deeply indebted to my family, Julia and Lilli their love and support also in times when PhD work and family life seemed a bit contradictory....

Table of contents

General introduction

This thesis focuses on two-dimensional (2D) oxygen measurements in benthic aquatic systems employing porphyrin-based planar oxygen optodes and the modular luminescence lifetime imaging (MOLLI) system. It will be shown that porphyrin-based planar oxygen optodes are powerful tools for the visualisation of highly heterogeneous and dynamic oxygen distributions, superior to one-dimensional measuring techniques. The extent to which the optodes can be used in aquatic applications will be specified and the causes of their limited applicability for highly accurate and rapid quantitative determination of oxygen distributions will be identified and discussed.

Oxygen measurements

The sediment-water interface is an important and highly active horizon of aquatic environments. Intense production and degradation of organic matter takes place within a relatively narrow zone leading to an intensive exchange of solutes and particulate organic matter between the sediment and the water column. Sediments, microbial mats, biofilms and other compact microbial communities (e.g., marine snow) occurring in aquatic environments are therefore characterised by steep gradients of various physical and chemical parameters, such as light intensity, pH and oxygen, over distances ranging from less than 0.5 mm to a few millimetres (Revsbech and Jørgensen 1986). The interface is typically not a flat horizon but is characterised by heterogeneities, both at micro- and macro-scale (Jørgensen and Des Marais 1990; Aller et al. 1998). These heterogeneities are related to several factors such as flow conditions, organic carbon input and usability, temperature, and macro- and micro-fauna activity.

Dissolved oxygen is one of the most important parameters in biological systems as it is the terminal electron acceptor for aerobic heterotrophic processes as well as for products of anaerobic organic matter degradation (Canfield et al. 1993). Therefore the knowledge of oxygen concentration gradients is of paramount importance in understanding the function and regulation of microbial communities.

Different types of oxygen sensors are used to determine oxygen concentrations at high spatial and temporal resolution, whereby generally two main functional principles can be distinguished: electrochemical O_2 microsensors (O_2 microelectrodes) and optical O_2 microsensors (O_2 microoptodes). Additionally, these two different sensor types can be divided into needle-type and planar sensors. Needle-type sensors have small sensor tips

and can consequently measure oxygen at single points or one-dimensional profiles. Planar oxygen optodes, however, enable the measurement of oxygen distribution in two-dimensions

Electrochemical oxygen sensing

Since the introduction of electrochemical microsensors to microbial ecology, direct oxygen measurements with a resolution down to 50 μm have been possible (Revsbech et al. 1980). Probably the most frequently and widely used oxygen microsensor in environmental applications is the Clarke-type sensor (Revsbech 1989). It consists of an Ag/AgCl reference and a gold-coated cathode immersed in an alkaline electrolyte solution within a glass casing behind an ion-impermeable, but gas-permeable silicone membrane. The sensor tip of such an electrode is shown in (Fig.1). The measuring principle is based on the diffusion of oxygen from the outside through the silicone membrane towards the electrode and the reduction of oxygen at the cathode. An additional guard cathode prevents oxygen from diffusing from the bulk electrolyte towards the sensor tip.
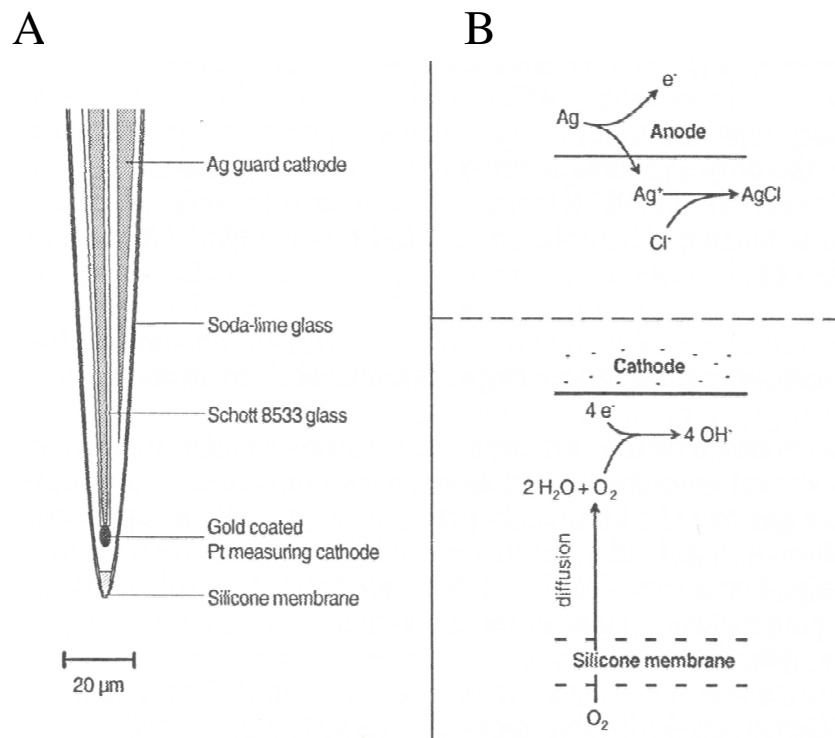

Figure 1: Clarke-type oxygen microsensor. (A) Detailed view of the sensor tip. (B) Scheme showing the measuring principle. Figure from Kühl and Revsbech (2001).

Clarke-type sensors can be made with tip diameters < 5 µm, exhibit detection limit of 0.1 µmol L^{-1}, have short response times (< 0.5 s), small stirring sensitivities (1 – 2 %), their output signal changes linearly with changing oxygen concentrations and are thus ideal tools for most applications in aquatic systems (Kühl and Revsbech 2001). However, their construction is time consuming and requires significant amount of training and in long-term measurements they often show inadequate signal stability.

Optical oxygen sensing

Optical methods have always played an important role in various fields of analytical science. Generally, the analyte interacts with an indicator and changes its optical properties. Colourimetry and photometry have been used to qualitatively determine chemical and biochemical species. A breakthrough resulted from the introduction of strip tests based on dry reagent chemistries allowing visual or instrumental evaluation of analytical results (Wolfbeis 1991). The pH paper stripe containing cellulose-immobilised pH colour indicator is probably the best known example. In the 1930`s Kautsky (1939) found that oxygen changed the luminescence properties of a specific fluorophore. After removal of oxygen the sensor regenerated after 1 - 2 seconds.

The optical oxygen measuring principle of the optodes used in this work is based on dynamic quenching of a fluorophore by oxygen. Oxygen molecules diffuse into a sensing layer where they react reversibly with the fluorescent dye. Upon absorption of excitation light, the electrons of the fluorophore molecule change from their ground energy level (S_0) to a higher energy level (S_1 or S_2). Because the excited state is energetically unfavourable the electrons return back to their ground level S_0 by emitting a quantum of luminescence light (Fig. 2). This emission is altered by the presence of oxygen molecules. Collision of oxygen with the excited dye results in a decrease of the intensity and/or lifetime of the emitted luminescence (Lübbers 1995), as schematically shown in Figure 3. Lifetime is defined as the time-interval after which the luminescence intensity decreases to 1/e times the initial intensity.

Commonly used oxygen indicators are ruthenium-diimine or platinum-porphyrin complexes immobilised in a polystyrene matrix (Papkovsky et al. 1992; Liebsch et al. 2000). These dye complexes offer relatively large Stoke`s shifts between the excitation (blue and green light) and the emission (red light) maximum and allow the use of standard optical filters to separate ambient and excitation light from the luminescence (Liebsch 2000).
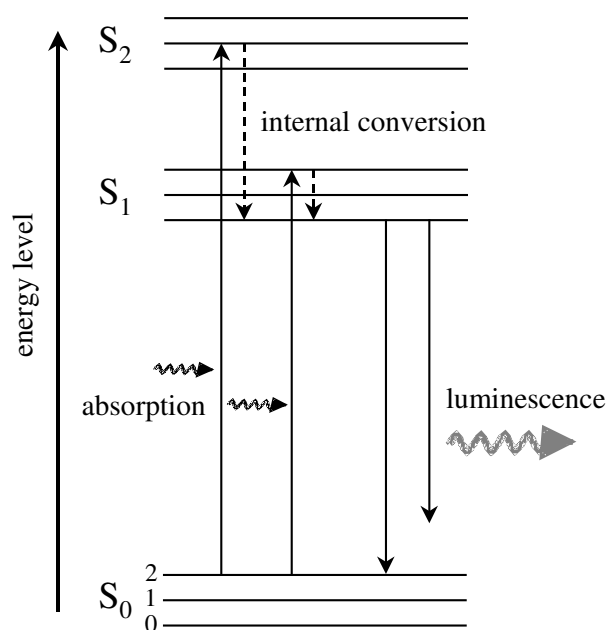
Figure 2: Simplified diagram of energy levels of an electron in a dye molecule. Absorption of a quantum of higher energy light (e.g., blue or green) leads to the excitation of the electron from its ground energy state (S_0) to an excited state (S_1 or S_2). By emitting luminescence, the electron returns back to its ground level. Internal decay due to thermal dissipation occurs, resulting in a longer wavelength of the luminescence compared to the absorbed light (so called Stoke's shift).
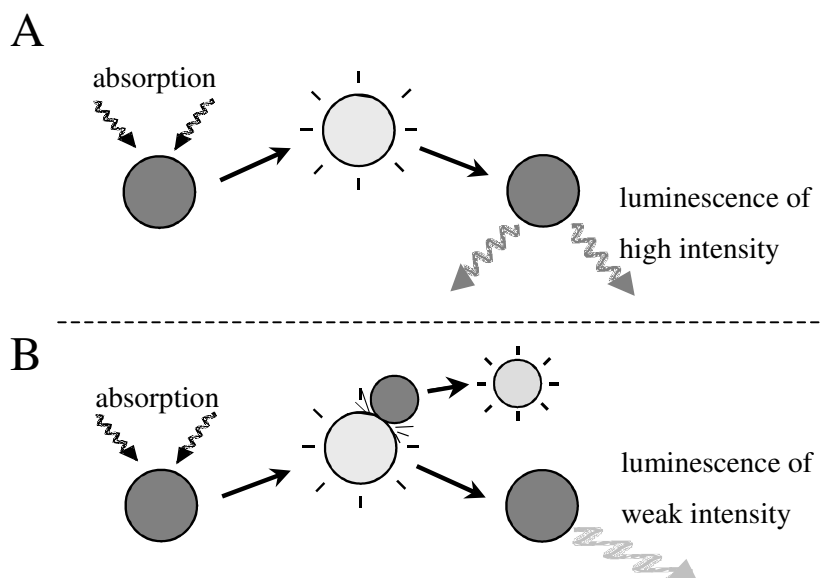

Figure 3:   Scheme of collisional quenching. (A) In the absence of oxygen the excited fluorophore returns to its ground state by emitting luminescence of higher intensity and longer lifetime. (B) When oxygen is present the luminescence is quenched, resulting in weaker intensity and shorter lifetime.

In contrast to microelectrodes, the used optodes show a nonlinear decrease in the signal (luminescence intensity or lifetime) with increasing oxygen concentrations (see chapter 5, Fig. 6). The calibration can be described by means of a two component model of the Stern-Volmer equation modified by Carraway et al. (1991) and allows for a two point calibration procedure of the optodes:

$$\frac{\tau}{\tau_0} = \frac{I}{I_0} = \frac{frac}{(1 + K_{sv} \times O_2)} + (1 - frac) \tag{1}$$

where τ_0, τ and I_0, I are the lifetime and intensity of luminescence in the absence and presence of oxygen, respectively, K_{sv} is the quenching efficiency or Stern-Volmer constant, O_2 is the oxygen concentration and frac is the fraction of the luminescence which is quenched by oxygen. The two point calibrations are usually done with the help of air saturated water and anoxic water or anoxic sediment samples at the experimental temperature and salinity as the oxygen solubility in water depends mainly on these two factors.

Oxygen microoptodes: Microooptodes were introduced into aquatic biology by Klimant et al. (1995). Their main advantage over microelectrodes is that they are easy and cheap to build, do not consume oxygen and feature good long-term stability. The measuring setup consists of an illumination module with the light source and optical filters, an optical fibre coupler, the optical microsensor, and a detection module with a fluorescence-detecting photomultiplier and a reference photodiode (Klimant et al. 1995). The sensor itself is constructed from a tapered optical fibre to which tip a thin layer of the sensor matrix is fixed. The optical fibre of the sensor is used for guiding both the excitation light to the dye at the sensor tip and the emitted luminescence signal to the photomultiplier (Fig. 4). Tip diameters are typically in the range of 30 – 50 μm, since smaller diameters would result in a strong decrease of the signal intensity (Klimant and Wolfbeis 1995; Holst et al. 1997).

Oxygen planar optodes: Several publications within the last decades have demonstrated that imaging of 2D solute distributions with luminescent indicators became a valuable tool in medicine, physics and biology. The first imaging systems were designed to measure oxygen concentrations and distributions of perfused tissue of rat livers (Rumsey et al. 1988) or oxygen partial pressures on skin surfaces and oxygen flux into the skin (Hartmann et al. 1997; Stücker et al. 1998; Liebsch 2000).
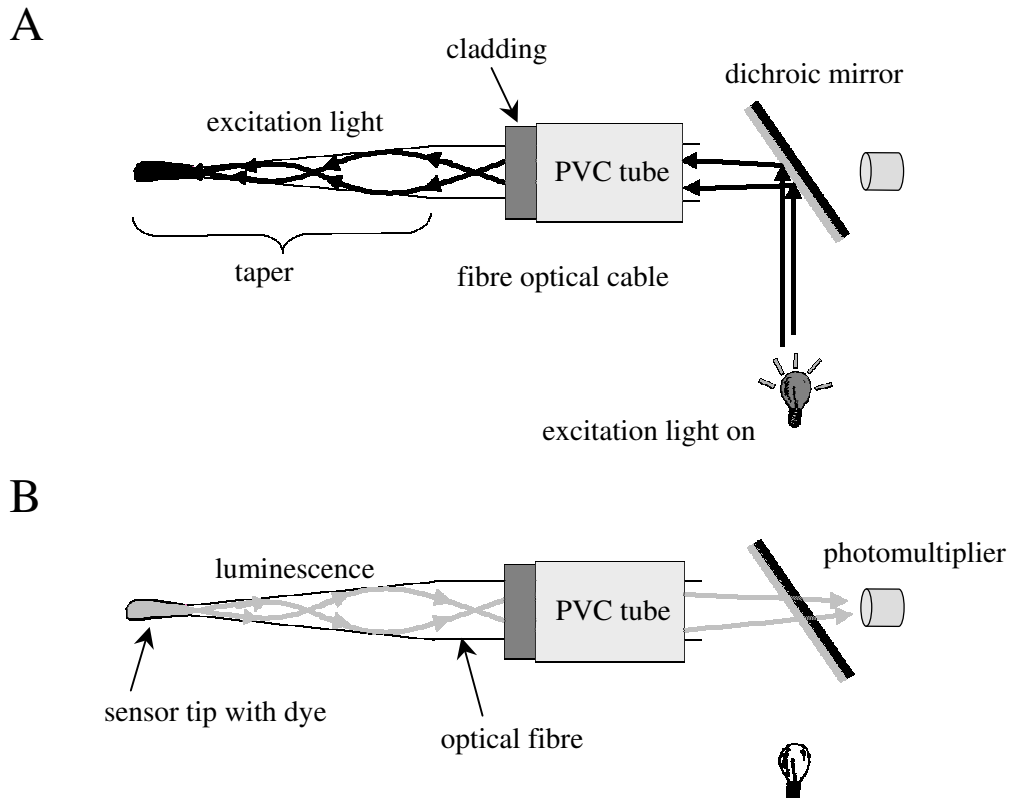
A

B

Figure 4: Schematic diagram of the measuring principle of microoptodes. (A) The excitation light is guided through an optical fibre and excites the oxygen sensitive dye at the sensor tip. (B) The emitted luminescence is guided trough the optical fibre and, after the excitation light is switched off, detected by a photomultiplier at the fibre end.

The first oxygen planar optode measuring system in aquatic science was introduced by Glud et al. (1996). Since then planar optodes have proven to be an attractive tool to measure heterogeneity and dynamics of oxygen concentrations in diverse aquatic systems such as photosynthetic and bioturbated sediments (Fenchel and Glud 2000; Holst and Grunwald 2001), permeable sandy sediments (Precht et al. 2004; Rasheed et al. 2004; Wild et al. 2004; Polerecky et al. 2005), corals and foraminifera (Holst and Grunwald 2001). First *in situ* measurements in photosynthetic and bioturbated sediments were also conducted (Glud et al. 2001; Wenzhöfer and Glud 2004).

In contrast to microoptodes, the sensor matrix containing the oxygen sensitive dye is deposited as a thin layer on a transparent support foil by a knife-coating process (Glud et al. 1996). The general imaging setup (see chapter 5, Fig.1) consists of the sensor fixed by transparent silicone to the inner wall of a transparent window of the experimental setup (e.g., an aquarium), a light source producing a relatively homogeneous light field to excite the optode, optical filters, a fast gateable CCD camera to image the luminescence, a trigger

device and a computer for control and image acquisition (e.g. Glud et al. 1996; Holst et al. 1998).

The first employed imaging system was able to measure the luminescence intensity. A drawback associated with intensity-based measurements is that the acquired images depend not only on the oxygen concentration but also on factors that are difficult to eliminate or control, such as varying background light, background luminescence and scattering effects, leaching and/or photobleaching of the oxygen-sensitive fluorophore and the distribution of the excitation light field (Liebsch et al. 2000; König et al. 2001).

A modular luminescence lifetime imaging (MOLLI) system was developed and first applied in marine microbiology by Holst et al. (1998). All of the above described undesirable factors of the intensity-based system are eliminated when a lifetime-based approach is used. For example, lifetime-imaging does not depend on a homogeneous fluorophore distribution across the foil, intensity variations due to leaching and/or photobleaching or the excitation light field distribution. Background luminescence can effectively be suppressed if it has a different decay time compared to that of the oxygen-sensitive fluorophore (Liebsch et al. 2000; Holst and Grunwald 2001).

Image acquisition and calculation of lifetime images: In the MOLLI system, lifetime image is measured by employing a rapid lifetime determination (RLD) method (Ballew and Demas 1989; Liebsch et al. 2000) schematically shown in Fig. 5. Following a short square-shaped light pulse from LEDs, luminescence is detected quantitatively in two different time-windows, referred to as W_1 and W_2. Thus, two integrated intensity images are obtained whose ratio is in each pixel related to the respective luminescence lifetime of the used indicator in the sensing layer. This ratio (W_1/W_2) is virtually independent of the overall signal intensity. When assuming a mono-exponential decay of luminescence intensity (i.e., a single lifetime) and an equal width of both windows (Δ_t), the lifetime (τ) can be calculated as (e.g. Holst and Grunwald 2001):

$$\tau = (\Delta_t + \Delta_2) / \ln (W_1/W_2), \qquad (2)$$

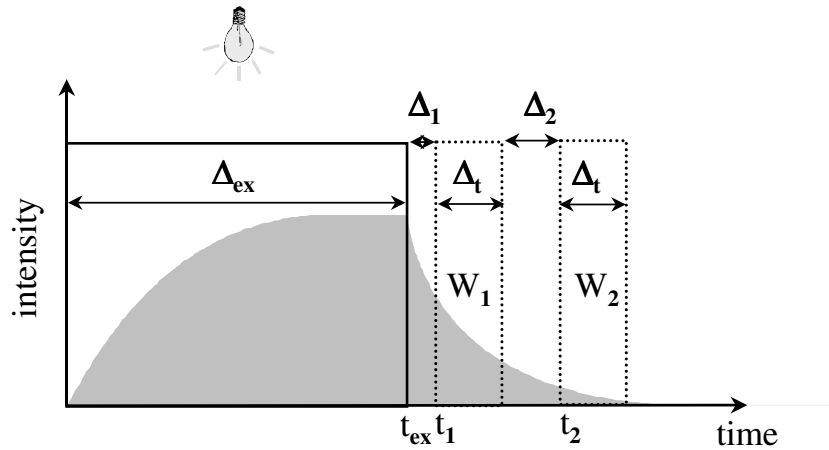where Δ_2 is the gap between the first and second windows (Fig. 5).

Figure 5: Scheme of the rapid lifetime determination (RLD) method. The fluorophore is excited by a short light pulse (Δ_{ex}). After a certain time interval (Δ_1) following the end of the light pulse, the emitted luminescence is detected (e.g., by a CCD camera) during two equally long time-intervals (Δ_t) separated by a gap (Δ_2). The luminescence lifetime (τ) can be calculated from the ratio of the intensities I_{w1} and I_{w2} measured during the first and second time-intervals (window 1 and 2). See text for more details.

For the actual calculation of the lifetime distribution using the "two-window" approach, the data acquisition process is separated into three measuring cycles (Fig. 6). Within each cycle the excitation light source is switched on for a certain amount of time to allow for a build-up of luminescence. Then the light source is switched off and, with a certain time delay (Δ_1, see Fig. 5), the camera shutter is opened for the duration Δ_t of the window W1, allowing the luminescence as well as the ambient background light to reach the CCD chip of the camera. This series of events is repeated within the cycle 1 and the luminescent light is integrated on the CCD chip. Thereafter the data of W_1, referred to as the image "window 1", is read out by the computer and stored in the memory. Then cycle 2 starts, whereby the camera shutter is opened for the duration Δ_t of the window W_2 after a longer time delay compared to cycle 1, namely at time t_2 (see Fig. 5). After these events have been repeated and the luminescent light has been integrated, the image "window 2" is transferred to the computer and the third cycle starts. In contrast to cycles 1 and 2, the excitation light is <u>not</u> switched on in cycle 3 and the camera shutter is opened again for the duration Δ_t. During this time, ambient background light is recorded by the CCD chip and transferred to the computer. This background image is subsequently subtracted from image "window 1" and "window 2" and all three images are stored on the hard disk of the computer as 12-bit TIFF images. To improve the signal-to-noise ratio of the acquired images, each cycle can be repeated and the corresponding images are averaged.
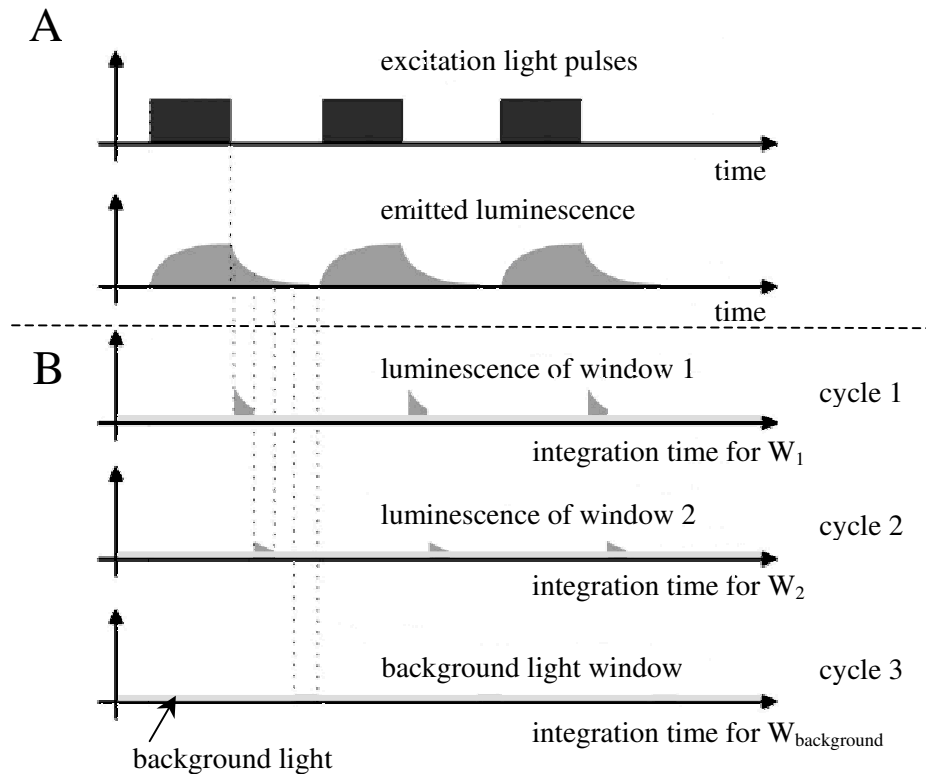
Figure 6: Scheme of the triggering and timing of the excitation light source and camera detecting the luminescence signal implemented in the MOLLI system. Panel (A) shows the general timing of the excitation light pulses and the corresponding luminescence, which is repeated for all three measuring cycles. The luminescence signal may be superposed with the background light of constant intensity. Panel (B) shows the cycles during which the camera integrates the luminescence signal of the windows 1 and 2 (see Fig. 5) and the background light used for the background correction of the two windows. Figure modified after Holst and Grunwald (2001).

The dynamic range of lifetime values for the porphyrin-based planar optodes utilised in our measurements was typically between 15 and 65 µs at air saturation and zero oxygen concentration, respectively. The measurements settings used for the data acquisition were selected as $\Delta_{ex} = 20$ µs, $\Delta_t = 10$ µs, $\Delta_1 = 1$ µs and $\Delta_2 = 0$ µs. With the time of a single cycle typically ranging between 50 and 300 ms, selected so as to detect enough luminescence for "window 1" and "window 2", the described events within one cycle were repeated between approximately 1000 to 7000 times.

Transport mechanisms and exchange processes in marine sediments

The sediment bed is the most important site for accumulation, storage and biogeochemical transformation of organic matter in shallow aquatic environments (Canfield et al. 1993). These processes are linked to the overlying water by transport of solutes and particles into and out of the sediment (van Rees et al. 1996). The transport mechanisms in marine sediments are either molecular diffusion or mass flow processes. Diffusion is restricted to solutes and is driven by concentration gradients whereby no net water or sediment transport occurs. In contrast, mass flow processes are independent of concentration gradients but rely on net water and/or sediment transport and include not only solutes but also particles. Water transport is caused by bioirrigation activity of fauna or physical forcing (porewater advection), sediment is transported either by bioturbating fauna (reworking activity) as well as by bedform migration driven by bottom water hydrodynamics. When the bottom flows are weak, fine-grained sediments (cohesive sediments) can accumulate, whereas frequently occurring stronger bottom currents, which resuspend and winnow the sediment, will result in coarse-grained sediments.

Transport mechanisms in cohesive sediments

Molecular diffusion: In fine-grained deposits such as silty and muddy sediments (grain size ≤ 63 µm) the porewater is virtually unmoveable and physical solute transport is restricted to molecular diffusion. Net transport in diffusive processes is driven by thermally-induced random movement of molecules along solute concentration gradients from sites of high to low concentrations, corresponding to sources and sinks of the solutes, respectively. Fick`s first law of diffusion describes the flux (J) of solutes which is proportional to the height of the vertical concentration gradient (dC/dz) (e.g. Crank 1975):

$$J = - D_0 \, (dC/dz) \qquad (3)$$

where D_0 is the substrate-dependent diffusion coefficient in water at a given temperature and salinity.

Within sediments, diffusion occurs only in the porespace. As molecules have to take longer paths around the sediment particles to diffuse from high to low concentrations the effective diffusion coefficient in sediments is lower than in water. Fick`s first law must be modified to account for these constraints as:

$$J = - \phi \, D_s \, (dC/dz) \qquad (4)$$

where ϕ is the sediment porosity and D_s is the effective diffusion coefficient in the porewater. The relation between ϕ and D_s can be found in the literature for different types of sediments (Ullman and Aller 1982; Iversen and Jørgensen 1993; Boudreau 1996).

Figure 7 shows a typical oxygen concentration profile in a muddy sediment with stirred overlying seawater derived by an oxygen microsensor. Turbulent mixing due to relatively high fluid velocities (eddy diffusion) causes constant oxygen concentrations within the surface water. This mixing drops rapidly towards the sediment surface as the water velocity decreases (velocity at the sediment surface is zero) and just above the sediment a linear oxygen decrease is determined. This region, typically 0.2 – 1.2 mm thick in marine environments (Jørgensen 2001), was termed diffusive benthic boundary layer (DBL) as molecular diffusion is the only transport mechanism within this layer (Jørgensen and Revsbech 1985).
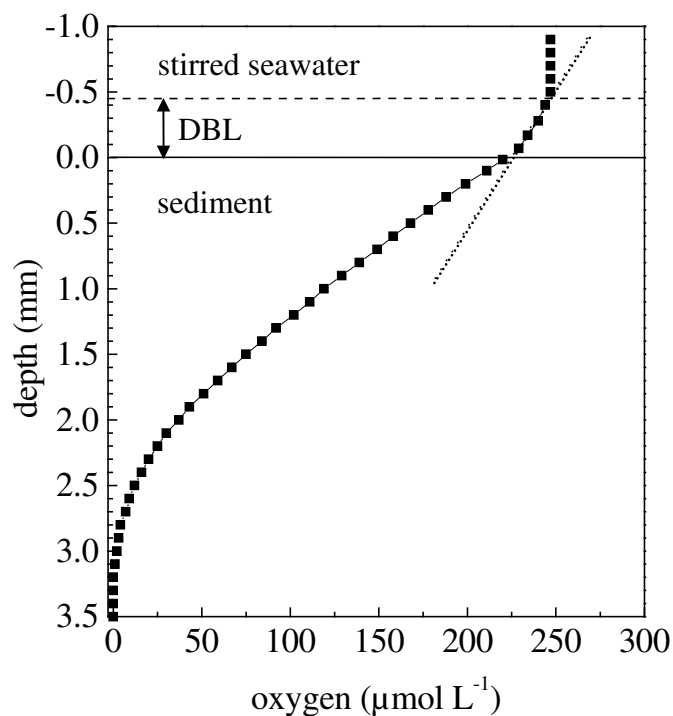

Figure 7: Typical oxygen profile measured with a Clarke-type microsensor in muddy sediment (Weddewarden, German North Sea). The thickness of the diffusive boundary layer (DBL) was approx. 450 µm. A line was fitted to the oxygen gradient within the DBL (dotted line). Horizontal lines indicate sediment surface (solid line) and the upper-most border of the DBL (dashed line).

The total oxygen uptake rate of the sediment will be restricted to the integrated total oxygen consumption in the upper most sediment layer as the maximum concentrations of oxygen in the bottom water and the oxygen consumption rates in the sediment will limit the maximum solute flux and the maximum distance which can be reached by diffusion (Jørgensen 2001). When very steep oxygen gradients between the sediment and the overlying water are present due to high sedimentary oxygen consumption rates, the DBL may completely limit oxygen consumption rates (Jørgensen and Revsbech 1985).

According to a simplified version of the Einstein-Smoluchowski relation the mean distance (Δx) which a molecule can cover by diffusion in a certain time (Δt) can be estimated (Adam et al. 1988):

$$\Delta x^2 = 2 \times D \times \Delta t \qquad\qquad (5)$$

where D is the diffusion coefficient of the solute. The fact that the time a molecule needs to cover a certain distance increases with the square of the distance, explains why transport by molecular diffusion is only efficient over short distances, one of the major characteristic of molecular diffusion. Therefore, in diffusion-dominated environments established solute distributions are relatively stable. However, when dramatic changes of the solute consumption in the sediment or concentration of the solute in the overlying water occur, this can result, e.g., in significant change of the oxygen penetration depth.

Solute exchange over the sediment-water interface in muddy sediments may be largely increased by benthic macrofauna due to bioirrigation and bioturbation activity (e.g. Aller 1982). The magnitude of biological transport relative to diffusive processes is primarily controlled by the abundance and activity of benthic macrofauna organisms. For coastal marine sediments, the balance between molecular diffusion and fauna mediated solute exchange is roughly 50 – 50 % (Jahnke 2001). Molecular diffusion prevails in muddy sediments only where benthic macroorganisms are absent, such as anoxic basins (e.g. large areas of the deep parts of the Baltic Sea) or where their abundance is relatively small (e.g. the majority of deep sea locations). Usually biogenic transport is most intense in the uppermost sediment layer near the sediment-water interface, where benthos is numerous due to the presence of oxygen. The presence of burrow-building, bioirrigating fauna, i.e. filter-feeding organisms, will increase the solute exchange by enlarging the potential effective exchange area from the visible sediment surface also to the burrows walls within the sediment (Aller 1988; Kristensen 1988; Wenzhöfer and Glud 2004). Although the final

delivery of oxygen through the burrow walls also occurs via diffusion, the burrows can not be considered as simple extension of the sediment surface, as the fauna activity regulates the oxygenation status of the burrow lumen.

Bioirrigation activity: Borrowing animals ventilate their burrows for a multitude of reasons such as acquirement of oxygen and food particles from the overlying water column and flushing of toxic reduced substances out of the burrow (Kristensen 1988; Kristensen 1989; Aller 2001). Benthic filter-feeding organisms, e.g., may transport substantial volumes of surface water for nourishment and respiration through their burrows by ventilation activity. Thereby oxygen-rich surface water is pumped into deeper sediment depths and vice versa. Filter-feeding may provide a rapid and efficient pathway for solutes and particulate matter into and out of the sediment and locally increases the oxygen penetration depth (Riisgard and Larsen 2000; Aller 2001). Often burrows are only flushed periodically which will result in temporally unstable redox conditions (Kristensen et al. 1985). When no ventilation activity is present, the burrow typically will get anoxic, allowing NH^{4+}, Fe^{2+}, and Mn^{2+} to diffuse into the burrow lumen.

The magnitude of temporal and spatial heterogeneity of the geochemical zonation will therefore be influenced by periodically burrow ventilation activity and the complex three-dimensional structure of the burrows (Aller 1994; Wenzhöfer and Glud 2004), in contrast to the more stable and horizontally laminated zonation, which is predominant when fauna is absent in diffusion-controlled sediments.

Bioturbation activity: The search for food and the construction of burrows (bioturbation activity) may effectively mix the upper sediment horizon and disrupt the original stratification of the sediment, which will result in enhanced exchange rates of solutes (Aller 1982) as well as in the transport of particles across the sediment-water interface and within the sediment (Graf and Rosenberg 1997). Physical reworking of the upper sediment layer by supercritical bottom flow can have a similar effect (Wheatcroft 1992).

Transport mechanisms in coarse-grained permeable sediments

The above described transport mechanisms are also present in sandy sediments, but as they are characterised by larger grain-sizes than cohesive sediments, porewater can flow through the interstices. This permits an additional transport mechanism called advection by means of physically induced mass flow of porewater.

Advection: Advective porewater flow is always driven by pressure gradients, which are counteracted by friction in the porespace depending on viscosity of the fluid medium and

the permeability of the sediment. Darcy`s law describes the relation between the porewater flow velocity (u), the sediment permeability (k) and porosity (ϕ), the porewater viscosity (μ) and the spatial pressure gradient (∇p):

$$u = (k/\phi \times \mu) \times \nabla p \qquad\qquad (6)$$

Sediment permeabilities exceeding 1×10^{-12} m^2 allow advective porewater flow driven by pressure gradients that is faster than diffusive transport, whereby significant porewater flow trough the upper layers of sandy sediments can be caused by pressure gradients of less than 1 Pa Huettel and Gust (1992a). Pressure gradients in aquatic sediments may originate from density gradients (density-driven convection), unidirectional currents (current-induced advection) or waves (wave-induced advection). In the following section only current and wave-induced advection are discussed in detail.

Current-induced advection

Figure 8 schematically shows the pressure field around a sediment mound with direction and magnitude of the porewater flow velocities in a flume experiment with unidirectional flow conducted by Huettel et al. (1996).
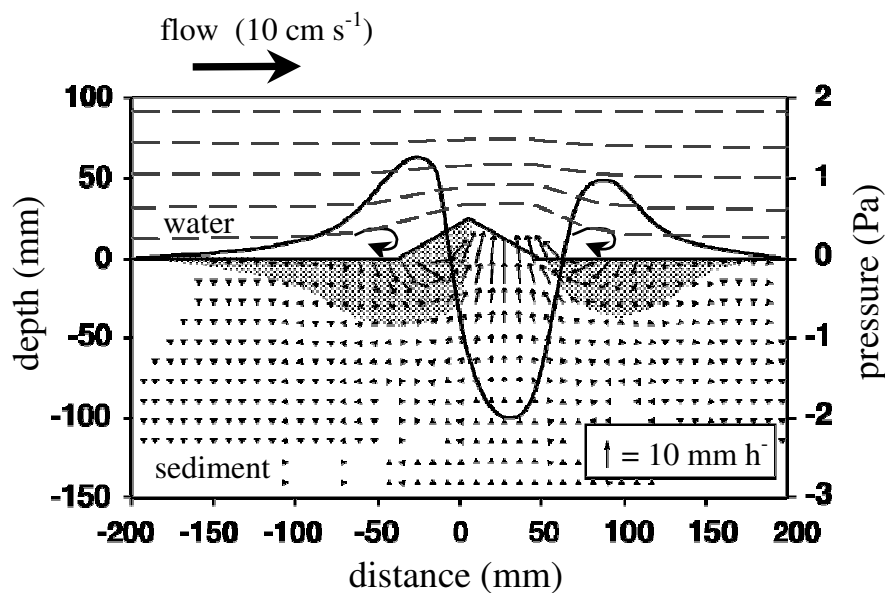

Figure 8: Scheme of unidirectional water flow (dashed lines) in a straight open channel deflected by a protruding topography, the associated pressure field (solid line) and the corresponding advective porewater flow field. Shaded areas show water intrusion zones, arrows in the sediment indicate direction and magnitude of advective porewater flow. Figure modified after Huettel et al. (1996).

The water flow was undisturbed well up- and downstream of the mound, whereas directly upstream of the obstacle the flow was deflected upward (deceleration of flow) and a recirculation zone developed. This resulted in a pressure increase at the sediment surface. In the zone right behind the top of the mound the flow detached from the surface where flow velocities were highest and a pressure minimum occurred. The second recirculation zone behind the mound was coupled to another zone of relatively high pressure. The magnitude of the pressure gradients developing at the sediment surface were studied in flume setups, e.g., with diverse artificially designed bioroughness elements representing burrows, mounds, shells, or benthic organisms resting on the sediment surface (Huettel and Gust 1992a; Huettel et al. 1996). It was found that the pressure gradients are positively correlated with the bottom water flow velocity as well as the height of the obstacles.

A characteristic porewater circulation pattern will develop around an obstacle under unidirectional flow. Up- and downstream of the obstacle, where high pressure is present, bottom water is forced into the sediment, whereas at the low pressure region porewater leaves the sediment. As the low pressure centre is not directly located at the highest point of the obstacle in unidirectional flow systems, porewater leaves the sediment at the downstream flank of the obstacle resulting in an asymmetrical circulation pattern (Fig. 8). Because the water volume which is forced into and out of the sediment has to be balanced and the fact that the areas of intrusion are bigger than extrusion, the porewater velocities have to be higher in the upwelling region compared to the regions of intrusion. Several flume studies using dyes to visualise porewater flow showed this porewater flow pattern (Thibodeaux and Boyle 1987; Huettel and Gust 1992a; Huettel et al. 1996; Elliott and Brooks 1997). Generally the vertical extension of the porewater flow field in sediments with a homogeneous permeability equals approx. the ripple wavelengths (Rutherford et al. 1995). Porewater velocities can range from mm h^{-1} and cm h^{-1} (Savant et al. 1987; Huettel and Gust 1992a; Huettel et al. 1996) up to m h^{-1} in gravel beds exposed to fast bottom flow as can be found in river environments (Thibodeaux and Boyle 1987).

Wave-induced advection

When the water depth is lower than half of the wavelength of surface gravity waves, oscillating bottom flow near the sediment surface occurs (Shum 1992).

Flat bed: The passage of surface gravity waves introduce hydrostatic pressure gradients caused by wave crests and troughs at the sediment surface, which will set the porewater into pulsing rotation. Riedl et al. (1972) introduced the term "subtidal pump" and proposed based on field observations that this mechanism could lead to enhanced exchange rates

between the sediment and the overlaying water. The same process was described by Rutgers van der Loeff (1981) as enhanced diffusivity in the upper most sediment layer of sandy sediment under low and moderate wave action.

Malan and McLachlan (1991) developed an *in situ* benthic chamber setup with flexible tops to allow "wave pumping" activity within the chamber. These authors could show that oxygen consumption and solute fluxes were correlated with wave action. Wave tank experiments focusing on solute exchange processes by Precht and Huettel (2003) suggested that the effect of "wave pumping" might be of minor importance as its separation from advection induced by wave-driven oscillatory bottom currents is not easy. This advective process will occur at the same time when sediment topography is present but is based on a totally different mechanism that will be described below.

Rippled bed: Advection through permeable sediments due to the interaction of oscillating boundary layer and sediment topography has been measured by Webb and Theodor (1968) and Webb and Theodor (1972). Their *in situ* experiments in sandy sediments showed that dye injected into sediment ripple troughs tended to exit the sediment at ripple crests, suggesting the existence of porewater circulation cells, whereby the flow rate of the porewater depended on the surface gravity wave height and the permeability of the sediment. The same physical principle as in unidirectional flow systems drives the advection where oscillating bottom flow interacts with obstacles protruding into the water column: Pressure differences develop, e.g., over a ripple sediment bed, as accelerated flow above ripple crests causes lower pressure than in ripple troughs.

A two-dimensional computational model was presented by Shum (1993), which calculated the trajectories of porewater particles under a rippled sediment bed over one wave period. The model suggested that porewater flow could extend down to sediment depths of several ripple heights over a wide range of wave conditions and sediment characteristics. In contrast to unidirectional flow, the porewater circulation pattern is symmetric (caused by similar strengths of the bottom flow in both directions), with porewater leaving the sediment at the ripple crest and overlying water forced into the sediment at the ripple flanks and troughs (Fig. 9) as observed by Webb and Theodor (1968) and Webb and Theodor (1972) and proposed by Shum (1992). This flow pattern was approved recently by wave tank experiments (Precht and Huettel 2003; Precht et al. 2004) as well as *in situ* experiments (Precht and Huettel 2004). Wave-induced porewater velocities ranged from 2 – 50 cm h^{-1} in a wave tank experiment (Precht et al. 2004) with decreasing velocities towards deeper sediment depths. *In situ* experiments showed median

porewater velocities of ~ 26 cm h^{-1} measured *in situ* under relatively calm wave conditions at a Mediterranean site (Precht and Huettel 2004) and 6 – 53 cm h^{-1} with combined effects of *in situ* tide- and wave-induced currents on the USA Middle Atlantic Bight shelf (Reimers et al. 2004).
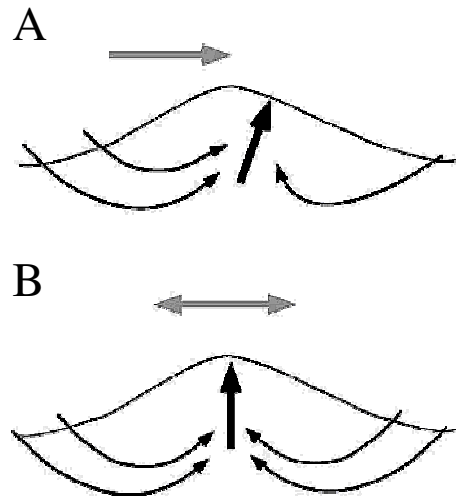

Figure 9: Comparative overview of the general porewater flow fields in permeable sediments under unidirectional (A) and oscillating bottom flow (B). Porewater is released close to the ripple crest at ripple flanks or directly at ripple crests driven by unidirectional flow (A) and oscillatory flow (B), respectively. Figure modified after Precht and Huettel (2004).

Consequences of advective transport

Advective transport of solutes: When the interaction of boundary-layer flow and sediment topography enables dynamic advective porewater flow, the solute exchange at the sediment-water interface can exceed transport by molecular diffusion by several orders of magnitude. In the presence of small mounds (height ≤ 2,5 cm) the interfacial water exchange was measured as dye release into the overlying water and fluxes up to 3 orders of magnitude compared to molecular diffusion were calculated (Huettel and Gust 1992a). Wave tank experiments conducted by Precht and Huettel (2003) revealed that the total exchange over the sediment-water interface of a rippled bed with oscillating bottom flow was up to 50 times the exchange rate by diffusion and 2 – 15 times the advective exchange over a flat bed.

Any solute in the water column and the porewater can be transported relatively fast across the sediment-water interface and within the sediment by advection. Electron acceptors such as oxygen can be supplied at high rates to the sedimentary organisms.

Laboratory (under unidirectional as well as oscillatory bottom flow) and *in situ* measurements experiments showed that advective supply of oxygen can result in fairly deep oxygen penetration depths in the range of several centimetres (Forster et al. 1996; Lohse et al. 1996; Ziebis et al. 1996; Precht et al. 2004; Reimers et al. 2004; de Beer et al. 2005). Indications for an effective advective removal of dissolved inorganic nitrogen species, silicate and phosphate was inferred from hydrodynamic conditions, low porewater concentrations as well as from the shape of porewater concentration profiles (Gehlen et al. 1995; Marinelli et al. 1998; D'Andrea et al. 2002). Additionally inhibitory products such as ammonium and hydrogen sulphide are effectively removed (Ziebis et al. 1996; Huettel et al. 1998).

It is considered that microbial organic matter degradation is increased by enhanced solute exchange (Forster and Graf 1995; Aller and Aller 1998). The supply with oxygen and sulphate has been identified as key factor determining remineralisation rates (Froehlich et al. 1979; Jørgensen and Sorensen 1985; Enoksson and Samuelsson 1987). Furthermore, transfer of nutrients as well as electron acceptors towards surface-associated sedimentary bacteria might be increased in the presence of fluid flow (van Loosdrecht et al. 1990; Logan and Kirchman 1991). All of these processes will have considerable consequences for biogeochemical processes and sediments influenced by advective processes may thus be considered as favourable locations for microbial communities showing increased metabolic activity.

Heterogeneous complex three-dimensional spatial distributions of solutes will be caused by the combination of biogeochemical reactions and advective transport processes. This could be shown for the biologically important solute oxygen in laboratory studies under unidirectional as well as oscillatory boundary flows (Ziebis et al. 1996; Precht et al. 2004). Advective porewater flushing caused a largely increased oxygenated sediment volume as well as zones where anoxic porewater reached the sediment surface, whereby the oxic-anoxic transition zone was greatly enlarged. Therefore not only vertical but also horizontal oxygen gradients of similar steepness developed as predicted by models for wave-induced advection in permeable sediments with rippled surface topography (Shum 1993). Huettel et al. (1998) also showed this complex pattern for NO_3^-, NH_4^+, Fe^{2+} and Mn^{2+} in a flume study. Up- and downstream of the sediment mounds, high concentrations of nitrate due to enhanced nitrification was detected in the advectively oxygenated sediment volumes. In contrast, high concentrations of NH_4^+, Fe^{2+} and Mn^{2+} were present in the anoxic upwelling regions. The three-dimensional distribution of solutes and the biogeochemical transition

zones in natural sediments are not static but highly dynamic. The factors controlling advective processes like bottom water hydrodynamics, sediment topography and permeability can change in time scales from seconds to seasons (Huettel et al. 2003). Short-term effects (seconds to minutes) result from changes of velocities and directions of the boundary flow pattern. Tides and local winds can influence currents in time scales of minutes to days. Bioturbating and bioirrigating benthic fauna can change the topography dramatically within hours to days (Wheatcroft 1992). But topography changes can occur also much faster. Sediment ripple propagation velocities of a few cm h^{-1} to more than 50 cm h^{-1} were recorded (Rutherford et al. 1993; Traykovski et al. 1999; Doucette et al. 2002).

One possible exception to these predominantly fast changes due to topography features could be the development of stationary topography features, e.g., stationary sediment ripples after a storm event in larger waterdepths. Sediment ripples may develop when the bottom flow is sufficiently high, and remain as stationary sediment topography features after the storm event. Thus, the sediment may be affected by advective processes over considerably periods of time in which relatively weak flow predominates. By this "memory effect" (Precht et al. 2004) a temporally stable three-dimensional biogeochemical zonation could establish.

These temporal and spatial changes of advection have strong influence on the sedimentary biogeochemistry and organisms living in the sediment. When bottom flows increase and decrease the rates of advection may considerably change, but the porewater flow field will remain the same (Rutherford et al. 1995; Precht et al. 2004). In contrast, when topography changes occur, e.g., sediment ripples propagate, they are trailed by their porewater flow field alternately exposing sediment volumes to oxic and anoxic conditions whereby the entire biochemical zonation of the advectively influenced sediment horizon will be changed (Precht et al. 2004; Janssen et al. in prep.). This could potentially intensify sediment metabolism as oxidised and reduced compounds can be exchanged fast across short distances. Generally, bacteria located in the transition zone of oxic and anoxic sediment regions show high activities and organic matter remineralisation is enhanced, especially when oxic and anoxic conditions oscillate (Aller 1994; Huettel et al. 1998).

Advective transport of particles: Advection will not only transport solutes but also suspended particles, whereby organic matter from the overlying water could be transported into the sediment. As the porewater velocities decrease with sediment depth, the particles get trapped in distinct layers perpendicular to the porewater flow direction. Studies with tracer particles or phytoplankton showed that particle could be transported several cm deep

into the sediment. Mainly grain size and permeability were found to determine the flux and penetration depth of these particles (Huettel and Rusch 2000; Rusch and Huettel 2000 ; Ehrenhauss and Huettel 2004; Ehrenhauss et al. 2004a). This supply of organic matter to sedimentary organisms is very important especially when high hydrodynamic forces are present and particles cannot settle on the sediment surface before they could be invoked into the sediment by biological (Huettel 1990) or hydrological (Jenness and Duineveld 1985) sediment mixing processes.

Results of Forster et al. (1996); Huettel and Rusch (2000); Ehrenhauss and Huettel (2004); Ehrenhauss et al. (2004a) and Ehrenhauss et al. (2004b) suggest that the advective transport of organic particles such as phytoplankton, bacteria and detritus into the sediment enhanced sedimentary microbial activity and degradation occurred faster compared to the overlying water. This increased degradation activity is most likely the result of several factors. Mechanical stress within the sand probably breaks up cells and intensified contact with bacteria due to fluid-motion make the organic matter easier available for bacteria attached to sand grains (Huettel and Rusch 2000). In the region where these particles are mainly trapped the co-occurrence of organic matter and oxygen as well as other electron acceptors combined with effective transport of inhibitory products will accelerate degradation activity (Ziebis et al. 1996; Huettel et al. 1998).

Aim of the thesis

This thesis focuses on two-dimensional (2D) oxygen measurements in aquatic systems using planar oxygen optodes and the modular luminescence lifetime imaging (MOLLI) system. Special emphasis was placed on characterising recently developed porphyrin-based planar oxygen optodes and testing their applicability to different biological systems. Depending on the system, the requirements for the oxygen sensing technique such as temporal and spatial resolution, quality of the oxygen data as well as robustness and long-term stability, vary. A substantial part of the work was dedicated to finding biological systems where the application of these new optodes would be most advantageously.

In the first experiment (chapter 2) the effects of porewater advection on the oxygen distribution and dynamics in natural sediment was to be investigated in a laboratory wave tank with the help of a planar optode. The porewater advection was driven by wave-generated bottom flow interacting with either stationary or mobile sediment ripples. Their influence on the sedimentary oxygen dynamics was the focus of this experiment.

The second study (chapter 3) was designed to evaluate a newly developed method which allows for the determination of depths profiles of potential oxygen consumption rates in permeable sediments. The method is based on percolation of the sediment with oxygen-rich water and monitoring the oxygen in the sediment with a microelectrode (one-dimension) or in two-dimensions with a planar oxygen optode. The method was tested and compared to standard flux and benthic chamber methods with permeable sediments cores under strictly controlled conditions.

The objective of the third experiment (chapter 4) was to investigate the influence of advective and diffusive transport mechanisms on the aerobic degradation of particular organic matter (POM) in permeable sediment. The means by which advection might enhance the degradation rates was the focus of this study. Degradation rates were quantified directly by measuring the carbon and nitrogen content of POM samples and indirectly by measuring two-dimensional distributions of OCR using planar oxygen optodes.

The fourth study (chapter 5) was designed to describe the characteristics of porphyrin-based planar oxygen optodes such as light-guidance, noise behaviour, temporal and spatial resolution, long-term stability and robustness. The causes of the methodological limitations

were identified, discussed and possible solutions to improve the optode`s applicability are suggested.

Several laboratory applications were tested (chapter 6) to investigate the applacability of porphyrin-based planar optodes on a variety of processes in different aquatic systems. Subjects of investigations were bioirrigation activity; photosynthesis of microbial mats; oxygen uptake rates of foraminifera; radial oxygen loss of seagrass roots; temperature dependence of oxygen consumption rates of permeable sediments and the possibility of distinguishing between the biological and chemical contribution to the total sedimentary OCR of permeable sediments. The goal of this study was the identification of the advantages and limitations offered by the use of porphyrin-based planar oxygen optodes and the lifetime-based oxygen imaging technique.

References

Adam, G, P Läuger, and G Stark. 1988. Physikalische Chemie und Biophysik. Edited by G. Adam, P. Läuger and G. Stark. 2nd Edition. Springer Verlag.

Aller, R. C. 1982. The effects of macrobenthos on chemical properties of marine sediment and overlying water, p. 53-102. *In* P. L. McCall and J. S. Tevesz, [eds.]. Animal-sediment relations. The biogenic alteration of sediments. Topics in Geobiology. Plenum Press.

Aller, R. C., P. O. J. Hall, P. D. Rude, and J. Y. Aller. 1998. Biogeochemical heterogeneity and suboxic diagenesis in hemipelagic sediments of the Panama Basin. Deep-Sea Research Part I-Oceanographic Research Papers **45**: 133-165.

Aller, R.C. 1988. Benthic fauna and biogeochemical processes in marine sediments: the role of burrow structures, p. 301-338. *In* T. H. Blackburn and J. Sørensen, [eds.]. Nitrogen cycling in coastal marine environments. John Wiley.

Aller, R.C. 1994. Bioturbation and remineralization of sedimentary organic-matter - effects of redox oscillation. Chemical Geology **114**: 331-345.

Aller, R.C., and J.Y. Aller. 1998. The effect of biogenic irrigation intensity and solute exchange on diagenetic reaction rates in marine sediments. J. Exp. Mar. Biol. Ecol. **56**: 905-936.

Aller, Robert C. 2001. Transport and reactions in the bioirrigated zone, p. 269-301. *In* B. P. Boudreau and B. B. Jørgensen, [eds.]. The Benthic Boundary Layer. Oxford University Press.

Ballew, R. M., and J. N. Demas. 1989. An error analysis of the rapid lifetime determination method for the evaluation of single exponential decays. Analytical Chemistry **61**: 30-33.

Boudreau, B. P. 1996. The diffusive tortuosity of fine-grained unlithified sediments. Geochim. Cosmochim. Acta **60**: 3139-3142.

Canfield, D. E., B.B. Jørgensen, H. Fossing, R. Glud, J. Gundersen, N. B. Ramsing, B. Thamdrup, J. W. Hansen, L. P. Nielsen, and P. O. J. Hall. 1993. Pathways of organic carbon oxidation in three continental margin sediments. Marine Geology **113**: 27-40.

Carraway, E. R., J. N. Demas, B. A. Degraff, and J. R. Bacon. 1991. Photophysics and Photochemistry of oxygen sensors based on luminescent transition-metal complexes. Analytical Chemistry **63**: 337-342.

Crank, J. 1975. The Mathematics of Diffusion. 2nd edition ed. Oxford University Press Inc.

D'Andrea, A. F., R. C. Aller, and G. R. Lopez. 2002. Organic matter flux and reactivity on a South Carolina sandflat: The impacts of porewater advection and macrobiological structures. Limnol. Oceanogr. **47**: 1056-1070.

de Beer, D., F. Wenzhofer, T.D. Ferdelman, S. Boehme, M. Huettel, J. E. E. von Beusekom, M. E. Böttcher, N.   Musat, and N. Dubilier. 2005. Transport and mineralization rates in North Sea sandy intertidal sediments Sylt- Rømø basin, Wadden Sea. Limnol. Oceanogr. **50**: 113-127.

Doucette, J. S., E. S. Harvey, and M. R. Shortis. 2002. Stereo-video observation of nearshore bedforms on a low energy beach. Marine Geology **189**: 289-305.

Ehrenhauss, S., and M. Huettel. 2004. Advective transport and decomposition of chain-forming planktonic diatoms in permeable sediments. J. Sea Res. **52**: 179-197.

Ehrenhauss, S., U. Witte, S. L. Buhring, and M. Huettel. 2004a. Effect of advective pore water transport on distribution and degradation of diatoms in permeable North Sea sediments. Mar. Ecol. Prog. Ser. **271**: 99-111.

Ehrenhauss, S., U. Witte, F. Janssen, and M. Huettel. 2004b. Decomposition of diatoms and nutrient dynamics in permeable North Sea sediments. Cont. Shelf Res. **24**: 721-737.

Elliott, A. H., and N. H. Brooks. 1997. Transfer of nonsorbing solutes to a streambed with bed forms: Laboratory experiments. Water Resour. Res. **33**: 137-151.

Enoksson, E., and M.O. Samuelsson. 1987. Nitrification and dissimilatory ammonium production and their effects on nitrogen flux over the sediment-water interface in bioturbated coastal sediments. Mar. Ecol. Prog. Ser. **36**: 181-189.

Fenchel, T., and R. N. Glud. 2000. Benthic primary production and O_2-CO_2 dynamics in a shallow-water sediment: Spatial and temporal heterogeneity. Ophelia **53**: 159-171.

Forster, S., and G. Graf. 1995. Impact of irrigation on oxygen flux into the sediment: Intermittent pumping by *Callianassa subterranea* and "piston-pumping" by *Lanice conchilega*. Marine Biology. **123**: 335-346.

Forster, S., M. Huettel, and W. Ziebis. 1996. Impact of boundary layer flow velocity on oxygen utilisation in coastal sediments. Mar. Ecol. Prog. Ser. **143**: 173-185.

Froehlich, P.N. , G.P. Klinkhammer, M.L. Bender, N.A. Luedtke, G.R. Heath, D. Cullen, P. Dauphin, D. Hammond, B. Hartman, and V. Maynard. 1979. Early oxidation of organic matter in pelagic sediments of the eastern equatorial Atlantic: suboxic diagenesis. Geochim. Cosmochim. Acta **43:** 1075-1090.

Gehlen, M., H. Malschaert, and W. R. Van Raaphorst. 1995. Spatial and temporal variability of benthic silica fluxes in the southeastern North Sea. Continental Shelf Research **15**: 1675-1696.

Glud, R. N., N. B. Ramsing, J. K. Gundersen, and I. Klimant. 1996. Planar optrodes: A new tool for fine scale measurements of two-dimensional O_2 distribution in benthic communities. Mar. Ecol. Prog. Ser. **140**: 217-226.

Glud, R. N., A. Tengberg, M. Kuhl, P. O. J. Hall, I. Klimant, and G. Holst. 2001. An in situ instrument for planar O-2 optode measurements at benthic interfaces. Limnol. Oceanogr. **46**: 2073-2080.

Graf, G., and R. Rosenberg. 1997. Bioresuspension and biodeposition: A review. Journal of Marine Systems **11**: 269-278.

Hartmann, P., W. Ziegler, G. Holst, and D. W. Lubbers. 1997. Oxygen flux fluorescence lifetime imaging. Sensors and Actuators B-Chemical **38**: 110-115.

Holst, G., R. N. Glud, M. Kuhl, and I. Klimant. 1997. A microoptode array for fine-scale measurement of oxygen distribution. Sensors and Actuators B-Chemical **38**: 122-129.

Holst, G., and B. Grunwald. 2001. Luminescence lifetime imaging with transparent oxygen optodes. Sensors and Actuators B-Chemical **74**: 78-90.

Holst, G., O. Kohls, I. Klimant, B. König, M. Kuhl, and T. Richter. 1998. A modular luminescence lifetime imaging system for mapping oxygen distribution in biological samples. Sensors and Actuators B-Chemical **51**: 163-170.

Huettel, M. 1990. Influence of the lugworm *Arenicula marina* on porewater nutrient profiles of sand flat sediments. Mar. Ecol. Prog. Ser. **62**: 241-248.

Huettel, M., and G. Gust. 1992a. Impact of bioroughness on interfacial solute exchange in permeable sediments. Mar. Ecol. Prog. Ser. **89**: 253-267.

Huettel, M., and A. Rusch. 2000. Transport and degradation of phytoplankton in permeable sediment. Limnol. Oceanogr. **45**: 534-549.

Huettel, M., W. Ziebis, S. Forster, and G.III. Luther. 1998. Advective transport affecting metal and nutrient distribution and interfacial fluxes in permeable sediments. Geochim. Cosmochim. Acta **62**: 613-631.

Huettel, M., W. Ziebis, and S. Forster. 1996. Flow-induced uptake of particulate matter in permeable sediments. Limnol. Oceanogr. **41**: 309-322.

Huettel, M., H. Røy, E. Precht, and S. Ehrenhauss. 2003. Hydrodynamical impact on biogeochemical processes in aquatic sediments. Hydrobiologia **494**: 231-236.

Iversen, N., and B.B. Jørgensen. 1993. Diffusion-coefficients of sulfate and methane in marine-sediments - Influence of porosity. Geochim. Cosmochim. Acta **57**: 571-578.

Jahnke, Richard A. 2001. Constraining organic matter cycling with benthic fluxes, p. 302-319. *In* B. P. Boudreau and B. B. Jørgensen, [eds.]. The Benthic Boundary Layer. Oxford University Press.

Janssen, F., H Roy, U. Werner, and U. Witte. in prep. Sediment surface topographies and bottom water flow: An in situ case study on the fundamentals of porewater advection.: in prep.

Jenness, M. Ian, and G. C. A. Duineveld. 1985. Effects of tidal currents on chlorophyll a content of sandy sediments in the southern North Sea. Mar. Ecol. Prog. Ser. **21**: 283-287.

Jørgensen, B.B. 2001. Life in the diffusive boundary layer, p. 348-373. *In* B. P. Boudreau and B. B. Jørgensen, [eds.]. The benthic boundary layer: transport processes and biogeochemistry. Oxford Univ. Press.

Jørgensen, B.B. , and D.J. Des Marais. 1990. The diffusive boundary layer of sediments: oxygen microgradients over a microbial mat. Limnol. Oceanogr. **35**: 1343-1355.

Jørgensen, B.B., and N. P. Revsbech. 1985. Diffusive boundary-layers and the oxygen-uptake of sediments and detritus. Limnol. Oceanogr. **30**: 111-122.

Jørgensen, B.B., and J. Sorensen. 1985. Seasonal cycles of O_2, NO_3^- and SO_4^{2-} reduction in estuarine sediments - The significance of a NO_3^- reduction maximum in spring. Mar. Ecol. Prog. Ser. **24**: 65-74.

Klimant, I., V. Meyer, and M. Kuhl. 1995. Fiberoptic oxygen microsensors, a new tool in aquatic biology. Limnol. Oceanogr. **40**: 1159-1165.

Klimant, I., and O. S. Wolfbeis. 1995. Oxygen-sensitive luminescent materials based on silicone-soluble ruthenium diimine complexes. Analytical Chemistry **67**: 3160-3166.

König, B., G. Holst, R.N. Glud, and M. Kuehl. 2001. Imaging of oxygen distributions at benthic interfaces: A brief review, p. 63-71. *In* J. Y. Aller, S. A. Woodin and R. C. Aller, [eds.]. Organism-Sediment Interactions. University of South Carolina Press.

Kristensen, E. 1988. Benthic fauna and biogeochemical processes in marine sediments: microbial activity and fluxes, p. 275-299. *In* T. H. Blackburn and J. Sørensen, [eds.]. Nitrogen cycling in coastal marine environments. John Wiley.

Kristensen, E. 1989. Oxygen and carbon-dioxide exchange in the Polychaete *Nereis-virens* - Influence of ventilation activity and starvation. Marine Biology **101**: 381-388.

Kristensen, E., M. Jensen, and T. Andersen. 1985. The impact of polychaete (*Nereis-virens sars*) burrows on nitrification and nitrate reduction in estuarine sediments. J. Exp. Mar. Biol. Ecol. **85**: 75-91.

Kühl, M., and N. P. Revsbech. 2001. Biochemical microsensors for boundary layer studies, p. B. P. Boudreau and B. B. Jørgensen, [eds.]. The benthic boundary layer. Oxford University Press.

Liebsch, G. 2000. Time-resolved luminescence lifetime imaging with optical chemical sensors thesis, University of Regensburg.

Liebsch, G., I. Klimant, B. Frank, G. Holst, and O. S. Wolfbeis. 2000. Luminescence lifetime imaging of oxygen, pH, and carbon dioxide distribution using optical sensors. Applied Spectroscopy **54**: 548-559.

Logan, B. E., and D. L. Kirchman. 1991. Uptake of dissolved organics by marine-bacteria as a function of fluid motion. Marine Biology **111**: 175-181.

Lohse, L., E.H.G. Epping, W. Helder, and W. van Raaphorst. 1996. Oxygen pore water profiles in continental shelf sediments of the North Sea: turbulent versus molecular diffusion. Mar. Ecol. Prog. Ser. **145**: 63-75.

Lübbers, D. W. 1995. Optical Sensors for Clinical Monitoring. Acta Anaesthesiologica Scandinavica **39**: 37-54.

Malan, Daniel E., and Anton McLachlan. 1991. In situ benthic oxygen fluxes in a nearshore coastal marine system: a new approach to quantify the effect of wave action. Mar. Ecol. Prog. Ser. **73**: 69-81.

Marinelli, R. L., R. A. Jahnke, D. B. Craven, J. R. Nelson, and J. E. Eckman. 1998. Sediment nutrient dynamics on the South Atlantic Bight continental shelf Limnol. Oceanogr. **43**: 1305-1320.

Papkovsky, D. B., J. Olah, I. V. Troyanovsky, N. A. Sadovsky, V. D. Rumyantseva, A. F. Mironov, A. I. Yaropolov, and A. P. Savitsky. 1992. Phosphorescent Polymer-Films For Optical Oxygen Sensors. Biosensors & Bioelectronics **7**: 199-206.

Polerecky, L., U. Franke, U. Werner, B. Grunwald, and D. de Beer. 2005. High spatial resolution measurement of oxygen consumption rates in permeable sediments. Limnol. Oceanogr.: Methods **3**: 75-85.

Precht, E., U. Franke, L. Polerecky, and M. Huettel. 2004. Oxygen dynamics in permeable sediments with wave-driven pore water exchange. Limnol. Oceanogr. **49**: 693-705.

Precht, E., and M. Huettel. 2003. Advective pore water exchange driven by surface gravity waves and its ecological implications. Limnol. Oceanogr. **48**: 1674-1684.

Precht, E., and M. Huettel. 2004. Rapid wave-driven advective pore water exchange in a permeable coastal sediment. J. Sea Res. **51**: 93-107.

Rasheed, M., C. Wild, U. Franke, and M. Huettel. 2004. Benthic photosynthesis and oxygen consumption in permeable carbonate sediments at Heron Island, Great Barrier Reef, Australia. Estuarine Coastal and Shelf Science **59**: 139-150.

Reimers, C. E., H. A. Stecher, G. L. Taghon, C. M. Fuller, M. Huettel, A. Rusch, N. Ryckelynck, and C. Wild. 2004. In situ measurements of advective solute transport in permeable shelf sands. Cont. Shelf Res. **24**: 183-201.

Revsbech, N. P. 1989. An oxygen microelectrode with a guard cathode. Limnol. Oceanogr. **55**: 1907-1910.

Revsbech, N. P., and B.B. Jørgensen. 1986. Microelectrodes: Their use in microbial ecology. Adv. Microb. Ecol. **9**: 293-352.

Revsbech, N. P., B.B. Jørgensen, and T. H. Blackburn. 1980. Oxygen in the sea bottom measured with a microelectrode. Science **207**: 1355-1356.

Riedl, R. J., N. Huang, and R. Machan. 1972. The subtidal pump: a mechanism of interstitial water exchange by wave action. Marine Biology **13**: 210-221.

Riisgard, H. U., and P. S. Larsen. 2000. Comparative ecophysiology of active zoobenthic filter feeding, essence of current knowledge. J. Sea Res. **44**: 169-193.

Rumsey, W. L., J. M. Vanderkooi, and D. F. Wilson. 1988. Imaging of phosphorescence - a novel method for measuring oxygen distribution in perfused tissue. Science **241**: 1649-1651.

Rusch, A., and M. Huettel. 2000. Advective particle transport into permeable sediments - evidence from experiments in an intertidal sandflat. Limnol. Oceanogr. **45**: 525-533.

Rutgers van der Loeff, Michiel M. 1981. Wave effects on sediment water exchange in a submerged sand bed. Neth. J. Sea Res. **15**: 100-112.

Rutherford, J. C., J. D. Boyle, A. H. Elliott, T. V. J. Hatherell, and T. W. Chiu. 1995. Modeling benthic oxygen-uptake by pumping. J. Environ. Eng.-ASCE **121**: 84-95.

Rutherford, J. C., G. J. Latimer, and R. K. Smith. 1993. Bedform mobility and benthic oxygen-uptake. Water Research **27**: 1545-1558.

Savant, S. A., D. D. Reible, and L. J. Thibodeaux. 1987. Convective transport within stable river sediments. Water Resour. Res. **23**: 1763-1768.

Shum, K.T. 1992. Wave-induced advective transport below a rippled water-sediment interface. J. Geophys. Res. **97**: 789-808.

Shum, K.T. 1993. The effects of wave-induced pore water circulation on the transport of reactive solutes below a rippled sediment bed. J. Geophys. Res. **98**: 10289-10301.

Stücker, M., L. Schulze, G. Pott, P. Hartmann, D. W. Lubbers, A. Rochling, and P. Altmeyer. 1998. FLIM of luminescent oxygen sensors: clinical applications and results. Sensors and Actuators B-Chemical **51**: 171-175.

Thibodeaux, L. J., and J. D. Boyle. 1987. Bedform-generated convective transport in bottom sediment. Nature **325**: 341-343.

Traykovski, P., A. E. Hay, J. D. Irish, and J. F. Lynch. 1999. Geometry, migration, and evolution of wave orbital ripples at LEO-15. J. Geophys. Res.-Oceans **104**: 1505-1524.

Ullman, W. J., and R. C. Aller. 1982. Diffusion-Coefficients in Nearshore Marine-Sediments. Limnol. and Oceanogr. **27**: 552-556.

van Loosdrecht, M. C. M., J. Lyklema, W. Norde, and A. J. B. Zehnder. 1990. Influence of Interfaces on Microbial Activity. Microbiological Reviews **54**: 75-87.

van Rees, K. C. J., K. R. Reddy, and P. S. C. Rao. 1996. Influence of benthic organisms on solute transport in lake sediments. Hydrobiologia **317**: 31-40.

Webb, J. E., and J. Theodor. 1968. Irrigation of submerged marine sands through wave action. Nature **220**: 682-683.

Webb, J. E., and J. L. Theodor. 1972. Wave-induced circulation in submerged sands. Journal of the Marine Biological Association of the United Kingdom **52**: 903-914.

Wenzhöfer, F., and R. N. Glud. 2004. Small-scale spatial and temporal variability in benthic O2 dynamics of coastal sediments: Effects of fauna activity. Limnol. Oceanogr. **49**: 1471-1481.

Wheatcroft, R. A. 1992. Temporal variation in bed configuration and one-dimensional bottom roughness at the mid shelf STRESS site. Cont. Shelf Res. **14**: 1167-1190.

Wild, C., M. Rasheed, U. Werner, U. Franke, R. Johnstone, and M. Huettel. 2004. Degradation and mineralization of coral mucus in reef environments. Mar. Ecol. Prog. Ser. **267**: 159-171.

Wolfbeis, O.S. 1991. Fiber optic chemical sensors and biosensors. CRC Press.

Ziebis, W., M. Huettel, and S. Forster. 1996. Impact of biogenic sediment topography on oxygen fluxes in permeable seabeds. Mar. Ecol. Prog. Ser. **140**: 227-237.

Overview of the enclosed chapters

The main part of this thesis comprises 4 manuscripts and one chapter, presented here all as chapters.

Chapter 2

Elimar Precht, Ulrich Franke, Lubos Polerecky and Markus Huettel

Oxygen dynamics in permeable sediments with wave-driven pore water exchange

This study was initiated by M. Huettel, E. Precht and U. Franke. E. Precht and U. Franke conducted the experiments. U. Franke was responsible for the oxygen measurements and evaluation of the oxygen data. U. Franke wrote the corresponding material and methods part of the manuscript and provided with the co-authors editorial help and input for the entire manuscript. The manuscript has been published in Limnology and Oceanography © American Society of Limnology and Oceanography Inc. 2004.

Chapter 3

Lubos Polerecky, Ulrich Franke, Ursula Werner, Björn Grunwald and Dirk de Beer

High spatial resolution measurements of oxygen consumption rates in permeable sediments

D. de Beer, U. Franke and L. Polerecky initiated this study. L. Polerecky, U. Franke and U. Werner conducted the experiments. L. Polerecky and U. Franke evaluated the data and wrote the manuscript with editorial help and input of U. Werner and D. de Beer. This manuscript has been accepted for publishing in Limnology and Oceanography: Methods © American Society of Limnology and Oceanography Inc. 2004.

Chapter 4

Ulrich Franke, Lubos Polerecky, Elimar Precht, and Markus Huettel

Wave tank study of particulate organic matter degradation in permeable sediments

U. Franke and M. Huettel initiated this study. U. Franke conducted the experiments, evaluated the data and wrote the manuscript with the editorial help and input of all co-authors. This manuscript has been submitted to Limnology and Oceanography.

Chapter 5

Ulrich Franke, Gerhard Holst and Lubos Polerecky

Characteristics of porphyrin-based planar optodes: consequences for applicability in aquatic systems

This study was initiated by U. Franke, L. Polerecky and G. Holst. U. Franke and L. Polerecky conducted the experiments. U. Franke evaluated the data and wrote the manuscript with editorial help and input of L. Polerecky. This manuscript is in preparation for submission to Limnology and Oceanography.

Chapter 6

Ulrich Franke, Tjeerd Bouma, Emmanuelle Geslin, Gerhard Holst, Henk Jonkers, Stephanie Köhler-Rink, Gloria Peralta, Ursula Werner and Lubos Polerecky

Applications of porphyrin-based planar oxygen optodes and the modular luminescence lifetime imaging (MOLLI) system in aquatic environments

This chapter gives an overview of experiments which have been carried out during the whole PhD period on diverse biological systems in aquatic environments. Studies were initiated and conducted by U. Franke and the co-authors. U. Franke evaluated the data and wrote the chapter with editorial help and input of the co-authors.

Oxygen dynamics in permeable sediments with wave-driven pore water exchange

Elimar Precht, Ulrich Franke, Lubos Polerecky, and Markus Huettel*

Max Planck Institute for Marine Microbiology, Celsiusstrasse 1, D-28359 Bremen, Germany

*Present address: Florida State University, Department of Oceanography, 0517 OSB, West Call Street, Tallahassee, Florida 32306-4320, USA

Abstract

The effects of advective pore water exchange driven by shallow water waves on the oxygen distribution in a permeable ($k = 3.3 \times 10^{-12}$ to 4.9×10^{-11} m^2) natural sediment were studied with a planar oxygen optode in a wave tank. Our experiments demonstrate that pore water flow driven by the interaction of sediment topography and oscillating boundary flow changes the spatial and temporal oxygen distribution in the upper sediment layer. Oxygenated water intruding in the ripple troughs and deep anoxic pore water drawn to the surface under the ripple crests create an undulating oxic–anoxic boundary within the upper sediment layer, mirroring the topographical features of the sediment bed. Anoxic upwelling zones under ripple crests can separate the oxic sediment areas of neighboring ripple troughs with steep horizontal oxygen concentration gradients. The optode showed that migrating wave ripples are trailed by their pore water flow field, alternately exposing sediment volumes to oxic and anoxic pore water, which can be a mechanism for remobilizing particulate oxidized metal precipitates and for promoting coupled nitrification–denitrification. More rapid ripple migration (experimental threshold ~ 20 cm h^{-1}) produces a continuous oxic surface layer that inhibits the release of reduced substances from the bed, which under slowly moving ripples is possible through the anoxic vertical upwelling zones. Swift, dramatic changes in oxygen concentration in the upper layers of permeable seabeds because of surface gravity waves require that sediment-dwelling organisms are tolerant to anoxia or highly mobile and enhance organic matter mineralization.

Introduction

The dominant boundary layer flows in shallow marine environments are those generated by surface gravity waves. This dominance is reflected by the presence of wave ripples structuring large areas of shallow sandy sea beds that are abundant in coastal, estuarine, and shelf environments. Most of these sandy sediments are permeable ($k > 10^{-12}$ m^2) and thus allow interstitial water motion. Pressure differences at the sediment–water interface might drive interfacial solute transport through the surface layers of these beds. This advective transport can exceed transport by molecular diffusion by several orders of magnitude (Huettel and Webster 2001). In contrast, the major transport mechanisms in fine-grained muddy sediments are molecular diffusion and local bioturbation (Berner 1980; Aller 1982). Increased fluid exchange between sediment and overlying water affects the oxygen dynamics in permeable sediments and therefore also affects biogeochemical processes. Booij et al. (1991) showed in benthic chamber experiments that oxygen-rich water can be advected vertically into sandy sediment, which increased the Oxygen penetration depth in the sediment as a function of the flow velocity of the overlying water. Advective oxygen distribution in permeable sand because of unidirectional boundary flow interacting with sediment topography was studied by Ziebis et al. (1996), who showed that oxygen is transported rapidly and effectively into deeper sediment layers and could thus enhance mineralization of organic matter (Forster et al. 1996). This organic matter could be transferred from the boundary layer into the top centimeters of the sediments as suspended particles or phytoplankton by advection (Huettel et al. 1996; Huettel and Rusch 2000). As a consequence of these processes, advective pore water flow can generate a complex biogeochemical zonation in the sediment with areas of enhanced nitrification or iron precipitation and vertical channels through which ammonium and reduced metals are transported to the sediment surface (Huettel et al. 1998).

Surface gravity waves produce oscillating flows at the sediment-water interface by the wave orbital water motion (e.g., *see* p. 54 in Denny 1988) in areas with a water depth shallower than half the wavelength of the waves. The ability of such oscillating boundary flows to drive pore water flow was shown by Webb and Theodor (1968, 1972) by injecting dyed water into coarse, sandy, nearshore sediment and observing its reappearance at the sediment surface. Wave-driven in situ pore water velocities were measured by Precht and Huettel (2004). Shum (1992) calculated the pore water motion under a rippled bed over one wave period with a two-dimensional computational model, showing that the zone of advection extends several ripple heights below the ripple surface over a wide range of

wave conditions and sediment characteristics. These transport studies suggest that waves, by enhancing advective fluid exchange between sediment and overlying water, also affect the biogeochemical processes in permeable beds in the same way as unidirectional flows. Oxygen distributions underneath a rippled surface exposed to progressing waves modeled by Shum (1993) revealed that, in permeable beds, oxygen concentration gradients in the horizontal might be the same order of magnitude as those in the vertical. In a wave tank study quantifying the wave-induced advective interfacial exchange, Precht and Huettel (2003) showed that horizontal tracer concentration gradients migrate with sediment topography (ripple) propagation. These authors suggested that this could be of significance for sediment oxygen dynamics because sediments might alternately be exposed to changing oxygen concentrations.

The planar oxygen optode technique employed in this study to assess the oxygen dynamics in the sediment was introduced by Glud et al. (1996) and has been used successfully to measure oxygen production, consumption, and dynamics in marine systems (e.g., microbial mats, Glud et al. 1998, 1999). Glud et al. (2001) also developed an in situ instrument for planar O_2 optode measurements at benthic interfaces.

The aim of this study was to elucidate the effects of advection driven by wave-generated oscillating boundary flow interacting with mobile sediment topography on the oxygen dynamics of natural sediment. To achieve this goal, experiments were carried out in natural sandy sediment in a laboratory wave tank with a planar oxygen optode.

Materials and methods

Sediment and sediment preparation

The sediment used in this study was collected in an intertidal flat at Sylt Island in the German North Sea (55°02'N, 08°26'E) in February 2001 at a temperature of 4°C. Sediment was sampled in two layers: the top 2 cm, then down to 20 cm depth. These sediments were transported separately and were combined again in the laboratory wave tank within 24 h of sampling. The wave tank was filled with ~1,750 liters of artificial seawater (Instant sea[TM]) with a salinity of 31 and kept at a constant temperature of 17°C. The sediment surface was leveled by the foraging activity of a small *Carcinus maenas* crab, which also eliminated the initially abundant *Hydrobia ulvae* mud snails.

The sediment then was left under a constant recirculating unidirectional flow of ~ 5 cm s^{-1} (at 10 cm above the bed) for 12 months to regain a quasi-natural balance. Infauna consisted mostly of oligochaetes of the Tubificidae family living in the upper 2 cm of the sediment. No nourishment was added to the wave tank during the first months after the setup to prevent accumulation of nutrients. Starting 8 weeks before and during the experiments, powdered dried red algae (ground to a particle size between 125 and 250 mm) equivalent to an input of 1 g m^{-2} was added biweekly by suspending the material and evenly distributing it in the wave tank.

Sediment analyses

At the sediment sampling site, sediment cores (2.6 cm diameter, 12 cm long) were taken for measurement of in situ permeability and porosity. Three representative sediment samples were additionally taken for grain size analyses. Before and after the experiments, sediment cores (2.6 cm diameter) were taken in the wave tank for analyses of permeability (~12 cm long), porosity (10 cm long), and grain size distribution (10 cm). Additionally, grain sizes and permeability of the upper 2.5 cm of the sediment were assessed.

For porosity and pore water analysis, the sediment subcores taken in-situ and from the laboratory wave tank were sectioned into 1-cm-thick horizontal slices. Porosity averaged over depth, as calculated from wet and dry (after drying until constant weight at 60° C) weights of the sediment slices, was 37.1 % (SD = 2.0, n = 10) in situ, 34.0 % (SD = 2.3, n = 20) before the experiments, and 36.2 % (SD = 3.8, n = 30) before the experiments, and 36.2 % (SD = 3.8, n = 30) after the experiments. The sediment subcores used to assess the permeability were sealed after sampling and stored at 48C until the measurements were carried out within a few days. Permeability was assessed by the constant head method (Klute and Dirksen 1986) directly on the retrieved sediment cores. Values for density and dynamic viscosity were calculated after Krögel (1997). In situ sediment permeability was 7.6×10^{-12} m^2 (SD = 1.4×10^{-12} m^2; n = 4) and wave tank permeability 3.3×10^{-12} m^2 (SD = 0.8×10^{-12} m^2; n = 2), with higher permeability of the surface sediment (upper 2.5 cm) of 4.9×10^{-11} m^2 (SD = 0.04×10^{-11} m^2; n = 3). In situ grain size distribution was determined by desalination, drying, and sieving with a set of eight calibrated sieves. The median grain size of the sediment was 180 µm.

Wave tank setup

The laboratory wave tank used in this study was made of clear acrylic and had an open channel length of 520 cm with a rectangular cross section (50 cm high, 47 cm wide). Two

acrylic boxes were put into the open channel section (upstream box: 240 cm long, downstream box: 120 cm long, both 19 cm high and spanning the entire width of the channel) such that the gap between the two boxes had a width of 120 cm and could be filled with sediment (Fig. 1). Filled with a sediment layer of 22 cm depth, this setup amounted to a sediment volume of 124 dm^3. The two boxes in the open channel section were covered with 3 cm of sediment to create an overall even surface with uniform roughness throughout the open channel section. Initially, the sediment surface was level, and all subsequent ripple formation was the response of the bed to the applied wave action. Waves were generated at the upstream end of the wave tank with a paddle driven by an electric motor, controlling wave amplitude by the stroke of the eccentric and wave frequency via motor speed. This setup permitted reproducible generation of sinusoidal waves of selected amplitude and frequency. At the downstream end of the wave tank, the dissipation of the waves was achieved by an artificial beach made of an acrylic plate 1 m long covered by a 10 cm thick mat of highly permeable plastic foam, causing the waves to run up and break.
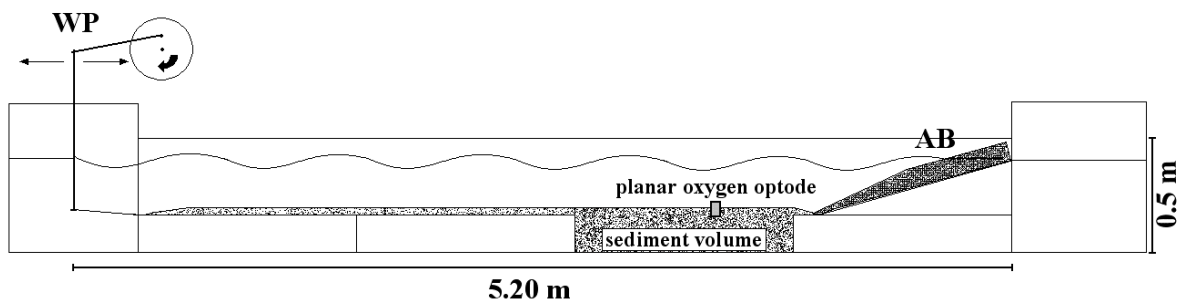

Figure 1: Wave tank setup; WP = wave paddle, AB = artificial beach.

Hydrodynamics

The hydrodynamic conditions in the wave tank were measured with a three-beam DANTEC ™ LDA (laser doppler anemometer) system in the backscatter mode. This LDA technique allows three- dimensional measurements of the flow velocity in a spheroidal measuring volume 600 µm long and 70 µm in diameter. During the experiments, vertical velocity profiles (120–0.5 mm above the sediment) of the horizontal and vertical velocities were measured above unrippled sections of the experimental sediment surface. In the water layer closer than 6 mm to the sediment–water interface, the LDA setup only allowed the measurement of the horizontal velocity component. During the experiments in which

ripples formed, the root mean square values of the horizontal velocity (U_{RMS}) 12 cm above the sediment surface ranged from 0.12 to 0.14 m s^{-1}. In the experiments with flow not sufficient to initiate sediment mobilization, U_{RMS} was ~ 0.06 m s^{-1}.

Oxygen measurements

The two-dimensional oxygen distribution was measured with a planar semitransparent oxygen optode (3.7 cm wide, 5.7 cm high) glued to the inside wall of the wave tank such that 2.7 cm of the optode was above and 3 cm was below the level sediment–water interface. The optical oxygen measurement is based on the dynamic or collisional quenching of the luminescence of an indicator by oxygen (Kautsky 1939). Commonly used oxygen indicators are platinum-porphyrins embedded in a polystyrene matrix (Papkovsky et al. 1992; Liebsch et al. 2000).

The planar sensing foils comprised two layers: a transparent polyester support foil (125 mm thick, Goodfellow) and the sensing layer, which was spread by knife. The luminescent oxygen indicator (59 mg) platinum(II) mesotetra (pentafluorophenyl) porphyrin (Pt-PFP, Porphyrin Products) was dissolved in 14.7 g chloroform (Merck, Darmstadt) and 1.63 g polystyrene (Sigma-Aldrich). To increase the amount of excitation light within the sensing layer, 1.63 g titanium dioxide particles (TiO_2 , 5 mm, Aldrich) were added. These particles do not interfere with the quenching but enhance the signal by scattering. Therefore, they increase the output luminescence signal at the expense of loosing a clear view of the structure behind the sensor (Klimant and Wolfbeis 1995). The concentration of the fluorophore in the cured sensing layer was 1.8 % (w/w). The thickness of the semitransparent sensing layer was approximately 30 µm, resulting in an overall thickness of the planar optode of 155 µm.

The O_2 distribution measurements were conducted by the specially developed modular luminescence lifetime imaging system, MOLLI, as described by Holst et al. (1998) and Holst and Grunwald (2001). The planar optode was illuminated by blue (λ_{max} = 475 nm) excitation light of diodes (LEDs, HLMP-CB 15, Agilent), and the luminescence (λ_{max} = 647 nm) emitted by the optode was filtered with a red optical filter (80 % transmission at ≥620 nm; Deep Golden Amber, LEE-Filters) to remove most of the reflected excitation light. The luminescence images of the planar optode were recorded by a charge-coupled device (CCD) camera (SensiCam, PCO) with a resolution of 640 × 480 pixels. The images covered an area of 25.6 × 19.2 mm. Taking the thickness of the sensing layer (30 µm) and the spatial resolution of the imaging system into account, the spatial

resolution of the oxygen images was 40×40 mm pixel^{-1}. In order to determine the distribution of oxygen concentrations, the two-dimensional luminescence lifetime distributions were evaluated by the rapid lifetime determination (RLD) method (Woods et al. 1984; Ballew and Demas 1989; Liebsch et al. 2000). Further image processing was carried out with a custom-made computer program (Holst and Grunwald 2001). The planar optode was calibrated before and after the experiments by recording images corresponding to 0 % and 100 % air saturation. The measured luminescence lifetime distributions were converted into oxygen concentration values by a modified two-component model of the Stern–Volmer equation (Klimant et al. 1995; Holst and Grunwald 2001).

The accuracy of the oxygen measurements of the optode, as determined with 11 high-frequency measurements, was ± 7 % of air saturation at 70–90 % air saturation and ± 2.5 % at 0–10 % air saturation. The lower accuracy at higher oxygen concentrations occurs because higher oxygen content leads to a weaker luminescence signal. The stability of the optode was checked by calibrations before and after the experiments, and the calibration function of the sensor foil did not change significantly during 1.5 yr of experiments. The rate at which the optode could accurately follow changes is ~1 Hz, which is significantly lower than the measuring intervals employed (minutes).

Sediment topography

The sediment relief in front of the planar optode had to be assessed simultaneously with the oxygen measurements. This was achieved by a CCD camera positioned on the side of the wave tank opposite the planar optode. The camera's field of vision covered the area of the planar optode and was fixed slightly elevated relative to the optode in a 10° downward angle so that the sediment topography directly in front of the optode did not obstruct vision (Fig. 2). The camera was triggered simultaneously with the diodes that emitted the excitation light for the oxygen measurements. Thus, the obtained images showed the planar optode with the background light of the diodes and was partly darkened by the respective sediment relief. The sediment relief was assessed from these images with an edge-detecting algorithm that used the transition between dark and light regions of the image corresponding to the sediment surface relief. With three fluorescently marked reference points, the horizontally mirrored image of the sediment surface relief and oxygen distribution images could be aligned precisely. The sediment relief line was superimposed on the oxygen distribution images in a batch conversion routine. Time sequences of the resulting composite images were combined to produce animations of the oxygen dynamics in the sediment, simultaneously showing the changes of the sediment relief.
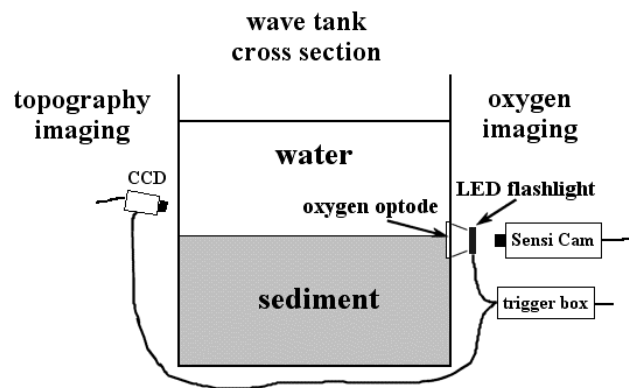
Figure 2: Side view of the setup for the simultaneous oxygen and surface topography imaging in the wave tank.

Experiments

To assess pore water velocities and pore water flow patterns under typical wave conditions, an experiment was carried out with waves equivalent to those in experiments 2, 5, 6, and 7 (Table 1). Prior to an experiment, the sediment surface was leveled. After the waves were switched on, ripples formed (wavelength = 2.5 cm, amplitude = 0.5 cm), and Rhodamine WT solution was injected into the sediment at various locations adjacent to the transparent wave tank wall next to the planar optode-ripple troughs and crests included. The development of the dye clouds in the sediment was recorded in high-resolution photographs taken at distinct time intervals (15 or 60 s). From the dye migration, the pore water velocities could be assessed. Seven successful wave tank oxygen dynamics experiments were conducted between April and June 2002. All experiments were carried out with surface gravity waves of variable lengths and heights. The bed was smoothed before the experimental runs, and no artificial roughness elements were placed on the sediment surface. Exceptions were experiments 3 and 4, which were carried out with the remaining sediment topography of the previous experiment 2 to test the case of identical sediment topography and decreased flow velocities. During all experiments, oxygen images measured by the planar optode, together with the sediment relief images, were recorded. The experimental parameters relevant to the different experimental settings are listed in Table 1.

Table 1: Experimental parameters.

Experiment	Exp 1	Exp 2	Exp 3	Exp 4	Exp 5	Exp 6	Exp 7
date	16 May 02	16 May 02	27 May 02	30 May 02	05 Jun 02	26 Jun 02	08 Jul 02
duration (h)	4.5	15	1.5	3.5	26	5	36
waves							
wave height (cm)	8	8	7	3	8	8	8
wave length (cm)	80	70	80	120	70	70	70
period (s)	0.75	0.75	0.8	1	0.75	0.75	0.75
flume							
water depth (cm)	20	17	17	17	17	16.5	17
sediment depth (cm)	20	20	20	20	20	20	20
measurements							
LDA (Laser Doppler Anemometer)	No	Yes	No	Yes	No	No	Yes
ripples							
sediment surface	level and smooth	level and smooth	existing topography	existing topography	level and smooth	existing topography	level and smooth
first ripples (min)	15	15	0	0	15	0	15

Results

Ripples

Orbital wave ripples formed in all experiments with smooth sediment surfaces in a matter of minutes (Table 1). However, the ripple evolution did not occur in a regular manner and uniformly in all experiments. Usually, ripples evolved in patches and spread over the rest of the sediment surface. Therefore, it could take some time until ripples formed in front of the planar optode. Ripple migration did not occur continuously and was characterised by variable velocities. Moreover, it could be observed that in the first experiment, ripple evolution was generally slower, which can most likely be attributed to EPS (extracellular polymeric substances) excreted by active organisms on the sediment surface. This effect was however not investigated further in the experiments.

Pore water velocity

A symmetrical advective flow pattern develops when the oscillating boundary flows interact with the wave ripples. Water enters the sediment at the ripple troughs and leaves it at the ripple crests. Figure 3 shows the directions of pore water movement with the corresponding velocities assessed from the measurements of the injected dye clouds. Pore water velocities are higher closer to the sediment and lie in the range of centimeters to decimeters per hour.
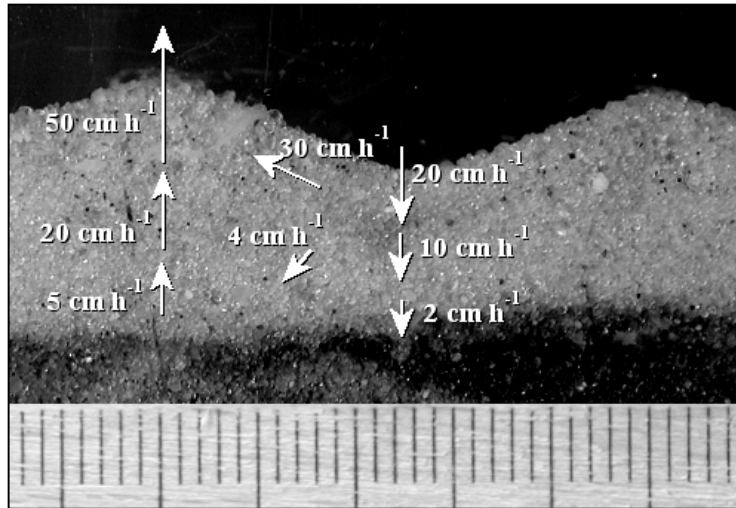
Figure 3: Summary of pore water velocity measurements conducted with soluble tracer. The arrows indicate the observed pore water directions and are not to scale. The mm scale of the image is shown at the bottom.

Oxygen measurements

The average oxygen penetration depth into the sediment under stagnant conditions without waves was ~3 mm. This oxygen distribution, governed predominantly by molecular diffusion, was only locally altered by oligochaete bioirrigation (Fig. 4a).

After the waves were switched on, but prior to the formation of sediment ripples in front of the planar optode, the oxygen penetration depth slowly increased to 5 mm within ~ 80 min (Fig. 4b). This effect can be attributed to advection associated with small-scale surface roughness or wave pumping (Riedl et al. 1972).

Figure 4a, b shows non saturation oxygen values in the water column. This is an effect that occurs when large anoxic areas are imaged by the oxygen optode. Because of reflections of the luminescent light within the acrylic wave tank wall, anoxic regions of the studied area affect the measurements in neighboring oxic regions. Although a reverse influence also takes place, the former is more pronounced because of the stronger luminescence intensity generated within anoxic regions. This effect lowers the spatial resolution of the oxygen images, but on a lower spatial scale than required to observe the principles of the processes studied here.

After ripples formed in front of the planar optode, the changes in the oxygen distribution in the sediment as a result of the ensuing advective pore water flows could be recorded with the optode. Upwelling of anoxic pore water from lower sediment layers led to an oxygen-depleted zone underneath the ripple crests. In the ripple troughs, oxygen-rich water from the water column was forced into the sediment, generating oxygenated zones in

the sediment that reached a maximum depth of 1 cm (wave amplitude = 8 cm, wavelength = 80 cm; ripple amplitude = 0.4 cm, ripple wavelength = 2.9 cm). Thus, the pore water flows produced an oxygen distribution pattern reflecting the structure of the ripple topography, with alternating oxic and anoxic zones associated with ripple troughs and crests, respectively (Fig. 4c). This oxygen distribution led to steep horizontal oxygen concentration gradients underneath the ripple crests (Fig. 5).
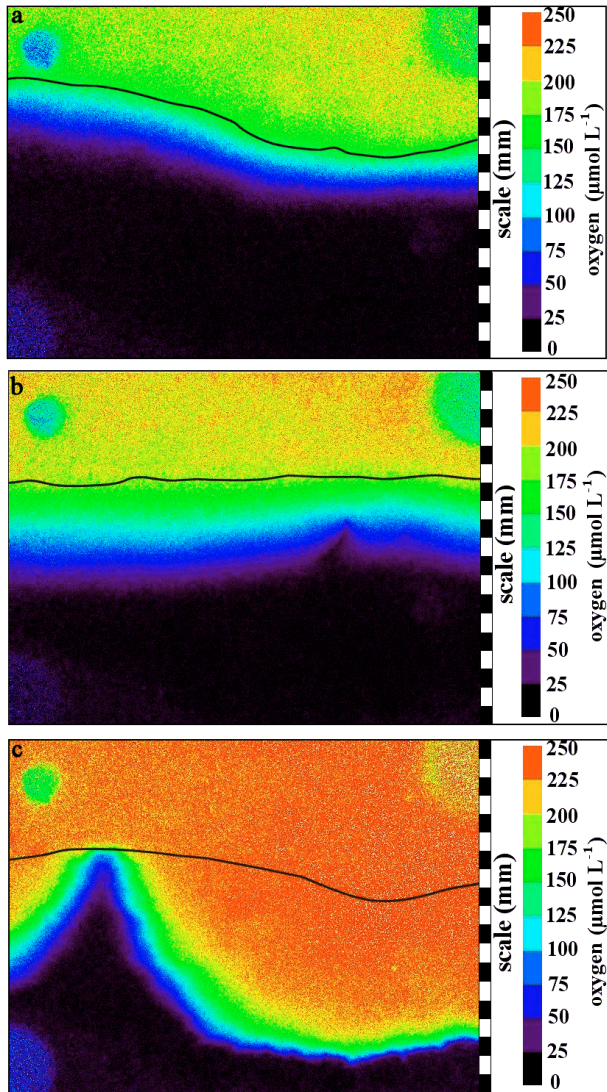

Figure 4: a) Oxygen image under stagnant conditions without waves (Exp. 3). The black line indicates the sediment surface relief; b) Oxygen image demonstrating an increased oxygen penetration depth under oscillating flow in the absence of sediment topography (Exp. 6). The black line indicates the sediment surface relief; c) Image of oxygen distribution linked to a stationary sediment ripple under oscillating flow (Exp. 1). The black line indicates the sediment surface relief, each black and white bar of the scale corresponds to one mm.
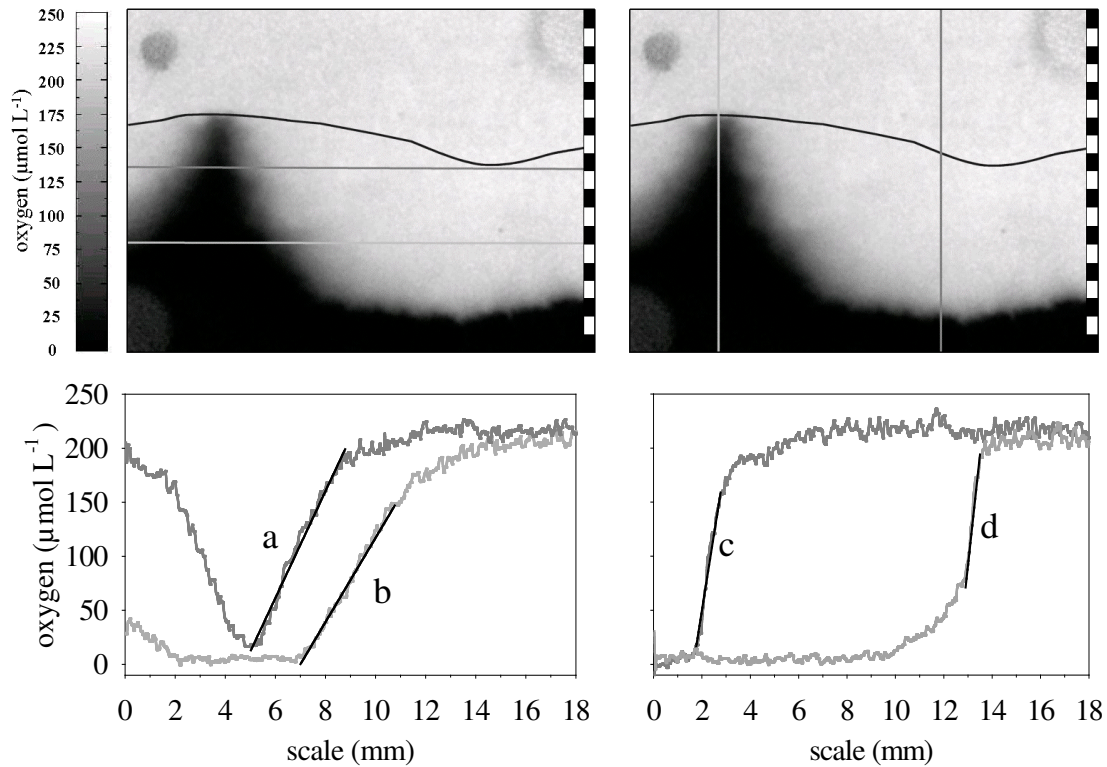
Figure 5: Horizontal (left) and vertical (right) oxygen concentration profiles extracted from an optode image underneath a stationary ripple under oscillating flow (Experiment 1). The black lines indicate the sediment surface relief; the grey lines show the extracted profiles. The depicted gradients of the oxygen concentration profiles correspond to a = 49 µmol L^{-1} mm^{-1}; b = 39 µmol L^{-1} mm^{-1}; c = 150 µmol L^{-1} mm^{-1}; d = 190 µmol L^{-1} mm^{-1}.

In the experiments with existing sediment ripples at the optode and flow that was not strong enough to initiate further sediment movement, it could be observed that the final oxygen distributions in the sediment were similar regardless of the hydrodynamic forcing. With decreasing wave energy, the time needed to reach the final equilibrium was increased (from 46 min in experiment 3 to 216 min in experiment 4), showing that the pore water flow pattern is dependent on the sediment topography, whereas the pore water velocity is dependent on the magnitude of the hydrodynamic forcing. With even lower bottom flows, higher oxygen consumption, or both in the sediment, one can expect the equilibrium oxic-anoxic boundary to be shifted upward in the sediment because the reduced input of oxygen-rich water into the sediment cannot cover the demand of oxygen-consuming processes in the sediment.

In the case of sediment ripples migrating in front of the planar optode, the pore water flow field and the associated oxygen distribution migrated with the ripples, alternately exposing sediment to oxic and anoxic conditions. This is shown in Fig. 6a (upper panel) presenting a series of oxygen distribution patterns under slowly migrating ripples.

The effect of exposing sediment alternately to variable oxygen concentrations is depicted in Fig. 6b, showing oxygen profiles extracted from the same vertical row of pixels of the two-dimensional oxygen images as a function of time. This figure demonstrates how an initial equilibrium phase (75 min) was succeeded by a phase with ripple migration, causing pronounced oxygen changes in the sediment. The redox conditions at one single vertical profile in this case changed six times from anoxic to oxic within 90 min.
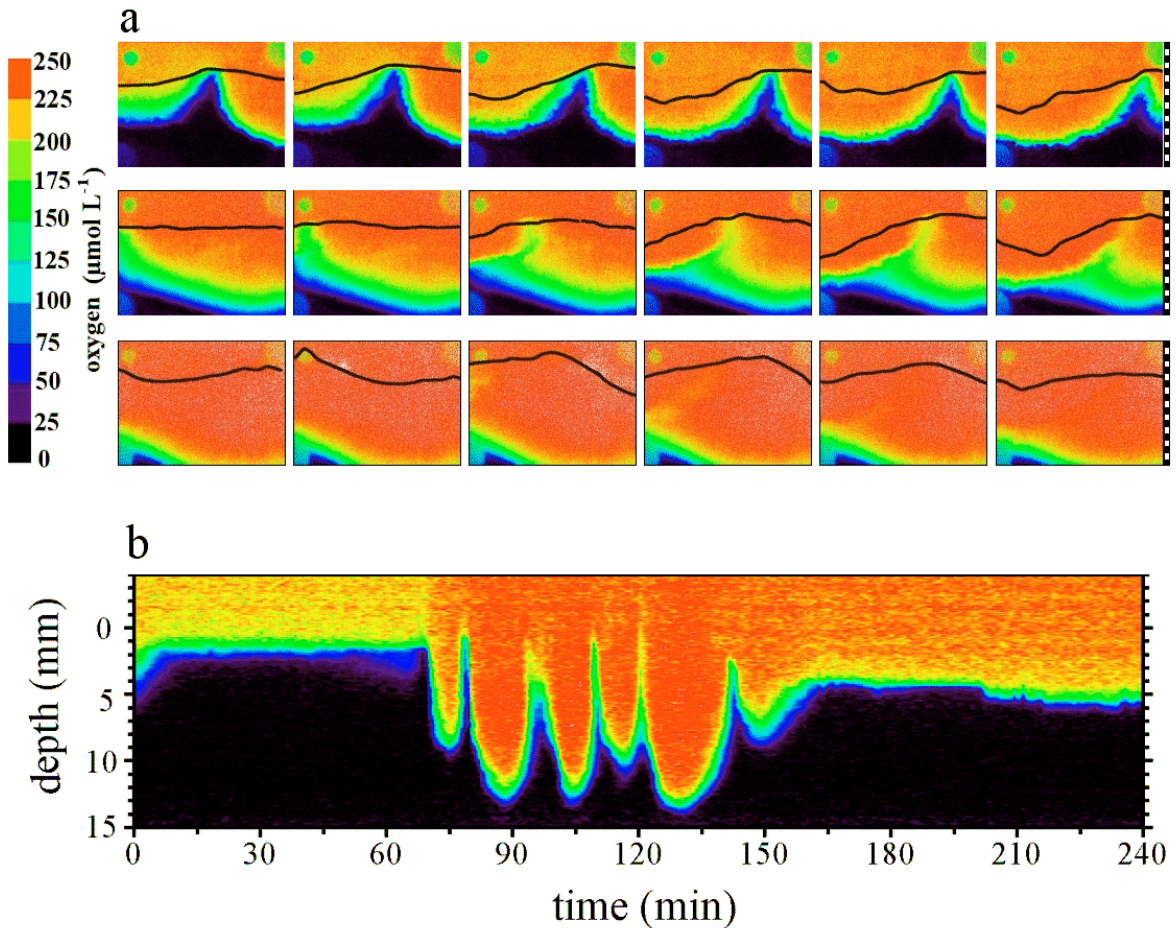

Figure 6: a) Time-series of images of oxygen distributions: Upper panel: under a slowly migrating ripple with a fully developed mobile upwelling zone (image interval: 1 min; experiment 6). Middle panel: under a migrating ripple with an upwelling zone lagging behind the ripple crest (image interval: 2 min; experiment 2). Lower panel: under a fast migrating ripple with no anoxic upwelling zone linked to ripple crests (image interval: 2 min; experiment 2). b) An example of a time-series oxygen profile extracted from one selected vertical row of pixels of the planar optode images, revealing a temporal exposure of the sediment to redox oscillations (experiment 6).

When ripples migrated faster, at rates of 10 to 20 cm h^{-1}, the oxygen-depleted zones started to lag behind the ripple crests and showed incompletely anoxic conditions (Fig. 6a, middle panel). When the ripple migration velocity in our experiments exceeded ~ 20 cm h^{-1}, the anoxic or oxygen-depleted zone underneath the ripple crest became

completely detached from the ripple topography, leading to a thick, uninterrupted oxygenated sediment surface layer (Fig. 6a, lower panel). This is in accordance with Elliott and Brooks (1997*a,b*), who found that release and trapping of pore water exchanges more water between the sediment and overlying water than advective pore water flow when the ripple migration velocity exceeds the pore water flow velocity.

The dynamics of the oxygen distribution become clearer in the animations that can be found in Web Appendix 1 (http://www.aslo.org/lo/toc/vol_49/issue_3/0693a1.html) or in the folder "Chapter-2-Movies" on a CD-Rom which can be made available upon request (contact: Ulrich Franke, Ostarastr. 5, 51107 Köln, e-mail: u.franke@fab-anlagenbau.com). The oxygen distribution in the sediment beneath a stationary ripple after the waves were switched on (corresponding to Fig.4a,c), as well as the oxygen dynamics in the sediment with slowly and fast-migrating ripples (corresponding to Fig. 6), are shown.

After the waves were switched off, the effects of the sediment's oxygen consumption could be observed with the optode. The oxic-anoxic boundary slowly moved upward until oxygen distributions reached the pre-experimental state with a homogeneous diffusive oxygen penetration depth of about 3 mm.

The oxygen consumption rates (OCRs) were calculated by fitting the changes in O_2 concentration over time (Fig. 7). In a pixel close to the sediment surface (circle), the O_2 concentration changed linearly with time, indicating that the effect of diffusion was negligible. The corresponding OCR, equivalent to the negative value of the slope of the O_2 decrease, was 0.32 ± 0.01 μmol L^{-1} min^{-1}.

The situation is different in a pixel close to the oxic-anoxic boundary (square). The decrease of O_2 with time is initially faster (~ 1.53 ± 0.07 μmol L^{-1} min^{-1} during the interval between 0 and 50 min) and gradually slows down (~ 0.28 ± 0.03 μmol L^{-1} min^{-1} during the interval between 150 and 200 min) because of the combined effects of oxygen consumption by the sediment and molecular diffusion that causes depletion of O_2. The influence of diffusion was determined by examining the images of O_2 distribution at the time intervals 0 - 50 min and 150 - 200 min. It was found that the rate of the observed O_2 depletion was enhanced by molecular diffusion during the first time interval, whereas it was slowed down by diffusion during the second time interval. Subtracting the contribution of molecular diffusion from the observed O_2 depletion rate, we found that the true OCR here was about 0.67 ± 0.07 μmol L^{-1} min^{-1}.

Because these two pixels are representatives of two extremes, we can conclude that the O_2 consumption rate varied across the oxic part of the sediment between 0.32 ± 0.01 and

0.67 ± 0.07 µmol L^{-1} min^{-1}. It should be noted that these values are expressed in terms of the volume of the pore water. If one wants to obtain the values expressed per volume of sediment, one would have to multiply them by porosity, which in our case was ~ 36 %.
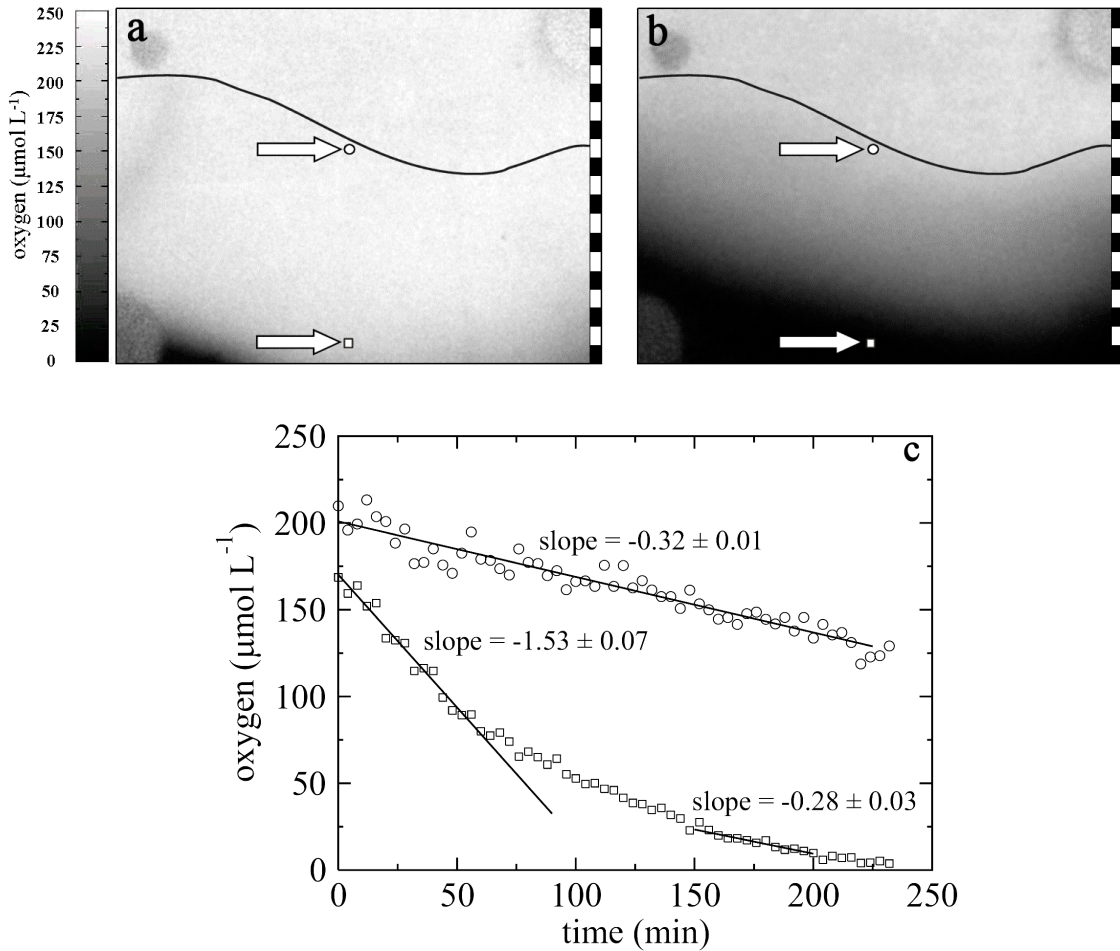

Figure 7: Assessment of the oxygen consumption rates in the sediment; a) Optode image of oxygen distribution directly after Experiment 1. b) Optode image of oxygen distribution 80 min after the experiment; the square and the circle (not to scale) indicate the areas of 3 × 3 pixels (~ 100 × 100 µm) over which the oxygen consumption rates were calculated. c) Fitting the changes of the O$_2$ concentration over time; circles: O$_2$ concentration close to the sediment corresponding to an OCR of 0.32 ± 0.01 µmol L^{-1} min^{-1}; squares: O$_2$ concentration deeper in the sediment, close to the initial oxic-anoxic boundary.

Discussion

We showed in a previous study (Precht and Huettel 2003) that the interaction of wave-generated oscillating boundary flows and ripple topography produced zones of up- and downwelling pore water in permeable sands that propagated with ripple migration. These finding suggested that waves can produce a complex and dynamic oxygen distribution in sandy sea beds that would strongly influence benthic organisms and sediment biogeochemistry.

Here, we demonstrated that wave-driven advective pore water flow associated with sediment wave ripples creates a pattern of sediment zones where oxygen-rich water is forced into the bed alternating with zones where anoxic pore water is drawn to the surface. The spatial and temporal distribution of these zones is closely related to the ripple topography and its changes. Because the oxygen distribution under such a rippled surface changes mainly in two dimensions, the planar oxygen optode technique proved to be a powerful tool to investigate the two-dimensional distribution and dynamics of oxygen distribution at the spatial and temporal scales of the pore water flow field.

Sediment permeability, magnitude of boundary currents, and ripple height and spacing control the advective pore water velocities, flow directions, and penetration depths (Huettel and Webster 2001). The advective penetration of a reactant like oxygen additionally depends on the consumption rates in the flushed sediment layers. Thus, the oxygen distribution pattern we observed is a complex result of oxygen injection into specific areas, with ensuing directed oxygen transport along streamlines, and sedimentary oxygen consumption characterized by a vertical gradient, with higher rates in the deeper layers. The waves transformed the smooth sediment with a thin, continuous, oxygenated surface layer into a rippled bed with a thick oxygenated layer interrupted by oxygen-depleted zones of upwelling deep pore water. Consequently, steep horizontal oxygen concentration gradients developed in the sediment, as had been predicted by Shum (1993).

The advective oxygen transport in our sediments from the wave–topography interaction was more than one order of magnitude faster than transport by diffusion (with our settings, 0.13 cm in 1 h), explaining the relatively deep oxygen penetration into a sediment with oxygen consumption rates of 0.33 - 0.67 μmol L^{-1} min^{-1}. In permeable sediments with a homogeneous permeability, the vertical extension of the pore water flow field equals approximately the ripple wavelengths (Rutherford et al. 1995). The maximum oxygen penetration depth we could observe in the ripple troughs was 14 mm, which corresponds to

18 mm below the flat sediment surface. With ripple wavelengths between 25 and 30 mm, the oxygen penetration depth we observed was only slightly lower than the sediment depth theoretically affected by advection, demonstrating the dominance of oxygen injection over oxygen consumption, although our sediment had consumption rates common in shelf sediments. Because of this dominance, pore water flushing caused by the interaction of oscillating boundary flows and ripple topography increased the oxic sediment volume more than threefold in our experiments compared with the situation of a stagnant water column and diffusive transport alone.

Biogeochemical zonation

In our previous wave tank experiments (Precht and Huettel 2003), sharp boundaries of the dye patterns developed, which revealed that the pore water drawn to the surface under the ripple crest mixes very little with pore water of adjacent sediment zones. The fluid basically flows to the surface along streamlines that do not cross, except for the mixing caused by dispersion in the porous medium. Because the pore water ascends from different biogeochemical reaction zones, a pattern develops with up welling flows that differ in their solute inventories. These pore water flows focus and narrow as they approach the ripple crest where fluid of different composition (and residence time in the sediment) emerges through narrow bands paralleling the crests (Fig. 8).
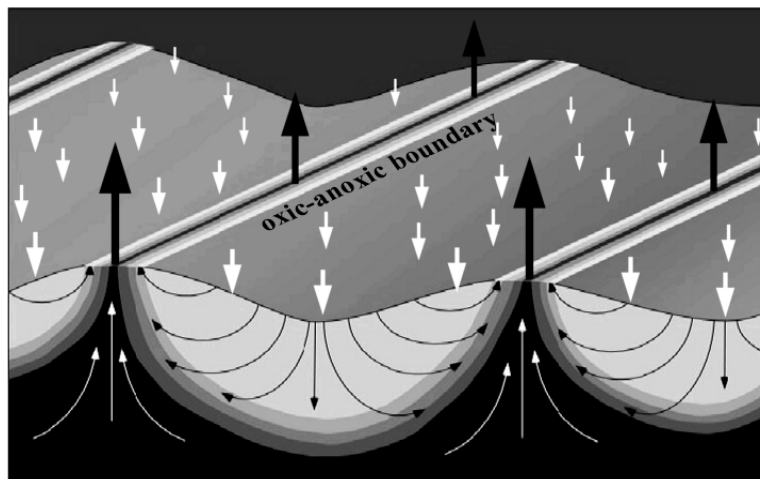

Figure 8: Schematic drawing of the biogeochemical reaction zones underneath stationary ripples created by wave-induced advective pore water flow. In the centre of the release areas, pore water from the deepest reaction zones emerges while at the outer edges of these areas, pore water leaves the sediment that resided shorter in the sediment and therefore has different solute content. Black arrows indicate flow out of the sediment, white arrows flow into the sediment.

With increasing distance from the center zone, these ''emergence bands'' release pore water from lesser and lesser depths and with shorter residence times in the sediment. As revealed by the oxygen concentration pattern under the stationary ripple (Fig. 4c), this produces bands of distinctly different geochemical characteristics at the sediment surface, which can be reflected, for example, by bands of different iron precipitates (Huettel et al. 1998). Microorganisms like sulfide oxidizers, denitrifiers, or iron oxidizers can profit from such patterns and the steep concentration gradients they produce (Fig. 5). Although the central upwelling zone might carry refractory dissolved organic matter (DOM), Fe^{2+}, and NH_4^+ to the surface, ''outer'' zones might release more labile DOM and NO_3^- resulting from enhanced organic matter decomposition and nitrification in the ripple slopes.

The situation in the ripple troughs is different. No solutes can be released from this area because molecular diffusion cannot counteract the water flow into the sediment. This implies that flux out of rippled permeable sediments averaged over larger areas only occurs through a fraction of the actual sediment surface area that is confined to the ripple crests.

In our experiments, the total width of the upwelling zone at the ripple crest was between 6 and 8 mm, while the sediment band separating these zones was ~ 20 – 24 mm wide. This resulted in an uptake : release area ratio of about 3, whereas the volume flow through both areas is the same for reasons of mass balance (which explains why the upwelling pore water flow reaches higher velocities than the downwelling flows; Fig. 3). Because the width of the upwelling zone linked to each ripple should be proportional to the ripple wavelength, we conservatively estimate that, also in natural environments, the flux from a permeable sediment into the water column occurs only in < 30% of the actual sediment surface areas in seabeds where advective exchange is effective. This demonstrates a major difference between sandy and cohesive sediment beds: in permeable seabeds, the fluxes are tightly linked to surface topography, and the fluxes out of the sediment occur in confined areas that are much smaller than the areas with fluxes into the sediment. In cohesive sediments, the mainly diffusive fluxes occur over the whole sediment surface in both directions, in and out of the sediment, with local hotspots, where directed bioturbative transport prevails.

The advective pore water motion and the linked oxygen distribution also affect the microbiological system, which in turn affects the biochemical zonation. Prior to the experiments, he sediment in our study was kept under constant recirculating flow for 12 months; thus, the microbiological community had time to adjust to the new conditions. During the experiments, the oxic–anoxic boundary shifted, which implies that either the

newly oxygenated zones became rapidly colonised by aerobes or that aerobic microorganisms were already present and became active. Because they are not the focus of this study, we have no information on these mechanisms. In later experiments, however, we can expect a microbial community that is tolerant against oxic and anoxic conditions and therefore adapted to the rapid changes in oxygen in the upper sediment layers.

Natural environments

The effect of wave action and bottom currents on interfacial pore water exchange was studied on an intertidal North Sea sandflat by Rutgers van der Loeff (1981). An increased apparent diffusivity in the upper 1.5 cm of the sandy sediments was measured. Measurements of pore water oxygen profiles in the North Sea by Lohse et al. (1996) revealed that the effective oxygen diffusion coefficients in the surface layers of sandy sediments could be >100 times higher than the molecular diffusion coefficients, which was attributed to turbulent diffusion driven by nearbottom currents. Moreover, Webb and Theodor (1968) and Precht and Huettel (2004) observed that wave-driven advective pore water flow is a natural process occurring in nearshore environments. Because the processes studied here are caused by the interaction of boundary flows and topography, it could be argued that in spite of small wavelength and shallow water depth, the laboratory results are applicable to natural permeable sediments affected by waves.

Sandy sediments are abundant in the global continental shelf environment (Emery 1968; de Haas et al. 2002), and sands like our experimental sediment with a median grain size of 180 mm are common on the shelf; for example, Cacchione et al. (1999) and Ogston and Sternberg (1999) describe shelf sands with a grain size of 125 - 250 μm and ripples of 9 cm wavelength at 60 m water depth.

Previous studies have shown that wave-induced boundary flows might reach the sediment surface in large areas of the global continental shelf down to > 100 m (Wiberg and Harris 1994; Harris and Wiberg 2001). The extent of the shelf areas affected by waves was numerically assessed by Harris and Coleman (1998): for example, in large areas of the southern North Sea, wave-induced flow exceeds the mobilisation threshold for quartz sands of 100 μm diameter 10-50 % of the time.

However, the wave ripples that formed during our experiments were of the orbital type (Wiberg and Harris 1994), with wavelengths between 2.5 and 3 cm. Under natural conditions, mainly anorbital ripples with comparable heights but longer wavelengths (~ 9 cm for a sediment of our grain size) are formed. This suggests that, in nature, wave-driven pore water advection affects greater sediment depths than in our experiments, given

that the permeability of the sediment is sufficiently high. As the pore water flow velocities decrease with depth, the oxic water entering the sediment in the ripple troughs will be deoxygenated by oxygen consumption because of the longer residence time in the sediment. Therefore, it is unlikely that the sediment depth affected by advective transport equals the actual sediment depth that is exposed to oxygen through advective flushing. Nevertheless, larger ripple spacing means that the sediment depth from which material can be released is increased. Thus, a storm event that produces or enhances bed ripples might affect sediment water exchange and penetration depth of advective pore flows much longer than its actual duration because of the persistence of the topography. After a storm, this ''memory effect'' might increase sedimentary biological and biogeochemical activity by the higher particle filtration and oxygen penetration associated with the ''new'' topography.

Effect of sediment topography

This study revealed four scenarios of advective interfacial exchange caused by waves dependent on the existence and mobility of sediment topography (Fig. 9).

(1) Sediment without significant topography: This scenario involves the development of a continuous oxidized sediment surface layer with a slightly increased oxygen penetration depth from small-scale advection, shear-driven Brinkman flow (Basu and Khalili 1999), and possibly wave pumping (Riedl et al. 1972). Additional solute release is caused by molecular diffusion and bioirrigation. The sediment is redox sealed, meaning that reduced substances that precipitate or are adsorbed under oxic conditions (e.g., Fe^{2+}) cannot penetrate from deeper, anoxic sediment layers to the surface because they are trapped in the oxidized surface layer.

(2) Sediment surface with stationary ripples: This scenario has vertically alternating oxic and anoxic surface layers, with the oxygen penetration depth locally increased by nearly one order of magnitude. The flushed sediment volume compared to stagnant conditions increases more than threefold. Upwelling of pore water from deeper sediment layers creates anoxic channels to the surface, through which reduced substances can be released to the water column. A horizontal geochemical zonation develops at the ripple crests with the deepest, and likely strongest, reduced pore water emerging in the center of the ripple crest. With increasing distance from this central upwelling, the pore water released from the ripple originates from less and less deeper zones, thus containing lesser amounts of reduced substances. The vertical anoxic upwelling zones under the ripple crests

might confine oxygen-dependent meiofauna to the sediment volume underneath the ripple troughs.

(3) Sediment surface with ripples moving slower than pore water: The flushed sediment volume relative to stagnant conditions increases more than threefold and is comparable with scenario 2. Mobile pore water upwelling zones, alternately exposing sediment volumes to oxic and anoxic conditions, enhance organic matter degradation in the upper sediment layer through associated redox oscillations (Aller 1994).

Anoxic upwellings passing through oxic zones could remobilize precipitated oxidized iron or manganese compounds and leach reduced Mn or Fe from the sediment. The cycling of Fe and Mn is believed to be closely linked to bioturbation because it constitutes the mechanism that transports oxidized precipitates into deeper, anoxic sediment layers, where they are remobilized (Aller 1990; Canfield et al. 1993). The mechanism we describe here opens a secondary pathway for the remobilization and cycling of oxidized metal precipitates.

Mobile vertical anoxic zones might cause migration of oxygen-dependent infauna and select for a bacterial community that is tolerant to oxygen and anoxic conditions. Sulfide oxidizers that depend on oxygen or that can store nitrate, like *Beggiatoa* (Jørgensen and Des Marais 1990) or *Thioploca* (Fossing et al. 1995; Huettel et al. 1996), might profit from alternating pore water down- and upwelling. Likewise, nitrifiers and denitrifiers could profit from this alternating exposure.

(4) Sediment with ripples moving faster than pore water: In this case, the upwelling of pore water is too slow to follow the ripple migration. A continuous oxic layer can develop that creates a redox-sealed sediment with an undulating oxic–anoxic interface. The sediment volume flushed by oxygen- rich water reaches a maximum under these circumstances (increased more than sixfold to stagnant conditions). Intensive mixing of upwelling and downwelling pore water within the sediment might cause layers with increased precipitation of redox-sensitive substances (e.g., the common ferric iron coatings on surface layer sands).

Between scenarios 3 and 4, there is a gradual transition. In our experiments, when the ripples propagated at velocities of < 10 cm h^{-1}, the oxygen-depleted zones under the ripple crests were fully developed with fully anoxic conditions in the centers (scenario 3). With ripple propagation velocities of > 20 cm h^{-1}, the upwelling zone became detached from the ripple crests (scenario 4). With pore water velocities between 10 and 20 cm h^{-1}, the oxygen-depleted zone trailed behind the ripple crest and showed only slight oxygen

depletion. Therefore, ripple migration velocity defines not only how long a sediment volume is exposed to anoxic conditions but also the degree of anoxia and which spectrum of substances can be ''leached'' from the sediment because of the passage of an oxygen-depleted or oxic zone (applicable to Fe, Mn, NO_3, NH_4, PO_4, and possibly to heavy metals like Pb, Cd, or Hg).
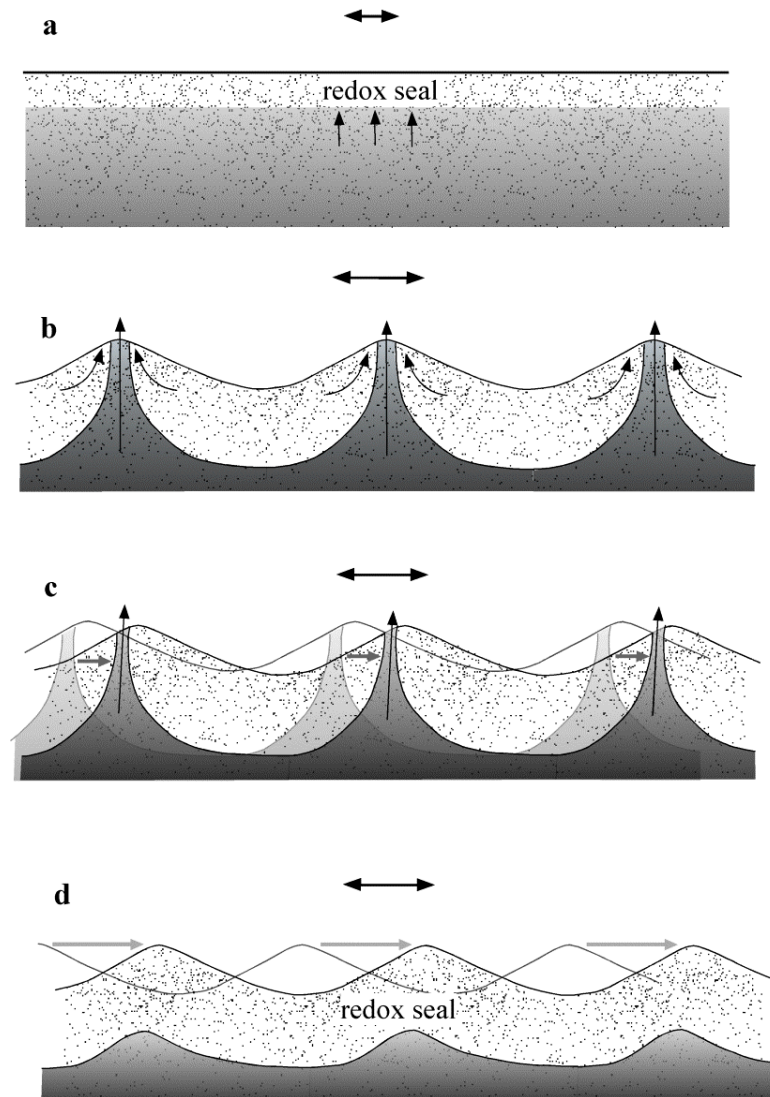

Figure 9: Schematic diagram of a) no sediment topography, oscillating flow; b) stationary ripples; c) ripples moving slower than pore water; d) ripples moving faster than pore water. Grey: anoxic pore water, arrows indicate water or pore water flow directions. See text for further details.

Doucette et al. (2002) measured the migration rates of wave ripples 45 m offshore at shallow water depths with ripple wavelengths and sediment grain sizes comparable to those in our study. They observed averaged ripple migration rates of 55 cm h^{-1}, which would mean that, at least in the highly mobile nearshore environment, scenario 4 of a

redox-sealed sediment with completely oxic surface layer occurs. Migration rates of larger wave ripples (ripple wavelengths typically 10 – 100 cm; sediment median grain size = 400 µm) were measured by Traykovski et al. (1999) at 11 m water depth, and it was found that these bedforms moved at velocities between 1 and 3 cm h^{-1}. These values show that all the scenarios we described for the flume sediment can occur in natural environments.

We conclude that surface gravity waves can control oxygen transport and distribution in shallow permeable sediments. Because this influence is affected by the formation of sediment wave ripples and associated advective pore water flows, the regularity of the ripple topography is reflected in the oxygen distribution pattern in the upper sediment layer, with alternating zones of oxic and anoxic sediment. This establishes a fundamental difference between fine-grained, impermeable sediments and sandy permeable beds. Although in the fine-grained beds the diffusive sediment–water solute exchange takes place everywhere at the surface and simultaneously in both directions (into and out of the sediment via diffusion and associated counterdiffusion), influx and efflux is spatially well separated in permeable sand beds, with solute penetration in the ripple troughs and solute release from the ripple crests (Fig. 10).

Thus, the fluxes into the sediment take place through a larger surface area than the fluxes out of the sediment. The separation of influx and efflux can generate a regular pattern of extremely different biogeochemical zones at the surface. The tight link between topography and pore water flow fields makes this distribution pattern highly dynamic, as ripples migrate or change their shape. Through the persistence of ripples after a storm event, this memory effect of the sea bed might control sediment metabolism a long time after such an event, through advective exchange caused by the interaction of boundary flows (e.g., tidal flows) and relict topography.
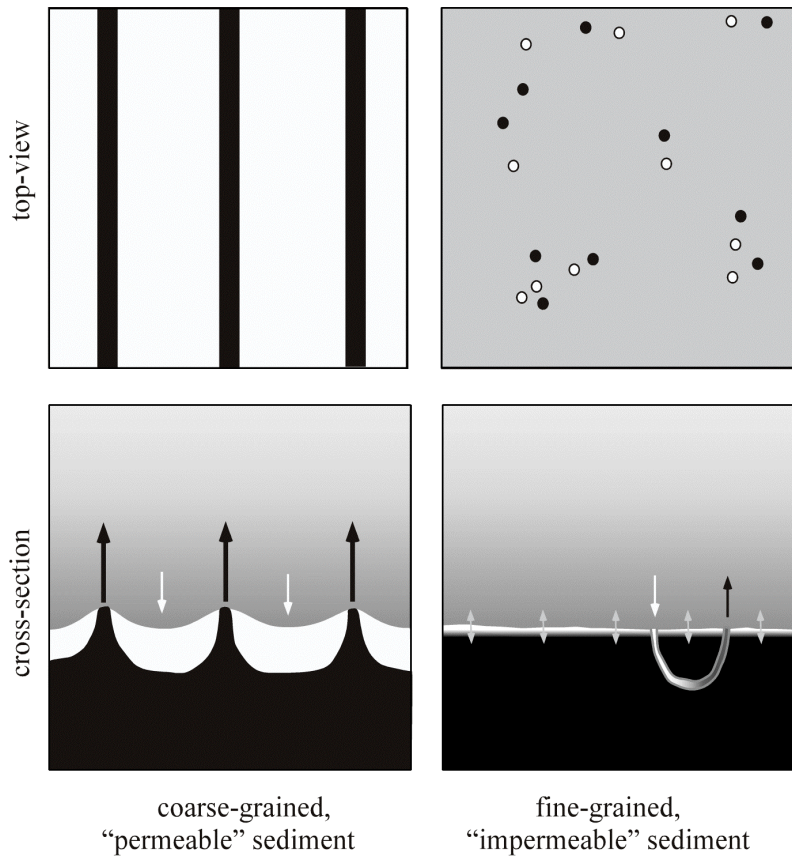
Figure 10: Top views (upper panels) and cross-sections of a coarse-grained, rippled, permeable sediment (left) and a fine-grained, impermeable bed (right). Black indicates solute flux from the sediment, white solute flux into the sediment, grey in the impermeable bed simultaneous flux into and out of the bed at the same location. The flux in and out of a rippled, permeable bed is limited to distinct zones of in- and outflow whereas the diffusive transport that prevails in fine-grained sediments occurs over the whole sediment surface area (with bioturbation producing local hotspots of transport).

Acknowledgements

References

Aller, R. C. 1982. The effects of macrobenthos on chemical properties of marine sediment and overlying water, p. 53-102. *In* P. L. McCall and M. J. S. Tevesz [eds.], Animal-Sediment Relations. Plenum Press.

Aller, R. C. 1990. Bioturbation and Manganese Cycling in Hemipelagic Sediments. Phil. Trans. R. Soc. Lond. A. 331: 51-68.

Aller, R. C. 1994. Bioturbation and remineralization of sedimentary organic matter: effects of redox oscillation. Chem. Geol. 114: 331-345.

Ballew, R. M. and J. N. Demas. 1989. An error analysis of the rapid lifetime determination method for the evaluation of single exponential decays. Anal. Chem. 61: 30-33.

Basu, A. J. and A. Khalili. 1999. Computation of flow through a fluid-sediment interface in a benthic chamber. Phys. Fluids. 11: 1395-1405.

Berner, R. A. 1980. Early Diagenesis-A Theoretical Approach. Princeton University Press.

Booij, K., W. Helder and B. Sundby. 1991. Rapid redistribution of oxygen in a sandy sediment induced by changes in the flow velocity of the overlying water. Neth. J. Sea Res. 28: 149-165.

Cacchione, D. A., P. L. Wiberg, J. Lynch, J. Irish and P. Traykovski. 1999. Estimates of suspended-sediment flux and bedform activity on the inner portion of the Eel continental shelf. Mar. Geol. 154: 83-97.

Canfield, D. E., B. Thamdrup and J. W. Hansen. 1993. The Anaerobic degradation of organic-matter in danish coastal sediments - Iron reduction, manganese reduction, and sulfate reduction. Geochim. Cosmochim. Acta. 57: 3867-3883.

de Haas, H., T. C. E. van Weering and H. de Stigter. 2002. Organic carbon in shelf seas: Sinks or sources, processes and products. Cont. Shelf Res. 22: 691-717.

Denny, M. W. 1988. Biology and the mechanics of the wave-swept environment. Princeton University Press.

Doucette, J. S., E. S. Harvey and M. R. Shortis. 2002. Stereo-video observation of nearshore bedforms on a low energy beach. Mar. Geol. 189: 289-305.

Elliott, A. H. and N. H. Brooks. 1997a. Transfer of nonsorbing solutes to a streambed with bed forms: Theory. Water Resour. Res. 33: 123-136.

Elliott, A. H. and N. H. Brooks. 1997b. Transfer of nonsorbing solutes to a streambed with bed forms: Laboratory experiments. Water Resour. Res. 33: 137-151.

Emery, K. O. 1968. Relict sediments on continental shelves of the world. Am. Assoc. Pet. Geol. Bull. 52: 445-464.

Forster, S., M. Huettel and W. Ziebis. 1996. Impact of boundary layer flow velocity on oxygen utilisation in coastal sediments. Mar. Ecol. Prog. Ser. 143: 173-185.

Fossing, H., V. A. Gallardo, B. B. Jorgensen, M. Huttel, L. P. Nielsen, H. Schulz, D. E. Canfield, S. Forster, R. N. Glud, J. K. Gundersen, et al. 1995. Concentration and transport of nitrate by the mat-forming sulfur bacterium *Thioploca*. Nature. 374: 713-715.

Glud, R. N., M. Kuhl, O. Kohls and N. B. Ramsing. 1999. Heterogeneity of oxygen production and consumption in a photosynthetic microbial mat as studied by planar optodes. J. Phycol. 35: 270-279.

Glud, R. N., N. B. Ramsing, J. K. Gundersen and I. Klimant. 1996. Planar optrodes: A new tool for fine scale measurements of two-dimensional O-2 distribution in benthic communities. Mar. Ecol. Prog. Ser. 140: 217-226.

Glud, R. N., C. M. Santegoeds, D. De Beer, O. Kohls and N. B. Ramsing. 1998. Oxygen dynamics at the base of a biofilm studied with planar optodes. Aquat. Microbial Ecol. 14: 223-233.

Glud, R. N., A. Tengberg, M. Kuhl, P. O. J. Hall, I. Klimant and G. Holst. 2001. An in situ instrument for planar O-2 optode measurements at benthic interfaces. Limnol. Oceanogr. 46: 2073-2080.

Harris, C. K. and P. L. Wiberg. 2001. A two-dimensional, time-dependent model of suspended sediment transport and bed reworking for continental shelves. Comput. Geosci. 27: 675-690.

Harris, P. T. and R. Coleman. 1998. Estimating global shelf sediment mobility due to swell waves. Mar. Geol. 150: 171-177.

Holst, G. and B. Grunwald. 2001. Luminescence lifetime imaging with transparent oxygen optodes. Sens. Actuator B-Chem. 74: 78-90.

Holst, G., O. Kohls, I. Klimant, B. Konig, M. Kuhl and T. Richter. 1998. A modular luminescence lifetime imaging system for mapping oxygen distribution in biological samples. Sens. Actuator B-Chem. 51: 163-170.

Huettel, M., S. Forster, S. Kloser and H. Fossing. 1996. Vertical migration in the sediment-dwelling sulfur bacteria *Thioploca spp* in overcoming diffusion limitations. Appl. Environ. Microbiol. 62: 1863-1872.

Huettel, M. and A. Rusch. 2000. Transport and degradation of phytoplankton in permeable sediment. Limnol. Oceanogr. 45: 534-549.

Huettel, M. and I. T. Webster. 2001. Porewater flow in permeable sediments, p. 144-179. *In* B. P. Boudreau and B. B. Jørgensen [eds.], The Benthic Boundary Layer. Oxford University Press.

Huettel, M., W. Ziebis and S. Forster. 1996. Flow-induced uptake of particulate matter in permeable sediments. Limnol. Oceanogr. 41: 309-322.

Huettel, M., W. Ziebis, S. Forster and G. I. Luther. 1998. Advective transport affecting metal and nutrient distribution and interfacial fluxes in permeable sediments. Geochim. Cosmochim. Acta. 62: 613-631.

Jørgensen, B. B. and D. J. Des Marais. 1990. The diffusive boundary layer of sediments: oxygen microgradients over a microbial mat. Limnol. Oceanogr. 35: 1343-1355.

Kautsky, H. 1939. Quenching of luminescence by oxygen. Trans Faraday Soc. 35: 216-219.

Klimant, I., V. Meyer and M. Kühl. 1995. Fiber-optic oxygen microsensors, a new tool in aquatic biology. Limnol. Oceanogr. 40: 1159-1165.

Klimant, I. and O. S. Wolfbeis. 1995. Oxygen-sensitive luminescent materials based on silicone-soluble ruthenium diimine complexes. Anal. Chem. 67: 3160-3166.

Klute, A. and C. Dirksen. 1986. Hydraulic conductivity and diffusivity: Laboratory methods, p. 687-734. *In* A. Klute [eds.], Methods of soil analysis - part 1 - physical and mineralogical methods. American Society of Agronomy.

Krögel, F. 1997. Einfluß von Viskosität und Dichte des Seewassers auf Transport und Ablagerung von Wattsedimenten (Langeooger Rückseitenwatt, südliche Nordsee). Berichte aus dem Fachbereich Geowissenschaften der Universität Bremen. 102: 168 pages.

Liebsch, G., I. Klimant, B. Frank, G. Holst and O. S. Wolfbeis. 2000. Luminescence lifetime imaging of oxygen, pH, and carbon dioxide distribution using optical sensors. Appl. Spectrosc. 54: 548-559.

Lohse, L., E. H. G. Epping, W. Helder and W. Vanraaphorst. 1996. Oxygen pore water profiles in continental shelf sediments of the North Sea - Turbulent versus molecular diffusion. Mar. Ecol. Prog. Ser. 145: 63-75.

Ogston, A. S. and R. W. Sternberg. 1999. Sediment-transport events on the northern California continental shelf. Mar. Geol. 154: 69-82.

Papkovsky, D. B., J. Olah, I. V.Troyanovsky, N. A. Sadovsky, V. D. Rumyantseva, A. F. Mironov, A. I. Yaropolov and A. P.Savitsky,. Phosphorescent polymer-films for optical oxygen sensors. Biosensors & Bioelectronics 7(3): 199-206.

Precht, E. and M. Huettel. 2003. Advective pore water exchange driven by surface gravity waves and its ecological implications. Limnol. Oceanogr. 48: 1674-1684.

Precht, E. and M. Huettel. 2004. Rapid wave-driven advective pore water exchange in a permeable coastal sediment. J. Sea Res.

Riedl, R. J., N. Huang and R. Machan. 1972. The subtidal pump: A mechanism of interstitial water exchange by wave action. Mar. Biol. 13: 210-221.

Rutgers van der Loeff, M. M. 1981. Wave effects on sediment water exchange in a submerged sand bed. Neth. J. Sea Res. 15: 100-112.

Rutherford, J. C., J. D. Boyle, A. H. Elliott, T. V. J. Hatherell and T. W. Chiu. 1995. Modeling benthic oxygen-uptake by pumping. J. Environ. Eng.-ASCE. 121: 84-95.

Shum, K. T. 1992. Wave-induced advective transport below a rippled water-sediment interface. J. Geophys. Res. 97: 789-808.

Shum, K. T. 1993. The effects of wave-induced pore water circulation on the transport of reactive solutes below a rippled sediment bed. J. Geophys. Res. 98: 10289-10301.

Traykovski, P., A. E. Hay, J. D. Irish and J. F. Lynch. 1999. Geometry, migration, and evolution of wave orbital ripples at LEO-15. J. Geophys. Res. 104: 1505-1524.

Webb, J. E. and J. Theodor. 1968. Irrigation of submerged marine sands through wave action. Nature. 220: 682-683.

Webb, J. E. and J. L. Theodor. 1972. Wave-induced circulation in submerged sands. J. Mar. Biol. Assoc. U.K. 52: 903-914.

Wiberg, P. L. and C. K. Harris. 1994. Ripple geometry in wave-dominated environments. J. Geophys. Res. 99: 775-789.

Woods, R. J., S. Scypinski, L. J. C. Love and H. A. Ashworth. 1984. Transient digitizer for the determination of microsecond luminescence lifetimes. Anal. Chem. 56: 1395-1400.

Ziebis, W., M. Huettel and S. Forster. 1996. Impact of biogenic sediment topography on oxygen fluxes in permeable seabeds. Mar. Ecol. Prog. Ser. 140: 227-237.

High spatial resolution measurement of oxygen consumption rates in permeable sediments

Lubos Polerecky , Ulrich Franke, Ursula Werner, Björn Grunwald and Dirk de Beer

Max-Planck Institute for Marine Microbiology, Celsiusstrasse 1, D-28359, Bremen

Abstract

A method is presented for the measurement of depth profiles of volumetric oxygen consumption rates in permeable sediments with high spatial resolution. When combined with in situ oxygen microprofiles measured by microsensors, areal rates of aerobic respiration in sediments can be calculated. The method is useful for characterizing sediments exposed to highly dynamic advective water exchange, such as intertidal sandy sediments. The method is based on percolating the sediment in a sampling core with aerated water and monitoring oxygen in the sediment using either an oxygen microelectrode or a planar oxygen optode. The oxygen consumption rates are determined using three approaches: (1) as the initial rate of oxygen decrease measured at discrete points after the percolation is stopped, (2) from oxygen microprofiles measured sequentially after the percolation is stopped, (3) as a derivative of steady-state oxygen microprofiles measured during a constant percolation of the sediment. The spatial resolution of a typical $3 - 4$ cm profile within a measurement time of $1 - 2$ h is better with planar optodes (≈ 0.3 mm) then with microelectrodes ($2 - 5$ mm), whereas the precision of oxygen consumption rate measurements at individual points is similar ($0.1 - 0.5 \, \mu mol \, L^{-1} \, min^{-1}$) for both sensing methods. The method is consistent with the established methods (interfacial gradients combined with Fick's law of diffusion, benthic-chambers), when tested on the same sediment sample under identical, diffusion-controlled conditions.

Introduction

Aerobic respiration plays an important role in the degradation of carbon and is typically estimated to account for 25 – 50 % of carbon mineralisation in coastal sediments. Two established methods have been used for the determination of areal oxygen consumption rates (OCR) in sediments, namely the diffusive oxygen uptake and the benthic-chamber total oxygen uptake methods. The first method, which will be referred to as the flux method, exploits the possibility provided by oxygen microelectrodes to measure diffusive oxygen microprofiles across the sediment-water interface (e.g., Revsbech et al. 1980; Glud et al. 1994). Using Fick's law of diffusion and a measured oxygen microprofile, one can calculate an areal diffusive oxygen uptake rate. However, to obtain an estimation of the possible lateral heterogeneity of areal rates, it is necessary to measure multiple microprofiles, which can be time consuming and requires constant conditions of the system during the measurements. The second method uses a sealed benthic chamber positioned at the surface of the sediment, enclosing a known area of the sediment surface and a known volume of the bottom water (e.g., Pamatmat 1971; Smith 1978; Glud et al. 1994). The areal OCR is evaluated from the temporal decrease of oxygen content in the overlying water in the chamber, which is determined either continuously by, e.g., an oxygen electrode or an oxygen microoptode present in the chamber (Glud et al. 1994; Tengberg et al. 1995; Glud et al. 1996) or by sampling the water from the chamber and analysing its oxygen content using the Winkler titration technique.

A known problem associated with the flux method is that the obtained areal OCR values can often underestimate the true uptake rates by not including the bio-irrigation activity of macrofauna living in the sediment (for citations, see Viollier et al. 2003). This problem is overcome by the benthic-chamber technique, where the measured decrease of oxygen reflects the respiratory activity of all organisms living in the sediment, including bio-irrigating macrofauna. However, the use of a benthic chamber may significantly alter the hydrodynamic conditions to which the measured sediment is exposed. The diffusive uptake of oxygen by the sediment depends considerably on the thickness of the diffusive boundary layer (DBL), which depends strongly on hydrodynamic conditions above the sediment surface. The water inside the chamber is therefore stirred so that the hydrodynamic conditions in the chamber resemble the natural situation as closely as possible.

Advection can be a highly effective transport process across the sediment-water interface (Huettel and Gust 1992; Huettel et al. 1996; Precht and Huettel 2003;

Precht et al. 2004), particularly in permeable sediments, which are common in coastal environments (Emery 1968; de Haas et al. 2002). Due to tidal pumping, waves or the interaction of the water flow with the surface topography (e.g., ripples), the sediments are flushed with oxygen-rich water, thus significantly enhancing rates of carbon mineralisation due to aerobic respiration. In advection-driven systems, the state of oxygenation of the sediment is often very dynamic, making the flux method, based on the measurement of steady-state diffusive microprofiles, unsuitable. Efforts have been made to mimic advective water exchange through the sediment-water interface inside benthic chambers. Cylindrical benthic chambers with stirring-induced radial pressure gradients, as a substitute for horizontal pressure gradients, served as model systems (Glud et al. 1996). Chambers with flexible walls were deployed to allow pressure variations driven by waves to propagate into the chambers (Malan and McLachlan 1991). However, these modifications cannot always mimic the highly dynamic conditions in the systems where advection is the dominant process of oxygen transport, thus limiting the use of benthic chambers under such circumstances.

Recently, an adaptation of eddy correlation to mass flow in aquatic systems was reported (Berg et al. 2003). The method is non-invasive and independent of the transfer mechanism of solutes through the sediment-water interface, which makes it suitable for the study of advective systems. Eddy correlation measures area-integrated fluxes of solutes such as oxygen. The footprint of the method is several square meters, which makes it an attractive tool for the assessment of total solute exchange. The measurement, however, cannot provide the functional information nor the small scale variability of the processes governing the solute uptake.

The dynamics of oxygen supply in advection-driven systems can be assessed by in-situ microprofiling using microelectrodes or planar optodes attached to autonomous profilers (Glud et al. 1994; Glud et al. 1999a; Glud et al. 2001; Wenzhöfer and Glud 2002). The variability of oxygen penetration can be determined with high temporal (ranging from a couple of seconds with an optode-based to 10–30 min with a microelectrode-based in situ profiler) and spatial (in the sub-millimeter range) resolutions. To estimate the rate of aerobic degradation of organic matter in such sediments, a method is needed for the determination of a depth profile of volumetric OCR with a comparably high spatial resolution. Once a depth profile of volumetric OCR is known, it can be integrated over the depth of oxygen penetration to obtain areal oxygen uptake rates of the sediment. Such a method was recently introduced by de Beer et al. (2005). It is based on percolating the

sediment in a sample core with air saturated water and observing the decrease of oxygen in the sediment after the percolation is stopped.

In this article four variations of the basic method introduced by de Beer et al. (2005) are described in detail. The first exploits alternating between the on and off periods of water flow through a sediment column and monitoring with a microelectrode the decrease of oxygen at distinct locations. The second procedure employs oxygen microprofiles measured repeatedly during a single flow-off period. In the third variation, planar oxygen optodes are used to monitor oxygen dynamics in the sediment, allowing a time-efficient determination of a two-dimensional map of OCR with a sub-millimeter spatial resolution. The fourth approach is based on the measurement of steady-state O_2 microprofiles during steady percolation of the sediment. Each of the method variations was tried using cores of permeable sandy sediment and compared with the flux and benthic-chamber methods under rigorously controlled conditions. Furthermore, the applicability and limitations of the method are critically assessed and discussed.

Materials and Procedures

Materials

The method was applied to permeable sandy sediments collected from an intertidal sandflat in the Wadden Sea (Janssand, near Neuharlingersiel, Germany). The sediment was collected from areas where flushing with oxygen-rich water was, due to waves and tidal pumping, intense and dynamic (the field data obtained by an autonomous microsensor profiler will be published elsewhere). The porosity of the sediment was $\phi = 0.45$, and the measurements were conducted using sea water (salinity 30) from the study site that was saturated with air at a temperature of 12° C (oxygen concentration 280 μmol L^{-1}).

The flow-through method is assembled as schematically shown in Fig. 1. A core with the sediment sample collected from an area of investigation is first fixed onto a stand so as to allow a flow of water through the sediment in the downward direction. Two types of sediment cores were used for the demonstration of the method reported here: a cylindrical plexiglass core (inner diameter 36 mm, height 200 mm, wall thickness 3 mm) and a rectangular stainless steel core (inner dimensions 70 × 75 mm, height 250 mm, wall thickness 2 mm). The plexiglass core was equipped with a rubber stopper into which a

valve was incorporated. The removable bottom of the steel core, also equipped with a valve, contained a depression (3 mm wide, 1 mm deep) with the dimensions fitting the dimensions of the core. The depression was filled with silicone which enabled water-tight enclosure immediately after the collection of the sediment sample.
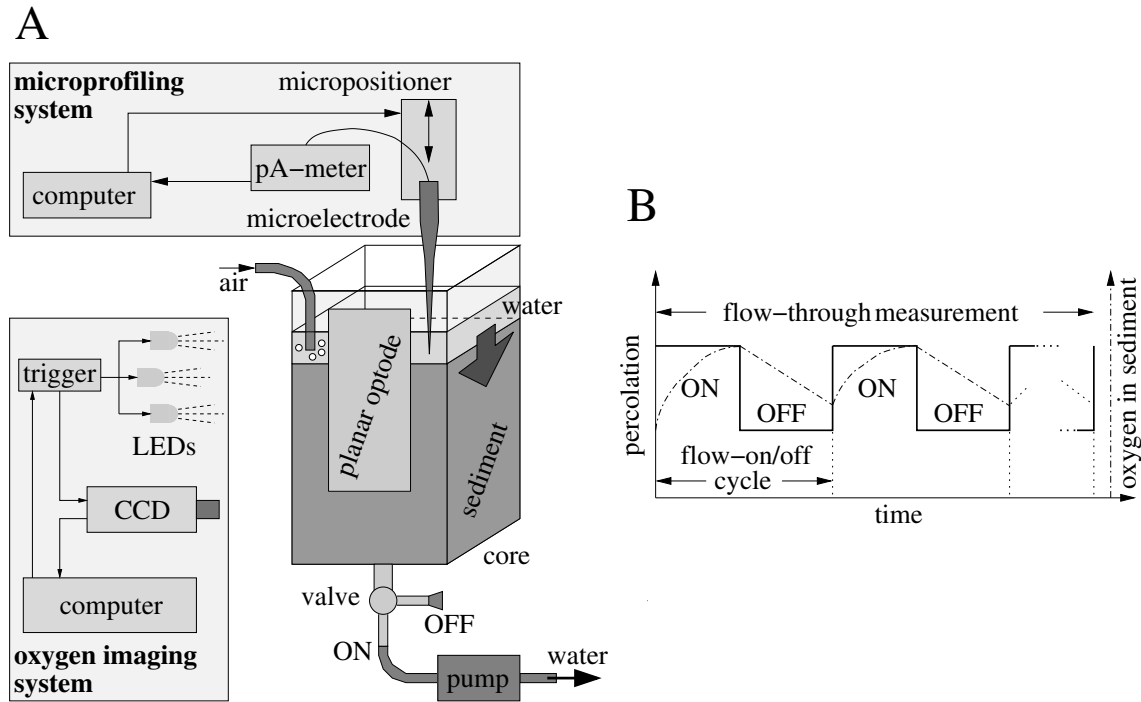

Figure 1: Schematic diagram of the (A) experimental configuration and (B) timing protocol of the flow-through method.

One side of the steel core contained a polycarbonate window (dimensions $50 \times 150 \times 4$ mm) glued to the steel by silicone. A semi-transparent planar oxygen optode was glued onto the polycarbonate plate by silicone grease (Elastosil, E4, Wacker) and the firm and water-resistant attachment was reinforced with tape at the foil edges. The foil was inside the core, enabling the measurement of oxygen in the water and sediment in direct contact with the wall. Details of the employed planar optode are given elsewhere (Precht et al. 2004).

The optode measurements were carried out using the MOLLI system (Holst et al. 1998; Holst and Grunwald 2001). The system consisted of a fast gateable CCD camera (SensiCam; PCO, Kelheim, Germany), a self-made triggering device, an array of blue LEDs (LXHL-LB5C, $\lambda_{max} = 470$ nm; Lumileds Lighting, San Jose, CA, USA) with a power supply and a red filter (Amber red; Lee Filters, Hampshire, UK). The measuring software

enabled computer-controlled acquisition of images with high spatial resolution and desired timing protocol. Oxygen images were calculated using the rapid lifetime determination method in combination with Stern-Volmer equation describing lifetime quenching by oxygen (Holst et al. 1998).

High spatial resolution oxygen microprofiles were measured with an oxygen microelectrode (Revsbech 1989), which was attached to a micromanipulator placed above the core. The micromanipulator was fixed onto a motorized stage (VT-80; Micos, Eschbach, Germany), enabling reproducible positioning of the sensor tip with 1 μm precision. The microelectrode was connected to a high-precision picoammeter, and the meter output was collected by a data-acquisition card (AI-16XE-50, data box CB68-LP; National Instruments, Austin, TX, USA). The microprofiling was facilitated by a computer program.

During the measurements, a constant water level above the sediment surface was maintained by a pump regulated by a float lever connected to an electrical switch. The overlying water was kept air-saturated by continuous bubbling with air.

When the permeability of the studied sediment permitted the flow of water solely due to gravity, a valve was used to regulate the speed of water percolation. When the sediment was less permeable, the valve was opened fully and a pump was used to suck the water through the sediment.

Basic theory

Each measurement of OCR consisted of two stages. In the first stage, referred to as the "flow-on" period, the sediment was percolated with air-saturated water. Subsequently, the percolation was stopped (this period is referred to as the "flow-off" period) and the decrease of oxygen in the sediment was recorded (Fig. 1B).

According to the diffusion equation, the rate of decrease of oxygen in the sediment during the flow-off period is determined by (i) the local oxygen consumption rate, denoted as R, and (ii) the local concentration variations, mathematically expressed by the diffusion term $D_s \Delta c$, Δ denoting the Laplacian operator and D_s being the diffusion coefficient of oxygen in the sediment (Crank 1975). The percolation speed and the duration of the flow-on period of the measurement are selected so that a steady and approximately homogeneous distribution of oxygen is reached in the sediment. This is an important experimental condition, as it guarantees that the diffusive term $D_s \Delta c$ is zero or negligible in comparison with the local consumption rate R at the time when the flow-off period starts.

If R is distributed inhomogeneously, local concentration gradients will develop, leading to the measured decrease of oxygen being influenced by the diffusion. Therefore, the local OCR was evaluated as the initial slope of the measured decrease of oxygen concentration.

An alternative approach for determining the depth profile of OCR is based on the theoretical description of the oxygen transport in permeable sediments driven mainly by advection. Under steady flow during the flow-on period, oxygen dissolved in the percolating water is respired on the way through the sediment. In a region of thickness Δz located at depth z of the sediment, the balance of the dissolved oxygen concentration, c, can be written as

$$v_f c(z + \Delta z) - v_f c(z) = -\phi A \Delta z R(z) \tag{1}$$

where v_f is the flow rate in $\mathrm{m^3\,s^{-1}}$, $R(z)$ is the local OCR[1] in $\mathrm{mol\,m^{-3}\,s^{-1}}$, ϕ is the porosity and A is the area of the horizontal cross-section in $\mathrm{m^2}$. This equation formulates that the amount of oxygen being transported by water flow at depth $z + \Delta z$ is reduced in comparison to that transported at depth z by an amount consumed in the volume $\Delta V = \phi A \Delta z$ with the consumption rate $R(z)$, which is assumed to be constant in the depth interval between z and $z + \Delta z$.

Considering that the depth difference, Δz, is infinitesimal and v_f is constant with depth, equation (1) can be rewritten in the form of a differential equation

$$-\frac{v_f}{\phi A}\frac{\partial c(z)}{\partial z} = R(z) \tag{2}$$

which is a one-dimensional equation describing the variation of an oxygen concentration profile in the sediment in a stationary situation, i.e., $\partial c(z)/\partial t = 0$, where constant advection is the dominant transport mechanism, i.e., $D_s \partial c / \partial z << v_f c(z) / A$. From this equation it follows that the depth profile of OCR can be determined from the derivative of a stationary oxygen profile during the flow-on period.

---

[1]Note that $R>0$ refers to oxygen consumption, while $R<0$ would represent oxygen production.

Measurement procedure

The measurement of the OCR profile was realised by four different approaches.

(a) *$O_2(t)$ measured at discrete depths by microelectrode* — An oxygen microelectrode was positioned at a specific depth in the sediment and the decrease of oxygen during the flow-off period was recorded. The duration of this period depended on the local oxygen consumption activity of the sediment, and was dynamically selected so that the observed decrease of oxygen was sufficient for precise determination of the slope (typically a couple of minutes). The local OCR was determined as an initial slope of the observed oxygen decrease, obtained by regression analysis. The microelectrode was then repositioned and the procedure was repeated until a complete OCR profile was measured.

(b) *Continuous O_2 profiling by microelectrode* — Oxygen microprofiles were measured continuously by a microelectrode during the flow-off period (Epping et al. 1999). The OCR profile was determined by subtracting oxygen concentrations measured at different times at individual depths and dividing each value of $\Delta c(z)$ by the time interval between the subsequent oxygen readings. This subtraction was carried out only for nonzero oxygen readings.

(c) *Continuous O_2 imaging by planar optode* — Continuous oxygen imaging was facilitated by the MOLLI system. During the flow-off period, oxygen images were recorded until a significant decrease of oxygen was observed in each pixel (typically for a couple of minutes up to an hour, if the consumption was very slow). The local OCR was determined by evaluating the initial slope of the oxygen decrease in each pixel, resulting in a two-dimensional (2D) map of OCR (see below).

(d) *O_2 profiling by microelectrode during steady-state flow-on period* — Oxygen microprofiles were measured during the flow-on period at different lateral positions. The depth profile of OCR was calculated from the steady state oxygen profiles using Eq. (2) and the known values of the flow speed, porosity and the cross-section of the sediment core.

Oxygen images were usually superposed with noise, which, depending on the optodes used, was up to $\pm 5\,\%$ of air saturation. The noise originated from the acquisition of fluorescence images by the CCD camera used and the way the oxygen images were calculated from the raw data (Holst and Grunwald 2001). Such noise levels introduced a complication when determining the initial slope of the oxygen decrease. In particular, when the oxygen images were recorded over sufficient time to ensure that the decrease in

oxygen was greater than the noise level in all pixels, the observed oxygen dynamics could be already influenced by the diffusion in some pixels while it was still unaltered in others. This was manifested by the increase or decrease of the observed slope of the oxygen signal in the 'diffusion-affected' pixels (depending on whether the pixel is surrounded by a region of a higher or lower consumption activity, respectively), while the linear decrease of oxygen remained unaltered in the 'diffusion-unaffected' pixels.

To distinguish between these types of behaviour with a statistical measure of significance, the following strategy was implemented in the pixelwise determination of the initial slope. The time evolution of oxygen in a pixel i of the image, denoted as $O_2(i;t)$, was fitted with polynomials between the 0th and 4th orders, i.e., $O_2(i;\ t) = P_0(i;\ t)$, or $O_2(i;\ t) = P_1(i;\ t), \ldots, or\ O_2(i;\ t) = P_4(i;\ t)$, where $P_k(t) = a_0 + a_1 t + \ldots + a_k t^k$ and each coefficient $a_k \equiv a_k(i)$ is a function of the pixel position. The parameters of the fitting polynomial were obtained by the procedure of minimising the sum of residues (Kleinbaum and Kupper 1978), i.e., by minimising the function $\chi_k^2(i) = \Sigma_{n=1}^N [O_2(i;t_n) - P_k(i;t_n)]^2$, N being the number of oxygen images considered in the fitting procedure.

The higher the order of the fitting polynomial, the better the quality of the fit, i.e., $\chi_0^2 \geq \chi_1^2 \geq \ldots \geq \chi_4^2$. However, even though the fit with a higher order polynomial is better than that with the lower order polynomial, it may not be significantly better. This consideration of a significant improvement of the fit was used to decide by which polynomial the observed evolution $O_2(i;t)$ was eventually fitted. The order of the fitting polynomial was selected as the maximum order K, such that the fit by a polynomial of any higher order, i.e., $P_{K+1},\ldots,P_{k=4}$, was not significantly better than the fit by the polynomial P_K. The significant improvement was determined by a statistical hypothesis testing described in textbooks (Sokal and Rohlf 1995), using the statistical significance level of 0.95. The OCR in the pixel i was then taken as the initial slope of the fitting polynomial (we refer to it as the most suitable polynomial), i.e., equal to the coefficient $a_1(i)$ when $K \geq 1$ or to zero when $K = 0$. This procedure was implemented in a program written in Matlab, enabling the calculation of an OCR image within seconds.

Assessment

O$_2$(t) measured at discrete depths by microelectrode

The speed of the air-saturated water flow through the sediment was adjusted by the valve to $v_f = 33$ cm^3 min^{-1} and the sediment was percolated for 10 min. The flow-off periods were between 4 and 11 minutes long and the corresponding time evolutions of oxygen were recorded at six depths between 5 and 30mm (Fig. 2A).
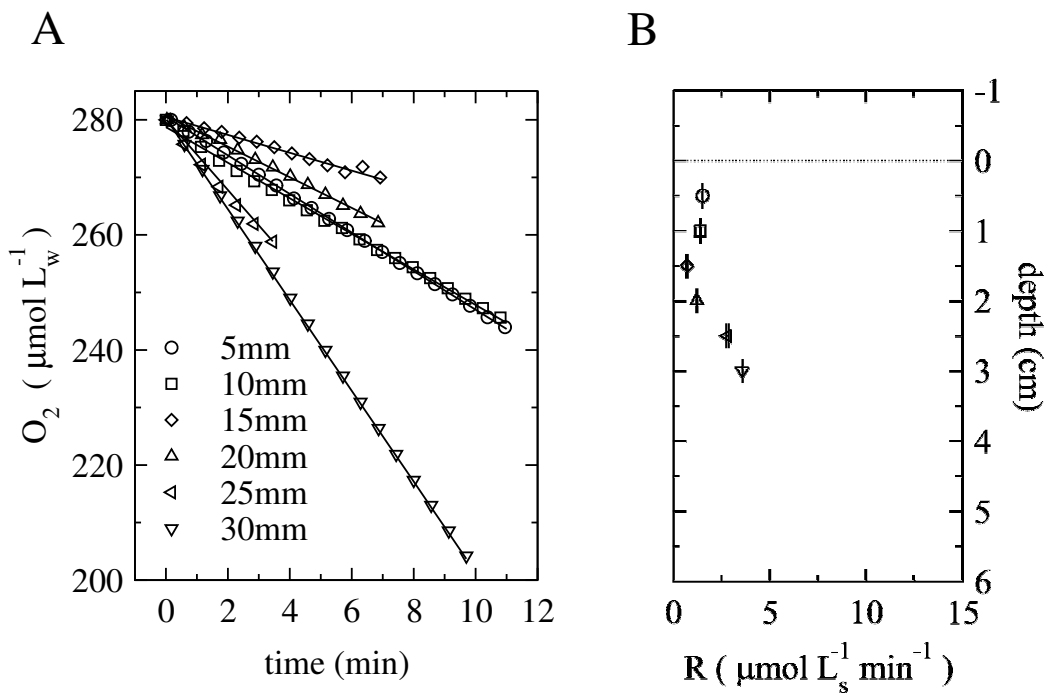
A   B

Figure 2: (A) Time evolution of the oxygen concentration measured at different sediment depths during the flow-off period of the flow-through experiment. (B) Corresponding oxygen consumption rates calculated as the initial slope of the oxygen decrease, corrected for the sediment porosity. The subscripts w and s refer to the volume of pore-water and sediment, respectively.

The linear decrease of oxygen at each measured depth suggested that the measurements were not influenced by diffusion during the measuring time. The values of OCR, determined from the slope of $O_2(i;t)$ and shown in Fig. 2B, were expressed per unit of the sediment volume.

One pump-on/off cycle lasted between approximately 15 and 20 minutes, resulting in the total time necessary to determine a single OCR profile of just under 2 hours. The precision of the determined OCR values, taken as the standard error of the slope of the

measured $O_2(t)$ at each position, was $0.01 - 0.1\,\mu mol L_s^{-1}\,min^{-1}$. Multiple flow-on/off cycles performed at each position showed that the measurements were reproducible with the same or lower variability. The spatial resolution was rather coarse (5 mm) and the profile was measured only at a single horizontal location (due to time constrains). A statistically representative determination of high resolution depth profiles of OCR would take several days to complete by this approach, unless multiple sensors are used simultaneously.

Continuous O_2 profiling by microelectrode

The approach based on continuous O_2 profiling by a microelectrode during the flow-off period was repeated on the same sediment core, however, at another horizontal position. Line #1 in Fig. 3A shows that initially, during the flow-on period (flow rate $v_f = 33\,cm^3\,min^{-1}$), oxygen was almost homogeneously distributed in the sediment. During the subsequent flow-off period, oxygen microprofiles were measured in time intervals of $15 - 30\,min$ with a step-size of 2 mm (lines #2 to #6 in Fig. 3A).
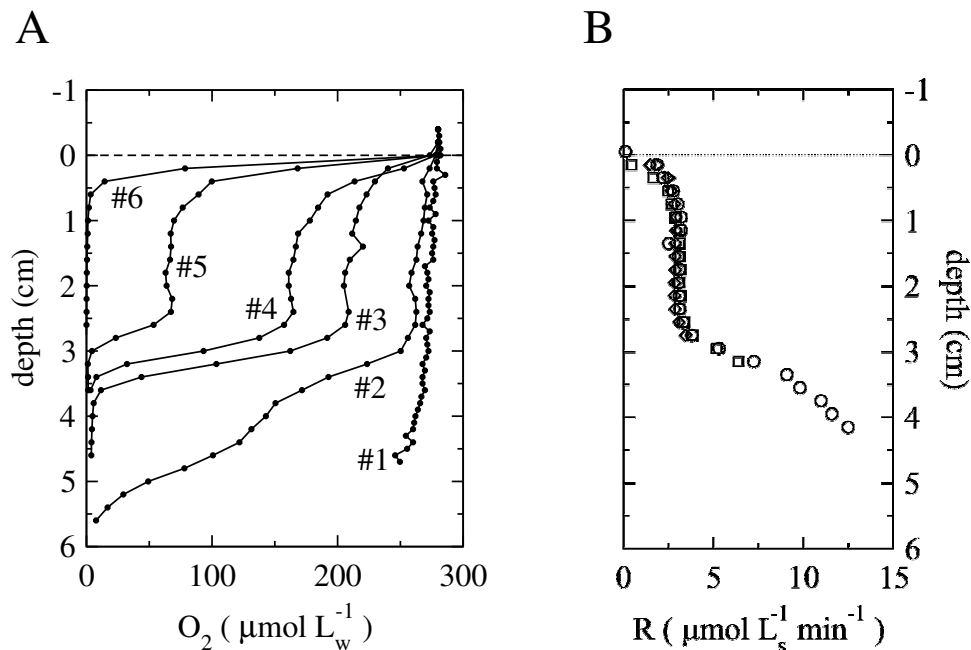

Figure 3: (A) Oxygen profiles measured during the flow-on (line #1) and flow-off (lines #2 to #6) periods of the flow-through measurement. Time differences between the starting points of profiles #2–#3, #3–#4, #4–#5 and #5–#6 were 17, 14, 30 and 34 min, respectively. (B) Corresponding profiles of oxygen consumption rates. Different symbols correspond to different profile pairs. The subscripts *w* and *s* refer to the volume of water and sediment, respectively.

The procedure described above resulted in OCR profiles shown in Fig. 3B. The OCR profiles obtained by the subtraction of different pairs of microprofiles were almost identical. The same procedure was conducted at another horizontal location, with similar results (data not shown).

The measured OCR profile is very close to that obtained by the approach employing the measurement of $O_2(t)$ at discrete depths, while the spatial resolution was improved (2 mm). However, since the sediment could be profiled at best every ≈ 15 min, the individual OCR determinations may include diffusion artifacts. For example, figure 3B shows that the measured OCR rapidly increases at depths immediately below 3 cm. This means that local concentration gradients developed during the measurement, leading to a possibly overestimated value of the measured OCR. A similar artifact may be observed near the sediment-water interface where oxygen may be renewed by diffusion from the overlying water, thus resulting in a possibly underestimated value of OCR.

The degree of under or overestimation can be estimated. This is done by approximating the diffusion contribution as $D_s \partial^2 c / \partial z^2 \approx D_s [c(z + \Delta z) + c(z - \Delta z) - 2c(z)] / \Delta z^2$, where $c(z)$ is the measured concentration profile and Δz is a depth interval. Using the values from the concentration profile #2 around $z = 3$ cm, $\Delta z = 0.4$ cm, and the diffusion coefficient in the sediment of porosity $\phi = 0.45$ of $D_s = 0.9 \, 10^{-5} \chi \mu^2 \sigma^{-1}$ (Boudreau 1996), the diffusive term amounts to $\approx$ -0.17 $\mu mol L_s^{-1} \min^{-1}$. Using the values from profile #5 around $z = 0.5$ cm and the same D_s and Δz, the diffusive term amounts to $\approx 0.54 \, \mu mol L_s^{-1} \min^{-1}$. Consequently, a conservative estimation of the inaccuracy of the measured OCR ranges between approximately -0.2 and 0.6 $\mu mol L_s^{-1} \min^{-1}$ for the deeper parts of the sediment ($z \geq 3$ cm) and for the locations close to the sediment-water interface ($z \leq 0.5$ cm), respectively. Thus the error induced by diffusion is less than 10%.

Since the OCR values obtained from different pairs of the measured oxygen profiles were similar, the OCR profile can be satisfactorily determined by measuring only two sequential profiles during the flow-off period. Thus, a depth profile of OCR between 0 and 4 cm with a spatial resolution of 2 mm could be determined with a needle-type microsensor within 30 – 60 min.

Continuous O$_2$ imaging by planar optode

The sediment sample was collected from the same site using a steel core with a window containing a planar oxygen optode. Approximately 2/3 of the optode was covered by the sediment and the remaining 1/3 by the overlying water.

The CCD camera was positioned so that the area of the planar optode (25×150 mm) resulted in an oxygen image of size 80×480 pixels, implying a spatial resolution of $\approx 300\,\mu$m. To minimise the noise of the oxygen images, 4 and 8 sequential images were averaged, resulting in a temporal resolution of ≈ 5 s and 10 s during the flow-on and flow-off periods, respectively.

Penetration of oxygen into the sediment during the flow-on period was observed in real time (see Fig. 4A–D). At a flow speed of 50 cm^3 min^{-1}, an approximately homogeneous distribution of oxygen in the sediment was reached after 8 min. Examples of the images recorded during the flow-off period, which lasted for 40 min, are shown in Fig. 4E–H. To check for the reproducibility of the measurement, the same procedure was repeated two more times.

Typical examples of time evolutions of the oxygen concentration in three selected pixels of the oxygen images are shown in Fig. 5. The pixels were selected to demonstrate different types of oxygen dynamics in the sediment. The data denoted as #1 in the bottom graph depict the decrease of oxygen concentration unaltered by diffusion during the entire duration of the flow-off period. On the other hand, the data denoted as #2 and #3 demonstrate how diffusion can increase and decrease the initial rate of oxygen consumption, respectively.

Figure 5 also shows the results of the fitting procedure. For example, the order of the most suitable polynomial fitting the data #1, #2 and #3 was 1, 3, and 2, respectively. The corresponding initial slopes, representing the local OCR, are depicted by the dashed lines. In addition to the local OCR, the fitting procedure also revealed the standard deviation of the initial slope, namely 0.05, 0.5 and $0.25\,\mu molL_s^{-1}\,\mathrm{min}^{-1}$ for data #1, #2 and #3, respectively. Thus the precision of the OCR values in a randomly selected pixel can be conservatively estimated as $\approx \pm\,0.5\,\mu molL_s^{-1}\,\mathrm{min}^{-1}$.
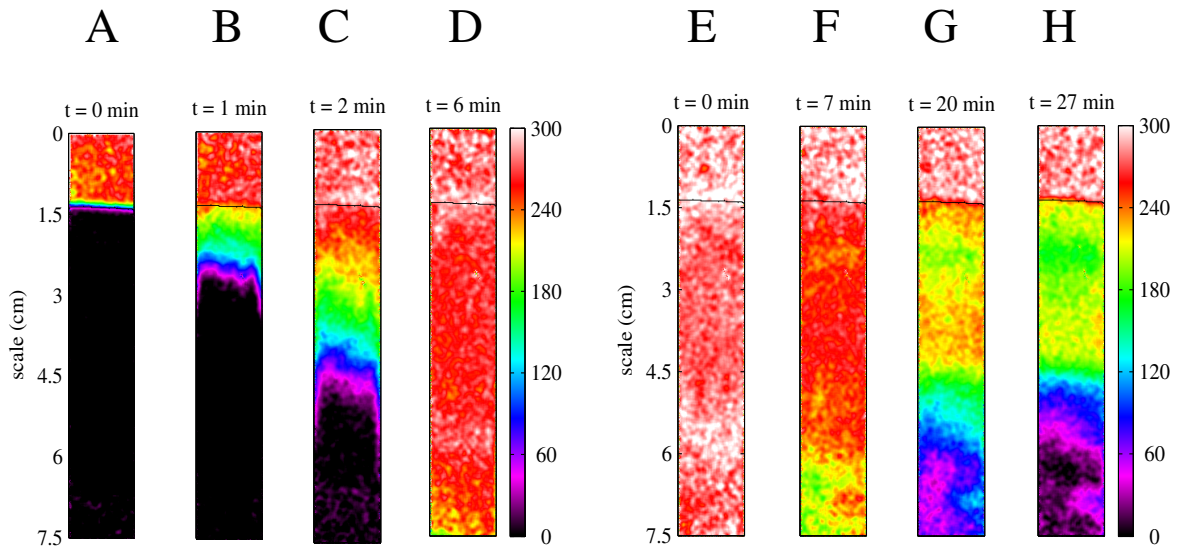
Figure 4: Examples of oxygen images during the flow-on (A–D) and flow-off (E–H) periods of the flow-through experiment. The solid lines at approximately 1.5 cm indicate the sediment surface. The color-bar on the right indicates the gradation of oxygen concentrations in $\mu mol L_w^{-1}$.
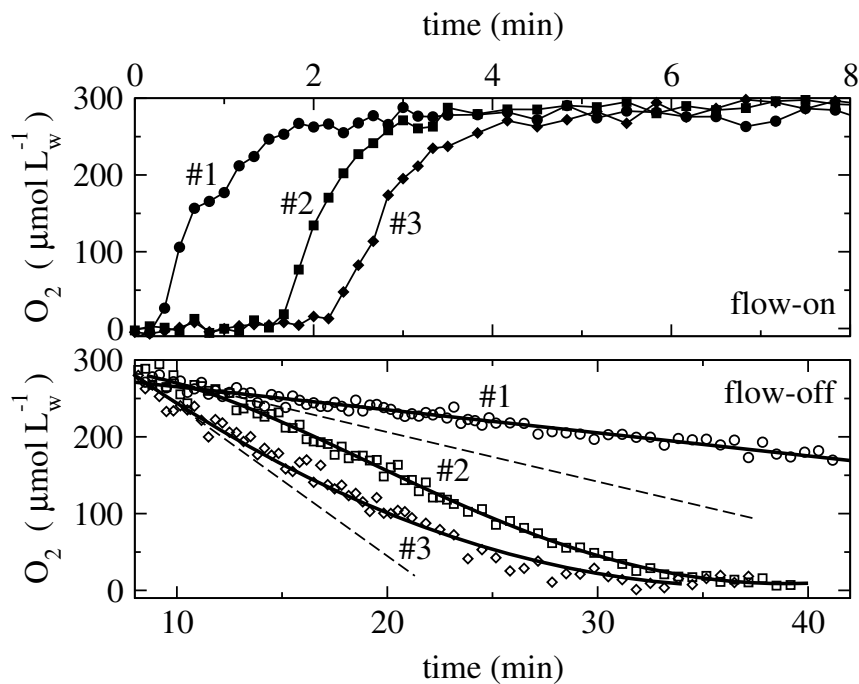

Figure 5: Examples of time evolutions of oxygen in three selected pixels as measured by the planar oxygen optode during the flow-on and flow-off periods. Data denoted as #1, #2 and #3 correspond to selected points located at depths of 1, 3 and 5 cm of the sediment, respectively. Symbols represent the experimental data, solid lines in the bottom graph the most suitable fitting polynomial (see text for more details) and dashed lines indicate the initial slope of oxygen decrease, representing the local OCR. For data #1, the dashed line is identical with the fitting line.
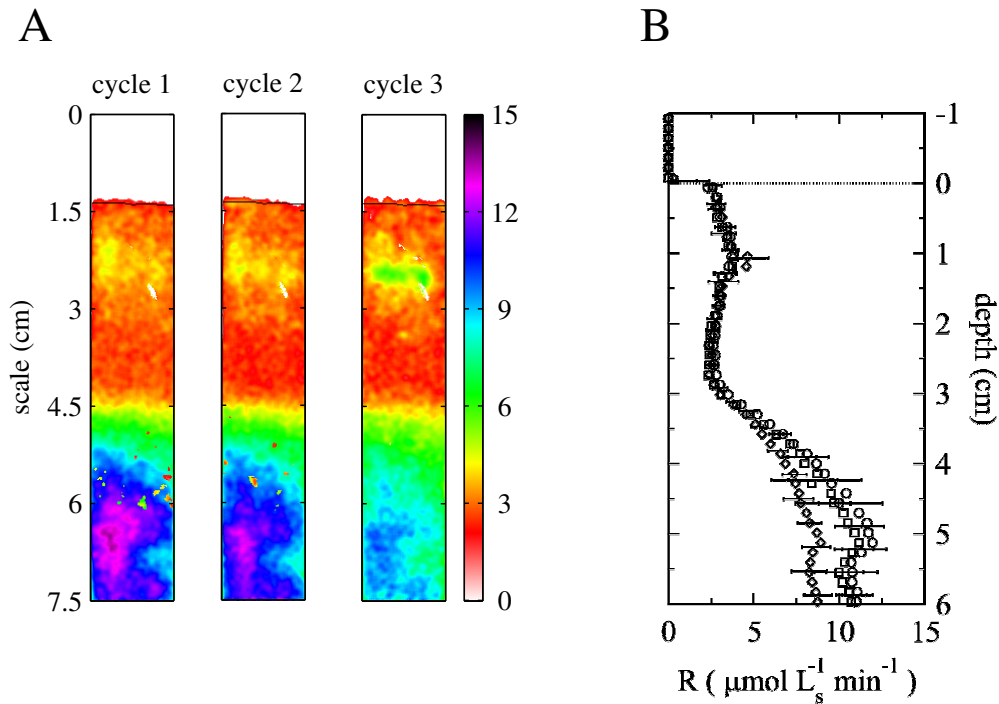
Figure 6: (A) Examples of OCR images obtained from three subsequent flow-through cycles. The color-bar to the right of the OCR images indicates the correspondence between the color and OCR in $\mu mol L_s^{-1} \min^{-1}$. (B) Depth profiles of OCR, obtained by horizontal averaging of the images, are also shown (circles, squares and diamonds correspond to the cycles 1, 2 and 3, respectively). The error bars represent the horizontal variability of the sediment's OCR. For clarity, only every 5th vertical data-point is depicted, i.e., every 1.5 mm.

After the fitting procedure was carried out in every pixel of the oxygen images, 2D maps of OCR across the entire observed section of the sediment were obtained (Fig. 6). After averaging the images in the horizontal direction, depth profiles of OCR were obtained, as shown in the same figure. The error bars, obtained as the standard deviations of the OCR values at the corresponding horizontal section, indicate the variability of sediment oxygen consumption over small horizontal scales.

The profiles obtained by planar optodes agree well with the profiles determined by the microelectrode based approaches (compare Fig. 6 with Figs. 2 and 3). This demonstrates a consistency of the measurement approaches. The planar optode based approach, however, provides a number of benefits.

Firstly, planar optodes enable the acquisition of a large amount of information during a single flow-on/off cycle of the flow-through measurement (Fig. 1B). In particular, the spatial resolution is optimal (≈ 300 µm, as compared to $2 - 5$ mm achieved by

a microelectrode in approximately the same measuring time) and both the vertical *and* horizontal small-scale variability of oxygen consumption activity of the sediment can be assessed. Secondly, since the planar optodes enable the observation of the oxygen distributions in real time, the timing of the flow-through measurement can be optimized dynamically.

A drawback of planar optodes is that the signal-to-noise ratio is lower than that of microelectrodes. This may lead to less precise OCR values (in the order of $\approx \pm 0.5 \, \mu mol L_s^{-1} \min^{-1}$, as mentioned above).

When using a microelectrode, OCR can be determined at any point in the sediment, which is an advantage in comparison to the planar optode based approach, where the measurement is restricted to the region of the sediment in direct contact with the optode. The OCR obtained by microelectrodes and planar optodes are similar, thus wall effects may be assumed to have been insignificant during this method demonstration.

Another potential drawback related to measurement with optodes is that the determination of oxygen requires intensive blue excitation light. If the sediment contains phototactic micro-organisms, the OCR could be altered if light exposure is long enough to allow for migration of such organisms towards the wall. Also, if photosynthetic micro-organisms were present in the sediment, oxygen production induced by the measuring light could influence the OCR measurement. However, such problems could be avoided by the use of optically isolated planar optodes (Glud et al. 1998, 1999b).

O₂ profiling during steady-state flow-on period

The flow-through method employing O₂ profiling by a microelectrode during the steady-state flow-on period was tested using the same sediment core characterized with the other microelectrode-based approaches. The water flow was, however, significantly lowered to v_f = 0.25 cm³ min⁻¹, which corresponded to a pore water flow velocity of 3.3cmh⁻¹. During the flow-on period, oxygen profiles were determined by a microelectrode at different horizontal positions. After approximately 2 hours, stationary oxygen profiles were measured, as shown in Fig. 7A. Each profile was fitted by a model describing advective transport of oxygen in the sediment (Eq. (2)), leading to a depth profile of OCR. These depth profiles were averaged and the resulting mean values together with the standard deviations are shown by symbols in Fig. 7B.

A

B

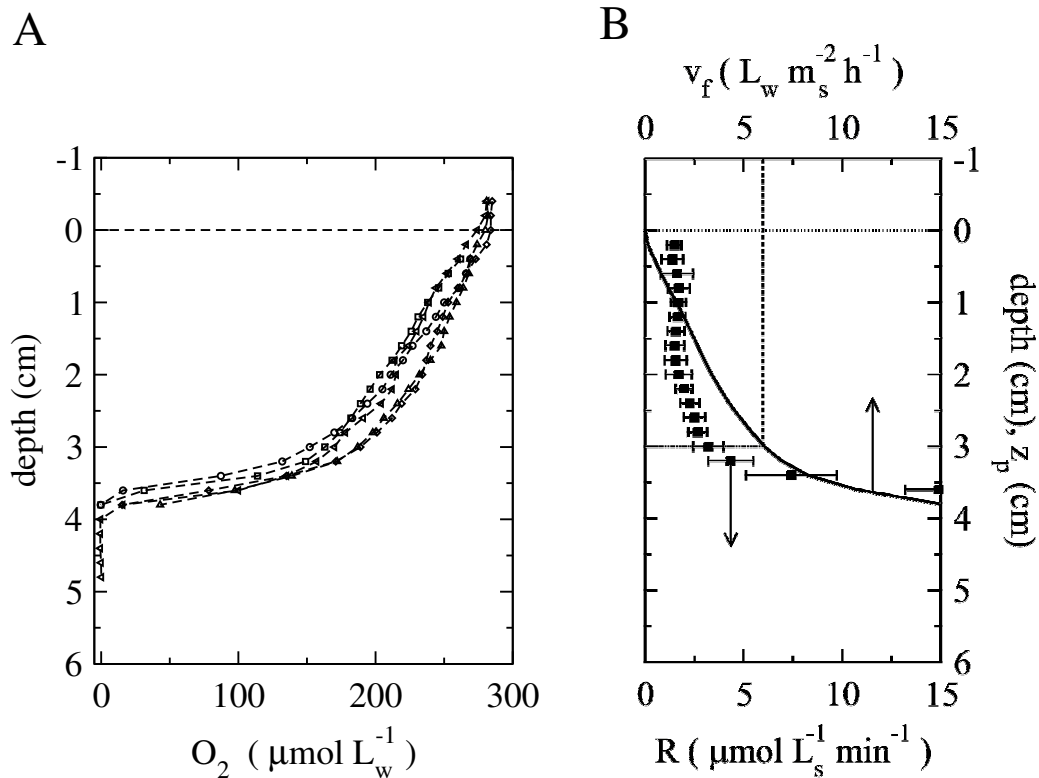$$v_f \left(L_w \, m_s^{-2} \, h^{-1} \right)$$

Figure 7: (A) Stationary oxygen profiles measured during the flow-on period at various horizontal positions. (B) Depth profile (symbols) of OCR obtained as the average of the OCR depth profiles calculated from Eq. (2) and the stationary profiles in A. The corresponding rate of water filtration through the sediment as a function of oxygen penetration depth z_p is depicted by a solid line.

The OCR values agree very well with those obtained by the alternative microelectrode based methods described above. The effect of diffusion, given by the second derivative of the profile multiplied by the diffusion coefficient, was also evaluated, but no significant influence on the OCR values was found.

Results obtained under steady flow can also be viewed as mimicking in situ oxygen profiles. An important parameter obtained by autonomous in situ profilers is the dynamic penetration depth of oxygen. The question is whether the volumetric exchange rate of water through the sediment could be estimated from this parameter.

Although natural flows are usually more complex (see below), the advective transport of pore water through many permeable sediments can be thought of as similar to that during the flow-on period of the flow-through measurements. During the measurement

described above, the oxygen penetration depth of $\approx 3.7\,$cm was achieved with the pore water flow of 3.3 cm h^{-1}, or the overlying water flow of 1.5 cm h^{-1} = 15 L m^{-2} h^{-1} (see the oxygen profiles in Fig. 7A). Thus, if such a penetration depth was observed by in situ microprofiling, it could be estimated that approximately 15 L of overlying water is hourly filtered through every m^2 of the sediment.

If another oxygen penetration depth was measured, additional "mimicking" measurements would not be necessary. Since the depth profile of OCR was already measured, advection-governed oxygen profile and thus the penetration depth can be modeled from Eq. (2). Denoting the oxygen concentration in the overlying water by c_0, penetration depth of oxygen by z_p, and assuming that the values of the pore water flow and porosity do not vary with depth, integration of Eq. (2) leads to $c_0 v_f / \phi A = \int_0^{z_p} R(z)dz$. Using this equation, which is nothing else than a simple oxygen balance for a steady-state vertical water flow, v_f can be estimated from the measured z_p and OCR profile $R(z)$, or vice versa.

The possible shape of $v_f(z_p)$ was calculated from the measured OCR profile and is shown by a solid line in Fig. 7B. When OCR is approximately constant (depths between 0 and 3 cm), the oxygen penetration depth increases roughly linearly with the flow rate. At $6\,L_w\,m_s^{-2}\,h^{-1}$, it reaches 3 cm, i.e., approximately 6 L of overlying water is filtered hourly through every m^2 of sediment when oxygen penetrates 3 cm deep. OCR rapidly increases below 3 cm and consequently the oxygen penetration depth is much less sensitive to the flow rate. For example, even though v_f doubles from $\approx 7.5\,L_w\,m_s^{-2}\,h^{-1}$ to $\approx 15\,L_w\,m_s^{-2}\,h^{-1}$, the penetration of oxygen increases only by as little as 5 mm (from ≈ 3.3 to $\approx 3.8\,$cm).

These observations suggest that in situ filtration rates of the sediment (pore water flow rates) could be estimated from OCR profiles when in situ oxygen penetration depths are also measured. This could be an interesting and attractive application of the flow-through method, since in situ filtration rates in permeable sediments have only been determined thus far by elaborate measurements of the displacement of an indicator (e.g., fluorescent dye or iodide) injected into the sediment (Precht and Huettel 2004; Reimers et al. 2004). One should, however, bare in mind the difference between the simple down-flow implemented in the flow-through method and the more complex water exchange in natural sediments (see Shum 1992; Shum and Sundby 1996; Huettel et al. 1996; Precht et al. 2004 for more on this topic).

The patterns of oxygen distributions resulting from the complex water exchange in permeable sediments can be determined in two dimensions (Precht et al. 2004; Wenzhöfer and Glud 2004). Provided that the directional field of the pore water flow is known, or can be to some extent reliably estimated, the model of advective transport expanded to two dimensions can be used together with the two-dimensional oxygen images to quantify the flow rate. Specifically, the process would involve (i) the calculation of the spatial derivative of concentration along the direction of the pore water flow vector, i.e., $\nabla_{\vec{s}} c$, where $\vec{s} \parallel \vec{v}_f$, and (ii) the calculation of the time derivative of concentration, $\partial c/\partial t$, determined from oxygen images acquired at different times. Consequently, neglecting the diffusive transport, the magnitude of the local flow rate (in cm h^{-1}) could be estimated from $v_f / \phi A \approx (\partial c / \partial t - R) |\nabla_{\vec{s}} c|^{-1}$, where R is the two-dimensional OCR distribution determined by the planar optode based flow-through method. The pursuit of such an interesting application would, however, require further investigation beyond the scope of this article.

Comparison of the flow-through method with the flux and benthic-chamber methods

The flow-through method was compared with the commonly used techniques for the determination of the areal oxygen consumption rates, i.e., the flux and benthic-chamber methods, under diffusion-dominated conditions. The purpose of this test was to confirm the consistency among the methods under well controlled conditions, where all methods are directly applicable.

The core with the planar optode was filled with sieved sediment of porosity $\phi = 0.45$. The water above the sediment was kept air saturated and stirred with a small propeller attached to a rotating axis. Stirring was minimal to ensure that transport was entirely diffusive.

Firstly, multiple microprofiles were measured by an oxygen microelectrode at different horizontal positions across the sediment surface area. The concentrations, which decreased by 23 ± 3 µmol L^{-1} over the average DBL thickness of 500 µm, were fitted by a diffusive model. Using the diffusion coefficient $D_w = 2 \times 10^{-5}$ cm^{2}s^{-1}, the average oxygen flux at the sediment-water interface was $J_{flux} = 5.4 \pm 0.9$ µmol m^{-2}min^{-1}.

The second step consisted of a planar optode based flow-through measurement with the flow-on period lasting approximately 2 min. At each horizontal position of the calculated OCR image, the vertical OCR profile was integrated over the penetration depth of oxygen

($\approx$ 5mm). The penetration depth was determined sufficiently long before and after the flow-through measurement, i.e., when oxygen distribution was governed by diffusion. This way, the obtained values could directly be compared with those from the first and next steps (see below). The resulting rates were averaged, leading to a total areal oxygen uptake rate of $J_{flow-through} = 5.0 \pm 1.0$ µmol m^{-2} min^{-1}.

Finally, a measurement mimicking the benthic-chamber experiment was carried out. Aeration of the overlying water was stopped and the chamber was closed with a lid. Stirring of the overlying water continued in order to maintain the same thickness of the diffusive boundary layer as during the diffusive flux measurement. The decrease of oxygen in the overlying water was monitored by an oxygen microelectrode positioned 1 cm above the sediment surface as well as by the planar optode, which extended well above the sediment surface. From the decrease, determined by regression analysis, the volume of the overlying water and the area of the sediment surface, the oxygen uptake rate was found to be $J_{chamber} = 5.3 \pm 0.1$ µmol m^{-2} min^{-1}.

The obtained values confirm that the three techniques lead to consistent results, when tested under equivalent, well controlled, diffusion-dominated conditions. However, since the flow-through method determines the potential volumetric OCR independently of the oxygenation status of the sediment, its applicability is much broader than that of the flux or benthic-chamber methods (see discussion for more on this topic).

It should be noticed that the standard deviation of the oxygen uptake rate obtained by the benthic-chamber method was approximately 9 – 10 times smaller than that obtained by the other two methods. This is understandable, as the standard deviations evaluated for the flux and flow-through methods represent the small-scale *horizontal variability* of the sediment with regard to the oxygen uptake rates, which is averaged by the benthic-chamber technique.

Effects of water percolation on the measurement

To identify potential artifacts induced by the percolation of air-saturated water through the sediment, results obtained by the planar optode based approach were further analyzed. The OCR images and the corresponding depth profiles of OCR displayed in Fig. 6 demonstrate that the OCR measured in cycle $N + 1$ were lower than those measured in cycle N in nearly all pixels. This was a consistently observed effect when the cycles were measured immediately one after the other. On the other hand, if the gap between the cycles was much longer, e.g., over night, a recovery in the measured OCR to the original values

was observed (data not shown). The effect was much more pronounced in deeper parts of the sediment (below 3 cm in the example discussed here), which coincided with a distinctly differently colored sediment (dark gray, almost black), as opposed to a light brown sediment of the top 3 cm.

This effect is most likely due to sediment stratification developed under natural conditions as a result of a highly dynamic, advection driven supply of oxygen into the sediment induced by waves and tidal pumping. Oxygen penetration depths of 2 – 3 cm are frequently observed by in situ profiler measurements (Walpersdorf, unpublished data), suggesting that the top sediment layer is inhabited mainly by aerobically respiring organisms, whereas reduced compounds accumulated in the deeper sediment. During the flow-through measurement, the pool of reduced compounds that can be easily oxidized contributed to the observed OCR in the deeper part of the sediment. As a result of this chemical oxidation, the size of the pool was reduced, resulting in the decreased contribution to the OCR observed in the subsequent measurement. On the other hand, when the sediment was kept anoxic for a longer time period, the pool could recover, resulting in a higher observed OCR.

Percolation of the sediment sample with aerated water is a prerequisite for the method, leading to a possible flushing out of compounds dissolved in the pore water from the sediment. Furthermore, rather lengthy percolation periods are required when a microelectrode based approach is employed. This may lead to a possible underestimation of the real oxygen consumption activity, as discussed above. However, as shown in Fig. 6, these effects are not significant in the part of the sediment that is naturally exposed to oxic conditions, which is the zone of primary interest.

Reimers et al. (2004) recently reported that the areal consumption rate of the same sediment volume could be enhanced by an increased percolation rate. Greater dispersion and penetration of oxygenated water into anoxic microenvironments within heterogeneous sediment at higher flow rates was suggested as a possible cause of this effect. Our measurements support this view, although additional experiments would be needed to exclude the possibility that respiration activities of microorganisms are enhanced by higher pore water flow rates. Using planar optodes, it was possible to monitor in real time the distribution of oxygen in the sediment. When OCR at some regions (not necessarily microscopic) of the sediment exceeded the supply of oxygen by the percolation at a specific flow rate, the regions remained anoxic. This would result in effectively zero potential volumetric OCR in these regions, leading after integration to lower areal OCR. If

the flow rate was increased until the entire sediment in front of the optode was oxic, the subsequently calculated OCR image showed significantly higher rates at these regions. Therefore, when sufficiently high percolation rates are used, the flow-through method provides an estimate of the maximum areal OCR. The percolation could, however, be modified to reflect the pore water flow conditions observed in situ (if such data exist), thus providing an estimate of the total oxygen uptake by the sediment experiencing close to natural conditions.

Comments and recommendations

The flow-through method is in principle a laboratory technique and cannot easily be applied in situ. However, since the experimental setup can be relatively easily assembled, it can be used as a field technique enabling the measurement immediately after the collection of the sample from a studied site.

The measurement procedure is simple and the software tools providing the subsequent analysis of the results were designed so that they could be operated by a trained non-specialist. Only minimal instrumentation (a micropositioner, an oxygen microelectrode and a data acquisition system) is required when the approach based on $O_2(t)$ measurements at discrete depths is employed. An additional automated micropositioning setup is preferable if the approaches based on continuous O_2 profiling during the flow-on or flow-off periods are used. With the access to a lifetime imaging system and planar oxygen optodes, full benefits of the flow-through method, namely the rapid determination of OCR in 2D with high spatial resolution, can be exploited. It is preferable to conduct planar optode measurements under dark conditions or at least at low ambient light intensities. No special light conditions are required for the microelectrode based approach, unless potential photosynthesis needs to be avoided. Typical merits characterizing each approach of the flow-through method are summarized in Tab. 1.

The flow-through method has a distinct advantage over the flux and benthic-chamber methods, as it quantifies the spatial distribution of *potential* oxygen consumption rates independently of the in situ conditions in the sediment. To determine actual in situ oxygen uptake rates, the results must be combined with information gathered when in situ oxygen distributions are measured in the sediment (Glud et al. 1994; Glud et al. 2001). It is not necessary to describe or mimic natural levels of flow complexity when quantifying OCR. It is only necessary to know over what depth to integrate the OCR profile.

Table 1: Duration, spatial resolution and precision of the different approaches of the flow-through measurement for a typical 3 – 4 cm vertical OCR profile determined by an oxygen microelectrode (ME) or planar optode (PO).

Measurement approach	Measurement time of one OCR profile	Spatial resolution (mm)	Precision ($\mu mol\ L^{-1}\ min^{-1}$)
$O_2(t)$ at discrete depths (ME)	2 hr	2 – 5	0.01 – 0.1
Continuous O_2 profiling (ME)	30 – 60 min	2	0.5
Continuous O_2 imaging (PO)	20 – 30 min	0.3	0.5
O_2 profiling during steady flow (ME)	2 – 4 hr	2	0.5

Due to the reliance of the flow-through method on supplementary information provided by benthic in situ profilers, its application may be costlier in comparison to, e.g., the benthic-chamber method. However, due to the above mentioned advantage, the flow-through method provides more accurate results in sediments with highly dynamic conditions (flow and oxygen penetration), where the use of benthic-chambers is limited and the flux method is not applicable.

The use of the flow-through method is limited in sediments with abundant burrowing and bioirrigating macrofauna. This is mainly because macrofauna can locally disturb the assessment of the rates by its irregular activity (i.e., water pumping) during the measurement. Another problem is that the respiring macrofauna can be easily missed if microelectrodes are used or if macrofauna are not located in sections of sediment in contact with planar optodes. Even though the volumetric respiration rates due to macrofauna can be determined, a straightforward quantification of areal OCR of the sediment would be problematic and the benthic-chamber or eddy-correlation technique would provide more reliable results.

The use of planar optodes facilitates a high spatial resolution measurement of OCR in two dimensions. This provides an insight into the sediment and the functional variability of the processes governing the oxygen uptake, e.g., differentiate between the microbial activity and bioturbation or bioirrigation, which is not possible using the benthic-chamber or eddy-correlation techniques.

In conclusion, the proposed method provides a feasible technique for the determination of volumetric oxygen consumption rates with high spatial resolution. The method is most

suitable for permeable sediments which can be easily percolated with water and which are naturally exposed to highly dynamic conditions. Of particular interest are sandy sediments, such as coral sands, intertidal or subtidal lithogenous sands, river beds, seep sediments.

Acknowledgments

References

P. Berg, H. Røy, F. Janssen, V. Meyer, B. B. Jørgensen, M. Huettel, and D. de Beer. Oxygen uptake by aquatic sediments measured with a novel non-invasive eddy-correlation technique. *Marine Ecology—Progress Series*, 261:75–83, 2003.

B. P. Boudreau. The diffusive tortuosity of fine-grained unlithified sediments. *Geochimica et Cosmochimica Acta*, 60(16): 3139–3142, 1996.

J. Crank. *Mathematics of Diffusion*. Oxford University Press, 2nd edition, 1975.

D. de Beer, F. Wenzhöfer, T. D. Ferdelman, S. Boehme, M. Huettel, J. E. E. von Beusekom, M. E. Boettcher, N. Musat, and N. Dubilier. Transport and mineralization rates in North Sea sandy intertidal sediments (Sylt-Rømø basin, Wadden Sea). *Limnology and Oceanography*, 50(1): 113-127, 2005.

H. de Haas, T. C. E van Weering, and H. de Stigter. Organic carbon in shelf seas: sinks or sources, processes and products. *Continental Shelf Research*, 22(5):691–717, 2002.

K. O. Emery. Relict sediments on continental shelves of the world. *Am. Assoc. Petroleum Geologists*, 52:445–464, 1968.

E. H. G. Epping, A. Khalili, and R. Thar. Photosynthesis and the dynamics of oxygen consumption in a microbial mat as calculated from transient oxygen microprofiles. *Limnology and Oceanography*, 44(8): 1936–1948, 1999.

R. N. Glud, S. Forster, and M. Huettel. Influence of radial pressure gradients on solute exchange in stirred benthic chambers. *Marine Ecology-Progress Series*, 141(1–3): 303–311, 1996.

R. N. Glud, J. K. Gundersen, B. B. Jørgensen, N. P. Revsbech, and H. D. Schulz. Diffusive and total oxygen-uptake of deep-sea sediments in the eastern south-atlantic ocean—in-situ and laboratory measurements. *Deep-Sea Research Part I—Oceanographic Research Papers*, 41(11–12):1767–1788, 1994.

R. N. Glud, I. Klimant, G. Holst, O. Kohls, V. Meyer, M. Kühl, and J. K. Gundersen. Adaptation, test and in situ measurements with O_2 microopt(r)odes on benthic landers. *Deep-Sea Research Part I—Oceanographic Research Papers*, 46(1):171–183, 1999a.

R. N. Glud, M. Kühl, O. Kohls, and N. B. Ramsing. Heterogeneity of oxygen production and consumption in a photosynthetic microbial mat as studied by planar optodes. *Journal of Phycology*, 35(2):270–279, 1999b.

R. N. Glud, C. M. Santegoeds, D. De Beer, O. Kohls, and N. B. Ramsing. Oxygen dynamics at the base of a biofilm studied with planar optodes. *Aquatic Microbial Ecology*, 14(3):223–233, 1998.

R. N. Glud, A. Tengberg, M. Kühl, P. O. J. Hall, I. Klimant, and G. Holst. An in situ instrument for planar O_2 optode measurements at benthic interfaces. *Limnology and Oceanography*, 46(8): 2073–2080, 2001.

G. Holst and B. Grunwald. Luminescence lifetime imaging with transparent oxygen optodes. *Sensors and Actuators B—Chemical*, 74 (1–3):78–90, 2001.

G. Holst, O. Kohls, I. Klimant, B. Konig, M. Kühl, and T. Richter. A modular luminescence lifetime imaging system for mapping oxygen distribution in biological samples. *Sensors and Actuators B—Chemical*, 51 (1–3):163–170, 1998.

M. Huettel and G. Gust. Impact of bioroughness on interfacial solute exchange in permeable sediments. *Marine Ecology Progress Series*, 89(2–3): 253–267, 1992.

M. Huettel, W. Ziebis, and S. Forster. Flow-induced uptake of particulate matter in permeable sediments. *Limnology and Oceanography*, 41(2):309–322, 1996.

D. G. Kleinbaum and L. L. Kupper. *Applied Regression Analysis and other Multivariable Methods*. Duxbury Press, 1st edition, 1978.

D. E. Malan and A. McLachlan. In situ benthic oxygen fluxes in a nearshore coastal marine system: a new approach to quantify the effect of wave action. *Marine Ecology Progress Series*, 73:69–81, 1991.

M. M. Pamatmat. Oxygen consumption by the seabed IV. Shipboard and laborator experiments. *Limnology and Oceanography*, 16:536–550, 1971.

E. Precht, U. Franke, L. Polerecky, and M. Huettel. Oxygen dynamics in permeable sediments with wave-driven pore water exchange. *Limnology and Oceanography*, 49(3):693–705, 2004.

E. Precht and M. Huettel. Advective pore water exchange driven by surface gravity waves and its ecological implications. *Limnology and Oceanography*, 48(4): 1674–1684, 2003.

E. Precht and M. Huettel. Rapid wave-driven advective pore water exchange in a permeable coastal sediment. *Journal of Sea Research*, 51:93–107, 2004.

C. E. Reimers, H. A. Stecher, G. L. Taghon, C. M. Fuller, M. Huettel, A. Rusch, N. Ryckelynck, and C. Wild. In situ measurements of advective solute transport in permeable shelf sands. *Continental shelf research*, 24:183–201, 2004.

N. P. Revsbech. An oxygen microelectrode with a guard cathode. *Limnology and Oceanography*, 34(2):474–478, 1989.

N. P. Revsbech, J. Sørensen, T. H. Blackburn, and J. P. Lomholt. Distribution of oxygen in marine sediments measured with microelectrodes. *Limnology and Oceanography*, 25(3):403–411, 1980.

K. T. Shum. Wave-induced advective transport below a rippled water-sediment interface. *Journal of Geophysical Research—Oceans*, 97: 789–808, 1992.

K. T. Shum and B. Sundby. Organic matter processing in continental shelf sediments — the subtidal pump revisited. *Marine Chemistry*, 53:81–87, 1996.

K. L. Smith. Benthic community respiration in NW Atlantic Ocean—insitu measurements from 40 to 5200 M. *Marine Biology*, 47(4):337–347, 1978.

R. R. Sokal and F. J. Rohlf. *Biometry*. W. H. Freeman and Company, 3rd edition, 1995.

A. Tengberg et al. 1995. Benthic chamber and profiling landers in oceanography—A review of design, technical solutions and functioning. *Progress In Oceanography*, 35(3):253–294, 1995.

E. Viollier, C. Rabouille, S. E. Apitz, E. Breuer, G. Chaillou, K. Dedieu, Y. Furukawa, C. Grenz, P. Hall, F. Janssen, J. L. Morford, J. C. Poggiale, S. Roberts, T. Shimmield, M. Taillefert, A. Tengberg, F. Wenzhöfer, and U. Witte. Benthic biogeochemistry: state of the art technologies and guidelines for the future of in situ survey. *Journal of Experimental Marine Biology and Ecology*, 285–286:5–31, 2003.

F. Wenzhöfer and R. N. Glud. Benthic carbon mineralization in the Atlantic: a synthesis based on in situ data from the last decade. *Deep-Sea Research Part I-Oceanographic Research Papers*, 49(7):1255–1279, 2002.

F. Wenzhöfer and R. N. Glud. Small-scale spatial and temporal variability in coastal benthic oxygen dynamics: Effects of fauna activity. *Limnology and Oceanography*, 49:1471–1481, 2004.

Wave tank study of particulate organic matter degradation in permeable sediments

Ulrich Franke[1], Lubos Polerecky, Elimar Precht[2] and Markus Huettel[3]

Max Planck Institute for Marine Microbiology, Celsiusstrasse 1, D-28359 Bremen, Germany

[1] Corresponding author (ufranke@mpi-bremen.de)

[2] Present address: DHI Wasser & Umwelt Krusenberg 31, 28857 Syke, Germany

[3] Present address: Florida State University, Department of Oceanography, 0517 OSB, West Call Street, Tallahassee, Florida 32306-4320, USA

Abstract

The influence of pore water flow and diffusive transport on the degradation of labile particular organic matter (POM: *Ulva lactuca* pieces) embedded in permeable sediment was studied in a wave tank. Pore water advection, induced by interaction of wave-driven oscillatory boundary flow and stationary sediment ripples, reproducibly exposed POM buried in the upper 2 cm of the sediment to oxic or anoxic conditions lasting between days and weeks. Planar oxygen optodes and carbon and nitrogen analyses were used to visualise and quantify the degradation rates. Oxygen consumption rates (OCR) were up to 18-times higher at locations of the buried POM compared to the surrounding sediment. Elevated OCR were also detected downstream the POM locations. Despite high permeability of the sediment and exposure to oxygenated pore water flows, suboxic and anoxic sites and suboxic porewater "plumes" developed at and downstream the locations of POM in otherwise oxygenated sediment regions. A large discrepancy between the measured total carbon loss of the *U. lactuca* discs and the carbon consumption calculated from the OCR measurements was observed, suggesting that bacterial degradation of POM and the final degradation of dissolved organic matter (DOM) became spatially decoupled by the porewater flow. Advection thus can enhance the rate of organic mater degradation by efficiently distributing DOM from "hotspots" of organic matter mineralisation to larger volumes of permeable sediments and associated microbial communities.

Introduction

Permeable sediments are abundant in the global continental shelf regions (Emery 1968; de Haas et al. 2002). These non-accumulating sands are generally poor in organic carbon and have been considered long time as relatively inactive habitats that do not contribute substantially to the cycling of organic matter (Boudreau et al. 2001). Recent studies, however, indicate that the low concentration of organics is more likely the result of rapid turnover and high exchange rates (Huettel et al. 1998; Rusch et al. 2003). When the interaction of boundary-layer flow (e. g., unidirectional or oscillatory flow induced by currents and gravity surface waves, respectively) and sediment topography enables dynamic advective porewater flow, the solute exchange at the sediment-water interface can exceed transport by molecular diffusion by several orders of magnitude (Rutgers van der Loeff 1981; Precht and Huettel 2004; Reimers et al. 2004). Advection increases significantly the oxygen penetration depth in sediments (Forster et al. 1996; Lohse et al. 1996; Ziebis et al. 1996a) as well as the transport of organic particles (Huettel et al. 1996; Rusch and Huettel 2000), resulting in enhanced sedimentary oxygen consumption and organic matter degradation (Forster et al. 1996; Ziebis et al. 1996b; Reimers et al. 2004).

The increased degradation activity in advective systems is most likely the result of several factors. Transport of nutrients towards the sedimentary bacteria, which can be the limiting factor under stagnant, diffusive-dominated conditions, is enhanced by fluid motion (van Loosdrecht et al. 1990). Furthermore, efficient directed transport of oxygen and other electron acceptors as well as organic matter from the overlying water to the sedimentary community, combined with fast transport of inhibitory products like ammonia and sulphide out of the sediment, possibly enhances bacterial activity under advection (Ziebis et al. 1996b; Huettel et al. 1998).

The biogeochemical reactions in the sediment and advective transport of organic particles and solutes result in a complex 3-dimensional zonation of oxygen, organic material, nutrients and heavy metals. In contrast to diffusion-dominated sediments, the zonation is highly dynamic, as it is tightly linked to rapidly changing sediment topography and overlaying water flow (Ziebis et al. 1996b; Huettel et al. 1998; Precht et al. 2004). Metabolic activity at the transition between oxic and anoxic zones is considered to be very intensive, especially when they oscillate (Aller 1994; Huettel et al. 1998).

If oxygen consumption due to oxidation of reduced species other than carbon (e. g., H_2S, Fe^{2+}, Mn^{2+} and NH_4^+) can be ignored, benthic oxygen uptake can be used for determining the total sediment remineralisation rates, as oxygen is the key electron acceptor for benthic degradation processes of organic matter (Canfield et al. 1993). In permeable sediments, the oxygen consumption is typically determined by sealable sediment enclosures, wherein natural flow conditions can be mimicked, namely either in flume setups (Forster et al. 1996; Ziebis et al. 1996b) or in diverse benthic chambers applicable for laboratory or in situ use (e.g., Malan and McLachlan 1991; Huettel and Gust 1992; Glud et al. 1996a). Other, more recent approaches include flow-through sediment column systems (Reimers et al. 2004) and the in situ eddy-correlation technique (Berg et al. 2003). By measuring the oxygen consumption integrated over the whole sediment volume affected by oxygenation, none of these methods can give insight into the possibly heterogeneous distribution of oxygen consumption rates (OCR) within the sediment. The only exception is the recently developed flow-trough method (de Beer et al. 2005; Polerecky et al. 2005), which enables the determination of OCR at submillimeter resolution.

The introduction of the planar oxygen optode technique to marine systems (Glud et al. 1996b) allowed to gaining more detailed insights into the oxygen distribution in sediments with high temporal and spatial resolutions, and planar oxygen optodes have been used in diverse applications (Glud et al. 1999; Precht et al. 2004; Wenzhöfer and Glud 2004). Of particular relevance is the flow-through method, where planar oxygen optodes are used to determine 2D maps of OCR with high spatial resolution (Polerecky et al. 2005).

The aim of this study was to assess the spatial variability of aerobic degradation of particular organic matter (POM) buried in permeable sediment, and to investigate possible influences of different transport modes (advective vs. diffusive) on degradation rates. Of particular interest was to identify the means by which advection can enhance the degradation. Experiments were conducted in a wave tank so as to mimic natural conditions. The degradation rates were quantified directly by measuring the carbon and nitrogen content of samples removed from the sediment and indirectly by measuring 2-dimensional distributions of OCR of buried POM samples using planar oxygen optodes.

Material and Methods

Wave tank set-up

Wave tank

Experiments were carried out in a laboratory wave tank (Precht et al. 2004) made of transparent acrylic, with dimensions of the open channel of $520 \times 50 \times 47$ cm ($l \times h \times w$) (Fig. 1A). A section of 120 cm in length located 240 cm downstream of the wave paddle was filled with natural sandy sediment (22 cm deep, volume ~ 124 dm^3). The wave tank was filled with artificial seawater (instant sea^{TM}) with salinity of 32, temperature was kept constant at 17°C.
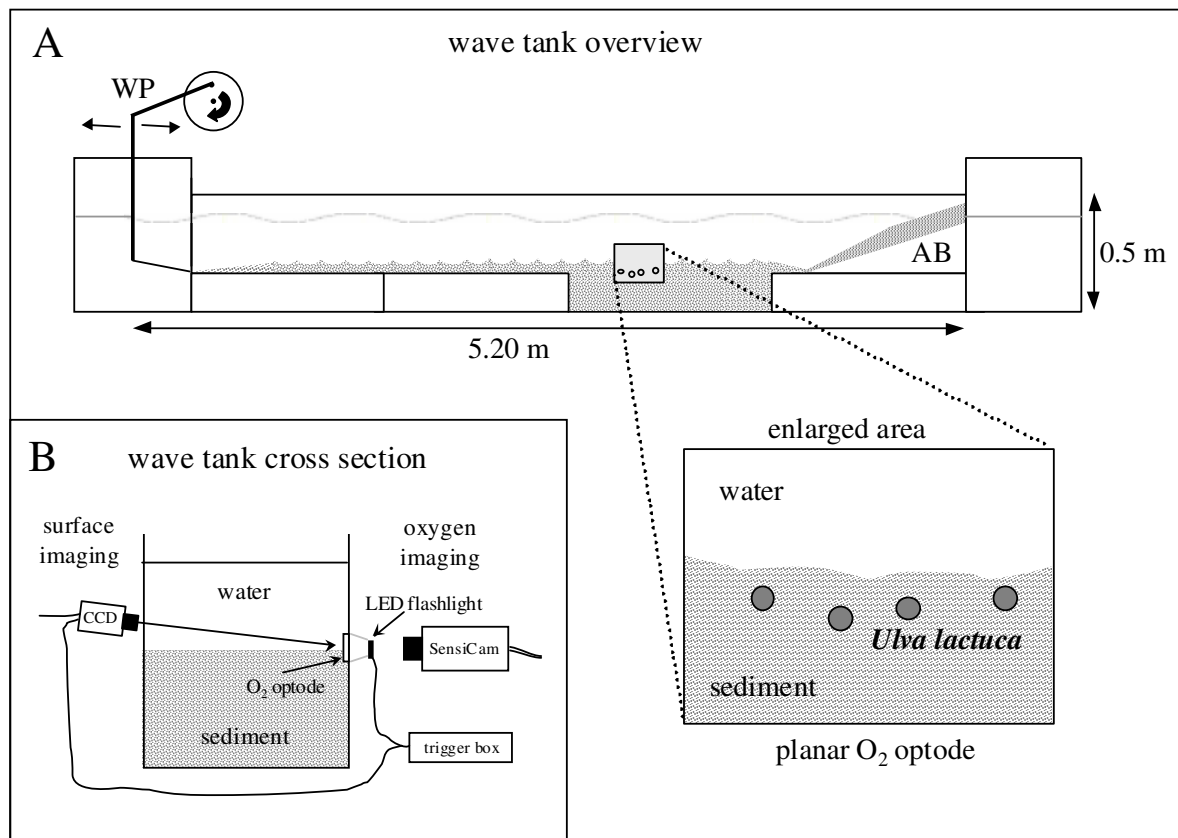
Figure 1: The experimental wave tank setup. A) Overview with locations of circular pieces of *U. lactuca* positioned in the sediment in front of the semi-transparent planar O_2 optode; WP = wave paddle, AB = artificial beach. B) Cross-section of the wave tank showing the setup for the simultaneous sediment surface and oxygen imaging.

The sediment was collected from the intertidal sand flat Hausstrand at Sylt Island in the German North Sea (55°02'N, 08°26'E) in February 2001. The top 2 cm and the deeper part (reaching down to ~ 20 cm) of the sediment were sampled separately and re-combined in the wave tank within 24 h.

Organic carbon (C) and nitrogen (N) contents of the top 5 cm of sediment, analysed using a Fisons NCS 1500 elemental analyzer, were 800 ± 25 (n = 5) and 30 ± 9 (n = 5) µg g^{-1} dry weight, respectively. Porosity, as calculated from the differences between wet and dry weights of sediment, was 35.2 %. Sediment permeability, measured using the constant head method (Klute and Dirksen 1986) was $(1.30 \pm 0.03) \times 10^{-11}$ m^2 (n = 3). The median grain size was 180 µm, as determined by sieving through a set of 8 calibrated sieves after desalination and drying of the sediment.

The sediment was kept under steady, recirculating unidirectional flow (~ 5 cm s^{-1} at 10 cm above the sediment surface) during the first ~ 12 months in order to re-establish natural balance. No nourishment was added during the first 10 months to prevent accumulation of nutrients. At that time infauna consisted mostly of oligochaetes of the Tubificidae family living in the upper ~ 2 cm of the sediment. Over a period of ~ 1 year, extensive advective process studies were conducted, during which food (powdered dried red algae, equivalent to an input of 1 g m^{-2}) was added biweekly to the sediment until three weeks before our experiments, when the nourishment was stopped. During our experiments, neither oligochaetes nor microphytobenthos were present. The top sediment horizon (1 – 3 cm thick) was frequently oxygenated by advection, while the deeper sediment layers remained reduced.

Sinusoidal waves were generated at the upstream end of the wave tank with a wave paddle driven by an electric motor (Fig. 1A). Wave amplitude was regulated by the stroke of an eccentric, while wave frequency could be varied by adjusting the motor speed. With this setup it was possible to generate and maintain either propagating or stationary sediment ripples on the sediment surface. Propagating ripples were produced by adjusting the water level to a height (h) of 19 cm above the sediment surface and the wave amplitude (a) to 7 cm, wavelength (λ) to 70 cm and frequency (f) to 1.25 Hz (settings 1). With these settings, root mean square value of the horizontal velocity directly above the sediment was $U_{RMS} \sim 0.12$ m s^{-1}, as measured with a three-beam DANTEC^{TM} LDA (Laser Doppler Anemometer). When the settings were changed to h = 15 cm, a = 5 cm, $\lambda = 80$ cm and f = 1.1 Hz (settings 2), resulting $U_{RMS} \sim 0.08$ m s^{-1}, the formed ripples remained stationary (Precht et al. 2004).

Two-dimensional (2D) oxygen distributions

2D oxygen distributions were measured with a semi-transparent planar oxygen optode (14 cm wide, 10 cm high) glued to the wave tank wall by transparent silicone (Elastosil® E4, Wacker). The optode consisted of 2 layers: a transparent polyester support foil and a sensing layer composed of 10 mg of fluorophore Platinum(II) meso - tetra (pentafluoro-phenyl) porphyrin (Pt-PFP) (Porphyrin Products), 490 mg Polystyrene (Sigma-Aldrich), 3 ml Chloroform (Merck) and 330 mg titanium dioxide (TiO_2) particles (< 5 µm, Aldrich). The concentration of the Pt-PFP in the cured sensing layer was 1.2 % (w/w), the thickness of the dry sensing layer was approximately 30 µm (see Precht et al. (2004) for details on sensor preparation).

The 2D oxygen measurements were done using the MOLLI system (Holst et al. 1998; Holst and Grunwald 2001) consisting of a fast gateable CCD Camera (SensiCam, PCO), two blue light emitting diodes (LEDs, Luxeon V Star Blue, λ_{max} = 470 nm, Lumileds), a red filter (Amber red, Lee) and a triggering device. The images (640 × 480 pixels) covered an area of 80 × 60 mm, resulting in a spatial resolution of 125 × 125 µm pixel^{-1}. Oxygen concentrations were calculated using the rapid lifetime determination (RLD) method combined with the Stern-Volmer equation, which describes the lifetime quenching by oxygen (Kautsky 1939; Holst et al. 1998).

Images of 0 and 100 % air saturation (AS) were taken before and after the long-term experiments and served as calibration images. The accuracy of the oxygen measurements, determined from 10 subsequent recordings, was between ± 2 % AS and ± 7 % AS in the regions of 0 – 10 % AS and 75 – 100 % AS, respectively. The lower accuracy at higher oxygen concentrations was caused by the weaker luminescence intensity signal, which decreased the signal to noise ratio, as well as by higher sensitivity of the foil's lifetime to changes in oxygen (for the latter effect see p. 220 in Glud et al. (1996)).

2D oxygen consumption rate (OCR) measurements

Oxygen was transported into the sediment by means of wave-induced advective porewater flow caused by flow-topography interactions (Precht et al. 2004). Initial steady state oxygen distributions were achieved by producing waves (using settings 2, see above) in the wave tank for a period of 3 - 5 h. When the waves were stopped, oxygen transport in the sediment was governed by molecular diffusion formally described by the diffusion equation $(\partial c/\partial t) = D_s \Delta c - R$, where $D_s \Delta c$ represents the diffusive transport in the sediment characterised by the diffusion coefficient D_s and $R > 0$ is the local OCR (note that $R < 0$

would describe oxygen production rate) (Crank 1975). The initial oxygen dynamics, $(\partial c/\partial t)_i$, were determined in 2D from oxygen images recorded every 30 s for 50 min after the waves were stopped using the algorithm described by Polerecky et al. (2005). The diffusive term was determined from the initial steady state 2D oxygen distribution, $D_s \Delta c_i$, where the calculation of $\Delta c_i = \partial^2 c_i/\partial x^2 + \partial^2 c_i/\partial y^2$ was based on the 2D Savitzky-Golay smoothing algorithm (Krumm2001:http://research.microsoft.com/users/jckrumm/SavGol/SavGol.htm). The local OCR was evaluated as

$$R = D_s \Delta c_i - (\partial c/\partial t)_i. \tag{1}$$

Since the effect of the wall (planar optode) on the diffusion could not be accurately determined, two effective diffusion coefficients were used to estimate the diffusion term, namely $D_{s1} = (\phi/\theta^2)$ with $D_s = 2.09 \times 10^{-6}$ cm^2 s^{-1} and $D_{s2} = D_w = 1.83 \times 10^{-5}$ cm^2 s^{-1}. D_{s1} was calculated according to Boudreau (1996) taking into account the sediment porosity ($\phi = 35.2$ %) and tortuosity ($\theta^2 = 1 - \ln(\phi^2) = 3.1$). D_w is the diffusion of oxygen in seawater (Salinity: 32; Temperature: 17°C) and was calculated according to Li and Gregory (1974). Image processing necessary for the calculation of the R-images based on Eq. (1) was implemented in Matlab[®].

Sediment topography

The sediment relief was imaged using a second CCD camera mounted on the other side of the wave tank channel (Fig. 1B) and triggered simultaneously with the oxygen imaging camera. The recorded surface images were aligned and superimposed with the oxygen images using Matlab[®] routines.

Particular organic matter

The marine green macroalgae *U. lactuca* (Chlorophycota, Ulvophyceae, "Sea Lettuce") is a very common species in marine coastal environments and produces membranous translucent thalli up to 30 cm across. Samples of *U. lactuca* were provided from the Alfred Wegener Institute for Polar and Marine Research (Helgoland Island), stored in artificial seawater (instant sea[TM], salinity 32, temperature 15°C) under 12 h light/12 h dark conditions. Circular pieces (5 mm diameter, dry weight 900 – 1200 mg) of *U. lactuca* were cut from a fresh large thallus and served as POM in the experiments.

Experimental procedure

Three different degradation scenarios of *U. lactuca* were investigated in the wave tank, each over a total period of 24 days:

Experiment 1: long term oxic conditions maintained by advective porewater transport;

Experiment 2: long term anoxic conditions, transport governed by diffusion;

Experiment 3: alternating oxic-anoxic conditions with periods of 3 days.

Prior to each experiment, ripples were generated at the planar optode (see above). Subsequently, 4 circular pieces of *U. lactuca* were placed directly flat against the optode at a sediment depth of 0.5 – 1.5 cm, preferentially under the ripple troughs (Fig. 1A). The *U. lactuca* discs could be kept under oxic conditions by maintaining advective pore water flow resulting from the interaction of continuous waves (settings 2) and stationary ripples. By stopping the waves, transport became diffusion-dominated and the discs could be kept under anoxic conditions.

In Exp. 1, the *U. lactuca* discs and the sediment surrounding them were kept oxic and under advection-dominated conditions by wave action for 24 days. The exceptions were the five OCR measurements conducted at intervals of 6 days, when the waves were stopped for approx. 1 hour (Tab. 1).

In Exp. 2, *U. lactuca* and the surrounding sediment were maintained under anoxic and diffusion-dominated conditions (no waves) for 24 days. The exceptions were the three OCR measurements performed on days 0, 12 and 24, when the waves (settings 2) were switched on for 4 – 5 h in order to oxygenate the sediment (Tab.1).

In Exp. 3, *U. lactuca* and the surrounding sediment were kept under alternating oxic (advection-dominated) and anoxic (diffusion-dominated) conditions of three days each over a total period of 24 days. OCR measurements were performed every 3 days (Tab. 1).

Table 1: Time-protocols of the three experimental scenarios specifying the conditions of *U. lactuca* and the surrounding sediment before the OCR measurements. Each OCR measurement lasted ~ 1 h. Stars (*) indicate the measurements after which 1 – 2 discs of *U. lactuca* were removed for the carbon and nitrogen analyses.

Exp.	total time of Exp.	intervals between the OCR measurements	number of the OCR measurement	conditions <u>before</u> the OCR measurement
1	24 days	6 days	1	advection: ~ 5 h
			2, 3*, 4, 5*	advection: 143 h
2	24 days	12 days	1	advection: ~ 3 h
			2*, 3*	diffusion: 283 - 284 h , advection: 4 - 5 h
3	24 days	3 days	1	advection: ~ 5 h
			2, 4, 6, 8	advection: 71 h
			3, 5*, 7, 9*	diffusion: 67 - 68 h, advection: 4 - 5 h

Analytical procedures

Plant material

A) Wave tank degradation experiments: After 12 days and at the end (24 d) of each experiment (Tab. 1), 1 - 2 circular pieces of *U. lactuca* were removed from the sediment and dried over night at 60°C. Each disc was cut into 4 pieces and analysed for total carbon and nitrogen content using a Fisons NCS 1500 elemental analyzer. The same procedure was applied to freshly cut *U. lactuca* stored in aerated, artificial seawater in the dark at 17°C, which served as controls.

B) Test tubes DOC experiment: To measure dissolved organic carbon (DOC) in the sediment produced either by *U. lactuca* itself or by the bacterial degradation of *U. lactuca*, *Ulva* discs (5 mm diameter) were placed at the wall of 21 test tubes (10 ml) and covered with ~ 1 cm^3 sterile sediment and 5 ml of artificial non-sterile seawater (salinity 32). Test tubes without algae addition served as controls. Every third day, *U. lactuca* discs were removed from 3 test tubes. The sediment was mixed by a vortex shaker and allowed to settle for 5 min. The water was decanted into a 10 ml syringe, filtered through a nylon

filter (Millex-GN Filter Unit, Millipore, pore size 0.2 µm) and kept frozen at - 20°C until analysis. The DOC analysis was conducted using a Shimadzu TOC-5050A total organic carbon analyzer, which determines the total dissolved carbon (TDC) and dissolved inorganic carbon (DIC). DOC was calculated by subtracting DIC from TDC.

Calculations of consumed carbon from OCR

To assess the amount of carbon mineralised during the wave tank experiments, the following procedure was performed. Firstly, the measured OCR was converted into carbon mineralisation rate (CMR) according to Florek and Rowe (1983) as

$$CMR \text{ (ng cm}^{-3} \text{ day}^{-1}) = OCR \text{ (ng cm}^{-3} \text{ day}^{-1}) \times 12/32 \times RQ, \qquad (2)$$

assuming a simplified reaction $CH_2O + O_2 \rightarrow CO_2 + H_2O$ for the organic matter degradation and a respiratory quotient (RQ) of 0.85 (Rowe et al. 1994). The factor 12/32 takes into account the carbon/oxygen molar weight ratio.

Secondly, it was assumed that the measured OCR at locations of the *Ulva* discs expanded over a half sphere of the disc diameter into the sediment (volume 0.033 cm^3). The total rate of mineralised carbon per disc of *U. lactuca* (ng disc^{-1}) was therefore obtained by multiplying the CMR in Eq. (2) by the volume 0.033 cm^3. As *U. lactuca* consists of only 2 cell layers and is only ~150 µm thick (Bobin-Dubigeon et al. 1997), this was a conservative estimate. The OCR of the sediment in central areas under ripple troughs were treated with the same procedure to allow for direct comparison with the CMR at the *Ulva* locations.

Thirdly, the temporal decrease of the calculated CMR was fitted with an exponential decay function and integrated over 24 days, resulting in the total amount of carbon mineralised over the experimental period. In Exp. 2 and 3, all OCR values measured after the prolonged anoxic (diffusion-dominated) degradation periods were additionally divided by a factor of 2. This was done because re-oxidation reactions of reduced inorganic substances, contributing to the measured OCR, were assumed to be equal to the biological oxygen respiration (Jørgensen 1982). Furthermore, it was assumed that this corrected OCR represented the anaerobic degradation rate during periods of anoxia.

Results

Sediment topography

   Due to the wave action, the sediment compacted and the ripples gradually flattened (see e.g. Figs. 2B, 2D and 3). These topography changes were, however, insignificant, except during the first 12 days of Exp. 1. Ripple wavelengths varied between 2 and 4 cm, ripple amplitudes between 0.1 and 0.4 cm (Tab. 2).

Table 2: Summary of the ripple wavelengths, ripple amplitudes and typical maximum oxygen penetration depths during the experiments.

Exp.	ripple wavelengths	ripple amplitudes	typical oxygen penetration depths under	
			advection	diffusion
1	2.5 - 4.0 cm	0.1 - 0.4 cm	1.3 - 2.4 cm	0.5 – 0.7 cm
2	1.4 - 2.5 cm	0.1 - 0.3 cm	0.5 - 1.8 cm	0.5 – 0.7 cm
3	~ 2.7 cm	0.2 - 0.4 cm	1.8 - 2.0 cm	0.5 – 0.7 cm

Steady state oxygen distributions

   Examples of steady state oxygen distributions, which were maintained under long term advective conditions in Exp. 1 and 3 and long term diffusive conditions in Exp. 2 and 3 (see Tab. 1) are shown in Figs. 2A-B and 2C, respectively. The streamlines indicating the pore water flow field in the figures were estimated according to Shum and Sundby (1996). Under advection, characteristic undulating patterns of oxygen rich porewater under ripple troughs and oxygen depleted porewater upwelling from deeper sediment layers under ripple crests developed (Precht et al. 2004). Oxygen penetration was enhanced under ripple troughs (0.5 – 2.4 cm) and strong vertical as well as horizontal oxygen gradients developed. When diffusive conditions lasted for more than 4 h, oxygen was completely consumed in deeper sediment layers and its penetration was limited to the top 0.5 – 0.7 cm (Tab. 2).

   Figures 2C and 2D demonstrate that steady local zones of reduced oxygen concentrations developed at as well as in the sediment downstream from the locations of the *U. lactuca* discs. This was caused by the enhanced oxygen consumption at the *Ulva* discs, which was comparable in magnitude to the advective oxygen supply. In contrast, no such oxygen-reduced zones were observed in the surrounding sediment, where the oxygen consumption was relatively low.
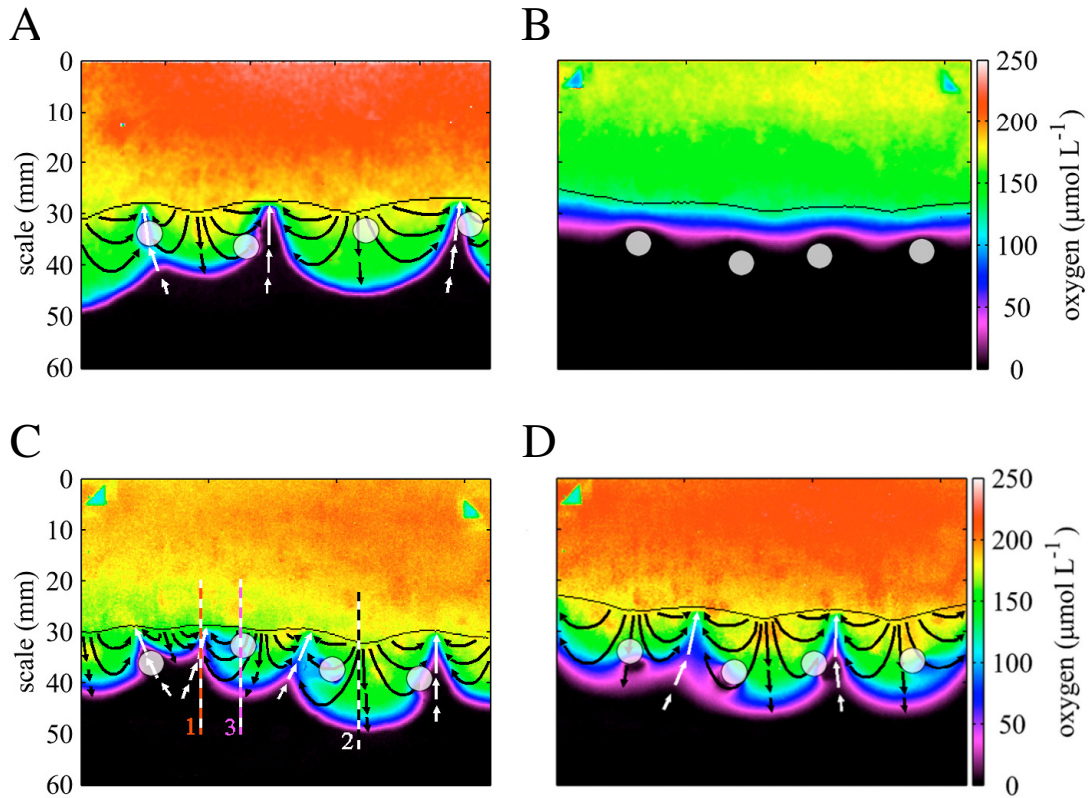
Figure 2: Typical steady state oxygen distributions during the long-term degradation experiments under oxic (A) and anoxic (B) conditions. Steady state oxygen distributions prior to OCR measurements in Exp. 1, 2 and 3 are shown in panels A, C and D, respectively. Circles show the positions of *U. lactuca* discs, black lines the sediment surface and the arrows indicate the approximate streamlines of the porewater flow estimated according to Shum and Sundby (1996) Vertical lines in panel C indicate three selected sediment regions from which vertical oxygen profiles were extracted and plotted as a function of time in Fig. 3.

Oxygen dynamics

To illustrate the qualitatively different dynamic behaviour of oxygen distributions and penetration depths in the sediment under advective and diffusive conditions, selected vertical oxygen profiles were plotted as a function of time (Fig. 3). Below ripple crests (Fig. 3A), anoxic porewater was initially driven towards the sediment surface after the transition from diffusion- to advection-dominated conditions. It became gradually mixed with oxygen rich porewater coming from the ripple flank, resulting in a slow increase of the oxygen penetration depth. Due to the absence of advection-driven upwelling of anoxic porewater after the waves were stopped, diffusion could deliver oxygen deeper into the sediment. Below ripple troughs (Fig. 3B), oxygen was pushed rapidly deeper into the sediment during advection, whereas oxygen penetration slowly decreased during diffusion.
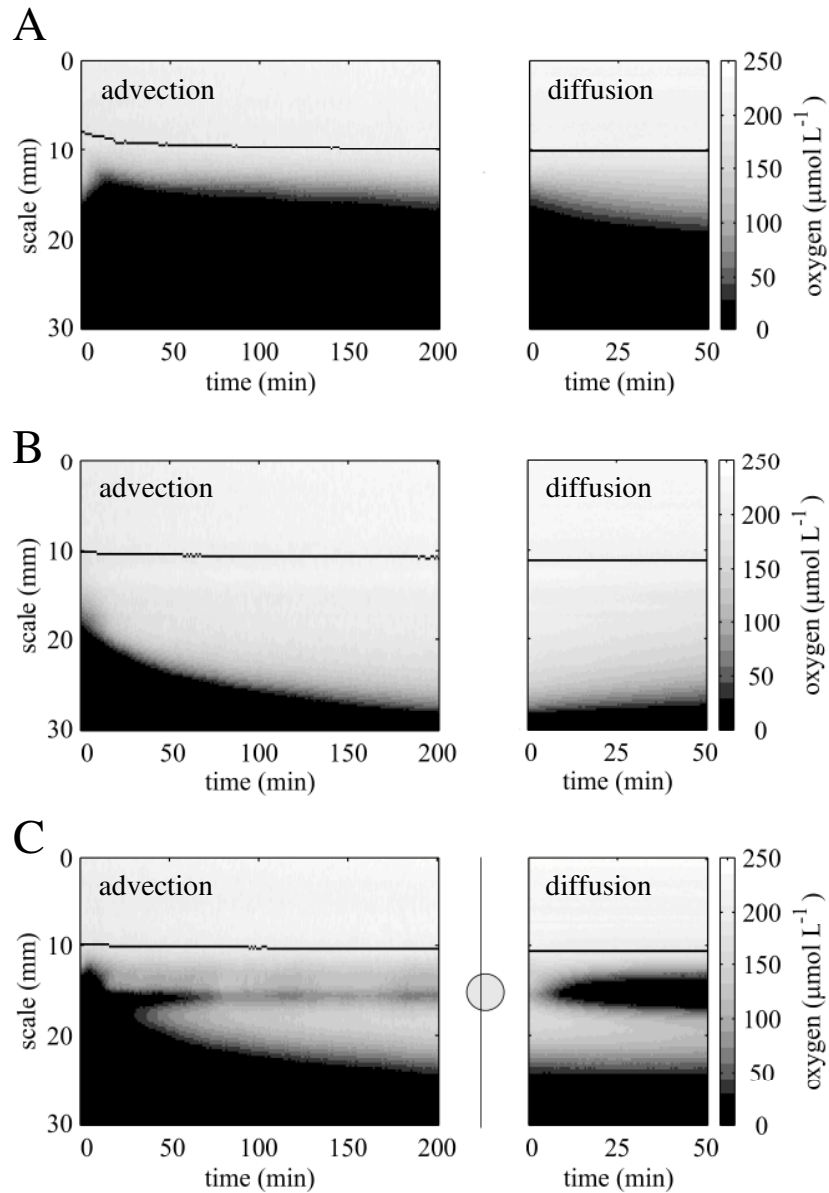
Figure 3: Typical time evolutions of selected vertical oxygen profiles under advection- and diffusion-dominated transport. The positions of the profiles in panels A, B and C are indicated in Figure 2C by the vertical lines 1, 3 and 2, respectively. The circle and the vertical line in panel (C) indicate the location of the *U. lactuca* disc in the sediment and the relative position of the extracted profile with respect to *Ulva*, respectively. The black horizontal lines show the sediment surface. The grey-scale was adjusted so as to enhance the contrast at lower oxygen concentrations. Note that the widths of the figures are not to scale.

The situation was qualitatively different when *U. lactuca* was present under a ripple trough (Fig. 3C). After the transition from diffusion- to advection-dominated conditions, the initial rapid advection-driven transport of oxygen into the sediment was temporally stopped after ~ 20 min at the position of the *Ulva* disc. This was caused by the elevated oxygen consumption that exceeded the mainly downward advective supply. Due to the 3D character of the porewater flow, oxygen was gradually transported below the *U. lactuca* disc from the surrounding sediment. However, a local suboxic region (< 70 µmol L^{-1}) remained at the position of the *U. lactuca* disc during the entire advective period. After the waves were stopped, the removal of oxygen was considerably faster at the location of the *U. lactuca* disc, where anoxia was reached within $15 - 70$ min, depending on the experiment. The presence of *Ulva* resulted in reversed oxygen gradients in deeper sediment during both advective and diffusive conditions.

The oxygen dynamics under advective and diffusive conditions are more clearly demonstrated in movies that can be found in the folder "Chapter-4-Movies" on a CD-Rom, which can be made available upon request (contact: Ulrich Franke, Ostarastr. 5, 51107 Köln, e-mail: u.franke@fab-anlagenbau.com). The movies show the development of steady state oxygen distribution beneath stationary sediment ripples after the *U. lactuca* discs were placed in the sediment and the waves were switched on (corresponding to Fig. 3C), as well as the oxygen dynamics after the waves were stopped.

2D OCR measurements

The effect of diffusion on the calculation of the 2D OCR distribution based on Eq. (1) is demonstrated in Fig. 4. Regions of oxygen increase ($(\partial c/\partial t)_i > 0$) can be seen in the up-welling regions of the $(\partial c/\partial t)_i$ image (Fig. 4A). As oxygen production due to photosynthetic organisms could be excluded, this must have been caused by diffusion. This is confirmed by the positive values in the upwelling regions of the $D_{s2} \Delta c_i$ image shown in Fig. 4B. When the lower diffusion coefficient (D_{s1}) was used to evaluate the diffusion contribution, the OCR image (Fig. 4C) calculated from Eq. (1) differed only slightly from the $(\partial c/\partial t)_i$ image, and the areas of apparent oxygen production could still be observed. By using the free water diffusion coefficient ($D_{s2} = D_w$), the apparent zones of oxygen production in the $(\partial c/\partial t)_i$ image were removed, but new oxygen production areas "emerged" in the OCR-image in the regions where the $(\partial c/\partial t)_i$ values were low, e.g., under ripple troughs and in ripple flanks (Fig. 4D). This suggested that the correct diffusion coefficient describing diffusion at the wall should probably lie between D_{s1} and

D_{s2}. Another possibility would be that the Δc_i image was not calculated satisfactorily in all pixels. In particular, due to the noise of the oxygen image, heavy smoothing (2D Savitzky-Golay Filter, polynomial of order 3, patch size of 17 x 17 pixels) had to be applied, which could have lowered Δc_i in pixels where oxygen gradients varied abruptly. The Δc_i values could also be artificially increased in areas with high oxygen concentrations, where the noise is larger, leading to the artefacts under ripple troughs.
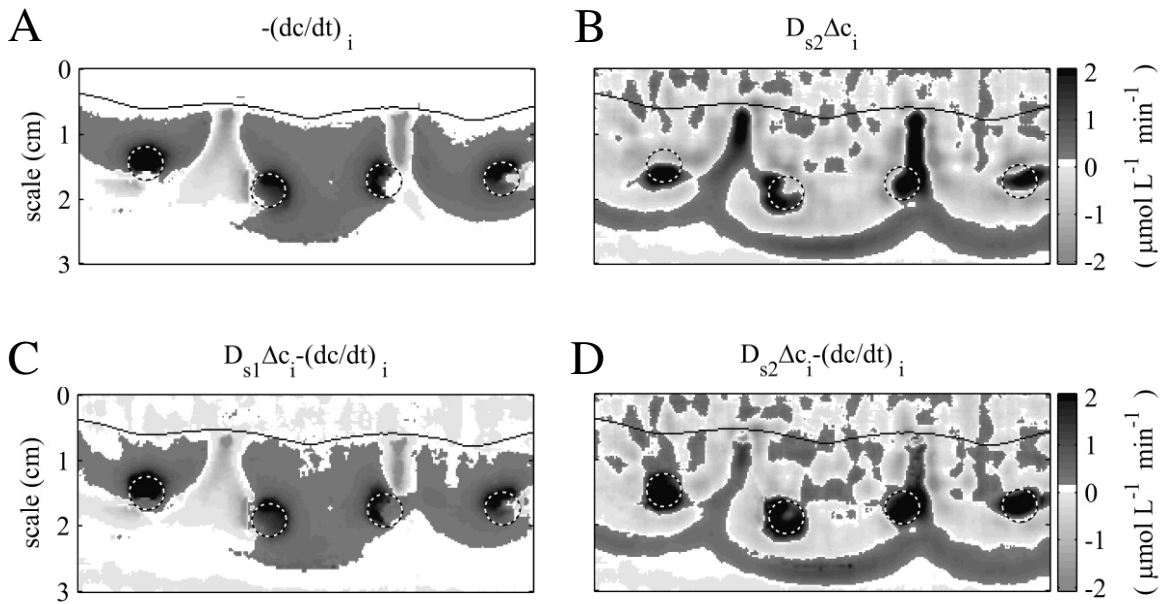
Figure 4: Comparison between the OCR images obtained without (A) and with the diffusion correction using the diffusion coefficient D_{s1} (C) and D_{s2} (D). The diffusion correction using D_{s2} is shown in (B). The images were cropped from the original size images (e.g., Fig.5). The black line indicates the sediment surface, circles indicate the positions of *U. lactuca*. Negative values represent oxygen production, whereas oxygen consumption is represented by positive values.

Table 3 shows that the systematic error introduced to the OCR values at the locations of *U. lactuca* discs by not including the diffusion-correction, i.e., by calculating the OCR image from $R = - (\partial c / \partial t)_i$, did not exceed $10 - 15$ %. Since the initial 2D oxygen distributions of the OCR measurements were very similar for each experiment (data not shown), this inaccuracy was the same for each calculated OCR image. Because the underestimation of the OCR values by maximum of $10 - 15$ % does not influence the main conclusions of our study, only the diffusion uncorrected OCR values ($R = - (\partial c / \partial t)_i$) will be presented below.

Table 3: OCR values (in µmol L^{-1} min^{-1}) averaged over selected *U. lactuca* discs (~ 5 mm diameter), calculated without (column 2) and with (columns 3 and 4) the diffusion correction. The standard deviations indicate the variability of the OCR values within the averaged area.

experiment	$R = - (\partial c / \partial t)_i$	equation (1) using D_{s1}	equation (1) using D_{s2}
1	4.5 ± 1.8	4.9 ± 2.3	5.1 ± 2.4
2	5.8 ± 3.0	5.9 ± 3.6	6.1 ± 4.0
3	2.9 ± 1.2	3.0 ± 1.7	3.2 ± 2.5

Typical OCR images are shown in Fig. 5. The positions of *U. lactuca* discs were clearly visible as areas of significantly elevated OCR values compared to the surrounding sediment. These areas were slightly larger (7.1 – 8.8 mm in diameter) than the actual size of the *U. lactuca* discs (5 mm in diameter). When the *Ulva* discs were removed (day 12 of the experiments), the regions of increased OCR disappeared (Fig. 5D). Peak sediment OCR values appeared at the transition zones between the oxic and anoxic sediment areas as well as close to *U. lactuca* discs. Lowest sediment OCRs were measured in the central areas of ripple troughs.

The OCR values were averaged over circular areas (5 mm diameter) either at locations of *U. lactuca* or in the central area under the ripple troughs for all conducted OCR measurements summarised in Tab. 1, and are shown in Fig. 6. OCR generally decreased during the experimental period of 24 d, most noticeably at and around the *U. lactuca* discs, where the oxygen consumption was initially highest.

At the locations of *U. lactuca* discs, OCR decreased exponentially (from ~ 4.5 to ~ 1.0 µmol L^{-1} min^{-1}) under long term oxic conditions (Exp. 1), whereas the values changed only slightly (from ~ 5.6 to ~ 5.0 µmol L^{-1} min^{-1}) when the degradation took place during prolonged anoxic conditions (Exp. 2). In Exp. 3, OCR decreased rapidly and increased slightly when the *Ulvas* were exposed to oxic and anoxic conditions, respectively. The overall decrease of OCR in this experiment was approx. exponential (from ~ 3.0 to ~ 0.5 µmol L^{-1} min^{-1}), as shown in Fig. 6A.

In contrast, only a minor decrease (from 0.22 – 0.29 to 0.15 – 0.25 µmol L^{-1} min^{-1}) in the sedimentary OCR was observed during 24 d of the experiments (Fig. 6B). The values were approx. 10 – 20 times lower than those at positions of *Ulvas* at the beginning of each experiment or during the entire Exp. 2. At the end of experiments with prolonged oxic

conditions (Exp. 1 and 3), the sediment values were only around 2 – 3 times smaller than the OCR at locations of *U. lactuca* discs.
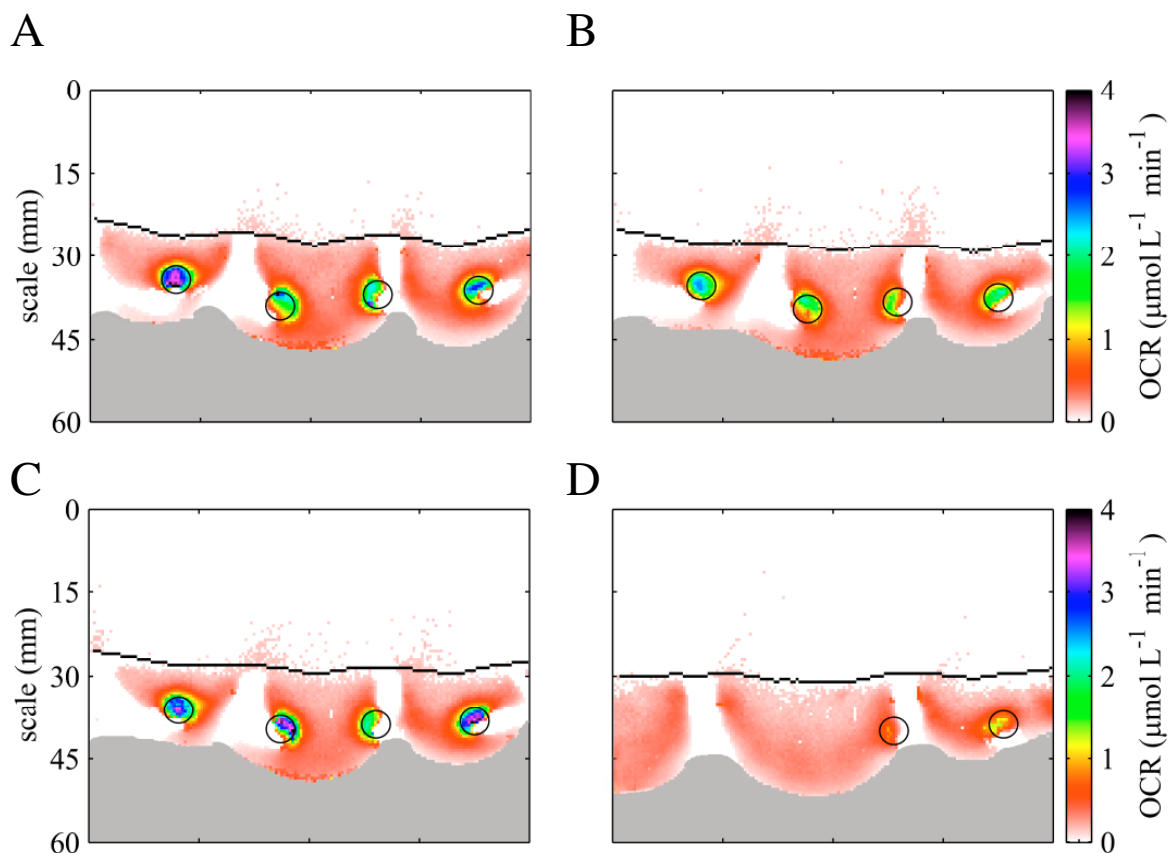

Figure 5: Typical examples of the calculated OCR images. Images A, B, C and D correspond to the OCR measurement number 1 (day 0), 2 (day 3), 3 (day 6) and 6 (day 15) of Exp. 3, respectively (see Table 1). OCR values are expressed per volume of porewater. Black horizontal lines indicate the sediment surface and circles show the locations of *U. lactuca* discs. Grey regions indicate deep sediment areas where no $(\partial c / \partial t)_i$ was measurable due to the lack of oxygen, whereas white regions in the sediment correspond to areas with $(\partial c / \partial t)_i > 0$.

Ulva lactuca analyses

Neither discs of *U. lactuca* taken out of the wave tank sediment for analysis after 12 and 24 days, nor the *U. lactuca* pieces from the test tubes experiment, nor the controls stored in non-sterile artificial seawater changed significantly their appearance during the experiments and all looked intact and greenish.

A) Wave tank degradation experiment: Carbon (C) and nitrogen (N) contents of *U. lactuca* varied considerably in all experiments. Carbon values ranged from 204 to

531 mg C g^{-1} dry weight (dw) with standard deviations (SD) of 30 – 112 mg C g^{-1} dw (n = 4). Nitrogen content of single discs varied between 9 – 26 µg N g^{-1} dw, SD = 1 – 4 µg N g^{-1} dw (n = 4). In all experiments, the total amounts of carbon and nitrogen per disc decreased significantly over 24 days for both *U. lactuca* discs buried in the sediment (Tab. 4, column 2) and the controls (data not shown). The remaining amounts, expressed relative to the initial values, are shown in Figure 7. Data demonstrate significantly enhanced degradation of *Ulva* buried in the sediment compared to the controls, however no differences between Exp. 1 – 3 were observed.

B) Test tubes DOC experiment: TDC and DIC concentrations in the test tubes with and without (control) *U. lactuca* were generally low (Fig. 8). Even though both TDC and DIC concentrations where higher and slightly increased in tubes containing pieces of *Ulvas*, the DOC concentrations were the same and remained constant during 18 days. Consequently, the increase in TDC was entirely due to the increase in DIC. Subtracting the DIC concentrations of controls from those of test tubes with *Ulvas* and fitting the results with a linear model (dotted line in Fig. 8B), the carbon turnover of 1.13 ng C per disc of *U. lactuca* (volume of 0.033 cm^{-3}) in 24 days was determined.
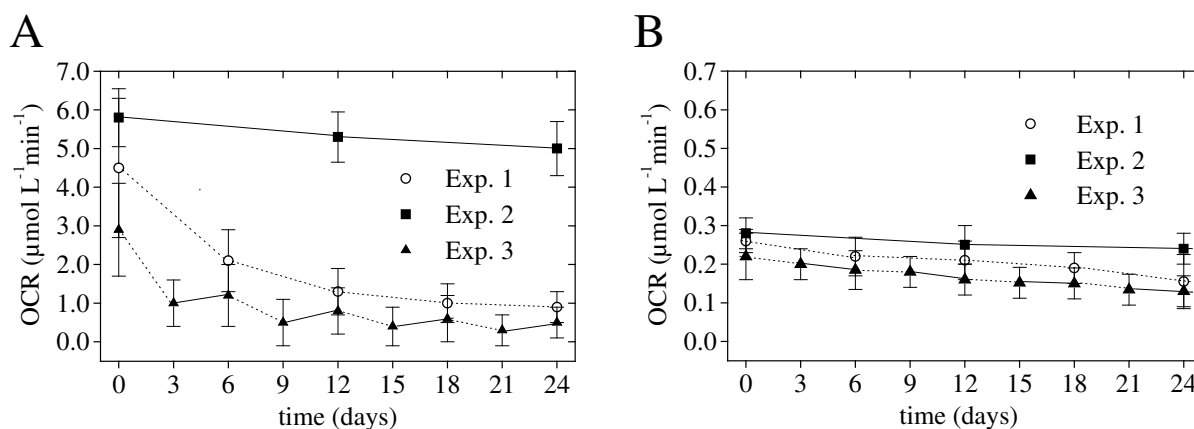
Figure 6: OCR values averaged over circular areas (5 mm diameter) at locations of *U. lactuca* (A) and in the central area under the ripple troughs (B). Error bars indicate the variability of the OCR over the averaged area. Solid and dotted lines represent the long-term anoxic and oxic periods preceding the OCR measurements, respectively. Note different scaling of graphs (A) and (B).

Table 4: Total carbon loss of *U. lactuca* derived from the C/N analysis and the OCR measurements during 24 days. Results were corrected for sediment porosity.

Exp.	C/N analysis (µg C / disc)	OCR measurements position of *U. lactuca* (µg C / 0.033 cm³)	OCR measurements *sediment* (µg C / 0.033 cm³)	equivalent sediment volume (cm³)
1	~ 250 (100 %)	~ 7.36 (3 %)	~ 0.83	~ 9.6
2	~ 150 (100 %)	~ 11.78 (8 %)	~ 1.15	~ 3.9
3	~ 200 (100 %)	~ 3.38 (2 %)	~ 0.68	~ 9.5

Calculations of consumed carbon

Total carbon loss derived from the OCR measurements (using Eq. (2) and data in Fig. 6A) accounted for no more than 8 % of the mineralised carbon determined from the C/N analysis (Tab. 4). This suggested that the main part of organic carbon originating from the *U. lactuca* discs was degraded in the surrounding sediment or in the overlying water. The CMR values of the surrounding sediment under ripple troughs were used to estimate the POM-free sediment volume needed to account for this difference (Tab. 4, column 5). The corresponding sediment volumes were approx. 100 – 300 times larger than the assumed effective volume of *Ulva* discs (0.033 cm³).
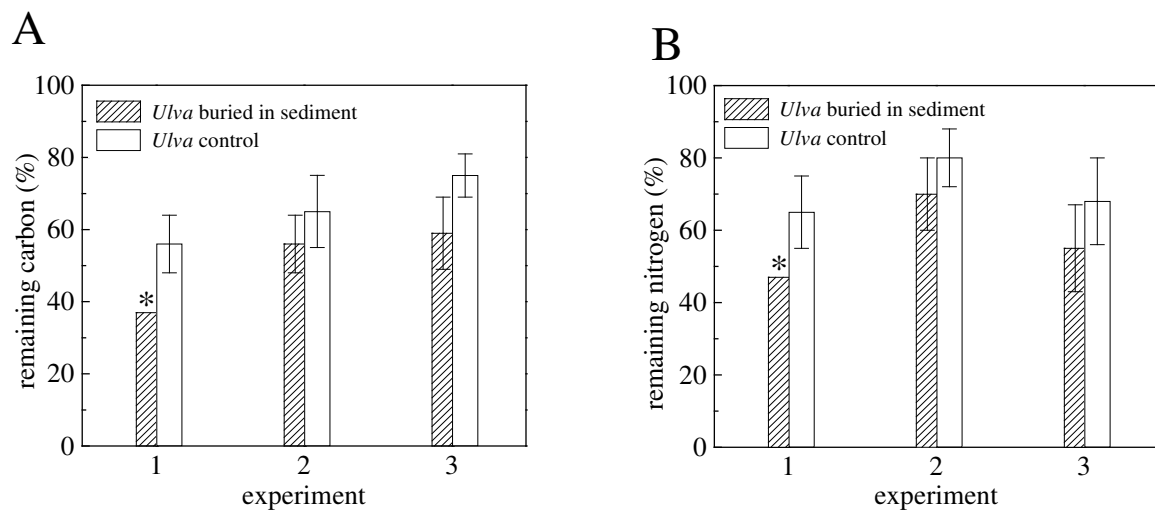
Figure 7: Remaining carbon (A) and nitrogen (B) contents of *U. lactuca* discs after 24 days of experiments expressed as a percentage of the initial values. Error bars were calculated from n = 2 samples, except for Exp. 1 (*) where one *U. lactuca* disc disappeared due to ripple migration.
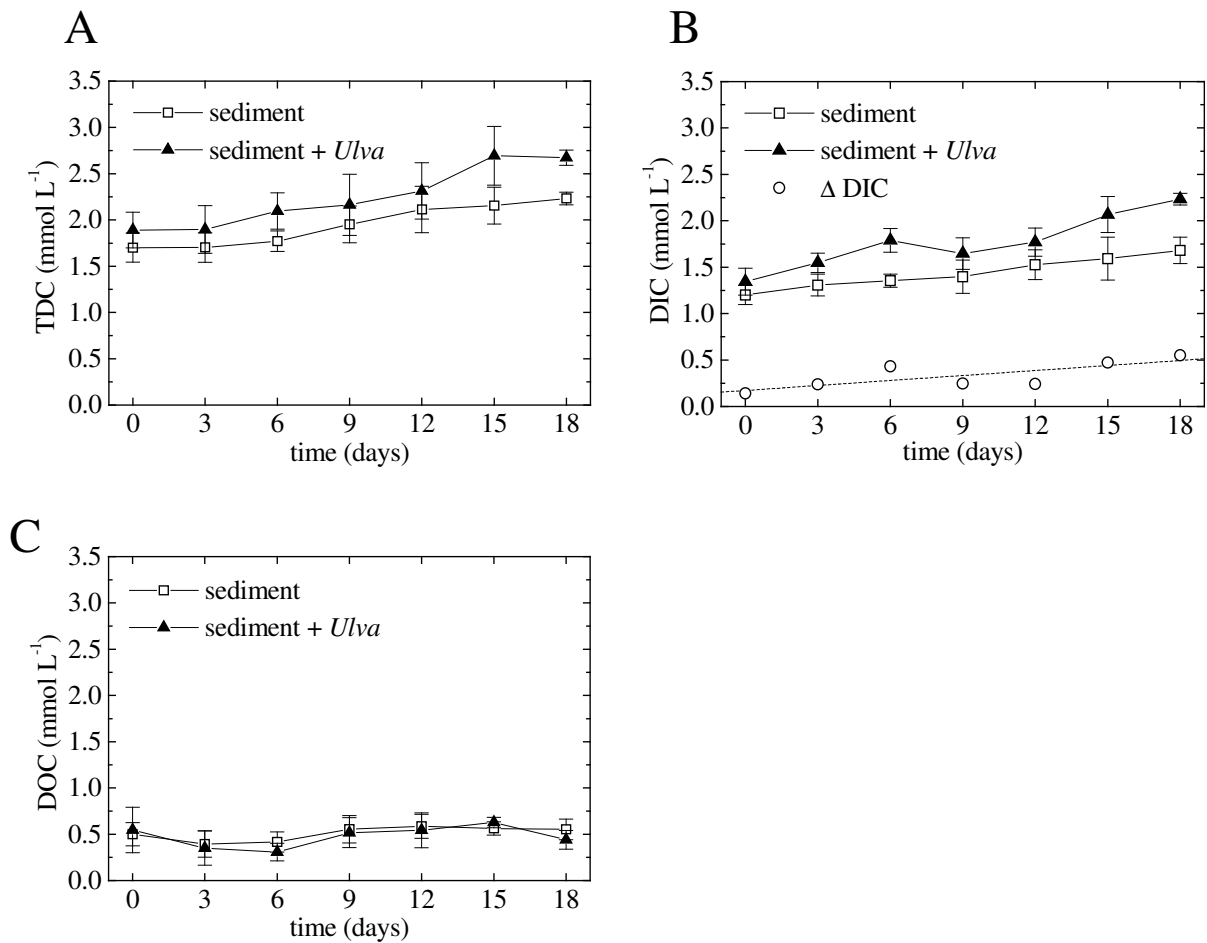
A

B

C

Figure 8: TDC (A), DIC (B) and DOC = TDC – DIC (C) concentrations as a function of time in a test tube experiment. Δ DIC denotes the difference between the DIC concentrations with and without *U. lactuca.* Standard deviations were calculated from n = 4 samples.

Discussion

In a previous study Precht et al. (2004) showed that advection caused by the interaction of wave-driven oscillatory flow and sediment topography creates alternating patterns of oxic and anoxic regions under ripple troughs and crests, respectively. These regions vary dynamically and may thus influence the conditions (either aerobic or anaerobic) of the organic matter degradation. By determining the total oxygen uptake (TOU) of the sediment using sealable flume-channels and chamber setups, "hotspots" of organic matter degradation within the sediment and their temporal development cannot be determined

because the measured signal is integrated over the whole sediment volume during a limited period of time. Here we present a technique where this lack of spatial and temporal resolutions is overcome and natural conditions are mimicked.

Labile POM in permeable sediments: "Hotspots" of degradation

Overlying water rich in oxygen, which is forced by advection into the sediment, becomes depleted in oxygen on its way through the sediment. The rate of depletion is determined by the porewater velocities and the local volumetric OCR. When the porewater velocities were high enough to transport quantities of oxygen exceeding by far the oxygen loss due to the OCRs in the sediment upstream and at *U. lactuca* discs, no significant change in the oxygen concentration in the vicinity of *U. lactuca* was measurable (see Fig. 2A). In contrast, when the OCR at the *U. lactuca* discs was high, porewater became depleted in oxygen, while passing across the *U. lactuca* discs, creating suboxic or anoxic sites in otherwise oxygenated sediment (Figs. 2C-D). The development of these anoxic sites in permeable sediment is the expression of intense degradation of particular organic matter (POM). This was observed also on a larger scale when large amounts of green algae were buried in permeable sediments and "black spots" developed at the sediment surface (Neira and Rackemann 1996).

During macrophyte decomposition, initially rapid leaching and dissolution of soluble materials associated with autolysis of cells occurs (Andersen and Hargrave 1984; Morand and Briand 1999). Then the labile macromolecules of POM are transformed into dissolved matter (DOM) by slower, bacteria-mediated decomposition using exoenzymes (Fenchel et al. 1998). In the last phase, recalcitrant, structural carbon, e. g., cellulose or hemicellulose, are degraded at very slow rates (Castaldelli et al. 2003). This gradual decrease of organic matter degradation rate was confirmed by our OCR measurements, namely by the exponential decrease of the observed OCR when *Ulvas* were exposed to prolonged oxic conditions. The last phase with the slow degradation rates occurred after 6 – 12 days. Similar decay pattern was found by Kristensen et al. (1995) and Kristensen and Holmer (2001). In contrast, due to the insufficient number of time points (limited by number of samples), the exponential decrease of the degradation rate of organic carbon and nitrogen of the *U. lactuca* could not be confirmed directly by the C/N-analysis.

During anoxic conditions, anaerobically produced inorganic compounds could accumulate in the diffusive distance from locations where the degradation took place. When oxygen is transported into the sediment by advection, not only the aerobic organisms

but also the reduced inorganic compounds (e. g., H_2S, Fe^{2+}, Mn^{2+}, and NH_4^+), which can be oxidised biologically and chemically, contribute to the OCR. In coastal sediments the rates of these reoxidation reactions are considered to be equal to (Jørgensen 1982) or even higher (Canfield et al. 1993) than the biological oxygen respiration rates. The accumulation of reduced inorganic compounds could be responsible for the persistently high and increasing OCR at positions of POM observed after prolonged anoxic conditions (Fig. 6, symbols connected by solid lines).

Generally, anaerobic degradation of fresh and labile organic matter can be as rapid as aerobic decomposition (e. g., Hulthe et al. 1998; Kristensen 2000), and oscillating oxic and anoxic periods could enhance organic matter degradation (Aller 1994). In our experiments, oxic and anoxic degradation conditions were induced by creating or stopping advective porewater flow, respectively. This changed not only the availability of oxygen but also the main transport mechanism of solutes. Advection is expected to enhance mineralisation of organic matter (Forster et al. 1996; Shum and Sundby 1996; Reimers et al. 2004). Not only oxygen is transported deep into the sediment (Forster et al. 1996; Lohse et al. 1996; Ziebis et al. 1996b), providing aerobic bacteria with the most favourable electron acceptor, but also inhibitory products like ammonia and sulphide as well as remnants of organic matter mineralisation are transported out of the sediment (Gehlen et al. 1995; Ziebis et al. 1996a; Huettel et al. 1998). Additionally, the transport rate of the electron-acceptors and/or substrate, which is often the limiting factor for bacteria attached to surfaces (e.g., sand grains or organic matter; (Rusch et al. 2003)), can be enhanced by fluid motion (van Loosdrecht et al. 1990). In our experiments, a large loss of carbon (up to 67 % of initial contents) and nitrogen (up to 53 % of initial contents) of *U. lactuca* buried in the sediment was detected. However, the highly variable C/N data did not reveal any significant differences between the amounts of carbon and nitrogen of the *U. lactuca* mineralised during prolonged oxic, anoxic and alternating oxic-anoxic conditions.

Decoupling of POM and DOM degradation in permeable sediments

When the main degradation of particular organic matter is accomplished by bacteria, POM is first converted into dissolved organic matter (DOM) (Fenchel et al. 1998). DOM is usually produced much faster by the bacteria attached to organic matter than it is consumed (Vetter et al. 1998). It was shown that DOM concentrations in porewater of surface sediments can be up to an order of magnitude higher than those in the overlying water (Chen et al. 1993; Martin and McCorkle 1993). In cohesive sediments the diffusive DOM

flux out of the sediment was found to be up to 10 % of the depth integrated sediment carbon degradation (Burdige and Homstead 1994; Alperin et al. 1999; Hee et al. 2001).

In our experiments, the organic carbon loss of the buried *U. lactuca*, determined directly by C/N analysis, was much higher than the carbon loss derived from the OCR measurements at the locations of the *U. lactuca* (Tab. 4). We explain this discrepancy by spatial decoupling of POM and DOM degradation due to advection driven porewater flow. This scenario is supported by the elevated OCR measured in the sediment downstream the positions of the *U. lactuca* discs (Fig. 5). The increased OCR in these zones was not visible when mainly diffusive conditions prevailed (Exp. 2, OCR-data not shown). Since the increase of OCR downstream of the *Ulva* pieces was relatively small and the zones were located within steep gradients of oxygen, the elevated OCR could be enhanced by the diffusion effect mentioned above (Fig. 4).

As opposed to the diffusive system, where the transport of DOM is slow, DOM in permeable sediments can be transported much more efficiently and spread over larger volumes of sediment. Consequently, the degraded POM will nourish more bacteria, and can thus result in a faster organic matter turnover. The volume of the affected sediment will depend on the porewater flow velocity and its direction, the abundance of bacteria living in the sediment and their ability to use the DOM as well as the adsorption of the DOM to sediment particles. We estimated this volume to be approx. 100 – 300 times the effective volume influenced by diffusion (Tab. 4). When the organic matter is located close to the sediment surface, the sedimentary produced DOM could be transported out of the sediment and remineralised in the overlying water.

This highlights a major difference between permeable and cohesive sediments (Fig. 9). In permeable sediments advection not only efficiently provides oxygen for aerobic degradation in the sediment, but also decouples POM and DOM degradation as well as enhances the transport of nutrients and labile DOM. In contrast, in cohesive sediments the locations of POM and the final degradation of DOM are more tightly linked because of the slow diffusive transport, with bioirrigation as an exception.

Variable influence of buried POM on carbon cycling under natural conditions

In natural environments, permeable sediments are abundant in the global continental shelf regions (Emery 1968; de Haas et al. 2002). Sediment surfaces down to water depths of >100 m can be reached by wave-induced boundary flows (Wiberg and Harris 1994; Harris and Wiberg 2001). Under natural conditions, sediment ripples develop when the boundary flow is sufficiently high. Even when the flow weakens and the ripples become

stationary, e. g., after storm events, the sediment is affected over extended time periods by advection. This "memory effect" (Precht et al. 2004) can result in a temporally stable 3-dimensional biogeochemical zonation. In the oxic/anoxic transition zone under ripple crests in the close vicinity to upwelling zones, bacteria could grow preferentially, because of "easy" access to oxygen, nutrients and DOM.
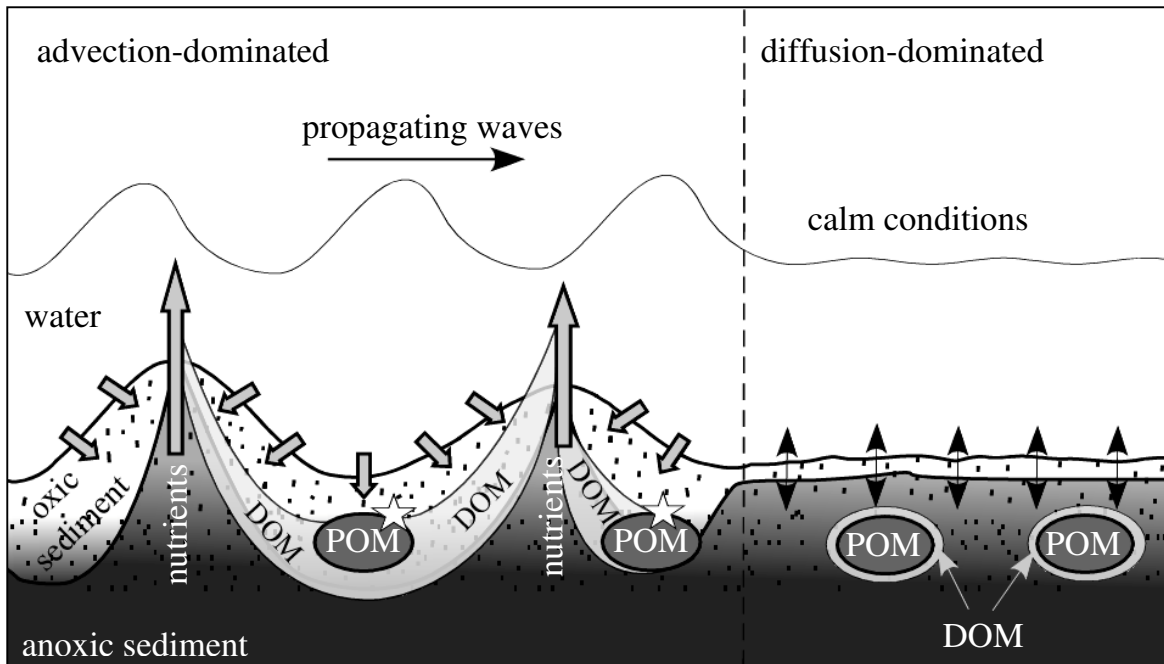

Figure 9: Scheme of POM degradation in permeable sediment under advective and diffusive conditions. *Advection-dominated conditions*: Interaction of oscillatory boundary layer flow and sediment topography results in advective porewater flow. Oxygen-rich surface water is forced deep into the sediment under ripple troughs, wheras anoxic water from deeper sediment horizons leaves the sediment at ripple crests. Bacteria-mediated aerobic degradation of labile particular organic matter (POM) is enhanced (☆) in the the advection affected sediment horizon (up to several cm in depth) by oxygen supply combined with transport of inhibiting products and remnants of organic matter degradation out of the sediment. Highly enhanced degradation activity can result in anoxic or suboxic (mirco) sites in oxygenated sediment. The pore water flow can spatially decouple POM and the final DOM degradation, whereby bacteria in a larger sediment volume could be nourished. DOM can even be transported out of the sediment. *Diffusion-dominated conditions*: during calm weather conditions transport processes are predominantly governed by diffusion. Degradation of buried POM is mainly driven by anaerobic bacteria as only a thin oxic surface layer (commonly a few mm) covers the anoxic sediment. Bacterial degradation activity can become diffusion limited. Additionally, inhibiting products can accumulate and decrease mineralisation activity. DOM and nutrients can spread only in the diffusive distance, affecting a small sediment volume.

However, scenarios of mobile sediment ripples will probably dominate shallow coastal areas due to strong and highly variable tidal currents and wave activity. Ripple propagation velocities range from 1-3 cm h^{-1} (Traykovski et al. 1999) to more than 50 cm h^{-1} (Doucette et al. 2002). Even if POM aggregations are buried in deeper sediment horizons, i.e., remain stationary with respect to the sediment movement associated with the ripple migration, they can influence different sediment volumes by fast advective transport of DOM. This is due to the tight coupling between the ripple propagation and advective porewater flow field (Precht et al. 2004). Therefore the bacteria attached to sand-grains of the top sediment layer are exposed to rapidly changing conditions. These bacteria have to be not only tolerant to both oxic and anoxic conditions, but also be able to react instantly when their favourable conditions, possibly lasting only minutes or hours, arise.

This fast reaction of the sedimentary aerobic bacterial community was detected in our experiments as up to 18 times higher OCR values at positions of *U. lactuca* compared to the surrounding sediment only minutes after the *U. lactuca* discs were placed into the sediment. That the bacteria living in the surrounding sediment and not the bacteria attached to the *U. lactuca* discs were the main degraders was confirmed by the negligible increase of DIC in a sterile sediment (dotted line in Fig. 8B).

We conclude that in permeable sediments, which represent advection dominated ecosystems, highly elevated aerobic mineralisation rates at locations of labile organic matter may lead to suboxic or anoxic (micro) sites in an otherwise oxygenated sediment. In these dynamic systems, the interaction of boundary flow and sediment topography can control transport of not only electron acceptors, nutrients and heavy metals (Huettel et al. 1998; Precht et al. 2004) but also DOM. Bacterial degradation of POM in the uppermost sediment layer affected by advective transport can lead to the spatial decoupling of POM mineralisation and final DOM degradation. The temporally and spatially changing advective DOM transport can consequently influence very dynamically bacterial communities living in large sediment volumes, which probably enhances organic matter degradation. Permeable sediments, considered as biocatalytic filters (Huettel et al. 2003), have therefore a large remineralisation potential, which cannot be always used fully, but can be expected to be able to react instantly to the input of labile organic material.

Acknowledgements

References

Aller, R. C. 1994. Bioturbation and remineralization of sedimentary organic-matter - Effects of redox oscillation. Chemical Geology **114**: 331-345.

Alperin, M. J., C. S. Martens, D. B. Albert, I. B. Suayah, L. K. Benninger, N. E. Blair, and R. A. Jahnke. 1999. Benthic fluxes and porewater concentration profiles of dissolved organic carbon in sediments from the North Carolina continental slope. Geochim. Cosmochim. Acta **63**: 427-448.

Andersen, F. O., and B. T. Hargrave. 1984. Effects of Spartina detritus enrichment on aerobic anaerobic benthic metabolism in an intertidal sediment. Mar. Ecol. Prog. Ser. **16**: 161-171.

Berg, P., H. Roy, F. Janssen, V. Meyer, B. B. Jørgensen, M. Huettel, and D. de Beer. 2003. Oxygen uptake by aquatic sediments measured with a novel non-invasive eddy-correlation technique. Mar. Ecol. Prog. Ser. **261**: 75-83.

Bobin-Dubigeon, C., M. Lahaye, F. Guillon, J. L. Barry, and D. J. Gallant. 1997. Factors limiting the biodegradation of Ulva sp cell-wall polysaccharides. Journal of the Science of Food and Agriculture **75**: 341-351.

Boudreau, B. P. 1996. The diffusive tortuosity of fine-grained unlithified sediments. Geochim. Cosmochim. Acta **60**: 3139-3142.

Boudreau, B.P., M. Huettel, S. Forster, R.A. Jahnke, A. McLachlan, J.J. Middelburg, P. Nielsen, F. Sansone, G. Taghon, W.R. Van Raaphorst, I. Webster, J.M. Weslawski, P. Wiberg, and B. Sundby. 2001. Permeable marine sediments: overturning an old paradigm. EOS Trans. Am. Geophys. Unioni **82**: 133-136.

Burdige, D. J., and J. Homstead. 1994. Fluxes of dissolved organic-carbon from Chesapeake Bay sediments. Geochim. Cosmochim. Acta **58**: 3407-3424.

Canfield, D. E., B. B. Jørgensen, H. Fossing, R. Glud, J. Gundersen, N. B. Ramsing, B. Thamdrup, J. W. Hansen, L. P. Nielsen, and P. O. J. Hall. 1993. Pathways of organic carbon oxidation in three continental margin sediments. Marine Geology **113**: 27-40.

Castaldelli, G., D. T. Welsh, G. Flachi, G. Zucchini, G. Colombo, R. Rossi, and E. A. Fano. 2003. Decomposition dynamics of the bloom forming macroalga Ulva rigida C. Agardh determined using a C-14-carbon radio-tracer technique. Aquatic Botany **75**: 111-122.

Chen, R. F., J. L. Bada, and Y. Suzuki. 1993. The Relationship between dissolved organic-carbon (Doc) and fluorescence in anoxic marine porewaters - Implications for estimating benthic Doc fluxes. Geochim. Cosmochim. Acta **57**: 2149-2153.

Crank, J. 1975. The Mathematics of Diffusion. 2nd edition ed. Oxford University Press Inc.

de Beer, D., F. Wenzhöfer, T.G., Ferdelman, S. Boehme, M. Huettel, J. E. E. von Beusekom, M. E. Böttcher, N. Musat, and N. Dubilier. 2005. Transport and mineralization rates in North Sea sandy intertidal sediments Sylt-Rømø basin, Wadden Sea. Limnol. Oceanogr. 50(1): 113-127.

de Haas, H., T. C. E. van Weering, and H. de Stigter. 2002. Organic carbon in shelf seas: Sinks or sources, processes and products. Cont. Shelf Res. **22**: 691-717.

Doucette, J. S., E. S. Harvey, and M. R. Shortis. 2002. Stereo-video observation of nearshore bedforms on a low energy beach. Marine Geology **189**: 289-305.

Emery, K.O. 1968. Relict sediments on continental shelves of the world. Am. Assoc. Pet. Geol. Bull. **52**: 445-464.

Fenchel, T., G.M. King, and T.H. Blackburn. 1998. Bactrial Biogeochemistry. The Ecophysiology of Mineral Cycling. 2nd ed. Academic Press.

Florek, R. J., and G. T. Rowe. 1983. Oxygen-consumption and dissolved inorganic nutrient production in marine coastal and shelf sediments of the Middle Atlantic Bight. Internationale Revue Der Gesamten Hydrobiologie **68**: 73-112.

Forster, S., M. Huettel, and W. Ziebis. 1996. Impact of boundary layer flow velocity on oxygen utilisation in coastal sediments. Mar. Ecol. Prog. Ser. **143**: 173-185.

Gehlen, M., H. Malschaert, and W. R. Van Raaphorst. 1995. Spatial and temporal variability of benthic silica fluxes in the southeastern North Sea. Cont. Shelf Res. **15**: 1675-1696.

Glud, R. N., S. Forster, and M. Huettel. 1996a. Influence of radial pressure gradients on solute exchange in stirred benthic chambers. Mar. Ecol. Prog. Ser. **141**: 303-311.

Glud, R. N., M. Kuhl, O. Kohls, and N. B. Ramsing. 1999. Heterogeneity of oxygen production and consumption in a photosynthetic microbial mat as studied by planar optodes. J. Phycol. **35**: 270-279.

Glud, R. N., N. B. Ramsing, J. K. Gundersen, and I. Klimant. 1996b. Planar optodes: A new tool for fine scale measurements of two- dimensional O-2 distribution in benthic communities. Mar. Ecol. Prog. Ser. **140**: 217-226.

Harris, C. K., and P. L. Wiberg. 2001. A two-dimensional, time-dependent model of suspended sediment transport and bed reworking for continental shelves. Comput. Geosci. **27**: 675-690.

Hee, C. A., T. K. Pease, M. J. Alperin, and C. S. Martens. 2001. Dissolved organic carbon production and consumption in anoxic marine sediments: A pulsed-tracer experiment. Limnol. and Oceanogr. **46**: 1908-1920.

Holst, G., and B. Grunwald. 2001. Luminescence lifetime imaging with transparent oxygen optodes. Sens. Actuator B Chem. **74**: 78-90.

Holst, G., O. Kohls, I. Klimant, B. Konig, M. Kuhl, and T. Richter. 1998. A modular luminescence lifetime imaging system for mapping oxygen distribution in biological samples. Sens. Actuator B Chem. **51**: 163-170.

Huettel, M., W. Ziebis, S. Forster, and G.III. Luther. 1998. Advective transport affecting metal and nutrient distribution and interfacial fluxes in permeable sediments Geochim. Cosmochim. Acta **62**: 613-631.

Huettel, M., W. Ziebis, and S. Forster. 1996. Flow-induced uptake of particulate matter in permeable sediments. Limnol. and Oceanogr. **41**: 309-322.

Huettel, M., and G. Gust. 1992. Solute release mechanisms from confined sediment cores in stirred benthic chambers and flume flows. Mar. Ecol. Prog. Ser. **82**: 187-197.

Huettel, M., H. Røy, E. Precht, and S. Ehrenhauss. 2003. Hydrodynamical impact on biogeochemical processes in aquatic sediments. Hydrobiologia **494**: 231-236.

Hulthe, G., S. Hulth, and P.O.J. Hall. 1998. Effect of oxygen on degradation rate of refractory and labile organic matter in continental margin sediments. Geochim. Cosmochim. Acta **62**: 1319-1328.

Jørgensen, B.B. 1982. Mineralization of organic-matter in the sea bed - the role of sulfate reduction. Nature **296**: 643-645.

Kautsky, H. 1939. Quenching of luminescence by oxygen. Trans Faraday Soc **35**: 216-219.

Klute, A., and C. Dirksen. 1986. Hydraulic conductivity and diffusivity: laboratory methods, p. 687-734. *In* A. Klute, [eds.]. Methods of soil analysis - part 1 - physical and mineralogical methods. American Society of Agronomy.

Kristensen, E. 2000. Organic matter diagenesis at the oxic/anoxic interface in coastal marine sediments, with emphasis on the role of burrowing animals. Hydrobiologia **426**: 1-24.

Kristensen, E., S. I. Ahmed, and A. H. Devol. 1995. Aerobic and anaerobic decomposition of organic matter in marine sediment: Which is fastest? Limnol. and Oceanogr. **40**: 1430-1437.

Kristensen, E., and M. Holmer. 2001. Decomposition of plant materials in marine sediment exposed to different electron accepters (O-2, NO3-, and SO42-), with emphasis on substrate origin, degradation kinetics, and the role of bioturbation. Geochim. Cosmochim. Acta **65**: 419-433.

Li, Y. H., and S. Gregory. 1974. Diffusion of ions in sea-water and in deep-sea sediments. Geochim. Cosmochim. Acta **38**: 703-714.

Lohse, L., E.H.G. Epping, W. Helder, and W. van Raaphorst. 1996. Oxygen pore water profiles in continental shelf sediments of the North Sea: Turbulent versus molecular diffusion. Mar. Ecol. Prog. Ser. **145**: 63-75.

Malan, D. E., and A. McLachlan. 1991. In situ benthic oxygen fluxes in a nearshore coastal marine system: a new approach to quantify the effect of wave action. Mar. Ecol. Prog. Ser. **73**: 69-81.

Martin, W. R., and D. C. McCorkle. 1993. Dissolved organic-carbon concentrations in marine pore waters determined by high-temperature oxidation. Limnol. and Oceanogr. **38**: 1464-1479.

Morand, P., and X. Briand. 1999. Anaerobic digestion of Ulva sp. 2. Study of Ulva degradation and methanisation of liquefaction juices. Journal of Applied Phycology **11**: 165-177.

Neira, C., and M. Rackemann. 1996. Black spots produced by buried macroalgae in intertidal sandy sediments of the Wadden Sea: Effects on the meiobenthos. J. Sea Res. **36**: 153-170.

Polerecky, L., U. Franke, U. Werner, B. Grunwald, and D. de Beer. 2005. High spatial resolution measurement of oxygen consumption rates in permeable sediments. Limnol. Oceanogr.: Methods **3**: 75-85.

Precht, E., U. Franke, L. Polerecky, and M. Huettel. 2004. Oxygen dynamics in permeable sediments with wave-driven pore water exchange. Limnol. and Oceanogr. **49**: 693-705.

Precht, E., and M. Huettel. 2004. Rapid wave-driven advective pore water exchange in a permeable coastal sediment. J. Sea Res. **51**: 93-107.

Reimers, C. E., H. A. Stecher, G. L. Taghon, C. M. Fuller, M. Huettel, A. Rusch, N. Ryckelynck, and C. Wild. 2004. In situ measurements of advective solute transport in permeable shelf sands. Cont. Shelf Res. **24**: 183-201.

Rowe, G. T., G. S. Boland, W. C. Phoel, R. F. Anderson, and P. E. Biscaye. 1994. Deep-sea floor respiration as an indication of lateral input of biogenic detritus from continental margins. Deep-Sea Res. Part II **41**: 657-668.

Rusch, A., and M. Huettel. 2000. Advective particle transport into permeable sediments - evidence from experiments in an intertidal sandflat. Limnol. and Oceanogr. **45**: 525-533.

Rusch, A., M. Huettel, C. E. Reimers, G. L. Taghon, and C. M. Fuller. 2003. Activity and distribution of bacterial populations in Middle Atlantic Bight shelf sands. Fems Microbiology Ecology **44**: 89-100.

Rutgers van der Loeff, M. M. 1981. Wave effects on sediment water exchange in a submerged sand bed. Neth. J. Sea Res. **15**: 100-112.

Shum, K. T., and B. Sundby. 1996. Organic matter processing in continental shelf sediments - the subtidal pump revisited. Mar. Chem. **53**: 81-87.

Traykovski, P., A. E. Hay, J. D. Irish, and J. F. Lynch. 1999. Geometry, migration, and evolution of wave orbital ripples at LEO-15. J. Geophys. Res. **104**: 1505-1524.

van Loosdrecht, M. C. M., J. Lyklema, W. Norde, and A. J. B. Zehnder. 1990. Influence of interfaces on microbial activity. Microbiological Reviews **54**: 75-87.

Vetter, Y. A., J. W. Deming, P. A. Jumars, and B. B. Krieger-Brockett. 1998. A predictive model of bacterial foraging by means of freely released extracellular enzymes. Microbial Ecology **36**: 75-92.

Wenzhöfer, F., and R. N. Glud. 2004. Small-scale spatial and temporal variability in benthic O2 dynamics of coastal sediments: Effects of fauna activity. Limnol. and Oceanogr. **49**: 1471-1481.

Wiberg, P. L., and C. K. Harris. 1994. Ripple geometry in wave-dominated environments. J. Geophys. Res. **99**: 775-789.

Ziebis, W., S. Forster, M. Huettel, and B. B. Jørgensen. 1996a. Complex burrows of the mud shrimp Callianassa truncata and their geochemical impact in the sea bed. Nature **382**: 619-622.

Ziebis, W., M. Huettel, and S. Forster. 1996b. Impact of biogenic sediment topography on oxygen fluxes in permeable seabeds. Mar. Ecol. Prog. Ser. **140**: 227-237.

Characteristics of porphyrin-based planar oxygen optodes: consequences for applicability in aquatic systems

Ulrich Franke, Gerhard Holst* and Lubos Polerecky

Max Planck Institute for Marine Microbiology, Celsiusstrasse 1, D-28359 Bremen, Germany

*Present address: PCO imaging AG, Donaupark 11, 93309 Kelheim, Germany

Abstract

By applying porphyrin-based planar oxygen optodes and the rapid lifetime determination technique in different aquatic biological systems, the characteristics of the used sensors were derived. The accuracy of the planar optodes was between $\pm 7 - 20$ % and $\pm 2 - 3$ % in the range around 100 % of air saturation and zero oxygen concentrations, respectively. The estimated minimum temporal resolutions were approximately 3 s for the transparent and semi-transparent optodes and 4 s for the optically isolated optodes. Minimum spatial resolutions were between $15 - 30$ and $35 - 70$ µm for the transparent/semi-transparent and optically isolated optodes, respectively. The long-term stability of continuously used semi-transparent optodes was more than 1.5 years. When used in systems with very steep oxygen gradients, anoxic regions influenced oxic regions by a light-guidance effect. Consequently, oxygen values in the oxic regions were underestimated and oxygen gradients at the oxic/anoxic transition zones were flattened. This effect was most pronounced when large anoxic areas were present and when the optode was glued to a thin transparent wall, such as the aquarium wall made of glass, PMMA or polycarbonate. The effect can be reduced by minimising the imaged anoxic area or by using thicker wall material for the measuring setup. Porphyrin-based oxygen optodes are a powerful tool for the measurement and visualisation of 2D oxygen distributions and dynamics in aquatic systems which do not require extremely fast and highly precise determination of oxygen distributions and gradients

Introduction

Due to the key role of oxygen in benthic aerobic degradation of organic matter, determination of oxygen distributions and exchange rates is very important when characterising benthic microbial communities. Since the time of their introduction to aquatic systems by (Revsbech et al. 1980), oxygen microelectrodes established themselves as a fundamental tool applied in the studies of the oxic zone with high spatial and temporal resolutions. Optical principle in oxygen sensing was first introduced by Klimant et al. (1995), who developed and applied the first oxygen microoptode in marine aquatic systems. This technology was further advanced by the introduction of planar oxygen optodes by Glud et al. (1996), which enabled the measurement of two-dimensional (2D) oxygen distributions with a comparable spatial resolution and thus considerably improved time efficiency of larger scale oxygen measurements.

The optical measuring technique is based on dynamic quenching of luminescence of a specific fluorophore by oxygen (Kautsky, 1939). By absorbing high energy light (blue or green), the fluorophore is excited from its ground level to a higher energy level. The return back to the ground level is accompanied by the emission of luminescence photons of different intensity and/or lifetime, which depends on oxygen concentration (Lübbers 1995).

Planar oxygen optodes consist in general of a fluorescent dye embedded in a polymer sensor matrix which is spread and fixed as a thin layer on a transparent supporting foil (Glud et al. 1996; Precht et al. 2004). The first utilised sensing technique was based on the measurement of luminescence intensity (Glud et al. 1996). This was further improved by employing a lifetime-based measuring approach (Holst et al. 1998). In contrast to the intensity-based measurements, lifetime imaging is not influenced by variable indicator concentrations in the sensor matrix. Intensity variations due to photobleaching or an inhomogeneous excitation light field and background luminescence can also be effectively suppressed (Liebsch et al. 2000; Holst and Grunwald 2001). With the intensity-based imaging system, only optically isolated optodes (sensing layer covered with an additional layer of black silicone) could be used to eliminate the effects of light scattering from an investigated sample, which would otherwise influence the oxygen determination. In contrast, the lifetime-based measuring system allowed also the use of transparent and semi-transparent optodes (Holst and Grunwald 2001).

Since their introduction, planar oxygen optodes were employed in several laboratory studies of diverse marine systems such as microbial mats (Glud et al. 1999), biofilms (Glud et al. 1998), photosynthetic and bioturbated sediments (Fenchel and Glud 2000; Holst and Grunwald 2001), permeable sandy sediments (Precht et al. 2004; Rasheed et al. 2004; Wild et al. 2004; Polerecky et al. 2005), corals and foraminifera (Holst and Grunwald 2001). First *in situ* applications in photosynthetic and bioturbated sediments were also reported (Glud et al. 2001; Wenzhöfer and Glud 2004). These studies demonstrated that oxygen optodes together with the intensity and/or lifetime imaging technique constitute a powerful tool for the visualisation and quantification of oxygen in diverse marine systems in two dimensions.

In this work, limitations of planar oxygen optodes are discussed in the context of biological applications in which the optodes have been or are being used. Characteristics of planar optodes such as light-guidance, signal-to-noise ratio, temporal and spatial resolutions, long-term stability and robustness are presented. The causes of the limitations are discussed and possible solutions are suggested.

Material and methods

Two-dimensional (2D) oxygen measurements

Planar oxygen optodes

The transparent and semi-transparent optodes consisted of 2 layers: a transparent polyester support foil (125 µm thick, Goodfellow) and a sensing layer spread on the support foil by knife-coating. The sensing layer was made of 10 mg of the luminescent oxygen indicator platinum(II) meso - tetra (pentafluorophenyl) porphyrin (Pt-PFP) (Porphyrin Products), 490 mg Polystyrene (Sigma-Aldrich) and 3 ml Chloroform (Merck). For semi-transparent optodes, 330 mg of titanium dioxide (TiO$_2$) particles (< 5 µm, Aldrich) were added to the matrix solution. By this process, the optode loses its transparency and the sensor appears milky, however, the sensor matrix becomes more robust (Klimant et al. 1995). In the preparation of optically isolated optodes, an additional layer of black silicone was knife-coated on top of the dry sensing layer (drying in air for ~ 5 - 10 min). The thicknesses of the dry sensing layer and the black silicone layer were approx. 15 - 30 µm and 20 - 40 µm, respectively. The planar optodes were glued with transparent silicone (Elastosil® E4, Wacker) onto flat transparent walls of diverse setups

(e.g., wave tanks, aquaria, square sediment corers) to facilitate oxygen measurements in the studied samples.

Oxygen imaging system

2D oxygen measurements were conducted with the modular luminescence lifetime imaging (MOLLI) system (Holst et al. 1998; Holst and Grunwald 2001). Blue light emitting diodes (LEDs: HLMP-CB 15, λ_{max} = 475 nm, Agilent, or Luxeon V Star Blue, λ_{max} = 470 nm, Lumileds) were used to create an approximately homogeneous excitation light field to illuminate the planar optodes. The red luminescence (λ_{max} = 647 nm) emitted by the optode was filtered by a red optical filter (Deep Golden Amber, LEE-Filters) to remove most of the reflected/scattered excitation light. A fast gateable CCD camera (SensiCam, PCO) with a resolution of 640×480 pixels recorded the luminescence images (Fig. 1).
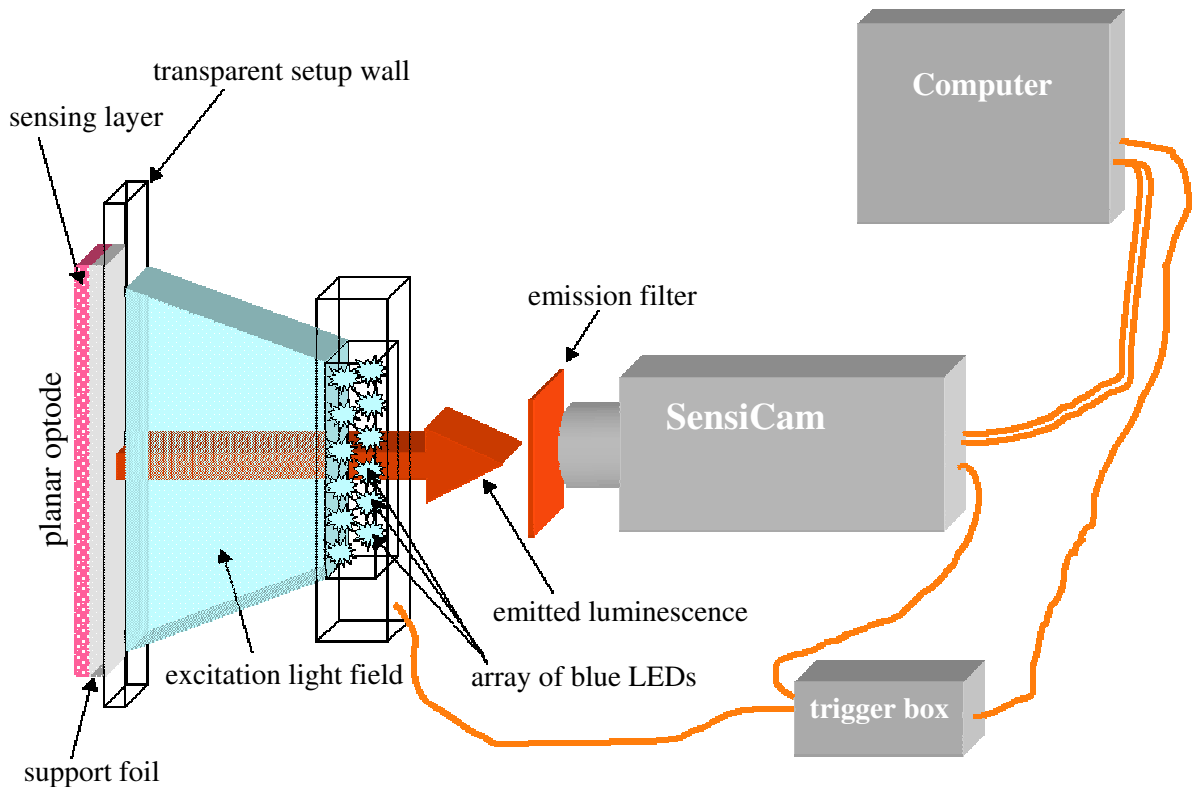
Figure 1: Scheme of the general oxygen imaging system.

Oxygen scanning system

Apart from illuminating the planar optode with a light field from LEDs, blue light from a laser-diode module (PVLS-3000, λ = 404 nm, Toptica Photonics) was also used. The laser light was shaped by line optics (OZ Optics) to form a thin laser-line (~ 200 µm wide and ~ 4 cm long in the distance of ~ 10 cm). With the help of a motorised micro-positioner

(HT-90, Micos), an aquarium equipped with the planar optode was moved up- and downwards (accuracy of +/- 2 µm) with respect to the fixed laser-line and the camera setup, thereby scanning the 2D oxygen distribution.

Image processing

The rapid lifetime determination (RLD) method (Ballew and Demas 1989; Liebsch et al. 2000) was employed to calculate the luminescence lifetime distributions. Lifetime values were converted into oxygen concentrations using a modified two-component model of the Stern-Volmer equation (Klimant et al. 1995; Holst et al. 1998). All experiments were conducted in the dark to minimise the effects of background light on the oxygen measurements. Further image processing was carried out with either a custom-made program developed in IDL$^®$ (Holst and Grunwald 2001) or Matlab$^®$ (Polerecky et al. 2005).

Calibration

Images of 0 and 100 % air saturation (AS) were taken before and after the experiments and served as calibration images. In contrast to a pixel-by-pixel calibration procedure (Glud et al. 1996; Wenzhöfer and Glud 2004), lifetime values averaged over several pixels (n > 100) served as calibration values. This was done because it was impossible to fix the used setups in such a way that the optode (e.g., fixed at a wall of an aquarium) and the camera remained precisely aligned during both the calibration procedure and the experiments.

One-dimensional (1D) oxygen measurements

For comparison, 1D high spatial resolution oxygen concentrations and oxygen microprofiles were measured with Clark-type oxygen microelectrodes (Revsbech 1989). The sensors had tip diameters of 10 – 20 µm, stirring sensitivities of < 1.5 % and response times of < 0.5 seconds. The microelectrodes were connected to a high-precision picoammeter whose signal was collected by a data-acquisition card (National Instruments) for PC data acquisition. Calibrations of the sensors were conducted at the experimental temperatures and salinities. Air-saturated water or water saturated with nitrogen gas as well as anoxic sediment parts, if present in the experiments, served for the determination of air saturation and zero oxygen calibration values, respectively. The sensors were attached to a micro-manipulator mounted on a motorised linear stage (VT-80, Micos) and placed above the sample, enabling reproducible positioning (precision +/- 1 µm) of the sensor tip.

Studied characteristics and experimental designs

Light-guidance effect ("spatial cross-talk" effect)

Planar oxygen optodes glued onto the aquaria walls were calibrated prior to the measurements and the lifetime values of τ_0 and τ_{100} corresponding to the 0% and 100% air saturation, respectively, were determined. The aquaria were subsequently filled with the intertidal mudflat sediment (German Wadden Sea) and a microbial mat (Jonkers et al. 2003). Oxygen images were calculated from the lifetime image measured by the MOLLI system using the calibration values τ_0 and τ_{100}.

Steady state 2D oxygen distributions and steep vertical oxygen gradients were used to determine the light guidance effects. Oxygen steady state in the microbial mats was achieved by illumination with a halogen lamp ($\sim$ 800 µmol photons m^{-2} s^{-1}). In the aquarium filled with mudflat sediment, steep oxygen gradients developed as a result of oxygen consumption by the sediment and continuous bubbling of the overlying water with air. The aquaria were filled with the sediment so that the sediment depth was the same in all aquaria.

To test the light-guidance effect at different experimental conditions, different transparent materials were used as walls in the aquaria. These included polymethylmethacrylate (PMMA, Malon, custom-made, product nr. 16) and polycarbonate (PC), both $\sim$ 7 mm thick, as well as quartz glass (Schott) of different thicknesses (2, 3, 5 and 10 mm). The surfaces of the PMMA and PC walls were coated with a special, scratch-resistant material (available as Axxis, Cadillac-Plastics or Lexan, Röhm or Makrolon, Bayer).

Signal-to-Noise ratio

The signal-to-noise ratio and accuracy of the planar optode were determined by repeated oxygen measurements (every 5 s) conducted in small flow-through aquaria, filled either with air saturated water or anoxic sediment. The oxygen concentrations were simultaneously measured with microelectrodes.

Temporal resolution

The temporal resolution was quantified by comparing parallel planar-optode and microelectrode measurements in oxygen-consuming intertidal permeable sediments and oxygen-producing/consuming Chiprana microbial mats. Oxygen concentrations in the permeable sediment were manipulated by starting and stopping the percolation with aerated water (flow-through method, as described by Polerecky et al. (2005)). Rapid

changes in oxygen concentrations in the microbial mats were induced by switching on and off the illuminating light from a halogen lamp.

Spatial resolution

The theoretical minimum spatial resolution of planar optodes was determined from the thickness of the sensing layers which was measured with the help of a high precision (+/- 1 µm) micrometer gauge (Wilson Wolpert).

Long-term stability and robustness of semi-transparent planar optodes

Calibration characteristics of the semi-transparent planar optodes, i.e., the dynamic range and luminescence intensity, were determined before, during and after extensive studies conducted in a wave tank (Precht et al. 2004). In these experiments, propagating sediment ripples were frequently created, resulting in the movement of sand grains along the surface of the optodes. Additionally, square sampling cores equipped with semi-transparent optodes, which were extensively applied in the flow-through measurements (Polerecky et al., 2005), were used to assess the robustness and durability of the optodes.

Results and discussion

Light-guidance effect

The influence of the spatial cross-talk effect is demonstrated in figures 2 and 3. Figure 2A shows 2D steady state oxygen distributions around the surface of a microbial mat. It can be seen that the larger is the covered part of the anoxic region under the mat surface (see pos 1 to 3), the more pronounced is the subsurface oxygen peak. The quantitative extent of this effect is better appreciated from Fig. 2B. When the anoxic region under the mat surface was fully covered (pos 1), peak oxygen concentrations in a selected profile reached above 400 µmol L^{-1}. On the other hand, maximum oxygen concentrations of ~ 320 µmol L^{-1} were determined if the anoxic region under the mat surface was uncovered (pos 3).

An alternative measurement of 2D steady oxygen distributions in the microbial mat was done by scanning the area of interest using a laser line. In this approach, only a very thin (~ 200 µm) region of the planar optode is illuminated at a time. If the scanning laser line is perpendicular to the oxygen gradients in the studied sample, the light guiding effect can effectively be reduced. This is demonstrated by pronounced oxygen peaks visible below the mat surface in the oxygen image reconstructed from the line-scan (Fig. 2C).
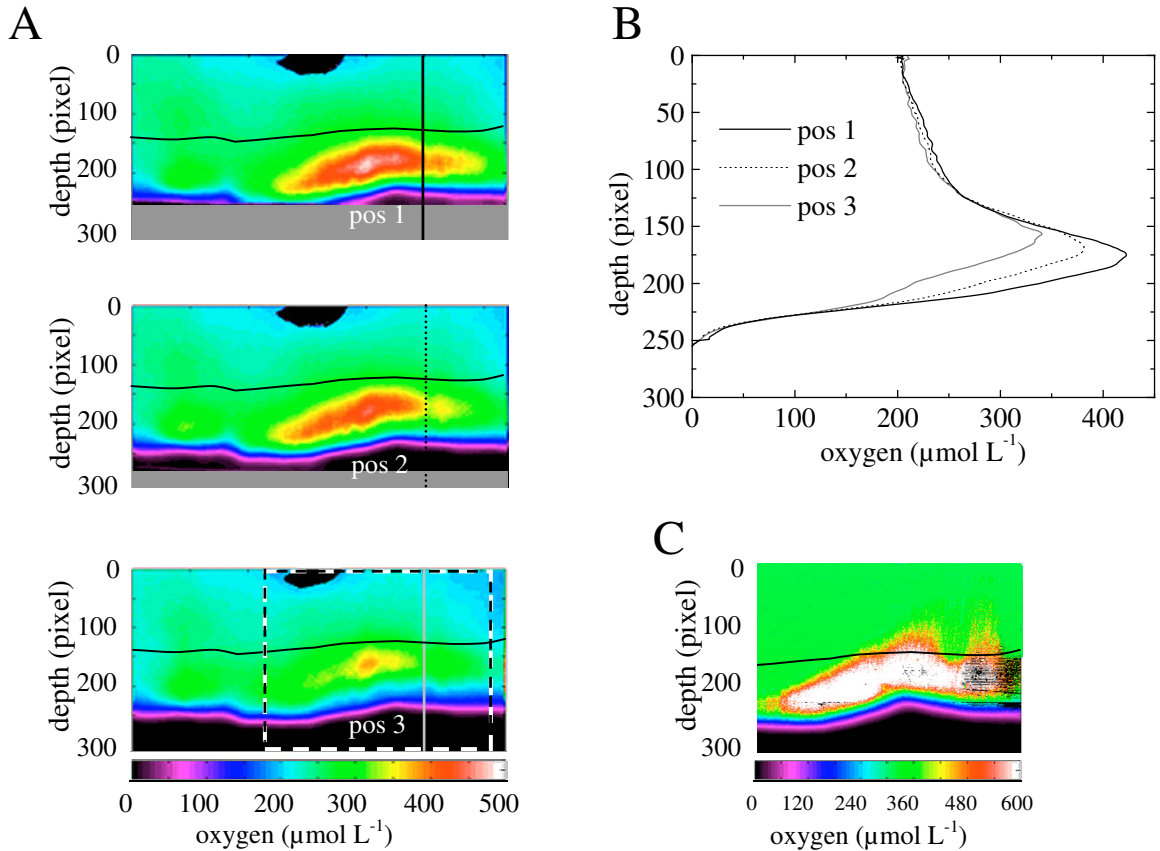
Figure 2: Correlation between the light-guidance effect and the size of the imaged anoxic region. (A) Steady state 2D oxygen distributions in a microbial mat at constant illuminating light intensity (~ 800 µE m^{-2} s^{-1}). The gray area depicts the extent of the cover over the anoxic parts of the mat which was employed to prevent the excitation light from reaching the planar optode. The size of the imaged anoxic part of the microbial mat increases from position 1 to position 3. (B) Vertical oxygen profiles extracted from the oxygen images in (A) at the position shown by the horizontal line (pixel x = 500). (C) Steady state 2D oxygen distribution in a microbial reconstructed from the scan by a laser-line. The area covered is indicated by dashed rectangle in image (A), pos 3. In all panels, black horizontal lines indicate the mat surface and each pixel corresponds to ~ 70 µm.

The measurements with the mudflat sediment show similar effects (Fig. 3). When the sediment is illuminated concomitantly with the overlying water, oxygen concentrations determined in the overlying water are underestimated (open symbols in Fig. 3). As soon as the anoxic sediment is covered, the values of oxygen concentration in the overlying water increase (filled symbols in Fig. 3). The increase is more pronounced when the planar oxygen optode is glued to a thinner wall, suggesting that the spatial cross-talk effect can be reduced by using a thicker wall (compare Fig. 3A and 3B). Tests with different materials

of the aquarium wall showed that the PMMA wall was better than the tested polycarbonate and glass walls (data not shown).

It can be summarized that when planar oxygen optodes are glued to a transparent wall (thickness of several millimeters) and a lifetime-based imaging approach is used for the determination of 2D oxygen distributions, oxygen concentrations measured in oxic areas are underestimated when the areas are close to anoxic regions. When these anoxic regions are covered from the outside of the aquarium wall to prevent the excitation of the planar optode in this part, the calculated oxygen concentrations in oxic regions increase. When the oxic regions are covered instead, no measurable effect is observed in anoxic regions (data not shown).
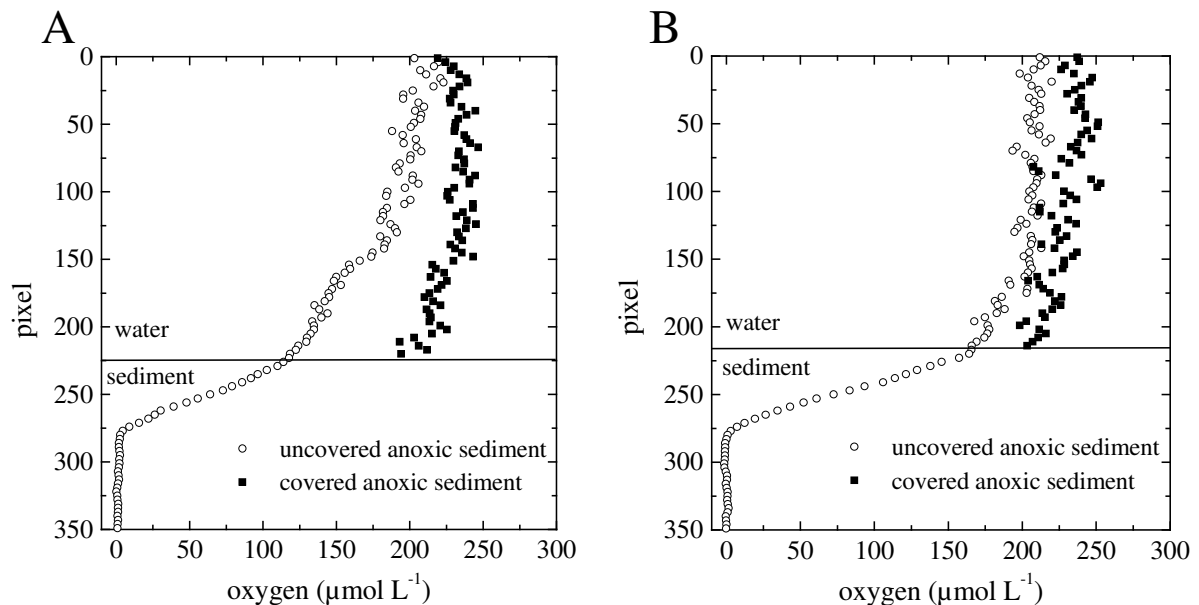
Figure 3: Vertical profiles extracted from oxygen images measured in a core filled with mudflat sediment. The anoxic sediment was either covered or uncovered by a light absorbing obstacle which prevented the blue excitation light from reaching the corresponding part of the planar oxygen optode. Panels (A) and (B) correspond to the situation where the thickness of the quartz glass, from which the aquarium wall equipped with the planar optode was constructed, was 2 and 10 mm, respectively. Each pixel corresponds to ~ 40 µm. For clarity, only every third data point is shown.

We refer to this as the spatial cross-talk effect and explain it as a consequence of light guidance in the sensor foil and/or in the aquarium wall to which the planar oxygen optode is glued (Fig. 4). Luminescence generated from the sensing layer in contact with anoxic regions has higher intensity and longer lifetime, whereas the luminescence originating from the oxic regions is weaker and has a shorter lifetime, both as a consequence of the

dynamic quenching by oxygen (Kautsky 1939). The light from the anoxic regions (e.g., point α in Fig. 4) "carrying" the longer lifetime information is guided to the oxic regions and vice versa, either through the support foil or the aquarium wall. Due to scattering, both the light with the shorter lifetime and a fraction of the guided light with the longer lifetime are detected by the CCD camera in the oxic region (point β in Fig. 4A). Consequently, the lifetime calculated by the RLD method in the oxic region appears longer as it would do if no light from the anoxic region was guided to the oxic region, resulting in the underestimated oxygen concentrations. The situation is reverse in anoxic regions of the sediment (point α in Fig. 4A), i.e., the concentrations may appear overestimated. However, this effect was not detectable in our experiments most likely due to the much lower intensity of the fluorescence light generated in the oxic regions.
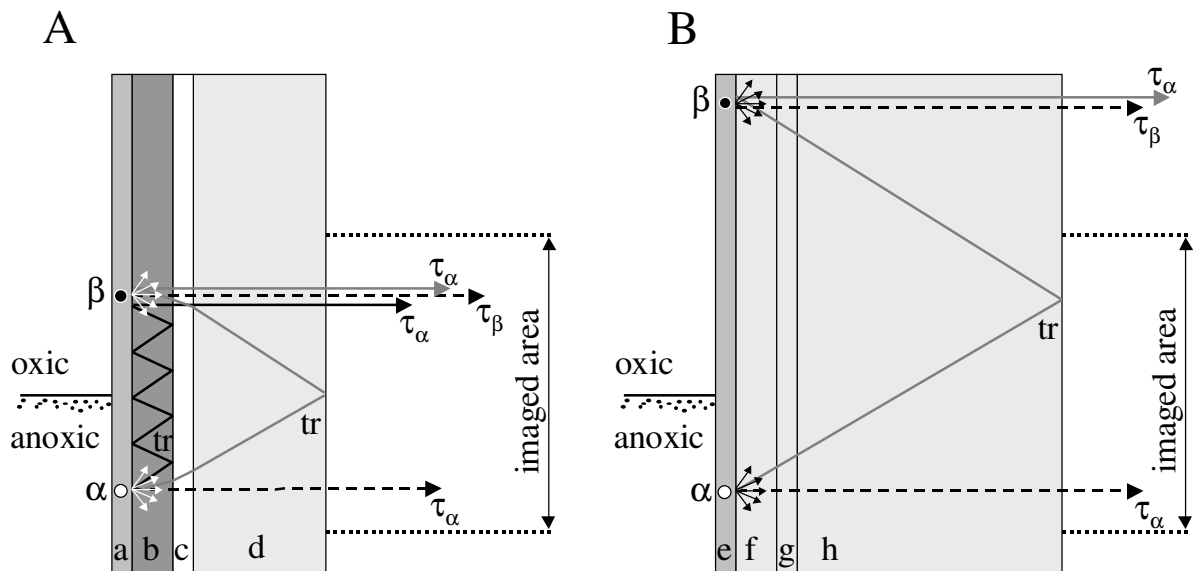
Figure 4: (A) Planar oxygen optode glued onto an aquarium wall: (a) sensing layer, (b) polyester (Mylar) supporting foil (refractive index n = 1.58), (c) silicone layer (n = 1.43), (d) aquarium wall, e.g., PMMA (n = 1.49), polycarbonate (n = 1.58) or quartz glass (n = 1.45 – 1.49). From point α (anoxic region), luminescent light of higher intensity and longer lifetime (τ_α) could be guided within the supporting foil (b) of the optode and/or within the aquarium wall (d) by total reflections (tr). Due to scattering at surfaces of a, b, c and d at point β, the light with lifetime τ_α can be decoupled out of the aquarium wall and may thereby superpose with the weaker and shorter lived (τ_β) luminescent light originating from point β (oxic region). (B) Alternative setup where the sensor matrix (e), supporting foil (f), immersion oil (g), and aquarium wall (h) have equal refractive indices. This should eliminate the light guidance through the supporting foil. Moreover, by choosing thicker wall material, the distance of points α and β affected by the light guidance can be increased to such an extent that the spatial cross-talk effect can be reduced or removed completely.

Considering the refractive indices of the layers between the sensing layer and the imaging camera, light guidance due to total internal reflections (TIR) at interfaces of the different materials is likely to happen inside the sensor support foil and/or within the aquarium wall (Fig. 4A). To minimise or remove the possibility of TIR, one could choose the same material (identical refractive indices) for the supporting foil and the wall to which the optode is attached and use index matching immersion oil instead of silicone to facilitate good optical contact (Fig. 4B). By using immersion oil, however, the optodes cannot be fixed as well as with silicone, thereby increasing the risk of detachment of the optode from the wall (e.g., when the measurements are conducted in wave tanks, flumes or *in situ,* where the sediment moves or the core is used for sediment sampling). Another possibility would be to spread the sensor matrix directly onto the wall of the used setup. This would, however, result in a limited flexibility of the setup, which is one of the advantages provided by the planar optode technology.

Noise characteristics

Compared to oxygen microelectrodes, planar optodes showed much higher noise levels. At 100 % air saturation (AS), the accuracy of the oxygen concentrations was $\pm\,7 - 20$ % AS, while it was $\pm\,2 - 3$ % AS around zero oxygen concentrations (Fig. 5). The higher noise at higher oxygen concentrations is caused by the weaker luminescence intensity signal (due to dynamic quenching by oxygen). Additionally, at high oxygen concentrations the sensitivity of the foil's lifetime to changes in oxygen is much lower (up to ~ 15 times for the used semi-transparent optodes), resulting in considerably higher noise in oxygen concentrations for the same noise in lifetime (Fig. 6). Averaging several oxygen images can reduce the noise levels, however this would result in an increased temporal resolution with which oxygen images can be acquired (see below).

Temporal resolution

The response time of the sensors is determined by the dye response time, thickness of the sensing and optically isolating layers and, in the water phase, by the thickness of the DBL (Glud et al. 1996). The apparent response time of the tested semi-transparent optodes was in the order of 1 s, as revealed by experiments conducted in highly oxygen-consuming sediments using both planar optodes and microelectrodes (data not shown). The response time was comparable to that for ruthenium-based optically isolated planar oxygen optodes described by Glud et al. (1996). In our experiments, the materials of the sensing layers were chosen because of their high oxygen permeability.
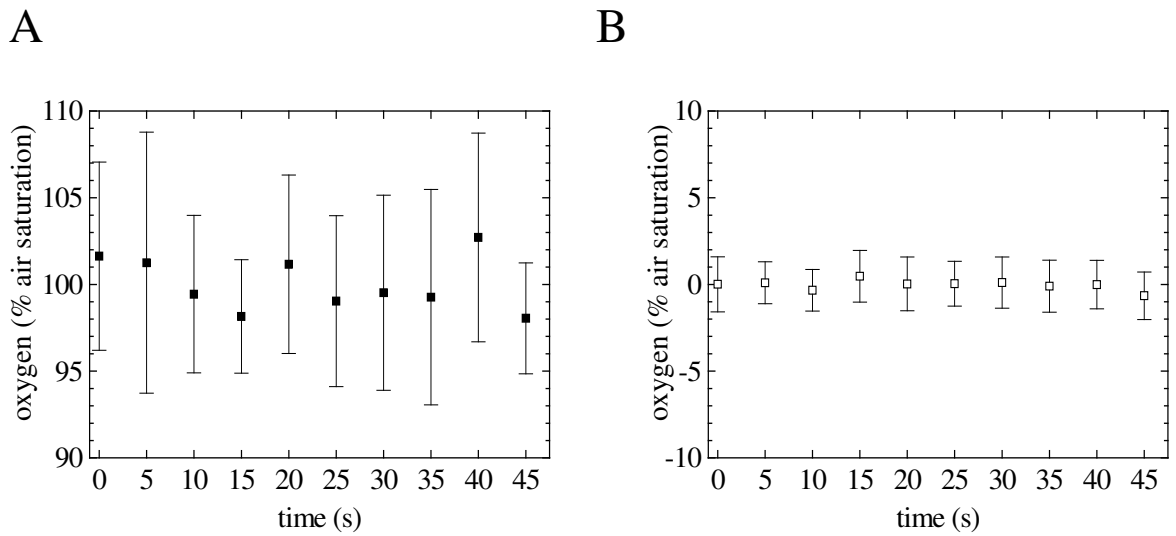
Figure 5: Oxygen concentrations measured by a semi-transparent planar optode surrounded by air-saturated water (A) and anoxic sediment (B). Standard deviations are derived from oxygen values of 4 (2×2) neighbouring pixels. Note different scale of y- axis in A and B.
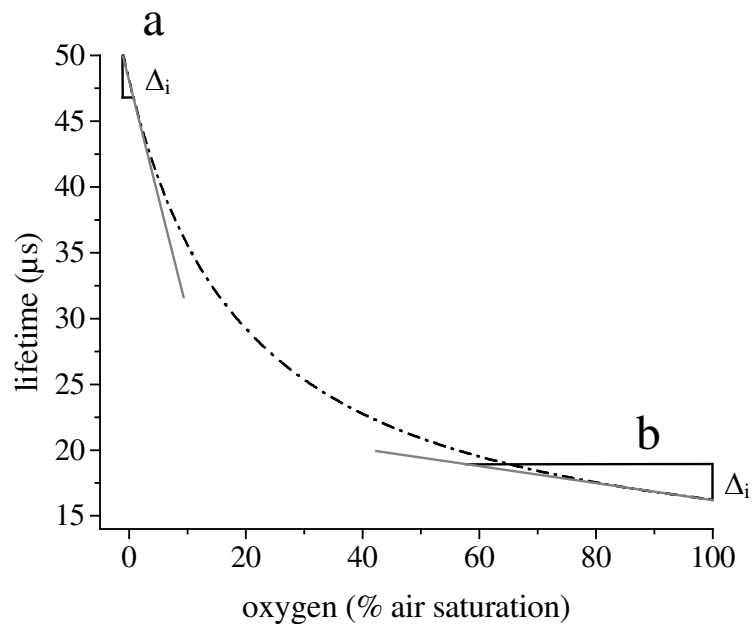

Figure 6: Typical calibration curve of the semi-transparent oxygen optode. The slope at 0 % air saturation (a) is ~ 15 times larger than the slope at 100 % air saturation (b). Therefore, a specific noise level of the lifetime (Δ_i) will result in ~ 15 times larger noise of the oxygen values at high oxygen concentrations (around air saturation) when compared to the noise levels at low oxygen concentrations.

The diffusion coefficients (D) of oxygen in the (polystyrene) sensor matrix and in silicone were $D_P = 1.1 \times 10^{-7}$ cm^2 s^{-1} (Bandrup et al. 2003) and $D_S = 1.7 \times 10^{-5}$ cm^2 s^{-1} (Crank and Park 1968), respectively. Considering the sensor matrix thickness of 15 – 30 µm, which are typical values for the used transparent and semi-transparent optodes, oxygen molecules would need 3 – 6 s to diffuse across the entire matrix. In optically isolated optodes, an additional 0.5 – 1 s would be needed for oxygen to diffuse through the silicone layer of 20 – 40 µm thickness, which would increase the sensor response time to 4 – 7 s.

In addition to the diffusive-limitation, the measurement procedure also limits the temporal resolution with which oxygen dynamics can be observed. To reduce the noise level of the oxygen images, 2 to 8 subsequently measured oxygen images were averaged. This resulted in a typical temporal resolution of 5 – 10 s and 7 – 15 s when transparent or semi-transparent and optical isolated optodes were used, respectively.

Spatial resolution

The spatial resolution of analyte imaging depends on the pixel resolution of the camera chip, the aperture of the objectives but also on lateral diffusion of the analyte in the sensing layer (Liebsch et al. 2000). Therefore, the theoretical minimum spatial resolution of planar optodes is determined by the thickness of the sensor layers and the spatial resolution could be improved by decreasing the sensing layer thickness. To achieve homogeneous sensing layers with the knife-coating process (Holst and Grunwald 2001), a minimum wet-layer thickness of ~ 50 µm is needed, resulting in a thickness of the cured sensing layer of 15 – 30 µm. The sensor matrix and, for optically isolated optodes, the additional black silicone layer are highly permeable for oxygen (see above). The transport within these layers is governed only by diffusion, i.e., oxygen molecules move randomly within the sensor matrix and the optical isolation. As a consequence, cross-diffusion within the layers will occur. The real spatial resolution is difficult to determine, as it is not easy to create extremely steep and well defined oxygen gradients next to the sensing layer. Therefore, the minimum spatial resolution of the used planar optodes was assumed to be in the range of the theoretical spatial resolution, taking into account the full sensing layer thickness, i.e., 15 – 30 µm for the transparent and semi-transparent optodes and 35 – 70 µm for the optical isolated optodes.

Because of the high noise levels, smoothing of the oxygen images is most often required for further data processing. Using the typical size of the smoothing kernel of 3 x 3 pixels, the spatial resolution will be increased to 50 – 200 µm.

Long-term stability and robustness

Long term stability of the first used oxygen optodes was between days and weeks (Klimant et al. 1995; Glud et al. 1996). During our experiments with semi-transparent planar optodes, the dynamic range as well as the intensity of the luminescence did not change significantly over ~ 1.5 years (Precht et al. 2004). Because of similar luminescence intensities, it is also likely that no bleaching or leaching of the fluorophore occurred during this period.

The robustness of the semi-transparent optodes was excellent. Mobile sandy sediment ripples neither harmed nor scratched the optode surface. No deterioration of the optodes was visible even after the cores with the attached optodes were pushed and retrieved into and out of porous sandy sediment many times.

Implications for applications in aquatic environments

One of the most important implication for biological applications employing the planar optode technique is given by the light guidance effect. This effect will cause the observed oxygen gradients to appear smaller than they are in reality. Furthermore, the absolute oxygen values in oxic regions can be (significantly) underestimated, particularly if these regions are close to anoxic areas. For example, in bioirrigated sediments where small oxic regions created by the pumping activity of benthic fauna (Kristensen 1981; Wenzhöfer and Glud 2004) are surrounded by large anoxic areas, the light guidance probably results in a strong underestimation of the oxygen concentrations inside the burrows. Therefore, special care has to be taken when such oxygen images are considered for further calculations.

The spatial cross-talk effect can be minimised by (i) selecting the materials of the optode, the aquarium wall and the fixation material (glue) so that they have the same (or very similar) refractive indices, or by (ii) increasing the thickness of the aquarium wall. However, if the experimental setup demands thin walls, optical oxygen determination using planar optodes will not provide accurate results in the entire range of oxygen concentrations.

Even though the light guidance effect is minimised when the laser-line scanning technique is employed, this approach is too slow to determine rapid oxygen changes which can occur, e.g., in porous or bioirrigated sediments (Precht et al. 2004; Wenzhöfer and Glud 2004) or in microbial mats (Glud et al. 1999). This technique is therefore suitable

only when steady state 2D oxygen distributions are of interest. Additionally, the laser and the line optics are delicate in handling and expensive.

To promote understanding and minimise the light guidance effect, further experiments are needed. In particular, tests should be performed with other combinations of materials for the aquarium wall, different thicknesses of the aquarium wall, etc.

Conclusions

Planar optodes described here can be satisfactorily used in applications where relatively noisy oxygen data can be tolerated and where temporal and spatial resolutions of several seconds and $50 - 100\,\mu m$, respectively, are sufficient. Due to their excellent long-term stability and robustness, the planar optodes are suitable oxygen sensors in long lasting experiments, especially when it is not possible to conduct frequent calibrations without disturbing the studied samples. The used planar optodes represent powerful tools also in experiments where the 2D oxygen dynamics need to be visualised but the highly accurate determination of oxygen concentrations is not too important.

Acknowledgements

References

Ballew, R. M., and J. N. Demas. 1989. An error analysis of the rapid lifetime determination Mmethod for the evaluation of single exponential decays. Analytical Chemistry **61**: 30-33.

Bandrup, J., E. H. Immergut, E. A. Grulke, A. Abe, and D. R. Bloch. 2003. Polymer Handbook. Edited by J. Bandrup, E. H. Immergut, E. A. Grulke, A. Abe and D. R. Bloch. 4th ed. John Wiley & Sons.

Crank, J. , and G.S. Park. 1968. Diffusion in Polymers. Edited by J. Crank and G. S. Park. 1st ed. Academic Press.

Fenchel, T., and R. N. Glud. 2000. Benthic primary production and O$_2$ - CO$_2$ dynamics in a shallow- water sediment: Spatial and temporal heterogeneity. Ophelia **53**: 159-171.

Glud, R. N., M. Kuhl, O. Kohls, and N. B. Ramsing. 1999. Heterogeneity of oxygen production and consumption in a photosynthetic microbial mat as studied by planar optodes. Journal of Phycology **35**: 270-279.

Glud, R. N., N. B. Ramsing, J. K. Gundersen, and I. Klimant. 1996. Planar optodes: A new tool for fine scale measurements of two- dimensional O-2 distribution in benthic communities. Marine Ecology-Progress Series **140**: 217-226.

Glud, R. N., C. M. Santegoeds, D. De Beer, O. Kohls, and N. B. Ramsing. 1998. Oxygen dynamics at the base of a biofilm studied with planar optodes. Aquatic Microbial Ecology **14**: 223-233.

Glud, R. N., A. Tengberg, M. Kuhl, P. O. J. Hall, I. Klimant, and G. Holst. 2001. An in situ instrument for planar O-2 optode measurements at benthic interfaces. Limnology and Oceanography **46**: 2073-2080.

Holst, G., and B. Grunwald. 2001. Luminescence lifetime imaging with transparent oxygen optodes. Sensors and Actuators B-Chemical **74**: 78-90.

Holst, G., O. Kohls, I. Klimant, B. König, M. Kuhl, and T. Richter. 1998. A modular luminescence lifetime imaging system for mapping oxygen distribution in biological samples. Sensors and Actuators B-Chemical **51**: 163-170.

Jonkers, H. M., R. Ludwig, R. De Wit, O. Pringault, G. Muyzer, H. Niemann, N. Finke, and D. De Beer. 2003. Structural and functional analysis of a microbial mat ecosystem from a unique permanent hypersaline inland lake: 'La Salada de Chiprana' (NE Spain). Fems Microbiology Ecology **44**: 175-189.

Kautsky, H. 1939. Quenching of luminescence by oxygen. Trans Faraday Soc **35**: 216-219.

Klimant, I., V. Meyer, and M. Kuhl. 1995. Fiberoptic oxygen microsensors, a new tool in aquatic biology. Limnology and Oceanography **40**: 1159-1165.

Kristensen, E. 1981. Direct measurement of ventilation and oxygen-uptake in 3 species of tubicolous polychaetes (Nereis Spp). Journal of Comparative Physiology **145**: 45-50.

Liebsch, G., I. Klimant, B. Frank, G. Holst, and O. S. Wolfbeis. 2000. Luminescence lifetime imaging of oxygen, pH, and carbon dioxide distribution using optical sensors. Applied Spectroscopy **54**: 548-559.

Lübbers, D. W. 1995. Optical sensors for clinical monitoring. Acta Anaesthesiologica Scandinavica **39**: 37-54.

Polerecky, L., U. Franke, U. Werner, B. Grunwald, and D. de Beer. 2005. High spatial resolution measurement of oxygen consumption rates in permeable sediments. Limnol. Oceanogr.: Methods **3**: 75-85.

Precht, E., U. Franke, L. Polerecky, and M. Huettel. 2004. Oxygen dynamics in permeable sediments with wave-driven pore water exchange. Limnology and Oceanography **49**: 693-705.

Rasheed, M., C. Wild, U. Franke, and M. Huettel. 2004. Benthic photosynthesis and oxygen consumption in permeable carbonate sediments at Heron Island, Great Barrier Reef, Australia. Estuarine Coastal and Shelf Science **59**: 139-150.

Revsbech, N.P. , J. Sørensen, T.H. Blackburn, and J.P. Lomholt. 1980. Distribution of oxygen in marine sediments measured with microelectrodes. Limnology and Oceanography. **25**: 403-411.

Wenzhöfer, F., and R. N. Glud. 2004. Small-scale spatial and temporal variability in benthic O2 dynamics of coastal sediments: Effects of fauna activity. Limnology and Oceanography **49**: 1471-1481.

Wild, C., M. Rasheed, U. Werner, U. Franke, R. Johnstone, and M. Huettel. 2004. Degradation and mineralization of coral mucus in reef environments. Marine Ecology-Progress Series **267**: 159-171.

Applications of porphyrin-based planar oxygen optodes and the modular luminescence lifetime imaging (MOLLI) system in aquatic environments

Ulrich Franke[1], Tjeerd Bouma[2], Emmanuelle Geslin[3,4], Gerhard Holst[1,5], Henk Jonkers[1], Stephanie Köhler-Rink[1], Gloria Peralta[2,6], Ursula Werner[1] and Lubos Polerecky[1]

[1] Max Planck Institute for Marine Microbiology, Celsiusstrasse 1, D-28359 Bremen, Germany

[2] Netherlands Institute of Ecology, Centre for Estuarine and Marine Ecology, P.O. Box 140, 4400 AC, Yerseke, The Netherlands

[3] Institute for Geology and Palaeontology, University of Tübingen, Sigwartstrasse 10, D-72076 Tübingen, Germany

[4] present address: Laboratory of Recent and Fossil Bio-indicators Dept. of Geology University of Angers, 49 045 Angers cedex - France

[5] present address: PCO imaging AG, Donaupark 11, 93309 Kelheim, Germany

[6] present address: Division of Ecology, Faculty of Marine and Environmental Sciences, University of Cadiz, Polígono del Río San Pedro s/n, 11510, Puerto Real (Cádiz), Spain), Spain

Acknowledgements

Introduction

Determination of oxygen distributions and exchange rates play important roles in characterising benthic microbial communities, as oxygen is the terminal electron acceptor for benthic aerobic processes as well as for products of anaerobic degradation of organic matter (Canfield et al. 1993). Revsbech et al. (1980) introduced microelectrodes to aquatic systems and these have become a fundamental standard tool applied in the studies of the oxic zone with high spatial and temporal resolutions (Kühl and Revsbech 2001). In 1995, microoptodes were introduced to the field of aquatic ecology by Klimant et al. (1995) as a cheaper, easily manufactured and long-term stable alternative to microelectrodes.

The measuring principle employed in microoptodes is based on dynamic quenching of luminescence of a specific fluorophore by oxygen (Kautsky 1939). The fluorophore molecule, when excited by a quantum of absorbed light, returns back from the higher energy level to the ground state by emitting a quantum of luminescence light. This emission is altered by the presence of oxygen molecules, resulting in a different intensity and/or lifetime of the luminescence in response to different oxygen concentrations (Lübbers 1995). The quenchable fluorophore is typically immobilised in a polymer matrix that is deposited on a tapered tip of an optical fibre. The optical fibre is used for both the delivery of the excitation light to the fluorophore and the guidance of the emitted luminescence to a signal-processing optoelectronic unit attached to the other end of the fibre (Klimant and Wolfbeis 1995).

Since microelectrodes and microoptodes can only be used for one-dimensional (1D) measurements, it is a difficult, time consuming and often impossible task to determine at micro and macro scales the spatial heterogeneity and temporal variability of oxygen in highly dynamic benthic systems. The 1D optical approach was improved by the introduction of planar oxygen optodes by Glud et al. (1996), which enabled the measurement of two-dimensional (2D) oxygen distributions with a comparable spatial resolution and thus considerably improved time efficiency of larger scale oxygen measurements. The sensing principle of a planar oxygen optode is the same as that of a microoptode, i.e., based on luminescence quenching by oxygen. However the polymer matrix containing the oxygen sensitive fluorophore is deposited as a thin layer on a transparent supporting foil.

The first utilised oxygen imaging system was entirely intensity-based. It consisted of a halogen lamp and a blue short-pass filter (≤ 450 nm) as an excitation unit, and a charge-

coupled device (CCD) camera, a red long-pass filter (≥ 610 nm) and a computer as the image acquisition and processing unit (Glud et al. 1996). To avoid scattering effects and potential stimulation of the biological sample by the excitation light, the optodes contained an additional thin layer of black silicone deposited on top of the sensing layer. The intensity-based oxygen imaging system was applied in the studies of sediments, biofilms and microbial mats (Glud et al. 1996; Glud et al. 1998; Glud et al. 1999).

A drawback associated with the measurement based on luminescence intensity is that the acquired images depend not only on the oxygen concentration but also on factors that are difficult to eliminate or control, such as varying background light, background luminescence and scattering effects, leaching and/or photobleaching of the oxygen-sensitive fluorophore and the distribution of the excitation light field (Liebsch et al. 2000; König et al. 2001). All of these undesirable factors are eliminated when a lifetime-based approach is used. For example, lifetime-imaging does not depend on a homogeneous fluorophore distribution across the foil, intensity variations due to leaching and/or photobleaching or the excitation light field distribution. Background luminescence can effectively be suppressed if it has a different decay time compared to that of the oxygen-sensitive fluorophore (Liebsch et al. 2000; Holst and Grunwald 2001).

A modular luminescence lifetime imaging (MOLLI) system suitable for high spatial resolution oxygen imaging in two and even three dimensions was first introduced and applied in marine microbiology by Holst et al. (1998). It consisted of an array of bright blue or green light emitting diodes (LEDs) serving as the excitation light source, a fast gateable CCD camera, a red emission filter (≥ 610 nm), a trigger controller and a computer used for the control and image acquisition (Holst et al. 1998; Holst and Grunwald 2001). Since its introduction, the luminescence lifetime imaging approach was employed in several laboratory studies of diverse marine systems such as photosynthetic and bioturbated sediments (Fenchel and Glud 2000; Holst and Grunwald 2001), permeable sandy sediments (Precht et al. 2004; Rasheed et al. 2004; Wild et al. 2004; Polerecky et al. 2005), corals and foraminifera (Holst and Grunwald 2001). First *in situ* applications in photosynthetic and bioturbated sediments were also conducted (Glud et al. 2001; Wenzhöfer and Glud 2004).

In addition to optically isolated planar oxygen optodes, transparent and semi-transparent optodes were also developed for the lifetime imaging approach. Transparent optodes enabled to link directly the structural elements of the studied biological sample and the measured oxygen distribution. However, they can only be applied to biological systems

where neither the sample itself nor the background structures move fast. This is because such movements could cause false calculation of oxygen values (Holst et al. 2001; Holst and Grunwald 2001). In contrast, semi-transparent optodes can be used in systems where the sample or background structures (e. g., propagating sediment ripples) move rapidly. This is because the milky appearance of the semi-transparent optodes, caused by scattering particles present in the matrix, prevents the moving particles (or other objects) behind the optode from influencing the calculation of oxygen distributions.

The first laboratory and *in situ* applications mentioned above demonstrated that oxygen optodes together with the intensity and/or lifetime imaging technique constitute a powerful tool for the visualisation and quantification of oxygen distributions and dynamics in diverse marine systems in two (planar optodes) and, to some extent, even three (dispersed dye or oxygen sensitive nano-particles) dimensions. They enable the measurement of oxygen distributions over relatively large areas (a few mm^2 to ~ 1 dm^2) with high spatial (~ 50 – 200 µm) and temporal (1 - 5 s) resolutions, thus considerably enlarging the amount of information that can be obtained from the studied system.

Here we report briefly on a number of unpublished laboratory applications using planar optodes which were conducted to study a variety of processes in different aquatic systems. In particular, microcosm experiments were utilised to visualise the impact of bioirrigation on the oxygen distribution in the surrounding sediment; oxygen measurements were carried out in a hypersaline microbial mat to assess the feasibility of the technology to measure high spatial resolution images of gross photosynthesis; experiments with foraminifera were conducted to assess oxygen distributions around and oxygen uptake rates of small three-dimensional objects; it was tested if planar optodes are a feasible tool for studying radial oxygen loss (ROL) from the rhizosphere of seagrass roots; the dependence of volumetric oxygen consumption rate (OCR) in permeable sandy sediment on temperature was studied using the planar optode based flow-through method; the possibility of distinguishing between the biological (due to microbial respiration) and chemical (due to oxidation of reduced compounds) contributions to the total sedimentary OCR was investigated by combining the planar optode based flow-through method with long-term incubation under oxic and anoxic conditions. The focus of theses experiments was the assessment of the applicability and the identification of the advantages and limitations offered by the use of the porphyrin-based planar oxygen optodes and the lifetime-based oxygen imaging technology.

Material and methods

Oxygen measurements

One-dimensional (1D) oxygen measurements

High spatial resolution oxygen microprofiles and photosynthesis measurements were measured with Clark-type oxygen microelectrodes (Revsbech 1989). The sensors had tip diameters of ~ 10 µm, stirring sensitivities of < 1.5 % and response times of < 0.2 seconds. The microelectrodes were connected to a high-precision picoammeter whose signal was collected by a data-acquisition card (National Instruments) for PC data acquisition. Calibrations of the sensors were conducted at the experimental temperatures and salinities. Air-saturated water or water saturated with nitrogen gas as well as anoxic sediment parts, if present in the experiments, served for the determination of air saturation and zero oxygen calibration values, respectively. The sensors were attached to a micro-manipulator mounted on a motorised linear stage (VT-80, Micos) and placed above the sample, enabling reproducible positioning (precision +/- 1 µm) of the sensor tip.

Two-dimensional (2D) oxygen distributions

Two-dimensional oxygen distributions were measured using optically isolated, transparent or semi-transparent planar oxygen optodes. The transparent and semi-transparent optodes consisted of 2 layers: a transparent polyester support foil (125 µm thick, Goodfellow) and a sensing layer. The sensing layer with the thickness of 15-30 µm was deposited on the support foil by knife-coating. The sensing layer was made of a mixture of 10 mg luminescent oxygen indicator platinum(II) meso - tetra (pentafluorophenyl) porphyrin (Pt-PFP) (Porphyrin Products), 490 mg Polystyrene (Sigma-Aldrich) and 3 ml Chloroform (Merck). For semi-transparent optodes 330 mg titanium dioxide (TiO$_2$) particles (< 5 µm, Aldrich) were added to the solution to increase the excitation efficiency by light scattering within the sensitive layer, whereby the transparency of the optode is lost and the sensor appears milky (Klimant et al. 1995). Optically isolated optodes were based on semi-transparent optodes but an additional layer of black silicone was added on top of the sensing matrix. The indicator/matrix cocktail and the black silicone layer were spread by a knife-coating process onto the polyester support foil and the sensor matrix, respectively. The thicknesses of the dry sensing layer and the black silicone layer were ~ 15 - 30 µm and ~ 20 - 40 µm, respectively.

Figure 1 shows the scheme of the general setup used for the 2D oxygen measurements. Planar optodes were glued with transparent silicone (Elastosil® E4, Wacker) to the inside of a transparent window of various aquaria and sediment cores, which were constructed so as to suit each particular application. Oxygen imaging was facilitated by the modular luminescence lifetime imaging (MOLLI) system (Holst et al. 1998; Holst and Grunwald 2001). The optodes were excited by either blue LEDs (HLMP-CB 15, λ_{max} = 475 nm, Agilent, or Luxeon V Star Blue, λ_{max} = 470 nm, Lumileds) or a blue laser-diode module (PVLS-3000, λ = 404 nm, Toptica Photonics). The laser light was shaped by line optics (OZ Optics) to form a thin laser line (~ 200 µm wide and ~ 4 cm long in the distance of ~ 10 cm). The red luminescence light (λ_{max} = 647 nm) emitted by the optode passed through a red optical filter (Deep Golden Amber, LEE-Filters) before being detected by a fast gateable CCD Camera (SensiCam, PCO, image size 640 $\times$ 480 pixels).

The rapid lifetime determination (RLD) method (Ballew and Demas 1989; Liebsch et al. 2000) was employed to measure the luminescence lifetime distributions. Lifetime values were converted into oxygen concentrations using a modified two-component model of the Stern-Volmer equation (Klimant et al. 1995; Holst et al. 1998). Further image processing was carried out with either a computer program developed in IDL® (Holst and Grunwald 2001) or Matlab® (Polerecky et al. 2005). Calibration was carried out before and after the experiments, whereby the lifetime values corresponding to 0 and 100 % air saturation (AS) were taken as an average of many pixels (n > 100) from the areas of the planar optode which were known to be anoxic and air saturated, respectively. All oxygen measurements were conducted in the dark to minimise the effects of the background light and prevent the possible production of oxygen in photosynthetically active samples.

Oxygen consumption rates

Under diffusive conditions, oxygen fluxes were calculated from steady state 1D oxygen profiles, which were either extracted from oxygen images or measured by oxygen microelectrodes. The profiles were fitted to Fick`s law (e.g. Crank (1975)) describing the diffusive oxygen flux as

$$J = - D_0 \, (dC/dz), \qquad\qquad (1)$$

where D_0 is the molecular diffusion coefficient for oxygen at a given temperature and salinity and C is the oxygen concentration at position z.
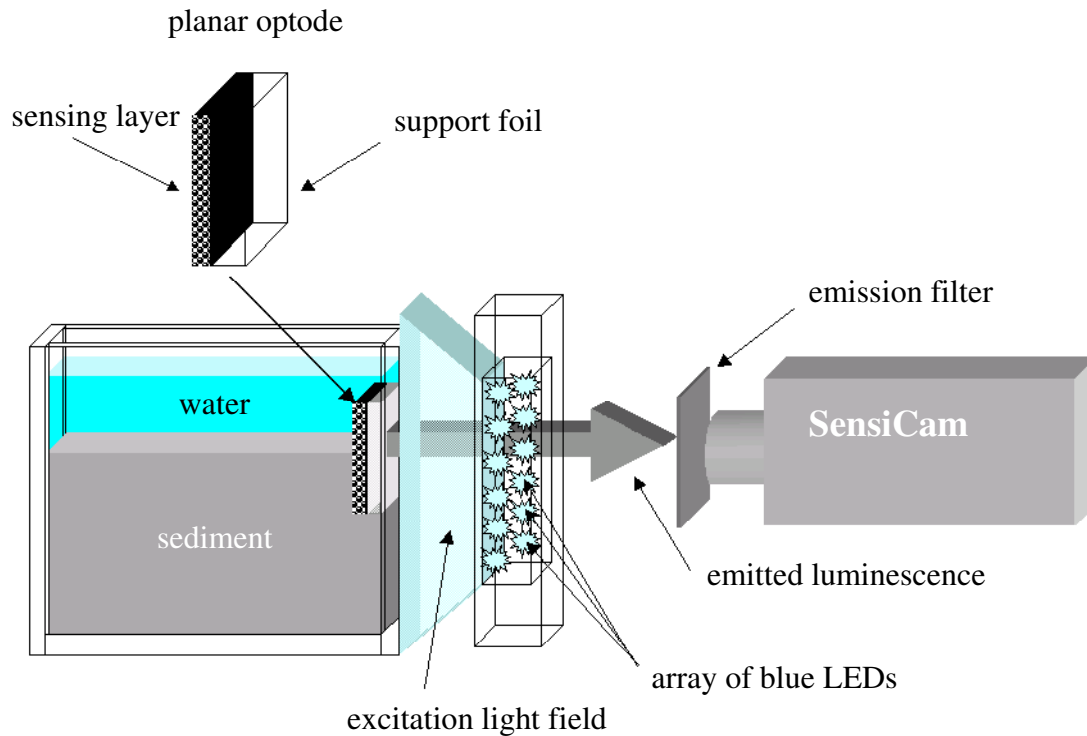
Figure 1: Schematic diagram of the general experimental setup comprising a sample and the oxygen imaging system.

Two-dimensional images of volumetric oxygen consumption rates (OCR) were determined from the time-series of 2D oxygen distributions measured by planar optodes. The OCR values were calculated as the initial slope of the oxygen change measured in each pixel, implementing the algorithm described in detail by Polerecky et al. (2005). All oxygen consumption rates were expressed per volume of sediment.

Biological applications

Bioturbation and bioirrigation experiments

Approximately 8 – 10 specimen of the polychaete *Hediste diversicolor* (O. F. Müller), which is known for its bioturbation and irrigation activity, were introduced into an aquarium filled with natural intertidal muddy sediment and habitat seawater (salinity 25). The aquarium was equipped with a flow system by which aerated surface water could be recirculated. Before the oxygen measurements were started, the sediment was allowed to settle and regain natural stratification for 1 – 2 days. Time series of oxygen distributions with image intervals ranging from seconds to minutes were recorded.

Microbial mat experiments

A piece of a hypersaline microbial mat (a detailed description of the microbial mat from the lake Chiprana, Spain, can be found in Jonkers et al. (2003)) was cut and placed in an aquarium in direct contact with an optically isolated semi-transparent planar oxygen optode and fixed on the other three sides by 2 % agar (Glud et al. 1999). The used aquaria were equipped with a flow system which facilitated recirculation of aerated or oxygen-depleted water above the mat.

The mat surface was approximately determined by first illuminating the mat samples (i.e., generating oxygen within the top part of the mat) and circulating oxygen-depleted water above the mat surface until steady state oxygen distributions were measured. Afterwards, the mat was darkened (resulting in anoxia in the top part of the mat) and oxic overlying water was circulated until steady state oxygen distributions were measured. The mat surface was taken as the position of the steepest vertical oxygen gradients. When the two steady state oxygen images were overlaid, both mat surface lines agreed well.

Mat samples were illuminated by white light from a fibre-optic halogen lamp. Volumetric gross photosynthesis (VGP) measurements were conducted applying the light/dark shift technique (Revsbech and Jørgensen 1983). Two-dimensional distributions of the VGP rates were calculated using the same algorithm as that used for the calculation of OCR (Polerecky et al. 2005). Steady state oxygen distributions developed at a fixed irradiance (~ 800 µmol photons m^{-2} s^{-1}) after approx. 30 min, as evaluated from the image series.

Foraminifera experiments

Experiments were conducted with two species of different sizes: *Ammonia beccarii* (Linné) and *Masselina secans* (d`Orbigne) with mean diameters of 0.8 and 1.4 mm, respectively. Oxygen distributions were measured by semi-transparent and transparent oxygen optodes, the latter enabling to link the oxygen distributions directly to the organism morphology. Single *A. beccarii* specimens were studied with an inverse microscope setup with a petri dish filled with air saturated sea water. *M. secans* specimens were studied in aquaria filled with natural muddy sediment and overlying sea water, which was bubbled constantly with an aquarium bubble stone. Prior to the experiments it was checked, by using the living and dead organisms, whether the scattering of light from a shell of the foraminifera had any influence on the oxygen measurement.

Organisms were added to the setups and time series of oxygen distributions were recorded in intervals of minutes to hours. Because the oxygen data were too noisy to

calculate 2D OCR from the time series (see Polerecky et al. (2005) for more details on this topic), uptake rates were estimated by calculating oxygen fluxes using Eq. (1) and the profiles extracted from the steady state oxygen images. The used diffusion coefficient (D$_0$) for oxygen in seawater (20°C, salinity 34) was D$_0$ = 1.98 × 10^{-5} cm^2 s^{-1} (Broecker and Peng 1974; Li and Gregory 1974). Assuming that the oxygen uptake did not vary across the surface of the organism, the approximate oxygen uptake rate by a single specimen was calculated by multiplying the oxygen flux with the surface of the specimen. The surface area (S) of *A. beccarii* was calculated assuming a half-sphere shape of the specimen, i.e., S$_{half-sphere}$ = 4/2 × π × r^2 (r = radius)**,** as used by Hannah et al. (1994). Alternatively, S was calculated assuming an ellipsoid shape of the specimen, where the surface of an ellipsoid was approximated by S$_{ellipsoid}$ ~ 2π(a^{P}b^P + b^{P}c^P + a^{P}c^P)$^{1/P}$, where P = ln3/ln2 and, in our case, a = b = radius, c = height/2 (http://home.att.net/~numericana/answer/ellipsoid. htm#thomsen).
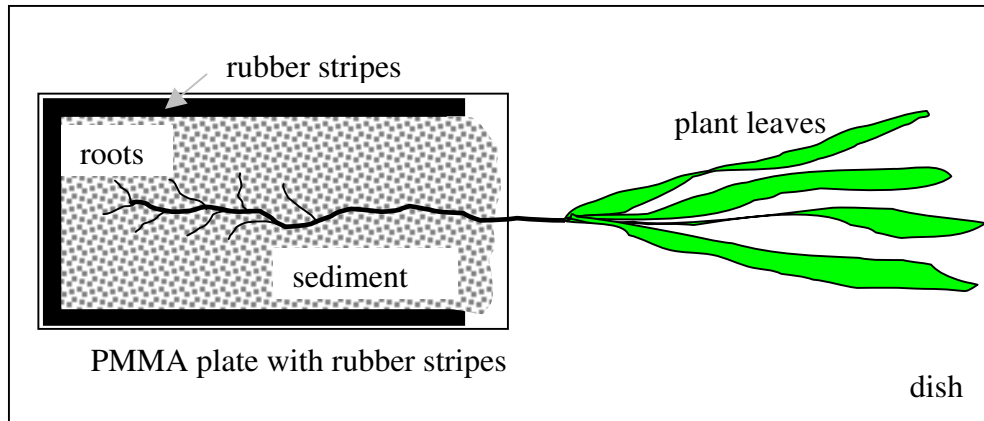
Seagrass experiments

Initial experiments with seagrass roots were done in large aquaria (size: l × h × w = 30 × 30 × 60 cm). At one side of the aquaria a transparent polymethylmethacrylate (PMMA) window was present on which a planar optode was fixed. Seagrass was planted close to the window and roots developed in direct contact to the optode. Because it was too difficult and time consuming to change the plants and sediment compositions in this type of aquaria, small cuvettes were used instead. The cuvettes were made of two transparent polymethyl-methacrylate (PMMA) plates, one equipped with a planar oxygen optode and the other with rubber slices (approx. 3mm thick) on three sides. Wet aerated sediment was placed between the rubber slices. The seagrass roots were carefully cleaned of the sediment in which they had been growing and then placed in the cuvette so that the shoot of the plant was sticking out of it and the roots were placed on top of the sediment (Fig. 2A). The cuvette was subsequently closed by putting on top the PMMA plate equipped with the planar optode, making sure that no air bubbles remained in the cuvette (Fig. 2B). The two plates were fixed by clamps and the cuvette was placed in a dish filled with seawater to prevent drying of the sediment and the plant.

Immediately after fixing the roots in the cuvette, oxygen images were taken in 10 s intervals and a 2D map of OCR of the sediment surrounding the roots was determined using the algorithm described by Polerecky et al. (2005). To induce radial oxygen loss (ROL) from the seagrass roots, the leaves of the plant were illuminated by a halogen lamp

while the roots were kept in the dark by covering the cuvette with a black cover. The black cover was temporarily removed and the halogen lamp switched off in 20-30 min intervals and oxygen images were taken. This was repeated over several hours until steady state was reached. To calculate the oxygen consumption rate of the used sediment according to Polerecky et al. (2005), oxygen image series were taken (image interval = 10 s).
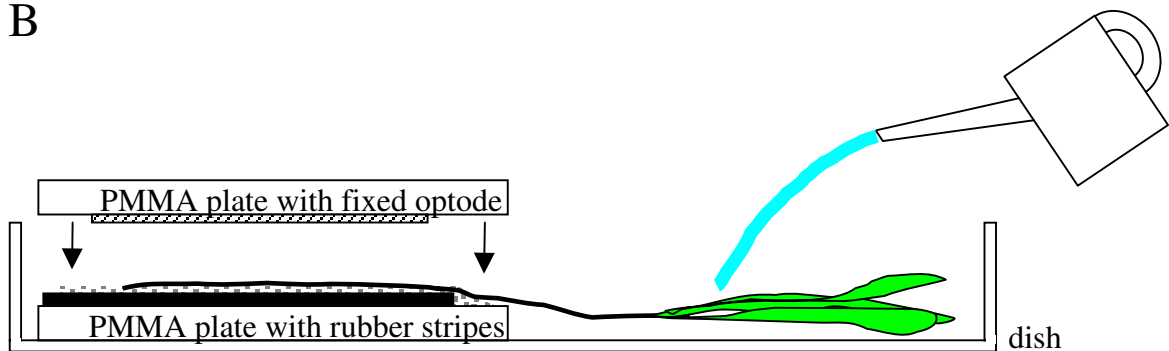
A

B

Figure 2: Top (A) and side (B) views of an experimental setup for the measurement of radial oxygen loss by seagrass roots. Illumination by the excitation light and the image acquisition by the CCD camera were done from above.

Temperature experiments

The dependence of volumetric OCR of natural permeable sediment on temperature was investigated by means of the flow-through method (Polerecky et al. 2005). Three undisturbed permeable sediment cores (for details of the stainless steel cores used, see Polerecky et al. (2005)) were collected from the intertidal sandflat Hausstrand located on

Sylt Island (German North Sea) in October 2003. The cores were transported into the laboratory and the flow-through measurements started ~ 8 h after the collection.

Volumetric OCRs were measured at 5 different temperatures (4, 10, 15, 20 and 26°C) in dark, temperature-controlled rooms. The measurements started at 4°C and proceeded through 10 to 26°C. In the end, OCRs were measured again at 4°C to assess the reproducibility. Sediment cores were allowed to acclimatise at each temperature for 24 h in the dark prior to the OCR measurements to ensure that no temperature gradients were present.

The measuring protocol is described in detail by Polerecky et al. (2005). The flow-on periods, during which the sediment cores were percolated with aerated artificial seawater (Instant sea^{TM}; salinity 32), lasted approx. 6 min (corresponding to 250 – 300 ml of seawater). The duration of the flow-off periods, when oxygen images were continuously recorded in 10-30 s intervals, varied depending on the temperature from 15 min (26°C) to 50 min (4°C).

From the time-series during the flow-off periods, two-dimensional images of OCR were determined as described by Polerecky et al. (2005). Values of volumetric OCR were averaged over 4 depth intervals (0 – 2, 2 – 4, 4 – 6 and 8 – 10 cm) for each temperature. These values were plotted against the inverse temperature (1/T) and fitted with the Arrhenius relation

$$OCR = A \times e^{-E_a / (R \times T)} \tag{2}$$

which describes the temperature dependence of OCR. This allowed the determination of the activation energy (E_a) of the processes governing the observed oxygen consumption. In Eq. (2), A is a constant, R is the gas constant (R = 8.31 J mol^{-1} K^{-1}) and T is the absolute temperature. Using E_a, the quotient of the rate increase after a 10°C temperature increase (Q_{10}) was calculated according to Thamdrup et al. (1998) as

$$Q_{10} = OCR(T+10°C) / OCR(T) = e^{E_a \times 10 / [R \times T \times (T+10)]} \tag{3}$$

Differentiation between the chemical and biological oxygen consumption rates

Due to the presence of reduced compounds in the sediment, oxygen consumption by means of chemical oxidation can be as high or even higher than that governed by biological respiration (Jørgensen 1982; Canfield et al. 1993). To investigate the possibility of differentiation between the chemical and biological contributions to the total

sedimentary OCR by applying the flow-through method, one of the cores used for the temperature experiments (see above) was subsampled at 0 – 2 and 8 – 10 cm depth intervals. The sediment subsamples (~ 30 cm^3) were homogenised, split into tree parts, transferred into Erlenmeyer flasks and covered with artificial sea water (Instant sea^{TM}; salinity 32), which was aerated by continuous bubbling with air. The sediments in the first and the other two flasks were used in experiments with short- and long-term exposures to oxygen, respectively.

In the short-term experiment, which was conducted at 20°C, approximately 6 cm^3 of the sediment of the upper sediment horizon (0 – 2 cm) was filled into a small flow-through core equipped with a planar optode. The sediment was exposed to oxygen by maintaining percolation with aerated seawater, which was recirculated. Eight flow-through measurement cycles were conducted in succession over the total measurement time of ~ 150 min. The duration of the flow-on periods was always 2 min, while the flow-off periods, during which the sedimentary OCR were determined, lasted for 13, 60 and 13 min for the flow-through cycles 1 – 6, 7 and 8, respectively. The timing was chosen so that the sediment did not reach anoxia during the cycles 1- 6 and 8, whereas it did remain anoxic for approximately 40 min after the cycle 7.

In the long-term experiment, the sediment in one of the flasks was left undisturbed (unstirred) for 8 days, whereas the sediment in the second flask was stirred on a cell-culture shaker for 8 days so that the sediment was in suspension. According to Thamdrup et al. (1998), most of the reduced compounds in the suspended sediment should become oxidised and the OCR measured after 8 days should mainly be caused by biological oxidation. On the other hand, both the chemical and biological contributions to the OCR measured after 8 days should be present in the undisturbed sediment. The volumetric OCRs were measured at the beginning and after 8 days by the flow-through method with the flow-on and flow-off periods lasting for 2 (corresponding to ~ 100 ml of seawater) an 13 min, respectively.

These OCR measurements were conducted at 4 different temperatures (4, 10, 15 and 20°C) Approximately 6 cm^3 of the sediment was taken from the Erlenmeyer flasks and filled into a small flow-through core (Fig. 3). The sediment was then flushed with ~ 100 ml of aerated artificial seawater and the volumetric OCRs were measured. After each OCR measurement, the sediment was returned into the respective Erlenmeyer flask and stored at the next temperature for 2.5 hours, either undisturbed or suspended, until the next OCR

measurement. The values of E$_a$ and Q$_{10}$ for each sediment sample were determined from the Arrhenius plots, as described in the previous section.
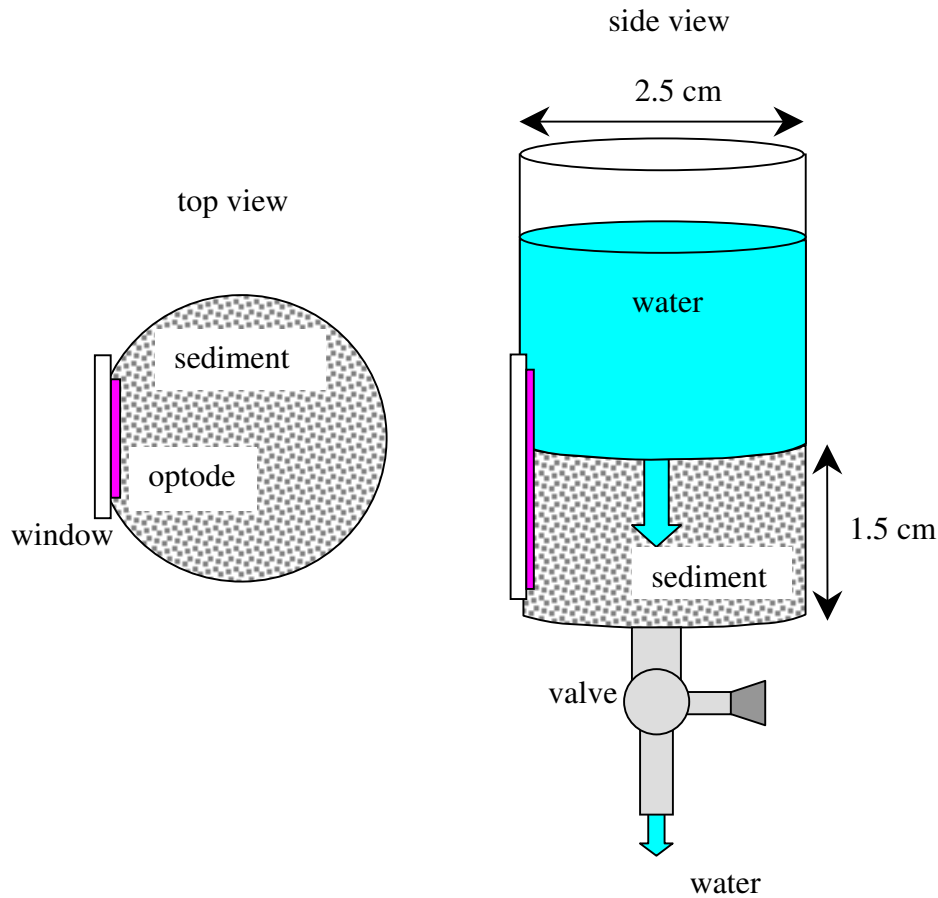
side view

top view

Figure 3: Schematic diagram of a small cylindrical core used for the measurements of oxygen consumption rates in small sediment samples by the flow-through method. A flat transparent window, to which a planar oxygen optode was glued, was fixed to a small opening cut at a side of the cylinder. The valve at the bottom of the core was used to adjust the percolation of the sediment with aerated seawater. Illumination by the excitation light and the image acquisition by the CCD camera were done from the side. Note that dimensions are not to scale.

Results and discussion

Bioturbation/bioirrigation experiments

Hediste diversicolor specimens started building burrows immediately after their introduction into the sediment-filled aquaria. Some of these burrows were in direct contact with the planar oxygen optode, allowing real-time monitoring of oxygen dynamics associated with the burrowing and pumping activity of the worms. Examples of typical oxygen distributions in and around the burrow are shown in Fig. 4A-C. To show more

clearly the irrigation and resting rhythms of the worm, oxygen data were averaged in two locations inside the burrow and plotted as a function of time (Fig. 4D). Increasing and decreasing oxygen concentrations in the burrows were interpreted as irrigation activity and resting phases of the animals, respectively. Rhythms were relatively stable, with irrigation and resting periods lasting for 1 and 1 – 2 min, respectively. Depending on the chosen location, oxygen concentrations in the burrow varied between approx. 100 and 10 or 80 and 30 µmol L^{-1} during the irrigation and resting periods, respectively. The entire oxygen dynamics can be found in the folder "Chapter-6-Movie" on a CD-Rom, which can be made available upon request (contact: Ulrich Franke, Ostarastr. 5, 51107 Köln, e-mail: u.franke@fab-anlagenbau.com).
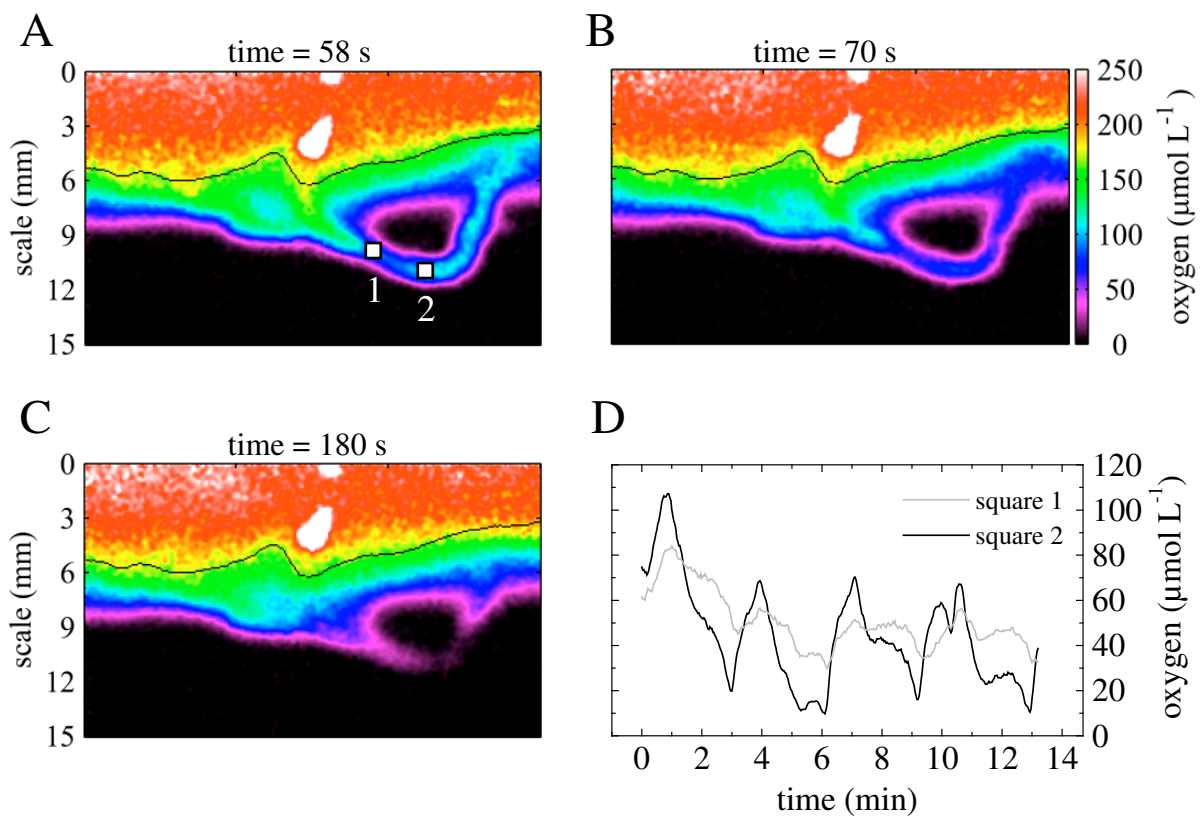

Figure 4: Examples of oxygen distributions in and around a burrow of *H. diversicolor* at different times during a 13 min long time-series (panels A-C). Mean oxygen concentrations at two positions inside the burrow, indicated as squares 1 and 2 in panel A (size of 5 × 5 pixels, depicted not to scale), as a function of time are also shown (panel D). Black horizontal lines in A - C indicate the sediment surface. The full movie showing the entire oxygen dynamics can be found in the folder "Chapter-6-Movie" on a CD-Rom, which can be made available upon request (contact: Ulrich Franke, Ostarastr. 5, 51107 Köln, e-mail: u.franke@fab-anlagenbau.com). Note that squares in (A) are not to scale.

The rates of the concentration change after the irrigation started or stopped differed considerably at the two selected locations (Fig. 4D). The two-dimensional situation around the whole burrow is depicted by the image of volumetric OCR determined during the resting phase within the time interval 60 and 180 s. OCR values ranged from 5 to 80 µmol L^{-1} min^{-1} (Fig. 5). Fenchel (1996a) determined, with the help of oxygen microelectrodes, the decrease of oxygen directly inside an empty *Hediste diversicolor* burrows after the burrows were flushed with aerated water. From these data we estimated OCR values of ~100 µmol L^{-1} min^{-1}, which is close to our measured maximum OCR.
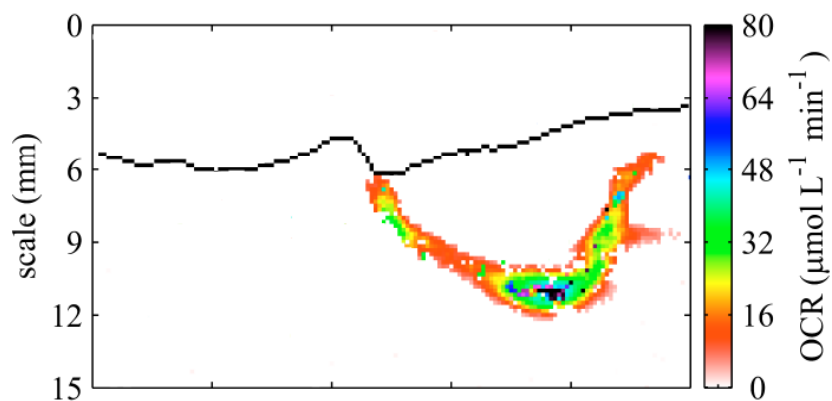

Figure 5: Two-dimensional distribution of OCR around the burrow of *Hediste diversicolor* calculated during the resting time interval 60 – 180 s. The black line indicates the sediment surface.

Hediste diversicolor has been described as a carnivore and/or scavenger, a detritivore, feeding partly on mud around the borrow opening, but also as a filter-feeder (Riisgard 1991 and references therein; Vedel and Riisgard 1993). The filter-feeding mechanism is based on a mucus net within the burrow and a water current created by undulating body movements of the polychaete. Suspended particles get trapped in the net, which is subsequently eaten. Riisgard (1991) found filter-feeding patterns of 1.5 ± 0.5 min of net spinning, 3 ± 1 min of water pumping and approx. 0.25 min of net eating. Similar patterns can be seen from the time series of oxygen concentrations obtained in our experiments (Fig. 4D). In contrast, Fenchel (1996a) found irregular pumping patterns with anoxia in the burrow when the worm partially or totally left the burrow during deposit-feeding on the sediment surface. As no such deposit-feeding on the surface was observed in our experiments, it can be assumed that the polychaetes in our experiments were most likely filter-feeding.

The activity of polychaetes is normally determined by recording their body movements (in strokes min^{-1}) with the help of infrared phototransducers (Riisgard 1991; Riisgard et al. 1992; Vedel et al. 1994), their ventilation rate with electromagnetic flow meters (in ml min^{-1}) (Kristensen 1981; Kristensen 1983a; Kristensen 1983b), or oxygen dynamics using oxygen microelectrodes (μmol L^{-1}) (Fenchel 1996a). Our measurements demonstrate that planar oxygen optodes constitute a useful tool using which such information as the rhythms of the worm activity and the effects of worm's pumping on the surrounding sediment can be determined with minimal effort. However, the extent to which the results can reliably be used as a quantitative measure of the worm's activity is limited, as a consequence of the light guidance effects and the fact that it is very difficult to assess the relative position of the borrow with respect to the wall formed by the planar optode.

As explained in more detail in chapter 5, the light guidance effect can result in underestimated values of oxygen concentrations determined inside or around the burrows by the planar oxygen optode. To determine the degree of this underestimation in the context of these experiments would, however, require further investigation.

Another problem associated with the use of planar optodes is that the exact position of the burrow relative to the optode is not easy to detect. Even when using transparent or semi-transparent optodes, it remains unclear whether the optode is in direct contact with the burrow lumen (burrow centre) or rather the burrow wall is sectioned at some specific distance from the burrow centre. As schematically shown in Fig. 6, these two situations would result in considerably different expected profiles of oxygen concentrations detected by the optode.

Wenzhöfer and Glud (2004) stated that the position of the burrow was identified in their experiments by a distinct break in the oxygen profiles crossing the apparent burrow inside. This could not be confirmed by our data, especially because at higher oxygen concentrations the noise of the oxygen data is more pronounced, whereby small oxygen changes are smeared. Nevertheless, even if such a break was detectable, the inability to determine exactly the relative position of the burrow and the optode would still cause that the estimation of exchange of oxygen across the burrow wall could be inaccurate.

Thus, it can be concluded that the presented technique can be used to visualise oxygen dynamics around bioirrigated burrows and show how irrigating fauna enhances the penetration of oxygen into otherwise anoxic sediment. However, further interpretation and calculations with the measured oxygen data is problematic and have to be done with care.
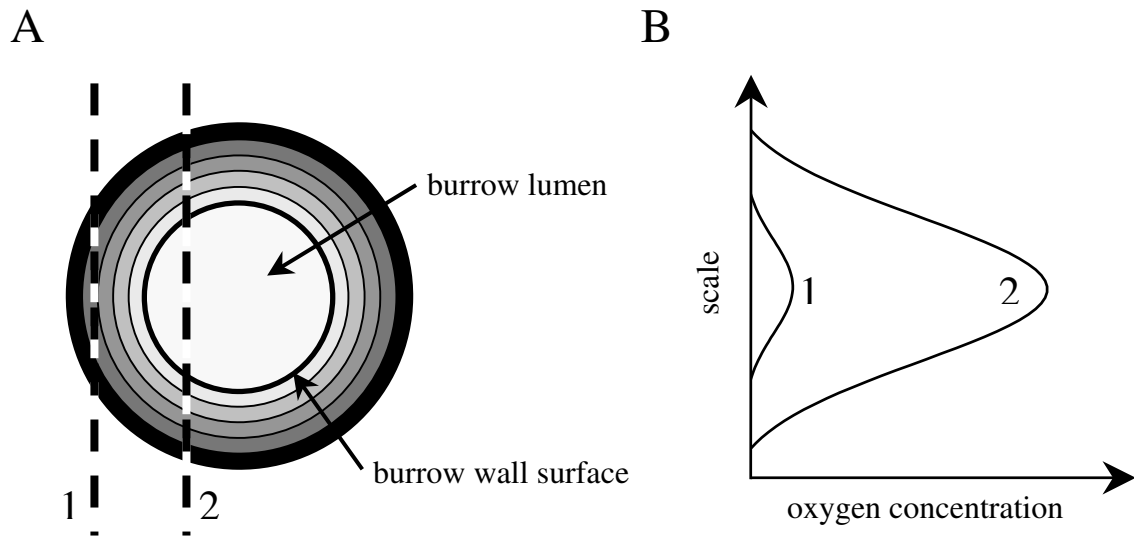
Figure 6: (A) Cross-section of a cylindrical polychaete burrow, schematically showing the oxic lumen and steep oxygen gradients within the burrow wall towards the anoxic surrounding sediment. Different oxygen concentrations are indicated by the different shades of grey, black corresponding to anoxia. Depending on the relative position of the optode and the burrow, indicated by dashed lines 1 and 2, the oxygen profile may differ considerably, as shown schematically by the corresponding curves in graph (B).

Microbial mat experiments

Examples of steady state oxygen distributions in a microbial mat kept in the dark and maintained under constant illumination are shown in Figs. 7A and 7B, respectively. During darkness oxygen penetration into the mat was limited to the top ~ 1 mm. When the mat was illuminated, oxygen penetration increased to ~ 3 mm and enhanced oxygen concentrations (up to 600 µmol L^{-1}) were detected in some regions of the mat. When, after the constant illumination, the light was switched off, oxygen was rapidly depleted inside the mat. An example of the oxygen distribution obtained 6.5 min after the light was switched off is shown in Fig. 7C.

Figure 7D shows the 2D distribution of volumetric gross photosynthesis rates (VGP) obtained from the time series of oxygen images recorded after the illuminating light was switched off. Typical VGP ranged from ~ 30 to ~ 80 µmol L^{-1} min^{-1}, which is in good agreement with the values of 30 - 120 µmol L^{-1} min^{-1} obtained from *in situ* microelectrode-based light/dark shift measurements conducted by Jonkers et al. (2003) at comparable light intensities.

It must be mentioned that the time series used for the determination of VGP lasted up to 6 min. This is considerably longer than the time interval typically employed in the light/dark shift method (< 1 to 2 s) (e.g. Revsbech and Jørgensen 1983; Epping et al. 1999). The need for such a long interval rose from the fact that the oxygen images obtained by planar optodes were very noisy, particularly at higher oxygen concentrations. For example, the noise could reach up to 80 % AS when the average oxygen concentrations were around 350 % AS. Due to such noise levels, the presented data should be considered only as approximate values of GPR.
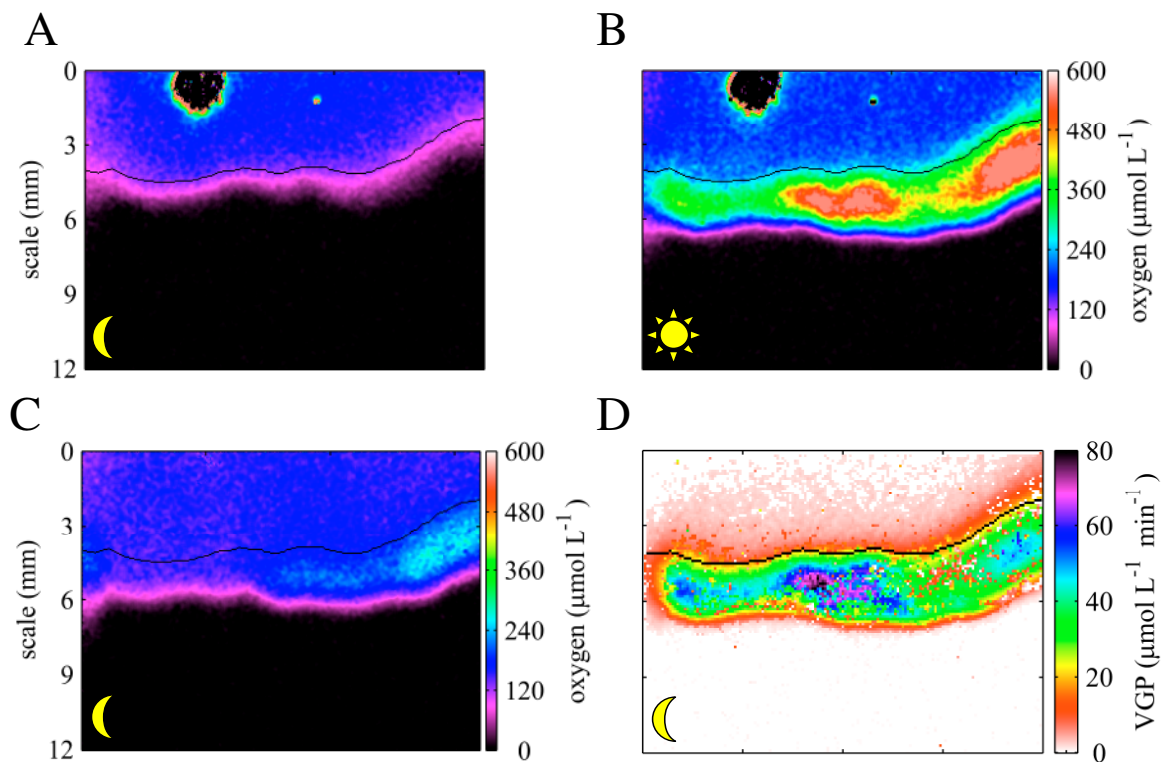

Figure 7: Typical steady state oxygen distributions in a microbial mat during darkness (A) and constant illumination (B). Oxygen distribution 6.5 min after the light was switched off is shown in (C). Two-dimensional distribution of the volumetric gross photosynthesis rate (VGP), obtained from the time-series recorded after the light was switched off, is shown in (D). Black lines indicate the mat surface.

Fitting each vertical profile of a steady state 2D oxygen distribution in a microbial mat by a diffusive model, Glud et al. (1999) were able to calculate a 2D distribution of net oxygen production and consumption rates with submillimeter spatial resolution. This was, however, not possible in our experiments, mainly due to the high noise level of the oxygen images.

In conclusion, the planar optode based technique is useful for visualisation of the small to large scale heterogeneities in oxygen distributions as well as of oxygen dynamics in microbial mats. However, the relatively high noise of the oxygen data, the problems associated with the cross-talk effect (see chapter 5) as well as the relatively small temporal resolution of the acquisition of oxygen images make the accurate 2D determination of gross and net rates of photosynthesis with submillimeter resolution difficult.

Foraminifera experiments

The experiments with living and dead foraminifera conducted with the inverse microscope setup revealed that the shells of the organisms did not influence the oxygen measurements by light scattering effects. At positions of living foraminifera a decrease in oxygen concentrations was detectable relative to the air saturated sea water (Fig. 8A). In contrast, at the location of dead foraminifera no change in oxygen concentration was visible (Fig. 8B).
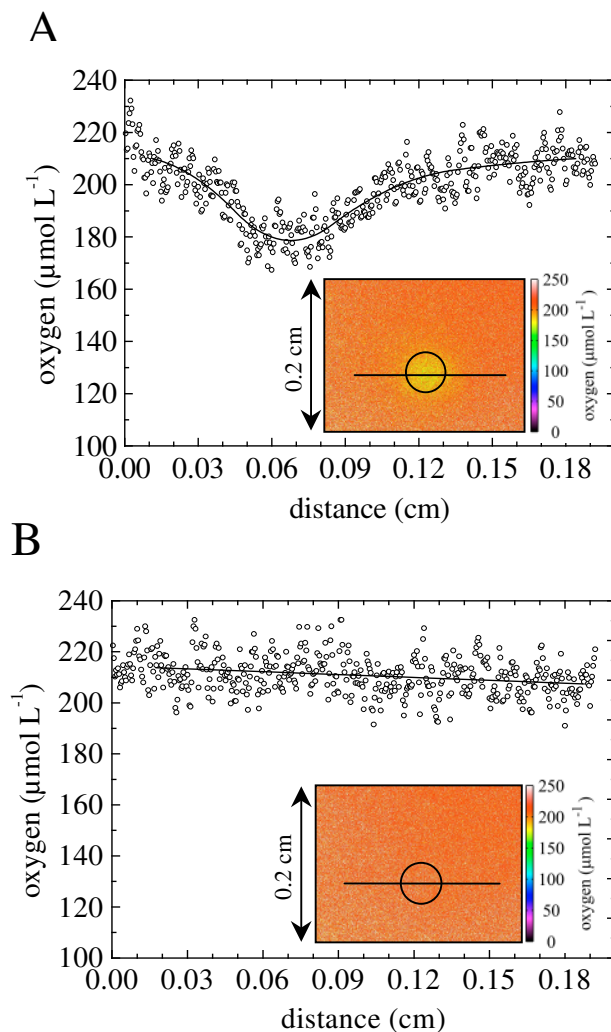

Figure 8: Oxygen distributions around a living (A) and dead (B) foraminifera (*Ammonia beccarii*) lying on top of a planar oxygen optode and surrounded by aerated seawater. Profiles extracted from the oxygen images, depicted in graph insets, were fitted by a diffusion model. Straight lines in the oxygen images show the positions of the extracted profiles, circles indicate the approximate silhouette of the foraminifera.

Although the noise of the oxygen data was pronounced, it was possible to fit oxygen profiles extracted from the oxygen images by a diffusion model. This procedure resulted in diffusive oxygen fluxes of 47 – 65 nmol cm^{-2} h^{-1} for one investigated specimen of *Ammonia beccarii*. Fluxes measured by oxygen microelectrodes on different specimens of *A. beccarii* were in the range of 18 – 150 nmol cm^{-2} h^{-1} (Köhler-Rink, pers. comm.), indicating that the results derived by the planar optode technique were realistic. Considering the dimensions a = b = radius ~ 0.3 mm and c = height/2 ~ 0.17 mm and the approximation of the shape of the specimen by a half-sphere and ellipsoid, oxygen consumption rates of 5.5 – 7.5 and 8.2 – 12.0 nl O$_2$ individual^{-1} h^{-1} were derived, respectively. These results are consistent with the cartesian diver respirometry experiments conducted with single specimen of *A. beccarii*, where respiration rates of 7.5 ± 2.78 nl O$_2$ individual^{-1} h^{-1} were determined (Hannah et al. 1994).

It should be noted that the oxygen uptake rates calculated from the oxygen fluxes determined by the planar optodes may be underestimated, namely due to the round shape of foraminifera specimen. The three-dimensional oxygen concentration profile created by the respiring foraminifera specimen is intercepted by the planar optode. Due to the small size and round shape of the specimen, oxygen gradients measured in the direction of the plane touching the specimen (Fig. 9A) may be smaller than those measured perpendicularly to its surface, as schematically depicted in Fig. 9B. The accuracy of the estimation of the oxygen uptake rates by means of planar optodes could be improved provided that the shape, orientation and the true distance of the specimen lying on the planar optode is known.

Time series of oxygen distributions in aquaria filled with relatively inactive sediment, characterised by deep oxygen penetration depths, showed that metabolic activity of *M. secans* could be detected and their movement along the aquarium wall could be followed as areas of locally reduced oxygen concentrations (Fig. 10). Exact positions of the organisms were determined through the transparent optode. Migration velocities of up to 1.5 mm h^{-1} were observed for a single specimen. The movement was generally along oxygen gradients towards higher oxygen concentrations, which could be interpreted as chemosensory motile behaviour (Fenchel 1996b).
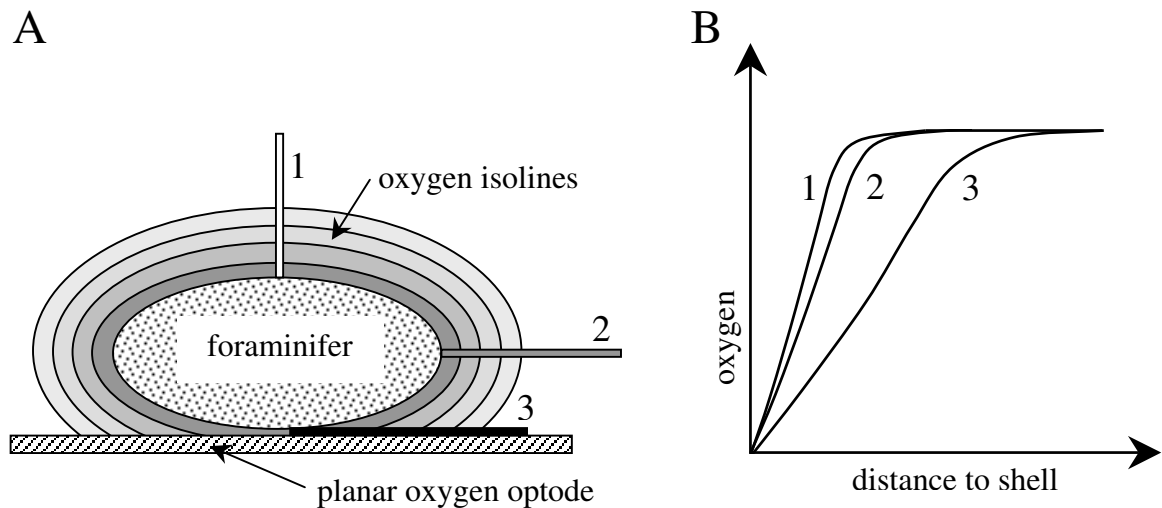
Figure 9: Schematic diagram depicting why the oxygen gradients around a foraminifera specimen measured by a planar oxygen optode can be underestimating the true values due to the round shape of the specimen. (A) Round-shaped foraminifera specimen lying on a planar oxygen optode. The concentric oxygen isolines are intercepted by the planar oxygen optode, resulting in an oxygen profile depicted by line 3 in graph (B). If the oxygen profiles were measured perpendicularly to the surface, e.g., with a microelectrode, the observed gradients would be larger, as depicted by lines 1 and 2 in graph (B). Note that the oxygen isolines (A) and profiles (B) are depicted only for qualitative demonstration purposes and may differ quantitatively from the correct shapes corresponding to the real situation.
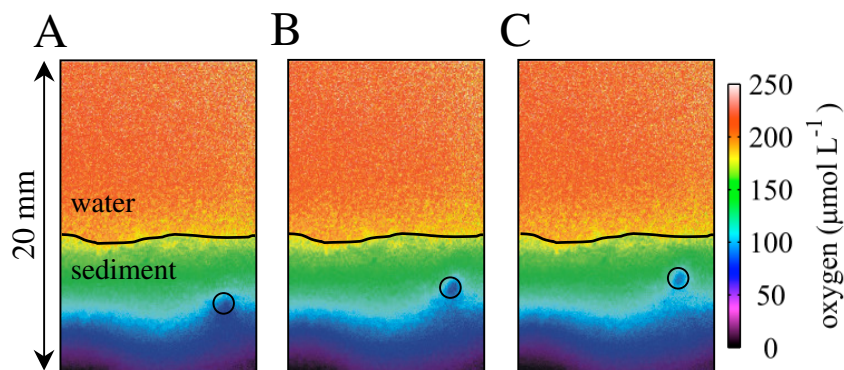

Figure 10: Oxygen distributions taken in time-intervals of 30 min demonstrating the moving activity of a foraminifera specimen in the sediment along the aquarium wall. The accurate location of the specimen (circles) as well as the sediment surface (horizontal line) could be determined because the measurements were done with the transparent oxygen optode.

Seagrass experiments

An increase of oxygen in the vicinity of a *Cymodocea rotundata* root was measured after ~ 5 h of constant illumination of the seagrass leaves (Fig. 11). However, only one experiment successfully demonstrated that ROL of seagrass roots could be measured with planar oxygen optodes. In a previous study, it could be shown that ROL measured in the seagrass *Halophila ovalis* decreased from the root tip towards the more basal region, which suggested that seagrass roots may contain a barrier to prevent loss of oxygen in the basal region (Connell et al. 1999). In our experiments the measured ROL was not close to the root tip, suggesting that the root could have been damaged when it was removed from sediment and cleaned before it was placed in the cuvette. One reason for the difficulties on measuring ROL could be the high rate of oxygen consumption in the surrounding sediment (OCR of up to ~ 140 µmol L^{-1} min^{-1} was detected). Oxygen released by the root was probably rapidly consumed by the sediment and thus could not be detected by the optode. Experiments by Pedersen et al. (1998) using oxygen microelectrodes showed that during illumination the oxic zone around the root extended only ~ 80 µm. As the spatial resolution of our measurements was in the range of 60 µm pixel^{-1}, the detection of ROL at this resolution is not very likely. Additionally, even an extremely thin layer of oxygen consuming sediment between the root and the optode could have circumvented the detection of ROL.

The main outcome of these first measurements was the design and construction of a suitable cuvette which allows fast and easy exchange of sediment. Using this cuvette setup and suitable sediment, it was recently possible to measure oxygen dynamics around seagrass roots (van der Welle et al., in prep.).
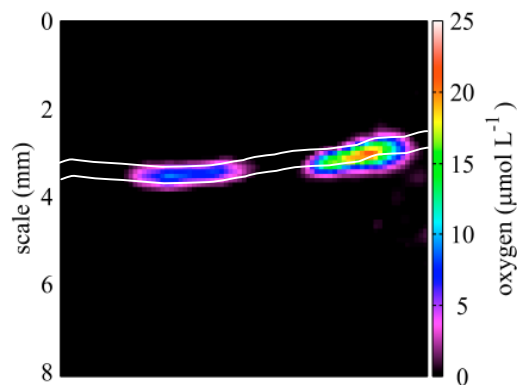

Figure 11: 2D oxygen distribution in sediment at the location of a seagrass root measured in a cuvette equipped with a planar oxygen optode. The white lines indicate the contour of the root.

Temperature experiments

Examples of 2D distributions of OCR measured in a core with intact, natural permeable sediment at various temperatures are shown in Fig. 12. Two sediment horizons with distinct OCR were clearly distinguishable. OCRs in the top 6 cm of the sediment were rather homogeneous and varied on average between 8 and 40 µmol L^{-1} min^{-1} for temperatures ranging from 4 to 26°C. These results are similar to those measured by de Beer et al. (2005) in the sediment collected from the same site in March and July, who determined using microelectrodes and the same flow-through method OCR values of 6 – 24 µmol L^{-1} min^{-1} for the top 6 cm of the sediment. In the deeper layers (8 – 10 cm), our measurements showed that OCRs were much more heterogeneous and varied on average from 26 to 100 µmol L^{-1} min^{-1} when temperatures changed between 4 and 26° C. OCR values determined during the second measurement at 4°C were lower by approx. 30 % at all sediment horizons (data not shown) in comparison to the OCR values measured initially at 4°C. Therefore only the first 4°C measurement was used for further calculations.
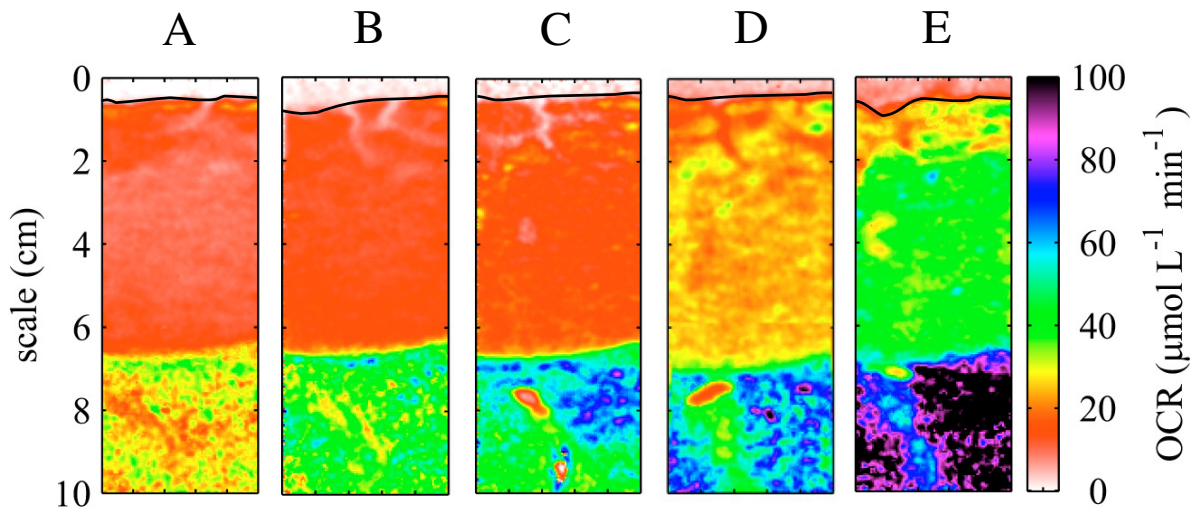

Figure 12: Examples of 2D distributions of OCR measured in a core with natural, intact permeable sediment at 4, 10, 15, 20 and 28°C corresponding to (A), (B), (C), (D) and (E), respectively. The black horizontal lines indicate the sediment surface.

Temperature dependence of OCRs averaged over four sediment horizons is shown in Fig. 13. OCR of the top three layers exhibited similar temperature dependence, which was also confirmed by similar values of the activation energy, $E_a \sim 60$ kJ mol^{-1}, and the quotient $Q_{10} \sim 2.5$. In contrast, the activation energy and quotient Q_{10} were considerably lower in the deeper sediment layers (horizon 8 – 10 cm), namely $E_a \sim 38$ kJ mol^{-1} and $Q_{10} \sim 1.8$.
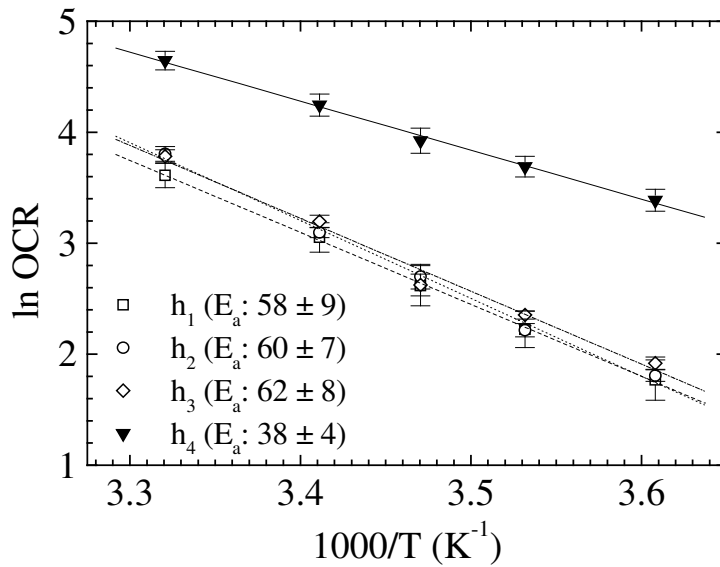
Figure 13: Arrhenius plots of OCR values averaged over 2×1 cm areas at four horizons in the intact permeable sediment (see Fig. 13 for examples of 2D distributions of OCR). Horizons h_1, h_2, h_3 and h_4 correspond to sediment depth intervals $0 – 2$, $2 – 4$, $4 – 6$ and $8 – 10$ cm, respectively. Error bars indicate the variability of OCR over the averaged areas. Activation energy (E_a in kJ mol^{-1}) calculated for each region is given in the legend.

The higher degree of homogeneity of OCR values and their temperature dependence in the top 6 cm of sediment implies a similar composition of the aerobic microbial community throughout this sediment horizon. Values of E_a and Q_{10} similar to ours were also found for sedimentary aerobic respiration rates of the top ($0 – 0.5$ cm) oxic sediment layers in Aarhus Bay (Denmark) and another temperate intertidal site (Weddewarden, German North Sea) (Thamdrup and Fleischer 1998; Thamdrup et al. 1998).

The lower E_a and Q_{10} values obtained for the deepest horizon were probably caused by the fact that the measured OCR represented predominantly oxygen consumption due to chemical oxidation of reduced compounds, which are generally characterised by Q_{10} values of approx. 2 (Adam et al. 1988). Aerobic organisms in these sediment horizons are probably relatively scarce and/or inactive because of infrequent oxidation events by advection. In situ oxygen profiling in the Sylt-Rømø basin in permeable sediments showed that advection caused prolonged oxygen penetration depths of $2 – 5$ cm (de Beer et al. 2005). Therefore, most likely anoxic conditions dominate in sediment depths of $8 – 10$ cm and solute transport is predominantly driven by diffusion. Inorganic compounds, e. g., H_2S,

Fe^{2+}, and Mn^{2+}, produced by anoxic degradation processes may easily accumulate under such conditions (Canfield et al. 1993). It is, however, problematic to compare our results directly with those of Thamdrup and co-workers, as the OCR rates changed considerably during the 6 days in our experiment (OCR measured at 4° C at the start and end of the experiments changed by ~ 30 %). Additionally to the temperature and the pool of inorganic compounds, also organic matter (substrate) can considerably influence oxygen respiration rates. Thamdrup et al. (1998) showed that after substrate addition the OCR could be doubled over a wide temperature range. Thus, the decrease in OCR, observed during the initial and final OCR measurements at 4° C, could be caused by the decreasing amounts of easy usable labile organic substrate due to washout effects (flow-on period) and increased metabolic activity during warm experimental conditions.

In these first temperature experiments, neither the substrate supply nor the concentration and reactivity of reduced inorganic substances were controlled or quantified, which causes difficulties in the interpretation and comparison of our results with others. Nevertheless, we demonstrated that the planar optode based flow-through technique can provide valuable supplementary information in the study of temperature characteristics of OCR in permeable sediments.

Differentiation between the chemical and biological oxygen consumption rates

When the sediment sample was exposed continuously to oxygen in the short-term experiment, the measured OCR values decreased rapidly from ~ 40 to 13 µmol L^{-1} min^{-1} during the first 4 cycles (first ~ 50 min of the experiment). During the subsequent 3 cycles the decrease levelled off at a value of ~ 11.5 µmol L^{-1} min^{-1}. After the sediment was exposed to approximately 40 min of anoxia prior to the 8th OCR measurement, a slight increase of OCR to ~ 12 µmol L^{-1} min^{-1} was observed (Fig. 14).

After 8 days of sediment incubation during the long-term experiment, OCR values in the aerated sediment were significantly lower than those measured in the sediment kept under anoxic conditions. Furthermore, no significant differences between the two investigated sediment horizons ($h_1 = 0 - 2$ cm and $h_4 = 8 - 10$ cm) were detectable for neither the aerated nor the non-aerated sediment samples. As shown in Fig. 15, average OCR values of the aerated sediment ranged between 0.3 (at 4 °C) and 3 µmol L^{-1} min^{-1} (at 20 °C). OCR values of the non-aerated sediment were approximately 20 – 100 times higher, ranging between 30 (at 4 °C) and 70 µmol L^{-1} min^{-1} (at 20 °C). Activation energies calculated from the Arrhenius plots also varied considerably, with E_a ~ 81 kJ mol^{-1} (Q_{10} ~

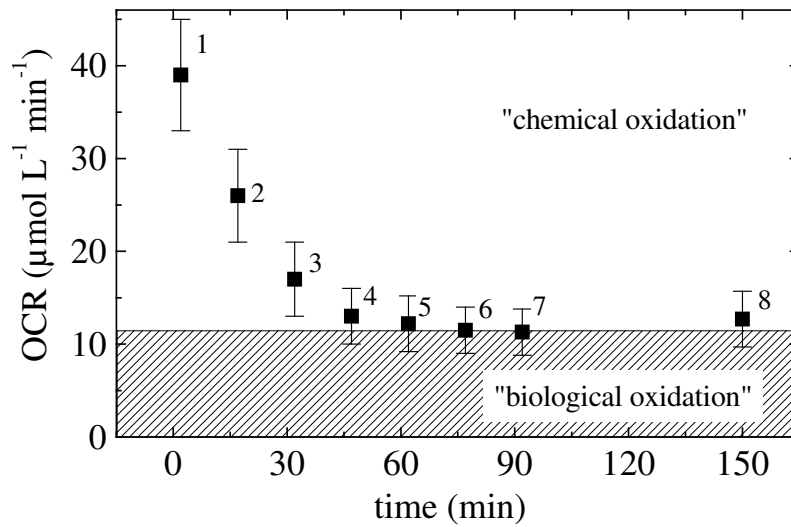3.4) and $E_a \sim 39$ kJ mol^{-1} ($Q_{10} \sim 1.8$) for the aerated and non-aerated sediment, respectively (Fig. 15).

Fig. 14: OCR values averaged over 0.5×1 cm of permeable sediment exposed to repeated aeration periods and OCR measurements. Aeration prior to the OCR measurements were 2 min (corresponding to ~ 100 ml of seawater), duration of OCR measurements # 1 – 6 and # 8 were 13 min, whereas the duration of the OCR measurement # 7 was ~ 60 min. Error bars indicate the variability of the OCR over the averaged area.

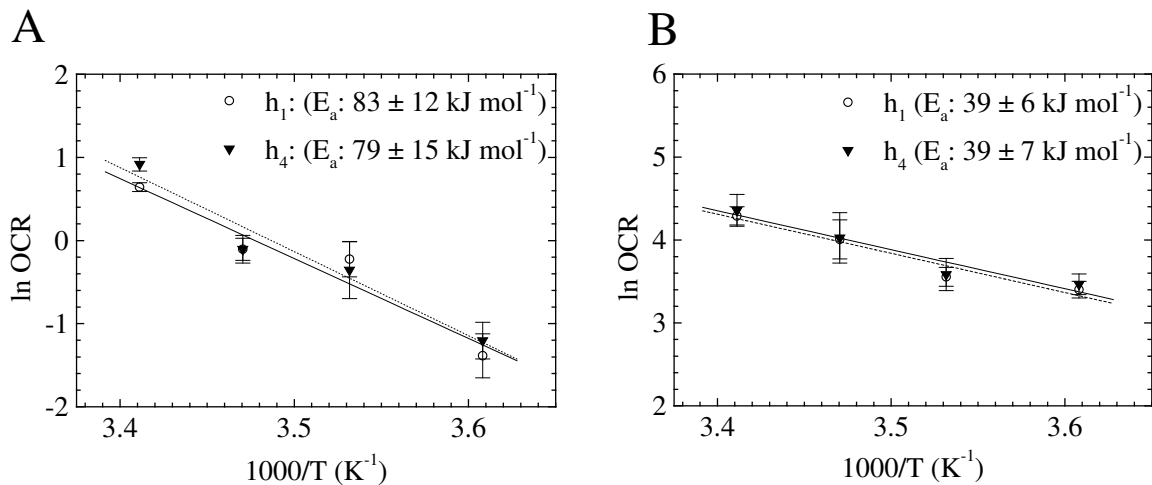Figure 15: Arrhenius plots and calculated activation energies (E_a) derived from the OCR measurements from 2 sediment horizons ($h_1 = 0 – 2$ cm, $h_4 = 8 – 10$ cm) of the subsampled sediment cores which were either aerated (A) or non-aerated (B) for 8 days. OCR values were averaged over an area of 0.5×1 cm, error bars indicate the variability of the OCR over the averaged area. For each region the calculated activation energy (E_a) is given in kJ mol^{-1} $\pm$ standard deviation, the corresponding Q_{10} values are ~ 3.4 for the aerated (A) and ~ 1.8 for non-aerated sediment (B). Note different scale of the ln (OCR) in (A) and (B).

A possible interpretation of these observations is as follows. In oxic sediment horizons, i.e., during oxic conditions, aerobic microorganisms utilise oxygen for organic matter degradation (OMD). When oxygen is absent, aerobes are inactive and OMD by anaerobic microbial processes like Fe-, Mn- and sulfate reduction takes over, resulting in the release of reduced compounds such as Fe^{2+}, Mn^{2+}, H_2S into the sediment (Canfield et al. 1993). If oxygen is not available for extended time periods and the main transport mechanism is diffusion, nutrients and reduced end products of anaerobic OMD can accumulate in the sediment. When oxic conditions arise again, not only the aerobic microorganisms contribute to the oxygen consumption, but also the pool of reduced compounds. We refer to these two pathways as the biological and chemical contributions to the sedimentary oxygen consumption.

The rapid decrease of the observed sedimentary OCR during the initial 40 – 60 minutes of the short-term experiment (Fig. 14) could be interpreted as the removal of the reduced compounds form the sediment by their oxidation with oxygen. If the pool of accumulated reduced compounds was differentiated by different reactivities towards oxygen, the component with the fastest reactivity was removed first, followed by the components with slower reactivity towards oxygen, etc. At the end of the 5th OCR measurement, i.e., after approximately 60 min of continuous exposure to oxygen, most of the reduced compounds that could become oxidised during the relatively short time of the OCR measurement were removed, resulting in the observed levelling off of the OCR. The constant values of the OCR at this stage of the short-term experiment, i.e., the OCR values measured at cycles 6 – 7 (Fig. 14), could be interpreted as the sum of the aerobic microbial respiration rate (biological contribution) and the oxidation rate of the reduced compounds reacting very slowly with oxygen. If the latter contribution could be neglected due to the relatively short OCR measurement, this type of experiment could be used to quantify the biological and chemical contributions to the sedimentary oxygen uptake, as indicated in Fig. 14 by the striped and white areas, respectively. After the sediment was left anoxic for ~ 40 min, a small fraction of the pool of reduced compounds could have been recovered due to the onset of anaerobic OMD, leading to the observed increase of OCR in the 8th cycle. It is known that particularly reduced iron is highly reactive with oxygen and very abundant in the studied sediment (Brüchert, pers. comm.). Therefore, the iron pool might be predominantly responsible for the chemical oxygen consumption.

The scenario described above is also supported by the results from the temperature measurements conducted after the long-term experiment (Fig. 15). During 8 days of

incubation under aerobic conditions, probably most reduced compounds were oxidised. On the other hand, reduced compounds became dominating in the sediment incubated under permanent anoxic conditions, which could explain the significantly higher OCR measured in the sediment incubated under anaerobic conditions. Additionally this could be the reason for the different temperature response of the sedimentary OCR measured after the long-term incubation. The activation energies determined for the aerated and non-aerated sediment were very similar to those determined for the top and bottom sediment horizons in the temperature experiments discussed in the previous section (compare figures 13 and 15), respectively. This supports the conclusion that the biological respiration and chemical oxidation were the dominant pathways of oxygen consumption in the aerated and non-aerated sediment samples, respectively. When compared to the value of E_a determined for the aerated sediment (Fig. 15A), E_a found in the sediment from the upper 6 cm in the temperature experiments (Fig. 13, horizons h_1-h_3) was slightly lower. This could be attributed to the fact that the activation energy determined for the top 6 cm of the sediment consisted of both the biological and chemical contributions in the temperature experiments. Another possibility would be that the microbial community changed their composition and thus their temperature response during the 8 days of incubation under aerobic conditions.

Interpretation of these results involves many assumptions about the processes taking place in the sediment which have to be checked by independent measurements. In particular, the dynamics of the reduced and oxidized iron (and possibly other) pools in the sediment need to be assessed independently to make the interpretation based entirely on oxygen measurements unambiguous. The conditions, e.g., organic matter content, under which the sediment was incubated over such relatively long time periods should also be controlled or at least characterized better. Nevertheless, it can be said that the planar oxygen optodes and the flow-through method utilized in a specially designed time and temperature protocols can, very rapidly and with a minimal effort, provide very useful information for the study of biogeochemical dynamics in permeable sediments.

Conclusions

Most of the presented applications showed that planar optodes cannot easily be used to measure and calculate highly accurate oxygen distributions and dynamics. Quantification of oxygen transport and conversion is therefore, in most cases, not satisfactory. Major problems which hamper quantification are the light guidance effect, relatively noisy oxygen data and slow time-response of the optodes (for details of these problems, see Chapter 5). Another problem is the planar geometry of the optode, whereby rounded

structures such as worm burrows or the organisms themselves impede determination of oxygen distributions and gradients. This problem could be addressed by developing models that realistically describe 3D oxygen distributions around the studied objects located at or near the planar optode.

On the other hand, planar optodes showed great potential in the study of temperature dependence of oxygen consumption rates in permeable sediments by means of the flow-through method. We showed that the planar optodes can help clarifying the contribution of chemical oxidation reactions to total OCR in permeable sediments, especially when combined with independent methods for the determination of the pools of reduced compounds. When qualitative determination and visualisation of the heterogeneity and dynamics of 2D oxygen data are the focus of interest (e.g., Precht at al. 2004; Franke et al, submitted), planar optodes represent a powerful tool, which is superior to one-dimensional measuring techniques provided by oxygen microoptodes or microelectrodes.

References

Adam, G, P Läuger, and G Stark. 1988. Physikalische Chemie und Biophysik. Edited by G. Adam, P. Läuger and G. Stark. 2nd Edition ed. Springer Verlag.

Ballew, R. M., and J. N. Demas. 1989. An error analysis of the rapid lifetime determination method for the evaluation of single exponential decays. Analytical Chemistry **61**: 30-33.

Broecker, W. S., and T. H. Peng. 1974. Gas-Exchange Rates Between Air and Sea. Tellus **26**: 21-35.

Canfield, D. E., B. B. Jorgensen, H. Fossing, R. Glud, J. Gundersen, N. B. Ramsing, B. Thamdrup, J. W. Hansen, L. P. Nielsen, and P. O. J. Hall. 1993. Pathways of organic carbon oxidation in three continental margin sediments. Marine Geology **113**: 27-40.

Connell, E. L., T. D. Colmer, and D. I. Walker. 1999. Radial oxygen loss from intact roots of Halophila ovalis as a function of distance behind the root tip and shoot illumination. Aquatic Botany **63**: 219-228.

Crank, J. 1975. The Mathematics of Diffusion. 2nd edition ed. Oxford University Press Inc.

de Beer, D., F. Wenzhöfer, T.D. Ferdelman, S. Boehme, M. Huettel, J. E. E. von Beusekom, M. E. Böttcher, N. Musat, and N. Dubilier. 2005. Transport and mineralization rates in North Sea sandy intertidal sediments Sylt- Rømø basin, Wadden Sea. Limnology and Oceanography. **50**: 113-127.

Epping, E.H.G., A. Khalili, and R. Thar. 1999. Photosynthesis and the dynamics of oxygen consumption in a microbial mat as calculated from transient oxygen microprofiles. Limnology and Oceanography. **44**: 1936-1948.

Fenchel, T. 1996a. Worm burrows and oxic microniches in marine sediments.1. Spatial and temporal scales. Marine Biology **127**: 289-295.

Fenchel, T. 1996b. Worm burrows and oxic microniches in marine sediments.2. Distribution patterns of ciliated protozoa. Marine Biology **127**: 297-301.

Fenchel, T., and R. N. Glud. 2000. Benthic primary production and O-2-CO2 dynamics in a shallow- water sediment: Spatial and temporal heterogeneity. Ophelia **53**: 159-171.

Franke, U., L. Polerecky, E. Precht, and M. Huettel. Visualisation of organic matter degradation in permeable sediments: a wave tank study. Limnology and Oceanography. **submitted**

Glud, R. N., M. Kuhl, O. Kohls, and N. B. Ramsing. 1999. Heterogeneity of oxygen production and consumption in a photosynthetic microbial mat as studied by planar optodes. Journal of Phycology **35**: 270-279.

Glud, R. N., N. B. Ramsing, J. K. Gundersen, and I. Klimant. 1996. Planar optrodes: A new tool for fine scale measurements of two-dimensional O$_2$ distribution in benthic communities. Marine Ecology-Progress Series **140**: 217-226.

Glud, R. N., C. M. Santegoeds, D. De Beer, O. Kohls, and N. B. Ramsing. 1998. Oxygen dynamics at the base of a biofilm studied with planar optodes. Aquatic Microbial Ecology **14**: 223-233.

Glud, R. N., A. Tengberg, M. Kuhl, P. O. J. Hall, I. Klimant, and G. Holst. 2001. An in situ instrument for planar O-2 optode measurements at benthic interfaces. Limnology and Oceanography **46**: 2073-2080.

Hannah, F., A. Rogerson, and J. Laybournparry. 1994. Respiration rates and biovolumes of common benthic foraminifera (Protozoa). Journal of the Marine Biological Association of the United Kingdom **74**: 301-312.

Holst, G., U. Franke, and B. Grunwald. 2001. Transparent oxygen optodes in environmental applications at fine scale as measured by luminescence lifetime imaging. Paper read at SPIE Vol. 4576: Advanced Environmental Sensing Technology II, at Boston, MA, USA.

Holst, G., and B. Grunwald. 2001. Luminescence lifetime imaging with transparent oxygen optodes. Sensors and Actuators B-Chemical **74**: 78-90.

Holst, G., O. Kohls, I. Klimant, B. König, M. Kuhl, and T. Richter. 1998. A modular luminescence lifetime imaging system for mapping oxygen distribution in biological samples. Sensors and Actuators B-Chemical **51**: 163-170.

Jonkers, H. M., R. Ludwig, R. De Wit, O. Pringault, G. Muyzer, H. Niemann, N. Finke, and D. de Beer. 2003. Structural and functional analysis of a microbial mat ecosystem from a unique

permanent hypersaline inland lake: 'La Salada de Chiprana' (NE Spain). Fems Microbiology Ecology **44**: 175-189.

Jørgensen, B.B. 1982. Mineralization of organic-matter in the sea bed - the role of sulfate reduction. Nature **296**: 643-645.

Klimant, I., V. Meyer, and M. Kuhl. 1995. Fiberoptic oxygen microsensors, a new tool in aquatic biology. Limnology and Oceanography **40**: 1159-1165.

Klimant, I., and O. S. Wolfbeis. 1995. Oxygen-sensitive luminescent materials based on silicone-soluble ruthenium diimine complexes. Analytical Chemistry **67**: 3160-3166.

König, B., G. Holst, R.N. Glud, and M. Kuehl. 2001. Imaging of oxygen distributions at benthic interfaces: A brief review, p. 63-71. *In* J. Y. Aller, S. A. Woodin and R. C. Aller, [eds.]. Organism-Sediment Interactions. University of south Carolina Press.

Kristensen, E. 1981. Direct Measurement of ventilation and oxygen-uptake in 3 species of Tubicolous Polychaetes (Nereis Spp). Journal of Comparative Physiology **145**: 45-50.

Kristensen, E. 1983a. Ventilation and oxygen-uptake by 3 species of *Nereis* (annelida, polychaeta).1. Effects of hypoxia. Marine Ecology-Progress Series **12**: 289-297.

Kristensen, E. 1983b. Ventilation and oxygen-uptake by 3 species of *Nereis* (Annelida, Polychaeta).2. Effects of temperature and salinity changes. Marine Ecology-Progress Series **12**: 299-305.

Kühl, M., and N. P. Revsbech. 2001. Biochemical microsensors for boundary layer studies. *In* B. P. Boudreau and B. B. Jørgensen, [eds.]. The benthic boundary layer. Oxford University Press.

Li, Y. H., and S. Gregory. 1974. Diffusion of Ions in Sea-Water and in Deep-Sea Sediments. Geochimica Et Cosmochimica Acta **38**: 703-714.

Liebsch, G., I. Klimant, B. Frank, G. Holst, and O. S. Wolfbeis. 2000. Luminescence lifetime imaging of oxygen, pH, and carbon dioxide distribution using optical sensors. Applied Spectroscopy **54**: 548-559.

Lübbers, D. W. 1995. Optical sensors for clinical monitoring. Acta Anaesthesiologica Scandinavica **39**: 37-54.

Pedersen, O., J. Borum, C. M. Duarte, and M. D. Fortes. 1998. Oxygen dynamics in the rhizosphere of Cymodocea rotundata. Marine Ecology-Progress Series **169**: 283-288.

Polerecky, L., U. Franke, U. Werner, B. Grunwald, and D. de Beer. 2005. High spatial resolution measurement of oxygen consumption rates in permeable sediments. Limnol. Oceanogr.: Methods **3**: 75-85.

Precht, Elimar, Ulrich Franke, Lubos Polerecky, and Markus Huettel. 2004. Oxygen dynamics in permeable sediments with wave-driven pore water exchange. Limnology and Oceanography **49**: 693-705.

Rasheed, M., C. Wild, U. Franke, and M. Huettel. 2004. Benthic photosynthesis and oxygen consumption in permeable carbonate sediments at Heron Island, Great Barrier Reef, Australia. Estuarine Coastal and Shelf Science **59**: 139-150.

Revsbech, N.P. , and B.B. Jørgensen. 1983. Photosynthesis of benthic microflora measured by the oxygen microprofile method: Capabilities and limitations of the method. Limnology and Oceanography. **28**: 749-756.

Revsbech, N.P. , J. Sørensen, T.H. Blackburn, and J.P. Lomholt. 1980. Distribution of oxygen in marine sediments measured with microelectrodes. Limnology and Oceanography. **25**: 403-411.

Riisgard, H. U. 1991. Suspension feeding in the Polychaete *Nereis-Diversicolor*. Marine Ecology-Progress Series **70**: 29-37.

Riisgard, H. U., A. Vedel, H. Boye, and P. S. Larsen. 1992. Filter-net structure and pumping activity in the polychaete *Nereis-Diversicolor* - effects of temperature and pump-modeling. Marine Ecology-Progress Series **83**: 79-89.

Thamdrup, B., and S. Fleischer. 1998. Temperature dependence of oxygen respiration, nitrogen mineralization, and nitrification in Arctic sediments. Aquatic Microbial Ecology **15**: 191-199.

Thamdrup, B., J. W. Hansen, and B. B. Jorgensen. 1998. Temperature dependence of aerobic respiration in a coastal sediment. Fems Microbiology Ecology **25**: 189-200.

van der Welle, M.E.W., L. Polerecky, G. Peralta, U. Franke, and T.J. Bouma. Spatial explicit quantification of oxygen dynamics in the rhizosphere: Measuring radial oxygen loss and respiratory oxygen consumption using a planar optode. **in prep.**

Vedel, A., B. B. Andersen, and H. U. Riisgard. 1994. Field investigations of pumping activity of the facultatively filter-feeding polychaete *Nereis-Diversicolor* using an improved infrared phototransducer system. Marine Ecology-Progress Series **103**: 91-101.

Vedel, A., and H. U. Riisgard. 1993. Filter-feeding in the polychaete *Nereis-Diversicolor* - growth and bioenergetics. Marine Ecology-Progress Series **100**: 145-152.

Wenzhöfer, F., and R. N. Glud. 2004. Small-scale spatial and temporal variability in benthic O2 dynamics of coastal sediments: Effects of fauna activity. Limnology and Oceanography **49**: 1471-1481.

Wild, C., M. Rasheed, U. Werner, U. Franke, R. Johnstone, and M. Huettel. 2004. Degradation and mineralization of coral mucus in reef environments. Marine Ecology-Progress Series **267**: 159-171.

Conclusions

The work presented in this thesis investigates two-dimensional (2D) oxygen distribution and dynamics in biological aquatic systems with the help of recently developed porphyrin-based planar oxygen optodes and the modular luminescence lifetime imaging (MOLLI) system.

The general characteristics of the used optodes were determined in experiments described in chapter 5. The accuracy of porphyrin-based oxygen planar optodes was relatively low with $\pm$ 7 – 20 % in the range around 100 % of air saturation and $\pm$ 2 – 3 % at zero oxygen concentration. The estimated minimum temporal resolution was approximately 3 s for transparent and semi-transparent optodes and 4 s for optically isolated optodes. Minimal spatial resolutions were between 15 – 30 and 35 – 70 µm for transparent/semi-transparent and optically isolated optodes, respectively. The long-term stability of continuously used semi-transparent optodes was longer than 1.5 years.

It is shown that planar optodes cannot easily be used to determine highly accurate oxygen distributions and dynamics, when very high spatial (< 15 µm) and temporal (< 3 s) resolutions are required (chapter 5 and 6). Major problems are the light guidance effect, relatively noisy oxygen data and the slow response time of the optodes. Also their planar geometry can cause problems when biological samples are investigated which feature round structures such as worm burrows or the organisms themselves (chapter 6).

One important limitation for the biological applicability of porphyrin-based oxygen planar optodes to biological systems is the light guidance effect (chapter 5). This can lead to a significant underestimation of absolute oxygen values in oxic regions if they are located close to anoxic areas, and also of oxygen gradients. The light guidance effect can be minimised by (i) selecting materials with the same (or very similar) refractive indices for the optode, the aquarium wall and the fixation material (glue), or by (ii) increasing the thickness of the aquarium wall. However, if the experimental setup demands thin walls, optical oxygen determination using planar optodes might provide inaccurate results for oxygen gradients at high oxygen concentrations. Even though the light guidance effect is minimised when the laser-line scanning technique is employed, it can only be employed for steady state 2D oxygen distributions.

The oxygen data measured with porphyrin-based planar optodes are robust enough to visualise 2D oxygen heterogeneities and dynamics qualitatively in various biological systems. However, when further accurate calculations and quantification of the oxygen

data are required, e.g., oxygen consumption rate (OCR) determination of single organisms or photosynthesis measurements (chapter 6), especially the noise and the light guidance effect can lead to inaccurate results. Therefore, special care has to be taken when such oxygen images are utilised for further calculations.

On the other hand, porphyrin-based oxygen optodes proved to be powerful tools in aquatic systems where qualitative determination and visualisation of the heterogeneity and dynamics of 2D oxygen distributions are the focus of interest. In these systems, where extremely fast and highly precise determination of oxygen distributions and gradients is less crucial, planar optodes are superior to one-dimensional measuring techniques provided by oxygen microoptodes or microelectrodes. One of the most appreciatory applications for planar optodes are permeable sediments (chapters 2, 3, 4 and 6). Planar optodes showed great potential in the study of oxygen dynamics and processes in permeable sediments. In these heterogeneous environments very dynamic oxygen changes can occur, not only at very small scale but also in scales of centi- and decimetres, dimensions which can be easily covered by planar optodes.

Established OCR methods, e.g., using interfacial oxygen gradients combined with Fick's law of diffusion, benthic-chambers or the eddy-correlation technique, only allow for the determination of areal OCR as the oxygen consumption is integrated over the total oxic sediment volume. To estimate possibly heterogeneous OCR within permeable sediments a method was developed that allowed for the determination of depth profiles of potential volumetric OCR (chapter 3). It is based on percolating the sediment core with aerated water and monitoring 1D or 2D oxygen changes in the sediment using oxygen microelectrodes or planar oxygen optodes, respectively. The method is useful for fast (minutes to hours) characterisation of sediments exposed to highly dynamic advective water exchange, such as intertidal sandy sediments. When combined with *in situ* oxygen microprofiles measured by microsensors, realistic areal rates of aerobic respiration in permeable sediments can be calculated (chapter 3).

The combination of the flow-through method and planar optodes could provide valuable supplementary information for clarifying the contribution of chemical oxidation reactions to total OCR in permeable sediments (chapter 6), when the pool of reduced compounds is determined with independent methods. Also the temperature characteristics of OCR in permeable sediments can be determined relatively fast, even on intact, undisturbed sediment cores.

Model calculations proposed that oxygen distributions underneath a rippled permeable surface exposed to progressing waves may be altered and horizontal gradients could occur. This complex two-dimensional oxygen distribution could not easily be assessed by classical one-dimensional approaches such as microelectrodes. Using planar optodes in a wave tank experiment (chapter 2) it was possible for the first time to directly visualise changes of the spatial and temporal oxygen distributions caused by wave-driven advective porewater flow. Oxygenated water intruding in the ripple troughs and deep anoxic porewater drawn to the surface under the ripple crests created an undulating oxic–anoxic boundary within the upper sediment layer, mirroring the topographical features of the sediment bed and resulting in steep vertical as well as horizontal oxygen gradients. The optode showed that slowly migrating wave ripples are trailed by their pore water flow field, alternately exposing sediment volumes to oxic and anoxic porewater. Rapid ripple migration (≥ 20 cm h^{-1}) produced a continuous oxic surface layer that inhibited the release of reduced substances from the sediment bed.

The influence of porewater flow and diffusive transport on the degradation of labile particular organic matter (POM) embedded in a natural permeable sediment was shown in chapter 4. Porewater advection, induced by interaction of wave-driven oscillatory boundary flow and stationary sediment ripples, reproducibly exposed POM to oxic or anoxic conditions lasting between days and weeks. OCRs were up to 18-times higher at locations of the buried POM compared to the surrounding sediment. Despite high permeability of the sediment and exposure to oxygenated porewater flow, suboxic and anoxic sites and suboxic porewater "plumes" developed at and downstream of the locations of POM in otherwise oxygenated sediment regions. A large discrepancy between the measured total carbon loss of the *U. lactuca* discs and the carbon consumption calculated from the OCR measurements was observed, suggesting that bacterial degradation of POM and the final degradation of dissolved organic matter (DOM) became spatially decoupled by the porewater flow. Advection thus can enhance the rate of organic mater degradation by efficiently distributing DOM from "hotspots" of organic matter mineralisation to larger volumes of permeable sediments and associated microbial communities.

The importance of permeable sediments for global carbon cycling and remineralisation processes is becoming increasingly acknowledged and applications using oxygen planar optodes can advance the understanding of these highly active and dynamic systems.

Manuscripts not included in this thesis

Transparent oxygen optodes in environmental applications at fine scale as measured by luminescence lifetime imaging

Gerhard Holst, Ulrich Franke and Björn Grunwald

Max Planck Institute for Marine Microbiology, Celsiusstrasse 1, 28359 Bremen, Germany

The manuscript has not been included in this thesis as U. Franke supplied only a part of the data on three-dimensional oxygen measurements. U. Franke aided in carrying out the experiments, and provided minor editorial help upon writing of the manuscript. The Manuscript can be made available upon request.

Abstract

Due to the **mo**dular **l**uminescence **l**ifetime **i**maging system (MOLLI) that has been developed within the last few years, it is possible to use oxygen sensors that are not optically isolated. Transparent planar optodes and dispersed nanooptodes for the first time enable a direct optical link between the chemical parameter to be measured (oxygen as an example) and the structure that is responsible for the distribution of the chemical parameter (corals as an example). Since the transparency as a principal quality of the optode allows to record structural images. The spatial resolution of the MOLLI imaging system is determined by a) the area size of the view field that is imaged onto the amount of pixels of the CCD-chip (640 x 480 in our case) and b) by the spatial limitations of the sensing layer. The latter means in case of the planar optode the thickness of the sensing layer and in case of dispersed nano-optodes the thickness of the excitation light field. We present biological applications of transparent planar optodes (thickness $\approx$ 5 - 10 µm) at two areal resolutions, a) 50 µm / pixel and b) 6 µm / pixel and one application of nano-optodes at 80 µm / pixel. The first application shows the oxygen production of endolithic cells that live in the skeleton of massive corals, measured in a cut coral sample that was illuminated through the planar oxygen optode with defined light energy levels to follow the oxygen production of these coral symbionts. Finally the oxygen production and consumption of coral symbionts are shown by dispersed oxygen nano-optodes in the medium. The specific set-up for the latter experiment will be discussed with the future implication of possible 3D measurements. Although the results all come from biological applications from coral reef environments, obviously the measuring system and the transparent sensors can be applied to a variety of environmental topics. At the moment similar optodes are under development for parameters like pH, CO_2 and temperature.

Benthic photosynthesis and oxygen consumption in permeable carbonate sediments at Heron Island, Great Barrier Reef, Australia

Rasheed[1], M., C. Wild[2], U. Franke[2], and M. Huettel[3]

[1] Marine Science Station, University of Jordan and Yarmouk University, P O Box 195, Aqaba, Jordan

[2] Max Planck Institute for Marine Microbiology, Celsiusstrasse 1, 28359 Bremen, Germany

[3] Florida State University, Department of Oceanography, 0517 OSB, West Call Street, Tallahassee, Florida 32306-4320, USA

The manuscript has not been included in this thesis as U. Franke supplied only the two-dimensional oxygen measurement data and provided minor editorial help upon writing of the manuscript. The Manuscript can be made available upon request.

Abstract

In order to investigate benthic photosynthesis and oxygen demand in permeable carbonate sands and the impact of benthic boundary layer flow on sedimentary oxygen consumption, in situ and laboratory chamber experiments were carried out at Heron Island, Great Barrier Reef, Australia. Total photosynthesis, net primary production and respiration were estimated to be 162.9 ± 43.4, 98.0 ± 40.7, and 64.9 ± 15.0 mmol C m^{-2} d^{-1}, respectively. DIN and DIP fluxes for these sands reached 0.34 and 0.06 mmol m^{-2} d^{-1}, respectively. Advective pore water exchange had a strong impact on oxygen consumption in the permeable sands. Consumption rates in the chamber with larger pressure gradient (20 rpm, 1.2 Pa between centre and rim) simulating a friction velocity of 0.6 cm s^{-1} were approximately two-fold higher than in the chambers with slow stirring (10 rpm, 0.2 Pa between centre and rim, friction velocity of 0.3 cm s^{-1}). In the laboratory chamber experiments with stagnant water column, oxygen consumption was eight times lower than in the chamber with fast stirring. Laboratory chamber experiments with Br^{-} tracer revealed solute exchange rates of 2.6, 2.2, 0.7 ml m^{-2} d^{-1} at stirring rates of 20, 10, and 0 rpm, respectively. In a laboratory experiment investigating the effect of sediment permeability on oxygen and DIC fluxes, a three-fold higher permeability resulted in two- to threefold higher oxygen consumption and DIC release rates. These experiments demonstrate the importance of boundary flow induced flushing of the upper layer of permeable carbonate sediment on oxygen uptake in the coral sands. The high filtration and oxidation rates in the sub-tropical permeable carbonate sediments and the subsequent release of nutrients and DIC reveal the importance of these sands for the recycling of matter in this oligotrophic environment.

Degradation and mineralization of coral mucus in reef environments

Wild, C.[1], M. Rasheed[2], U. Werner[1], U. Franke[1], R. Johnstone[3], and M. Huettel[4]

[1] Max Planck Institute for Marine Microbiology, Celsiusstrasse 1, 28359 Bremen, Germany

[2] Marine Science Station, University of Jordan and Yarmouk University, PO Box 195, Aqaba, Jordan

[3] Centre for Marine Studies, The University of Queensland, Brisbane, Queensland 4072, Australia

[4] Department of Oceanography, Florida State University, Tallahassee, Florida 32306-4320, USA

The manuscript has not been included in this thesis as U. Franke supplied only the two-dimensional oxygen measurement data and provided minor editorial help upon writing of the manuscript. The Manuscript can be made available upon request.

Abstract

With *in situ* and laboratory chamber incubations we demonstrate that coral mucus, an important component of particulate organic matter in reef ecosystems, is a valuable substrate for microbial communities in the water column and sandy sediments of coral reefs. The addition of coral mucus to the water of benthic chambers placed on lagoon sands in the coral cay Heron Island, Australia, resulted in a rapid and significant increase in both O_2 consumption and DIC production in the chambers. The permeable coral sands permitted the transport of mucus into the sediment with interfacial water flows, resulting in the mucus being mainly (> 90 %) degraded in the sediment and not in the water column of the chambers. A low ratio of 0.48 (*in situ*) to 0.64 (laboratory) for O_2 consumption/DIC production after the addition of coral mucus, and high sulfate reduction rates (SRR) in natural sediments which were exposed to coral mucus, suggest a large contribution of anaerobic processes to the degradation of coral mucus. Oxygen penetrated less than 5 mm deep into these sediments. The microbial reaction to mucus addition was rapid, with a calculated *in situ* C turnover rate ranging from 7 to 18 % h^{-1}. The degradation of coral mucus showed a dependency on the permeability of the carbonate sediments, with faster degradation and remineralization in coarse sands. This indicates the importance of permeable reef sediments for the trapping and degradation of organic matter. We suggest that coral mucus may have a function as a carrier of energy to the benthic microbial consumers.